Two-Grid hp-Version Discontinuous Galerkin Finite Element Methods for Quasilinear PDEs

Scott Congreve, BSc., MSc.

Thesis submitted to The University of Nottingham
for the degree of Doctor of Philosophy

July 2014

Abstract

In this thesis we study so-called two-grid hp-version discontinuous Galerkin finite element methods for the numerical solution of quasilinear partial differential equations. The two-grid method is constructed by first solving the nonlinear system of equations stemming from the discontinuous Galerkin finite element method on a coarse mesh partition; then, this coarse solution is used to linearise the underlying problem so that only a linear system is solved on a finer mesh. Solving the complex nonlinear problem on a coarse enough mesh should reduce computational complexity without adversely affecting the numerical error.

We first focus on the *a priori* and *a posteriori* error estimation for a scalar second-order quasilinear elliptic PDEs of strongly monotone type with respect to a mesh-dependent energy norm. We then devise an hp-adaptive mesh refinement algorithm, using the *a posteriori* error estimator, to automatically refine both the coarse and fine meshes present in the two-grid method. We then perform numerical experiments to validate the algorithm and demonstrate the improvements from utilising a two-grid method in comparison to a standard (single-grid) approach.

We also consider deviation of the energy norm based *a priori* and *a posteriori* error bounds for both the standard and two-grid discretisations of a quasi-Newtonian fluid flow problem of strongly monotone type. Numerical experiments are performed to validate these bounds. We finally consider the dual weighted residual based *a posteriori* error estimate for both the second-order quasilinear elliptic PDE and the quasi-Newtonian fluid flow problem with generic nonlinearities.

Keywords: hp-adaptivity; *a priori*; *a posteriori*; non-Newtonian fluids; discontinuous Galerkin finite element methods; two-grid; dual weighted residual

Acknowledgements

I would first like to thank my supervisor, Paul Houston, for the support and guidance he has provided throughout my PhD. I would also like to thank the University of Nottingham for providing the necessary funding to undertake this project.

I would also like to acknowledge the collaborative assistance and support of Prof. Thomas P. Wihler (Universität Bern) throughout this project, whose initial discussion with Paul prompted the study of the two-grid method. Similarly, the support and input of Prof. Endre Süli (University of Oxford) for the non-Newtonian fluid flow work was much appreciated.

Thank you also to all the fellow PhD students and post-doctoral researchers from the Mathematical Science department at Nottingham who have graced the coffee room over the years. You have all provided me with hours of fun and relief from work, and not forgetting the cakes, without which the whole PhD experience would have been much poorer. Special thanks must go to the other PhDs in the Scientific Computation and Analysis research group, especially Tom Bennison and Joe Collis, who have provided a useful sounding board for mathematical discussion.

Finally, thank you to family; my Mum and Dad, without whom this thesis would not exist, for providing support and financial help for my PhD and also my brother Michael for providing hours of relief from the stress of work, especially during the final write-up phase.

Contents

1 Introduction **1**

1.1 Nonlinear Problems . . . 1

1.2 Discontinuous Galerkin Finite Element Methods . . . 3

1.3 *A Posteriori* Error Estimation and Mesh Adaptivity . . . 8

1.4 Two-Grid Methods . . . 12

1.5 Outline of the Thesis . . . 14

2 Preliminaries **16**

2.1 Definitions and Notations . . . 16

2.1.1 Function Spaces . . . 16

2.1.2 Finite Element Discretisation . . . 18

2.1.3 Trace Operators . . . 20

2.2 DGFEM for Poisson's Equation . . . 21

2.2.1 Derivation of the DGFEM . . . 22

2.2.2 *A Priori* Error Analysis . . . 25

2.2.3 *A Posteriori* Error Analysis . . . 25

3 Two-Grid *hp*-DGFEM for Quasilinear Elliptic PDEs **27**

3.1 Standard *hp*-Version IP DGFEM . . . 29

3.1.1 *A Priori* Error Bound . . . 31

3.2 *hp*-Version Two-Grid DGFEM . . . 32

3.3 *A Priori* Error Bound . . . 32

3.4 *A Posteriori* Error Bound . . . 37

3.4.1 DG Decomposition . . . 39
3.4.2 Auxiliary Results . . . 40
3.4.3 Proof of Theorem 3.4 . . . 41
3.5 Summary . . . 45

4 Computational Implementation and Numerical Experiments 46
4.1 Validation of *A Priori* Error Bounds . . . 46
4.2 Two-Grid *hp*-Adaptive Mesh Refinement Algorithm . . . 47
4.2.1 Strategy One - Independent Fine and Coarse Grid Refinement . . . 49
4.2.2 Strategy Two - Linked Fine and Coarse Grid Refinement . . . 50
4.3 Adaptive Numerical Experiments . . . 52
4.3.1 Example 1: 2D Smooth Analytical Solution . . . 53
4.3.2 Example 2: 2D Singular Solution . . . 58
4.3.3 Example 3: 3D Singular Solution . . . 62
4.4 Summary . . . 64

5 Two-Grid *hp*-DGFEM Based on Single Newton Iteration 68
5.1 *hp*-Version Two-Grid DGFEM . . . 69
5.2 *A Priori* Error Analysis . . . 71
5.2.1 Auxiliary Results . . . 72
5.2.2 Proof of Theorem 5.3 . . . 75
5.3 *A Posteriori* Error Analysis . . . 76
5.3.1 Proof of Theorem 5.7 . . . 77
5.4 Numerical Experiments . . . 79
5.4.1 Validation of *A Priori* Error Bounds . . . 79
5.4.2 Validation of *A Posteriori* Error Bounds . . . 80
5.5 Summary . . . 88

6 *hp*-DGFEM for Non-Newtonian Fluids 89
6.1 Weak Formulation . . . 90

6.1.1 Variational Form . . . 90
6.1.2 Well-Posedness . . . 91
6.2 *hp*-Version DGFEM . . . 92
6.2.1 DGFEM Discretisation . . . 92
6.2.2 Well-Posedness of the DGFEM Formulation . . . 94
6.3 *A Priori* Error Analysis . . . 96
6.3.1 Proof of Theorem 6.5 . . . 97
6.4 *A Posteriori* Error Analysis . . . 102
6.4.1 Upper Bounds . . . 102
6.4.2 Local Lower Bounds . . . 103
6.4.3 Proof of Theorem 6.7 . . . 104
6.4.4 Proof of Theorem 6.8 . . . 112
6.5 Numerical Experiments . . . 117
6.5.1 Example 1: Smooth Solution . . . 118
6.5.2 Example 2: Cavity Problem . . . 119
6.5.3 Example 3: Singular Solution . . . 122
6.6 Summary . . . 124

7 Two-Grid *hp*-DGFEM for Non-Newtonian Fluids 125
7.1 Two-Grid *hp*-Version DGFEM . . . 126
7.1.1 *A Priori* Error Bound . . . 128
7.1.2 *A Posteriori* Error Bound . . . 133
7.2 Two-Grid *hp*-Version DGFEM Based on an Incomplete Newton Iteration 137
7.2.1 *A Priori* Error Bound . . . 138
7.2.2 *A Posteriori* Error Bound . . . 141
7.3 Numerical Experiments . . . 142
7.3.1 Validation of *A Priori* Error Bound . . . 143
7.3.2 Validation of *A Posteriori* Error Bound . . . 145
7.4 Summary . . . 154

8 DWR for *hp*-DGFEM for Quasilinear PDEs **155**

8.1 Second-Order Quasilinear PDE 155

8.1.1 *A Posteriori* Error Estimation 157

8.1.2 Two-Grid *hp*-Adaptive Mesh Refinement Algorithm 159

8.1.3 Numerical Experiments 160

8.2 Non-Newtonian Fluid Flow 171

8.2.1 *A Posteriori* Error Estimation 173

8.2.2 Numerical Experiments 174

8.3 Summary 186

9 Conclusions and Further Work **187**

9.1 Summary 187

9.2 Further Work 190

9.2.1 Extension to Generic Nonlinearities 190

9.2.2 More Complex Problems and Time-Dependence 190

9.2.3 Anisotropic Mesh Refinement 191

9.2.4 General Elements 191

Bibliography **I**

CHAPTER 1

Introduction

In this thesis we study the *a priori* and *a posteriori* error estimation of the discontinuous Galerkin finite element method (DGFEM) for classes of nonlinear partial differential equations (PDEs). In particular, we focus on so-called two-grid methods and the use of *a posteriori* error analysis for automatic hp-adaptive mesh refinement.

In this chapter we briefly outline the real world problems that give rise to nonlinear PDEs and, hence, why we are interested in them. We then discuss the DGFEM and the advantages of utilising this method compared to other numerical methods along with the necessity of deriving *a priori* error bounds. We also discuss *a posteriori* error estimation and its use in automatic mesh refinement for achieving an error in the numerical solution below a specific threshold. While the use of the standard DGFEM is fairly well developed within the literature, the generalisation to two-grid methods is quite recent; with this in mind, we present an overview of the two-grid method and give a brief description of the general principles behind the method.

1.1 Nonlinear Problems

Often in basic models a particular quantity of interest is modelled as linearly dependent on the known quantities; however, this is not always a realistic representation of the physical world observations. This can be demonstrated with the simple case of the displacement of a vertical rod (x) clamped at the lower end under a perpendicular force (P) at the upper end. Under small loads the displacement is modelled as proportional, or linear, to the force applied ($x = cP$); however, it is noted that experimental results

show that above a certain force the displacement becomes *nonlinear* with respect to the force applied as it is no longer proportional to the force, and the rod can even break; cf. Böhmer [41, Example 1.1].

In the field of continuum mechanics nonlinear partial differential equations arise fairly commonly. One of the most important nonlinear equations in the field of fluid dynamics, which we do not consider in this thesis, is the *incompressible* and *compressible Navier-Stokes* equations. The incompressible Navier-Stokes equations are given by

$$\begin{aligned} \rho\frac{\partial \boldsymbol{u}}{\partial t} - \nu\triangle\boldsymbol{u} + \rho(\boldsymbol{u}\cdot\nabla)\boldsymbol{u} + \nabla p &= \boldsymbol{f}, \\ \nabla\cdot\boldsymbol{u} &= 0, \end{aligned}$$

where $\boldsymbol{u} = (u_1, \ldots, u_d)^\top$ is the velocity vector, p is the pressure, ρ is the fluid density, ν is the viscosity, and $\boldsymbol{f}$ is the body force acting on the fluid. As can be seen this contains a nonlinear term $\rho(\boldsymbol{u}\cdot\nabla)\boldsymbol{u}$. The Navier-Stokes can be used to model the flow of water around a vessel, the airflow across an aircraft wing, fluid flow in a pipe and ocean currents to name just a few.

One thing to note is the term $\nu\triangle\boldsymbol{u}$ is linear with respect to $\boldsymbol{u}$ as it is modelling a Newtonian fluid flow [21], where the viscous stress arising from the flow is proportional to the local strain. Non-Newtonian fluids on the other hand do not obey this rule and, as a result, have a nonlinear second order term [167]. Non-Newtonian fluids include such common fluids as toothpaste, ketchup, paint and blood. One useful application of non-Newtonian fluid flows is in modelling the movement of a glacier, cf. Blatter [40], Colinge & Rappaz [62], Glowinski & Rappaz [99]. We also note that Bingham fluids [39, 146] are non-Newtonian and these have been used for the modelling of landslides [56, 113] and wire drawing in metal formation [67, 68, 127]. We study the above nonlinearity in this thesis, although we generally restrict to nonlinearities that are strongly monotone in type.

As noted above nonlinearities arise fairly commonly in interesting fields of study and, hence, solutions to problems are of this type are vitally important. Typically the

solutions to a nonlinear PDE cannot be determined by analytical methods, particularly in high dimensional space; therefore, the use of numerical methods is essential. In order to numerically solve a nonlinear PDE problem a variety of numerical methods exist, such as the finite difference, finite volume, boundary element and finite element methods, for example. We refer to the book by Böhmer [41] for an excellent overview of various numerical methods for the solution of fully nonlinear partial differential equations. In this thesis, we study the use of the *discontinuous Galerkin* finite element method (DGFEM) variant of the finite element method.

1.2 Discontinuous Galerkin Finite Element Methods

The original finite element method, subsequently referred to as the *continuous Galerkin* finite element method (CGFEM), was first developed during the 1950s and 1960s, independently by both engineers and mathematicians. We refer to the review article by Clough & Wilson [58] and the book by Babuška & Strouboulis [11] for background on this development. In the CGFEM the computational domain is divided into elements with the solution to the problem being approximated on each element by an elemental polynomial of a maximum order. The CGFEM assumes that the solution is continuous across the elemental boundaries and, hence, some of the degrees of freedom of the approximating polynomial for an element are shared with neighbouring elements to enforce this continuity condition. The CGFEM approximation to a PDE problem is typically defined directly from the underlying variational formulation by replacing the test and trial functions by piecewise polynomial functions, subject to the enforcement of appropriate boundary conditions. This results in a system of simultaneous equations to solve; in the case of a linear problem this leads to the matrix problem $\underline{A}\boldsymbol{x} = \boldsymbol{b}$, where $\underline{A}$ is a matrix and $\boldsymbol{x}, \boldsymbol{b}$ are vectors. For a nonlinear problem, a method for solving the resulting system of nonlinear equations is required; for example, the *damped Newton* method [147, Section 14.4].

One of the main issues with the CGFEM is that they display poor stability properties for convection-dominated and hyperbolic problems resulting in non-physical, highly

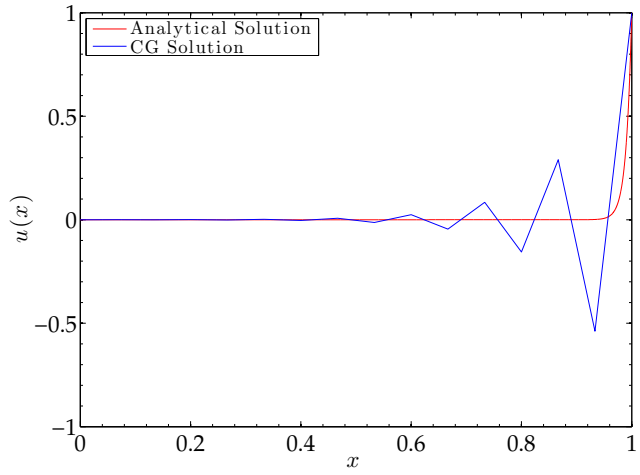

Figure 1.1: Analytical and continuous Galerkin FEM numerical solution to a convection-dominated convection-diffusion equation.

oscillatory, numerical solutions; modifications to the method have been developed to make them more stable, cf. Brooks & Hughes [49], Cangiani *et al.* [53], Fischer *et al.* [84], Franca *et al.* [85], Hughes *et al.* [126], Johnson & Nävert [129] and the references therein. For example, consider the one-dimensional convection-diffusion equation

$$-\epsilon u'' + Du' = 0, \qquad u(0) = 0, \qquad u(1) = 1,$$

which has the analytical solution

$$u(x) = \frac{1 - \mathrm{e}^{\mathrm{Pe}\, x}}{1 - \mathrm{e}^{\mathrm{Pe}}},$$

where $\mathrm{Pe} = {}^{D}/_{\epsilon}$ is the Péclet number. For a large Péclet number, i.e., $D \gg \epsilon$, the equation is convection dominated and results in an analytical solution almost exactly equal to the inflow boundary condition at $x = 0$, except for a boundary layer close to the outflow boundary $x = 1$ [49]. Figure 1.1 shows the analytical and CGFEM numerical solution when $\epsilon = 10^{-2}$ and $D = 1$, where the computational domain has been split into $N = 15$ elements of equal size $h = {}^{1}/_{N}$. On each element we approximate the solution using linear polynomials, which gives rise to $N + 1$ degrees of freedom, one at each elemental boundary shared between the elements on either side. Here we observe

that the numerical solution computed with the CGFEM results in highly oscillatory behaviour due to the presence of the boundary layer.

Discontinuous Galerkin finite element methods offer a class of alternative methods which attempt to address this stability problem. The initial development of DGFEMs was undertaken independently for hyperbolic, cf. Reed & Hill [150], and elliptic problems, cf. Arnold [7], Baker [14], Douglas & Dupont [75], Wheeler [171]; although we note that these papers do not refer to the method as the discontinuous Galerkin finite element method. We refer to the review article by Cockburn *et al.* [60], which provides an excellent overview of the development of DGFEMs. The initial article by Reed & Hill [150] focused on the neutron transport problem and was mainly an engineering article, in the sense that it focused on the algorithmic development of the method. Numerical experiments were performed to show that the DGFEM is numerically more stable than the CGFEM, but more computationally expensive. The reason for the extra computational expense arises from the fact that the DGFEM allows for discontinuities across elemental boundaries. In order to admit these discontinuities, the DGFEM does not share degrees of freedom between neighbouring elements, but imposes restrictions in the form of flux terms on the elemental boundary to attempt to minimise the jump between elements. As a result the DGFEM contains more degrees of freedom than the corresponding CGFEM; for example, in the one-dimensional convection-dominated equation considered earlier the DGFEM would result in nearly twice the number of degrees of freedom, or more precisely $2N$ degrees of freedom, as each element contains 2 independent degrees of freedom.

LeSaint & Raviart [134] undertook the first analysis of the DGFEM; they proved the existence and uniqueness of the numerical solution to the DGFEM formulation proposed by Reed & Hill [150]. In addition, LeSaint & Raviart [134] derived the first *a priori* error bound for the proposed method. An *a priori* bound bounds the error of the numerical solution, in some norm, from above in terms of the analytical solution and the mesh parameters, such as element size (h) and the degree of the elemental polynomials (k). Ideally as the mesh becomes finer, $h \to 0$ or $k \to \infty$, the value of the bound

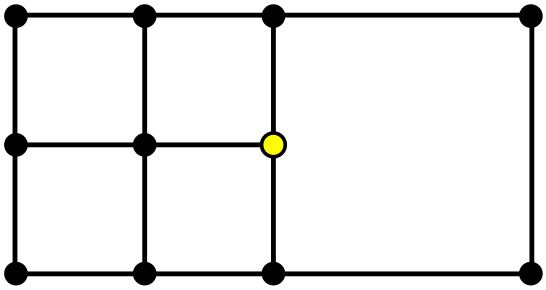

Figure 1.2: Mesh elements with a hanging node (highlighted in yellow).

should vanish; therefore, the error will also decrease, which proves that the error in the numerical solution converges to zero as the mesh is enriched. We refer to the articles by Johnson & Pitkäranta [130], Lin [135], Peterson [149], Richter [151] for further work concerning the *a priori* error analysis of the method, under the assumption that the polynomial degree of the approximating polynomial is fixed on all elements and does not change (so-called h-version FEMs). It is worth noting that degree 0 polynomials (piecewise constants) on each element essentially recovers the finite volume method.

Varying the polynomial degree across elements (p-version FEMs), as well as both the element size and polynomial degree (hp-version FEMs), can also be undertaken, cf. Schwab [158]. We note that the literature refers to polynomial degree refinement as p-refinement as p is usually used to denote polynomial degree; however, in this thesis we use k for polynomial degree to avoid conflict with the pressure function present in non-Newtonian fluid flows, but still refer to polynomial refinement as p-refinement for consistency with the literature; cf. Houston *et al.* [120, 121, 123]. We remark that the nature of the CGFEM means that it can be difficult to have two neighbouring elements with different polynomial degrees; whereas, with the DGFEM this is handled naturally by the method. Similarly, it is possible in a DGFEM to have elements with hanging nodes, cf. Figure 1.2, while the CGFEM method can not handle this situation as easily due to the requirement of continuity over elemental boundaries, cf. Šolín *et al.* [160]. The natural advantage of the p-version FEM is that they exhibit an exponential convergence rate with respect to the number of degrees of freedom, which is clearly more efficient than the h-version; cf. [156, 175]. It is worth noting that the advantage of hp-

version FEM is that h-refinement can be used to isolate singularities and non-smooth regions in the analytical solution, where p-version FEMs are unable to approximate the analytical solution accurately, and then perform p-refinement to achieve exponential convergence. As such we would expect hp-version FEMs to be able to achieve a lower error for fewer degrees of freedom compared to the h-version FEM. *A priori* error analysis for the hp-version of the DGFEM for hyperbolic PDEs has been undertaken, for example, by Bey & Oden [32], Houston & Süli [115], Houston *et al.* [118], Süli *et al.* [163].

The Reed & Hill [150] article and subsequent analysis [32, 115, 118, 130, 134, 135, 149, 151, 163] focusses on hyperbolic equations. The early work of the DGFEM for elliptic PDEs, cf. Arnold [7], Baker [14], Douglas & Dupont [75], Wheeler [171], focused on the *symmetic interior penalty* (SIP) DGFEM. We note that this is only one of many potential DGFEM formulations possible for elliptic problems. Two variants of the SIP DGFEM exist, the *nonsymmetic interior penalty* (NIP) [90, 119, 152, 163], and the *incomplete interior penalty* (IIP) [70, 71, 73, 164, 165] formulations. Other formulations that exists include the Babuška–Zlámal [13], Bassi–Rebay [17], Bassi *et al.* [18], Brezzi *et al.* [47, 48], Baumann–Oden [22, 145] and the *local discontinuous Galerkin* (LDG) [54, 55, 59, 61] FEMs. It is possible to derive all these of methods with a unified framework, cf. Arnold *et al.* [8, 9]. Essentially the original problem is written as a *flux formulation*, which contains numerical fluxes that approximate the analytical solution on the boundaries of the elements. Selection of different fluxes gives rise to the various methods mentioned above. In Chapter 2 we briefly outline this derivation for a generic *interior penalty* (IP) scheme for Poisson's equation; here, the scheme includes a parameter θ such that when $\theta = 1$ the NIP formulation is recovered, when $\theta = -1$ the SIP formulation is recovered and the IIP scheme is recovered in the case that $\theta = 0$.

For the treatment of nonlinear elliptic PDEs based on employing DGFEMs, we refer to the articles by Bustinza & Gatica [50], Gudi & Pani [100], Gudi *et al.* [101, 102] and Houston *et al.* [125], for example. Subsequent development of DGFEMs for non-Newtonian fluid flow problems has been undertaken by Bustinza & Gatica [51]; in-

deed, Bustinza & Gatica [51] derives *a priori* bounds for the LDG method applied to the quasilinear Stokes problem.

1.3 *A Posteriori* Error Estimation and Mesh Adaptivity

The issue with the *a priori* error analysis is that the bound on the error is usually in terms of the analytical solution. In the typical situation, where we do not know the analytical solution, it would not be possible to calculate a bound for the error in the numerical solution. With *energy norm* based *a posteriori* error estimation it is possible to derive an error bound for the error in the energy norm in terms of the numerical solution. For example, consider the h-version CGFEM method for the one-dimensional Poisson equation:

$$-u'' = f, \qquad u(0) = u(1) = 0.$$

Writing u_h to denote the CGFEM approximation, the following *a posteriori* error bound holds

$$\left\|u' - u_h'\right\|_{L^2(0,1)} \leq Ch \left\|\mathcal{R}(u_h)\right\|_{L^2(0,1)},$$

where C is a positive constant and $\mathcal{R}(\cdot)$ is the residual defined, elementwise, as

$$\mathcal{R}(v) = f + v'';$$

clearly, we have that $\mathcal{R}(u) \equiv 0$.

A key use of *a posteriori* error estimation is in adaptive mesh refinement, cf. Brenner & Scott [45, Chapter 9] and Eriksson *et al.* [82]. Here, the idea is to approximate a PDE on an initial mesh and then perform some form of mesh refinement with the aim of decreasing the error in the numerical solution. In theory we wish to continue refining the mesh until the error in the numerical solution is below a specific tolerance `TOL`, i.e.,

$$\left\|u' - u_h'\right\|_{L^2(0,1)} \leq \texttt{TOL}.$$

As the numerical error is unknown the *a posteriori* error estimate can be exploited, so

that the stopping condition for the criteria becomes

$$Ch \left\| \mathcal{R}(u_h) \right\|_{L^2(0,1)} \leq \texttt{TOL}. \tag{1.1}$$

Indeed, if (1.1) is satisfied, then the norm of the error will be below the desired tolerance. Essentially, we wish to perform the following algorithm to achieve our desired tolerance, cf. Eriksson *et al.* [82]:

Algorithm 1.1. *Choose an initial mesh* ${\mathcal{T}_h}^{(m=0)}$ *with mesh size* $h^{(m=0)}$

1. *Compute the corresponding FEM solution* $u_h^{(m)}$ *on the mesh* ${\mathcal{T}_h}^{(m)}$ *with mesh size* $h^{(m)}$.

2. *Given a computed* $u_h^{(m)}$ *on the mesh* ${\mathcal{T}_h}^{(m)}$ *with mesh size* $h^{(m)}$ *stop if*

$$Ch^{(m)} \left\| \mathcal{R}\left(u_h^{(m)}\right) \right\|_{L^2(0,1)} \leq \texttt{TOL},$$

   else, determine the new mesh ${\mathcal{T}_h}^{(m+1)}$ *with mesh size* $h^{(m+1)}$.

3. *Set* $m = m + 1$, *and go to Step 1.*

This is an important use of *a posteriori* error estimation as for most practical problems the aim is only to get a numerical solution that is 'good enough', or more accurately to a required tolerance. As a result, throughout this thesis we focus heavily on *a posteriori* error estimation and the application of these results to automatic mesh refinement. This algorithm naturally extends to any PDE problem, utilising different FEMs, as well as both p- and hp-version finite element methods. The key decision in this algorithm is selecting how to modify the existing mesh to order to create a new mesh for use in the next iteration; cf. Step 2. Eriksson *et al.* [82] proposes a method based on attempting to equidistribute the error across the mesh elements. To this end, the *a posteriori* error bound is split into elemental contributions; essentially for each element $\kappa \in \mathcal{T}_h$ we calculate

$$\eta_\kappa := Ch \left\| \mathcal{R}\left(u_h\right) \right\|_{L^2(\kappa)}.$$

The general aim of equidistribution methods is to refine or derefine elements based on the criterion

$$\eta_\kappa \approx \frac{\texttt{TOL}}{\sqrt{N}},$$

where N is the number of elements in the current mesh. Essentially if the local error indicator of an element is a significant amount larger than this criterion refine the element as many times as necessary to attempt to achieve this target. Bey *et al.* [33, 34] state an algorithm for deciding how many times to subdivide each element in order to equally distribute the error. Another technique is the so-called fixed fraction method. Here, for a fixed refinement percentage R and derefinement percentage D, the $R\%$ elements with the largest contribution to the error are refined and the $D\%$ elements with the smallest contribution are derefined. We note that there are many such algorithms available for selecting a new mesh and we refer to the book by Verfürth [170] for a summary. With the *a posteriori* analysis in the above outlined refinement algorithm there is no apparent guarantee that the error converges to zero as refinement progresses, unlike in *a priori* error estimation. However, for certain mesh refinement strategies convergence of the error to zero over the series of meshes generated by automatic mesh refinement has been shown; cf. Belenki & Diening [28], Binev *et al.* [38], Brenner & Scott [45, Chapter 9], Demlow & Stevenson [72], Dörfler [74], Morin *et al.* [144], Siebert [159], Stevenson [162], Veeser [169].

With hp-version FEMs an extra refinement decision is required. While the algorithms mentioned above will be useful for selecting elements to refine, with hp-version FEMs it is necessary to select whether to perform h-refinement, where mesh elements are divided into smaller elements, or p-refinement, where the polynomial degree of the approximating polynomial on that element is increased. Houston & Süli [116] outline an hp-adaptive mesh refinement algorithm, based on the general principle that p-refinement should occur on elements where the underlying analytical solution is locally smooth. As this is unknown, a technique for estimating the smoothness of the analytical solution is required. To this end, Houston & Süli [116] exploit the fact that

Legendre coefficients of smooth analytical functions decay to zero at an exponential rate. Employing this idea, an indicator can be derived to estimate the smoothness of the function; if this is below a certain threshold then p-refinement is performed, otherwise h-refinement is undertaken. We note that this work was motivated by the earlier work by Mavriplis [139]. Many different algorithms exist for choosing between h- or p-refinement; we refer to the articles by Mitchell & McClain [142, 143] for an overview and numerical experiments for the various techniques. These articles, however, do not include the recent work by Wihler [172, 173] and Fankhauser *et al.* [83], who propose an alternative method for estimating smoothness based on the use of Sobolev embeddings.

A posteriori error analysis for the IP DGFEM is more complicated then the above CGFEM analysis, but can be performed for two-dimensional problems via estimating DGFEM functions with conforming functions, cf. Houston *et al.* [120, 123, 124], Karakashian & Pascal [131]. For the extension to hexahedral elements in three-dimensions we refer to Zhu [181], Zhu *et al.* [183]. This is a key technique that we utilise throughout the *a posteriori* error estimation in this thesis. We note that although work has been done to derive *a posteriori* error bounds for the IP DGFEM scheme for scalar quasilinear problems, cf. Bi & Ginting [37], Houston *et al.* [125], minimal work has been performed for the non-Newtonian fluid flow problem; cf. Berrone & Süli [31] for work on the CGFEM formulation. In this thesis we, therefore, extend the work by Houston *et al.* [123, 125] to an incompressible non-Newtonian fluid flow.

The *a posteriori* error bounds discussed above focuses on bounding the error in an energy norm; however, it is also possible to perform dual weighted residual based *a posteriori* error estimation of the error for a target functional, such as the coefficient of lift or drag at a particular point or region in the computational domain. Here, the error estimate is usually an equality rather than an upper and lower bound. The initial work for this was developed by Becker & Rannacher [23, 24, 25], for continuous Galerkin finite element methods, cf. Bangerth & Rannacher [15], based on the use of duals for L^2-norm error estimation, cf. Eriksson *et al.* [82]. Work on extending this to DGFEMs has

been performed by Harriman *et al.* [108, 109] and Hartmann & Houston [110, 111, 112]. The advantage of using a dual weighted residual based *a posteriori* error bound over energy norm based adaptation occurs in the case when we are only concerned with the error for the specific target functional. In this situation the numerical solution away from a particular region may have a reduced effect on the error for the target functional; hence, an energy norm based adaptive routine may refine in regions of the domain that result in minimal reduction in the error. The dual weighted residual literature [23–25, 117] demonstrates numerically the fact that dual weighted residual based refinement results in lower error in the error functional for fewer degrees of freedom than energy norm based refinement in this situation.

1.4 Two-Grid Methods

As mentioned previously the DGFEM for linear PDEs results in solving a linear matrix problem; however, nonlinear problems need to be solved by an iterative method based on solving linearised versions of the equation. This naturally results in an increase in computational time and complexity compared to a linear problem. It is also possible that an iterative solver for a nonlinear problem may not converge to a solution. Xu [178, 179, 180] and Marion & Xu [138] first proposed the use of a *two-grid* method for solving a CGFEM for a quasilinear partial differential equation, based on earlier work for nonselfadjoint and indefinite problems [177] as a means to reduce computational complexity.

The principle of the two-grid method can be is summarised as follows. Let X and Y be two Hilbert spaces and write $\mathcal{N}(\cdot;\cdot,\cdot) : X \times X \times Y \to \mathbb{R}$ to denote a semilinear form, where $\mathcal{N}(\cdot;\cdot,\cdot)$ is linear with respect to the arguments to the right of the semicolon. We consider the variational problem of finding $u \in X$ such that

$$\mathcal{N}(u;u,v) = 0 \qquad \forall v \in Y.$$

We need to approximate this problem with a Galerkin approximation. To that end, we

construct sequences of finite-dimensional spaces $\{X_{h,k}\}$ and $\{Y_{h,k}\}$, parameterised by the mesh size h and the degree k of the approximating piecewise polynomial functions. A (standard) Galerkin approximation $u_{h,k}$ of u is sought in $X_{h,k}$ such that

$$\mathcal{N}_{h,k}(u_{h,k}; u_{h,k}, v_{h,k}) = 0 \qquad \forall v_{h,k} \in Y_{h,k},$$

where $\mathcal{N}_{h,k}(\cdot;\cdot,\cdot) : X_{h,k} \times X_{h,k} \times Y_{h,k} \to \mathbb{R}$. We refer to the above method as the standard formulation. The principle of the two grid method is as follows: given the 'coarser' finite element spaces $X_{H,K} \subseteq X_{h,k}$ and $Y_{H,K} \subseteq Y_{h,k}$, first solve the nonlinear problem of finding $u_{H,K} \in X_{H,K}$ such that

$$\mathcal{N}_{H,K}(u_{H,K}; u_{H,K}, v_{H,K}) = 0 \qquad \forall v_{H,K} \in Y_{H,K},$$

then, using $u_{H,K}$ to linearise the problem, compute the two-grid approximation by solving the problem of finding $u_{2G} \in X_{h,k}$ such that

$$\mathcal{L}_{h,k}(u_{H,K}; u_{2G}, v_{h,k}) = 0 \qquad \forall v_{h,k} \in Y_{h,k},$$

where $\mathcal{L}_{h,k}(\cdot;\cdot,\cdot) : X_{H,K} \times X_{h,k} \times Y_{h,k} \to \mathbb{R}$ is a *linearised* approximation to the original nonlinear problem on the fine finite element space. Xu [178, 179, 180] outlines the case when one step of a Newton method is employed, i.e.,

$$\mathcal{L}_{h,k}(u_{H,K}; u_{2G}, v_{h,k}) := \mathcal{N}'_{h,k}[u_{H,K}](u_{2G} - u_{H,K}, v_{h,k}) + \mathcal{N}_{h,k}(u_{H,K}; u_{H,K}, v_{h,k}),$$

where $\mathcal{N}'_{h,k}[u](\cdot, v)$ denotes the Fréchet derivative of $u \to \mathcal{N}_{h,k}(u; u, v)$, for fixed v, evaluated at u. In special cases a simpler form can be used, where the approximation is simply to use the coarse grid solution $u_{H,K}$ as the nonlinear argument, i.e.,

$$\mathcal{L}_{h,k}(u_{H,K}; u_{2G}, v_{h,k}) := \mathcal{N}_{h,k}(u_{H,K}; u_{2G}, v_{h,k}).$$

We emphasise the point that $\mathcal{L}_{h,k}(u;\cdot,\cdot)$ is linear for a fixed u. As the nonlinear problem

is now only solved on a coarse mesh we expect the computational complexity to be significantly reduced.

The initial articles by Xu [178, 179, 180] perform h-version *a priori* error analysis of the simpler case of utilising the coarse solution as the nonlinear argument, where the nonlinearity depends only on u; in this case an optimal convergence rate is achieved if $h = \mathcal{O}(H^{(k+1)/k})$, where k is fixed. A more general case is considered by Axelsson & Layton [10], who note that for certain regularity of the solution an optimal convergence of $\mathcal{O}(h^k)$ rate can be achieved when $h = \mathcal{O}(H^4)$ for piecewise linear polynomial elements. We remark that the two-grid method has been considered for the Navier-Stokes method, cf. Girault & Lions [98], Utnes [168], as well as reaction-diffusion equations, cf. Chen & Chen [57], Wu & Allen [176]. The two-grid method has also been considered for other numerical methods as well, such as the finite volume [35] and finite difference [69] methods.

Recently Bi & Ginting [36] extended the two-grid method to solving an h-version SIP formulation of the quasilinear problem

$$\nabla \cdot (\mu(\boldsymbol{x}, u)\nabla u) = f(\boldsymbol{x}).$$

A priori error analysis of the two-grid DGFEM found that the error bound in a mesh-dependent DG norm also has optimal convergence when $h = \mathcal{O}(H^{(k+1)/k})$.

We note that the literature for two-grid methods for DGFEMs is very sparse, with no development of hp-version *a priori* error bounds, *a posteriori* error analysis or automatic mesh refinement. The aim of this thesis, therefore, is to study hp-version DGFEMs and, more importantly, the use of *a posteriori* error analysis for the automatic hp-mesh adaptation of the two meshes employed within a two-grid method.

1.5 Outline of the Thesis

We first introduce the necessary definitions and notations used throughout this thesis in Chapter 2, as well as outlining the basic DGFEM for Poisson's equation. We then

start the original work of this thesis by studying in Chapter 3 the *a priori* and energy norm *a posteriori* error estimation for the two-grid version of the IP hp-DGFEM for a second-order quasilinear elliptic PDE with a strongly monotone nonlinearity, where the two-grid method is based on using the coarse solution as the nonlinear argument for the approximation on the fine mesh. In Chapter 4 we perform numerical experiments to validate the error bounds derived in Chapter 3. For the *a posteriori* error bound we need to be able to perform hp-adaptive mesh refinements on both the coarse and fine mesh used for the two-grid method; to this end, we develop in Chapter 4 a two-grid mesh adaptation algorithm. With this first two-grid method developed and validated we then study in Chapter 5 an alternative two-grid method based on employing one step of a Newton iteration on the fine mesh using the coarse solution as the inital guess. Chapter 5 contains both the *a priori* and *a posteriori* error analysis along with the numerical experiments to validate the error bounds.

Having studied the two-grid method for a nonlinear scalar PDE we wish to extend the analysis to a more complicated system of equations, such as a non-Newtonian fluid flow with a strongly monotone nonlinearity. In order to do this we first study in Chapter 6 the standard hp-version IP DGFEM for an incompressible non-Newtonian fluid flow problem, deriving both *a priori* and *a posteriori* error bounds, as well as performing numerical experiments to validate these bounds. Once the analysis of the standard method is established for the non-Newtonian fluid, we extend the analysis to the two-grid version in Chapter 7. Here, we study both variants of the two-grid method and compare the results numerically.

In Chapter 8 we study the *a posteriori* analysis of the two-grid method for both scalar second-order quasilinear elliptic PDEs and non-Newtonian fluid flow problems for target functionals of error based on the dual weighted residual technique for goal-oriented mesh refinement.

Finally, in Chapter 9 we summarise the results of this thesis and propose potential future developments in this area of research.

CHAPTER 2

Preliminaries

In this chapter we introduce the definitions and notations necessary to study discontinuous Galerkin finite element methods. We also briefly outline the IP DGFEM for the simple Poisson's equation as an introduction to the method.

2.1 Definitions and Notations

2.1.1 Function Spaces

Throughout this thesis we use function spaces based on a polygonal, or polyhedral, Lipschitz domain $D \in \mathbb{R}^d$, $d = 2, 3$, with boundary ∂D. We let $\mathbb{N}_0$ denote the set of all non-negative integers and define an n-tuple $\alpha = \{\alpha_1, \ldots, \alpha_n\} \in \mathbb{N}_0^n$, called the *multi-index*. We define the length of the multi-index α as the non-negative integer $|\alpha| = |\alpha_1| + \cdots + |\alpha_n|$ and $\partial^\alpha = \partial_1^{\alpha_1} \ldots \partial_n^{\alpha_n}$, where $\partial_j = \partial/\partial x_j$, for $j = 1, \ldots, n$.

We denote by $C(D)$ the set of all real-valued continuous functions defined on D, and define, for $k \in \mathbb{N}_0$, $C^k(D) = \{v \in C(D) : \partial^\alpha v \in C^k(D), |\alpha| \leq k\}$. We note that in the case when $k = 0$ we have $C^k(D) \equiv C(D)$.

We let $L^2(D)$ denote the set of all real-valued Lebesgue measurable functions v defined on D such that $|v|^2$ is integrable on D; this Hilbert space is equipped with the norm

$$\|v\|_{L^2(D)}^2 = \int_D |v|^2 \, \mathrm{d}\boldsymbol{x}.$$

With this notation we can now define, for $k \in \mathbb{N}_0$, the Sobolev space $H^k(D) = \{v \in$

$L^2(D) : \partial^\alpha v \in L^2(D), |\alpha| \leq k\}$, equipped with the seminorm

$$|v|^2_{H^k(D)} = \sum_{|\alpha|=k} \|\partial^\alpha v\|^2_{L^2(D)} ,$$

and norm

$$\|v\|^2_{H^k(D)} = \sum_{i=0}^{k} |v|^2_{H^i(D)}.$$

We note that for $k = 0$, we have $H^k(D) = L^2(D)$. We also define $L^\infty(D)$ as the set of all real-valued Lebesgue measurable functions v defined on D such that $|v|$ has a finite essential supremum; this is a Banach space with norm

$$\|v\|_{L^\infty(D)} = \operatorname*{ess\,sup}_{\boldsymbol{x}\in D} |v(\boldsymbol{x})|.$$

We further define the following spaces of functions, which are subspaces of the standard function spaces defined above. For $k \in \mathbb{N}$, we write $H^k_g(D)$ to denote the space of functions in $H^k(D)$ with trace g on ∂D, i.e., $H^k_g(D) = \{v \in H^k(D) : v = g \text{ on } \partial D\}$; similarly, $H^k_0(D)$ denotes the space of functions in $H^k(D)$ with zero trace on ∂D. We also let $L^2_0(D)$ denote the space of functions in $L^2(D)$ with zero mean over D, i.e., $L^2_0(D) = \{q \in L^2(D) : \int_D q \, \mathrm{d}\boldsymbol{x} = 0\}$.

Vector and Tensor Fields

We now extend the above notation for scalar-valued functions to both vector- and tensor-valued functions. For a function space $X(D)$, we write $[X(D)]^d$ and $[X(D)]^{d\times d}$ to denote the spaces of all vector and tensor fields, respectively, whose components belong to the function space $X(D)$. The norms for these spaces are denoted, for simplicity, as the same as the norm for $X(D)$.

For the vectors $\boldsymbol{v}, \boldsymbol{w} \in \mathbb{R}^d$ and matrices $\underline{\sigma}, \underline{\tau} \in \mathbb{R}^{d\times d}$ we define the operators:

$$(\nabla \boldsymbol{v})_{ij} = \frac{\partial v_i}{\partial x_j}, \quad (\nabla \cdot \underline{\sigma})_i = \sum_{j=1}^{d} \frac{\partial \sigma_{ij}}{\partial x_j}, \quad (\boldsymbol{v} \otimes \boldsymbol{w})_{ij} = v_i w_j, \quad \underline{\sigma} : \underline{\tau} = \sum_{i=1}^{d}\sum_{j=1}^{d} \sigma_{ij}\tau_{ij}.$$

Hence, we can write, for $\underline{\tau} \in \mathbb{R}^{d\times d}$, the Frobenius norm, $|\cdot| : \mathbb{R}^{d\times d} \to \mathbb{R}$, as $|\underline{\tau}|^2 = \underline{\tau} : \underline{\tau}$.

2.1.2 Finite Element Discretisation

In order to create a finite element method for a problem on the spatial domain $\Omega \subset \mathbb{R}^d$, $d = 2, 3$, with boundary $\Gamma = \partial\Omega$, we consider meshes $\mathcal{T}_h$ that partition Ω into disjoint open-element domains κ such that $\overline{\Omega} = \bigcup_{\kappa\in\mathcal{T}_h} \overline{\kappa}$. We assume that the family of subdivisions $\{\mathcal{T}_h\}_{h>0}$ is shape regular [42, pp. 61, 118 and Remark 2.2, p. 114] and each $\kappa \in \mathcal{T}_h$ is an affine image of a fixed master element $\widehat{\kappa}$; i.e., for each $\kappa \in \mathcal{T}_h$, there exists an affine mapping $T_\kappa : \widehat{\kappa} \to \kappa$ such that $\kappa = T_\kappa(\widehat{\kappa})$, where $\widehat{\kappa}$ is the open cube $(-1, 1)^3$ in $\mathbb{R}^3$ (hexahedral element) and either the open triangle $\{(x, y) : -1 < x < 1, -1 < y < -x\}$ or the open square $(-1, 1)^2$ (quadrilateral) in $\mathbb{R}^2$. We denote by h_κ the elemental diameter of $\kappa \in \mathcal{T}_h$ and set $h = \max_{\kappa\in\mathcal{T}_h} h_\kappa$. We let $\boldsymbol{n}_\kappa$ denote the unit outward normal vector to the boundary $\partial\kappa$ of element κ. We allow the meshes $\mathcal{T}_h$ to be '1-irregular', i.e., each face of any one element $\kappa \in \mathcal{T}_h$ contains at most one hanging node (which, for simplicity, we assume to be at the centre of the corresponding face) and each edge of each face contains at most one hanging node (yet again assumed to be at the centre of the edge). We assume that the family $\{\mathcal{T}_h\}_{h>0}$ is of 'bounded local variation', i.e., there exists a constant $\rho_1 \geq 1$, independent of element sizes, such that

$$\rho_1^{-1} \leq {}^{h_\kappa}/_{h_{\kappa'}} \leq \rho_1, \tag{2.1}$$

for any pair of elements $\kappa, \kappa' \in \mathcal{T}_h$ that share a common face $F = \partial\kappa \cap \partial\kappa'$. We store the element sizes in the vector $\boldsymbol{h} = \{h_\kappa : \kappa \in \mathcal{T}_h\}$.

For a non-negative integer k, we denote by $\mathcal{P}_k(\widehat{\kappa})$ the space of polynomials of total degree k or less on $\widehat{\kappa}$. When $\widehat{\kappa}$ is a hypercube (quadrilateral or hexahedral element), we also consider $\mathcal{Q}_k(\widehat{\kappa})$, the set of all tensor-product polynomials on $\widehat{\kappa}$ of degree k or less in each coordinate direction. We then define the function space $\mathcal{S}_k(\widehat{\kappa})$ to be

$$\mathcal{S}_k := \begin{cases} \mathcal{P}_k, & \text{if } \kappa \text{ is a triangle,} \\ \mathcal{Q}_k, & \text{if } \kappa \text{ is a hypercube.} \end{cases}$$

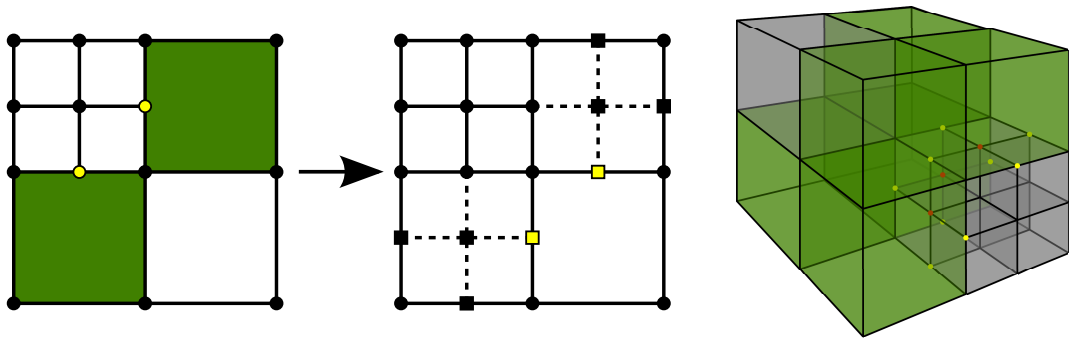

(a) 2D Mesh *(b)* 3D Mesh

Figure 2.1: (a) 2D mesh and (b) 3D mesh with hanging nodes. All elements marked in green are subdivided into 2^d elements to eliminate these hanging nodes (but introducing new hanging nodes) to create the auxiliary mesh, as demonstrated for the 2D mesh.

To each $\kappa \in \mathcal{T}_h$, we assign a polynomial degree $k_\kappa \geq 1$ (local approximation order), store these in a vector $\boldsymbol{k} = \{k_\kappa : \kappa \in \mathcal{T}_h\}$ and set $k_{\max} = \max_{\kappa \in \mathcal{T}_h} k_\kappa$. We suppose that $\boldsymbol{k}$ is also of bounded local variation, i.e., there exists a constant $\rho_2 \geq 1$, independent of the element sizes and $\boldsymbol{k}$, such that for any pair of neighbouring elements $\kappa, \kappa' \in \mathcal{T}_h$,

$$\rho_2^{-1} \leq {}^{k_\kappa}/_{k_{\kappa'}} \leq \rho_2. \tag{2.2}$$

We define an interior face F of $\mathcal{T}_h$ as the intersection of two neighbouring elements $\kappa, \kappa' \in \mathcal{T}_h$, i.e., $F = \partial\kappa \cap \partial\kappa'$. Similarly, we define a boundary face $F \subset \Gamma$ as the entire face of an element κ on the boundary. We denote by $\mathcal{F}_h^{\mathcal{I}}$ the set of all interior faces, $\mathcal{F}_h^{\mathcal{B}}$ the set of all boundary faces and $\mathcal{F}_h = \mathcal{F}_h^{\mathcal{I}} \cup \mathcal{F}_h^{\mathcal{B}}$ the set of all faces. For a face $F \in \mathcal{F}_h$ we define h_F as the diameter of the face and the face polynomial degree k_F as

$$k_F = \begin{cases} \max(k_\kappa, k_{\kappa'}), & \text{if } F = \partial\kappa \cap \partial\kappa' \in \mathcal{F}_h^{\mathcal{I}}, \\ k_\kappa, & \text{if } F = \partial\kappa \cap \Gamma \in \mathcal{F}_h^{\mathcal{B}}. \end{cases}$$

Since the mesh $\mathcal{T}_h$ is assumed to be 1-irregular we note that we can construct an auxiliary 1-irregular mesh $\mathcal{T}_{\tilde{h}}$ by subdividing all quadrilateral and hexahedral elements $\kappa \in \mathcal{T}_h$ whose edges contain at least one hanging node into 2^d sub-elements; Figure 2.1 demonstrates this for two- and three-dimensional quadrilateral and hexahe-

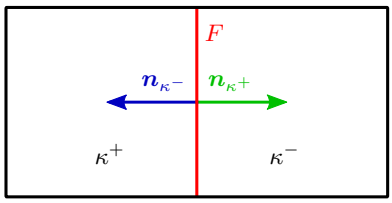

Figure 2.2: Unit outward normals to F for the elements κ^+ and κ^-, where $F = \partial\kappa^+ \cap \partial\kappa^-$.

dral meshes, respectively; cf. Zhu [181], Zhu & Schötzau [182], Zhu *et al.* [183]. We assume that triangular elements are *regularly reducible*, cf. Ortner & Süli [148], to eliminate hanging nodes in triangular elements on the auxiliary mesh.

2.1.3 Trace Operators

We shall now define some suitable face operators that are required for the definition of the DGFEM. Let q, $\boldsymbol{v}$, and $\underline{\tau}$ be scalar-, vector- and matrix-valued functions, respectively, which are smooth inside each element $\kappa \in \mathcal{T}_h$. Given two adjacent elements, $\kappa^+, \kappa^- \in \mathcal{T}_h$, which share a common face $F \in \mathcal{F}_h^{\mathcal{I}}$, i.e., $F = \partial\kappa^+ \cap \partial\kappa^-$, we write $q^\pm$, $\boldsymbol{v}^\pm$, and $\underline{\tau}^\pm$ to denote the traces of the functions q, $\boldsymbol{v}$, and $\underline{\tau}$, respectively, on the face F, taken from the interior of $\kappa^\pm$, respectively. With this notation, the averages of q, $\boldsymbol{v}$, and $\underline{\tau}$ at $\boldsymbol{x} \in F$ are given by

$$\{\!\{q\}\!\} = \frac{1}{2}(q^+ + q^-), \qquad \{\!\{\boldsymbol{v}\}\!\} = \frac{1}{2}(\boldsymbol{v}^+ + \boldsymbol{v}^-), \qquad \{\!\{\underline{\tau}\}\!\} = \frac{1}{2}(\underline{\tau}^+ + \underline{\tau}^-),$$

respectively. Similarly, the jumps of q, $\boldsymbol{v}$ and $\underline{\tau}$ at $\boldsymbol{x} \in F$ are given by

$$[\![q]\!] = q^+\boldsymbol{n}_{\kappa^+} + q^-\boldsymbol{n}_{\kappa^-}, \qquad [\![\boldsymbol{v}]\!] = \boldsymbol{v}^+ \cdot \boldsymbol{n}_{\kappa^+} + \boldsymbol{v}^- \cdot \boldsymbol{n}_{\kappa^-},$$
$$[\![\underline{\boldsymbol{v}}]\!] = \boldsymbol{v}^+ \otimes \boldsymbol{n}_{\kappa^+} + \boldsymbol{v}^- \otimes \boldsymbol{n}_{\kappa^-}, \qquad [\![\underline{\tau}]\!] = \underline{\tau}^+\boldsymbol{n}_{\kappa^+} + \underline{\tau}^-\boldsymbol{n}_{\kappa^-},$$

where $\boldsymbol{n}_{\kappa^\pm}$ denotes the unit outward normal vector on F to $\kappa^\pm$, respectively; cf. Figure 2.2. On a boundary face $F \in \mathcal{F}_h^{\mathcal{B}}$, we set $\{\!\{q\}\!\} = q$, $\{\!\{\boldsymbol{v}\}\!\} = \boldsymbol{v}$, $\{\!\{\underline{\tau}\}\!\} = \underline{\tau}$, $[\![q]\!] = q\boldsymbol{n}$, $[\![\boldsymbol{v}]\!] = \boldsymbol{v} \cdot \boldsymbol{n}$, $[\![\underline{\boldsymbol{v}}]\!] = \boldsymbol{v} \otimes \boldsymbol{n}$ and $[\![\underline{\tau}]\!] = \underline{\tau}\boldsymbol{n}$, with $\boldsymbol{n}$ denoting the unit outward normal vector on the boundary Γ.

With this notation, we note the following elementary identities for any scalar-,

vector- and matrix-valued functions q, $\boldsymbol{v}$, and $\underline{\tau}$, respectively:

$$\sum_{\kappa\in\mathcal{T}_h}\int_{\partial\kappa} q\boldsymbol{v}\cdot\boldsymbol{n}_\kappa\,\mathrm{d}s = \sum_{F\in\mathcal{F}_h}\int_F [\![q]\!]\cdot\{\!\{\boldsymbol{v}\}\!\}\,\mathrm{d}s + \sum_{F\in\mathcal{F}_h^{\mathcal{I}}}\int_F \{\!\{q\}\!\}[\![\boldsymbol{v}]\!]\,\mathrm{d}s, \tag{2.3}$$

$$\sum_{\kappa\in\mathcal{T}_h}\int_{\partial\kappa} \underline{\tau} : (\boldsymbol{v}\otimes\boldsymbol{n}_\kappa)\,\mathrm{d}s = \sum_{F\in\mathcal{F}_h}\int_F \underline{[\![\boldsymbol{v}]\!]} : \{\!\{\underline{\tau}\}\!\}\,\mathrm{d}s + \sum_{F\in\mathcal{F}_h^{\mathcal{I}}}\int_F \{\!\{\boldsymbol{v}\}\!\}\cdot[\![\underline{\tau}]\!]\,\mathrm{d}s. \tag{2.4}$$

Here, $\boldsymbol{n}_\kappa$ denotes the unit outward normal vector to the element $\kappa\in\mathcal{T}_h$. Finally, we note the following inequalities, which follows from the *inverse trace inequalities* [158, Theorem 4.76] and (2.1)–(2.2).

Lemma 2.1. *For any scalar-, vector- or matrix-valued functions q, $\boldsymbol{v}$, and $\underline{\tau}$, respectively, where $q|_\kappa\circ T_\kappa\in\mathcal{S}_{k_\kappa}(\widehat{\kappa})$, $\boldsymbol{v}|_\kappa\circ T_\kappa\in[\mathcal{S}_{k_\kappa}(\widehat{\kappa})]^d$ and $\underline{\tau}|_\kappa\circ T_\kappa\in[\mathcal{S}_{k_\kappa}(\widehat{\kappa})]^{d\times d}$ for all $\kappa\in\mathcal{T}_h$, there exists a positive constant C_T, independent of $\boldsymbol{h}$ and $\boldsymbol{k}$, but dependent on the constants ρ_1 and ρ_2 from (2.1) and (2.2), respectively, such that*

$$\sum_{F\in\mathcal{F}_h}\int_F h_F k_F^{-2}|\{\!\{q\}\!\}|^2\,\mathrm{d}s \le C_T\,\|q\|^2_{L^2(\Omega)}\,,$$

$$\sum_{F\in\mathcal{F}_h}\int_F h_F k_F^{-2}|\{\!\{\boldsymbol{v}\}\!\}|^2\,\mathrm{d}s \le C_T\,\|\boldsymbol{v}\|^2_{L^2(\Omega)}\,,$$

$$\sum_{F\in\mathcal{F}_h}\int_F h_F k_F^{-2}|\{\!\{\underline{\tau}\}\!\}|^2\,\mathrm{d}s \le C_T\,\|\underline{\tau}\|^2_{L^2(\Omega)}\,.$$

2.2 DGFEM for Poisson's Equation

In this section we briefly outline the IP DGFEM for Poisson's equation:

$$-\triangle u = f \qquad \text{in } \Omega, \tag{2.5}$$

$$u = 0 \qquad \text{on } \partial\Omega. \tag{2.6}$$

where $\Omega\subset\mathbb{R}^2$ is a bounded polygonal Lipschitz domain with boundary Γ and $f\in L^2(\Omega)$. For simplicity, we assume the mesh is conforming, i.e., no hanging nodes are present.

2.2.1 Derivation of the DGFEM

We briefly outline below the derivation of the IP DGFEM, cf. Arnold *et al.* [8, 9]. The first step is to rewrite Poisson's equation as a system of first order equations

$$\begin{aligned} \boldsymbol{\chi} = \nabla u, \qquad & -\nabla \cdot \boldsymbol{\chi} = f && \text{in } \Omega, \\ & u = 0 && \text{on } \Gamma. \end{aligned}$$

Multiplication by the test functions $\boldsymbol{\tau}$ and v, respectively, and integrating over an element $\kappa \in \mathcal{T}_h$ generates the *weak formulation*:

$$\begin{aligned} \int_\kappa \boldsymbol{\chi} \cdot \boldsymbol{\tau} \, \mathrm{d}\boldsymbol{x} &= -\int_\kappa u \nabla \cdot \boldsymbol{\tau} \, \mathrm{d}\boldsymbol{x} + \int_{\partial\kappa} u \boldsymbol{n}_\kappa \cdot \boldsymbol{\tau} \, \mathrm{d}s, \\ \int_\kappa \boldsymbol{\chi} \cdot \nabla v \, \mathrm{d}\boldsymbol{x} &= \int_\kappa f v \, \mathrm{d}\boldsymbol{x} + \int_{\partial\kappa} \boldsymbol{\chi} \cdot \boldsymbol{n}_\kappa \, \mathrm{d}s. \end{aligned}$$

By defining the spaces

$$\begin{aligned} V(\mathcal{T}_h, \boldsymbol{k}) &= \left\{ v \in L^2(\Omega) : v|_\kappa \circ T_\kappa \in \mathcal{S}_{k_\kappa}(\widehat{\kappa}), \kappa \in \mathcal{T}_h \right\}, \\ \boldsymbol{\Sigma}(\mathcal{T}_h, \boldsymbol{k}) &= \left\{ \boldsymbol{\tau} \in L^2(\Omega) : \boldsymbol{\tau}|_\kappa \circ T_\kappa \in [\mathcal{S}_{k_\kappa}(\widehat{\kappa})]^d, \kappa \in \mathcal{T}_h \right\}, \end{aligned}$$

the *flux formulation* may be derived: find $u_{h,k} \in V(\mathcal{T}_h, \boldsymbol{k})$ and $\boldsymbol{\chi}_{h,k} \in \boldsymbol{\Sigma}(\mathcal{T}_k, \boldsymbol{k})$ such that for all $\kappa \in \mathcal{T}_h$

$$\begin{aligned} \int_\kappa \boldsymbol{\chi}_{h,k} \cdot \boldsymbol{\tau}_{h,k} \, \mathrm{d}\boldsymbol{x} &= -\int_\kappa u_{h,k} \nabla \cdot \boldsymbol{\tau}_{h,k} \, \mathrm{d}\boldsymbol{x} + \int_{\partial\kappa} \widehat{u}_\kappa \boldsymbol{n}_\kappa \cdot \boldsymbol{\tau}_{h,k} \, \mathrm{d}s, && \forall \boldsymbol{\tau}_{h,k} \circ T_\kappa \in [\mathcal{S}_{k_\kappa}(\widehat{\kappa})]^d, \\ \int_\kappa \boldsymbol{\chi}_{h,k} \cdot \nabla v_{h,k} \, \mathrm{d}\boldsymbol{x} &= \int_\kappa f v_{h,k} \, \mathrm{d}\boldsymbol{x} + \int_{\partial\kappa} \widehat{\boldsymbol{\chi}}_\kappa \cdot \boldsymbol{n}_\kappa \, \mathrm{d}s, && \forall v_{h,k} \circ T_\kappa \in \mathcal{S}_{k_\kappa}(\widehat{\kappa}), \end{aligned}$$

where $\widehat{\boldsymbol{\chi}}_\kappa$ and $\widehat{u}_\kappa$ are the numerical fluxes, which approximate $\boldsymbol{\chi} = \nabla u$ and u, respectively, on the boundary of the element κ. It is necessary to express the numerical fluxes in terms of $\boldsymbol{\chi}_{h,k}$ and $u_{h,k}$. Summation over all elements gives

$$\int_\Omega \boldsymbol{\chi}_{h,k} \cdot \boldsymbol{\tau}_{h,k} \, \mathrm{d}\boldsymbol{x} = -\int_\Omega u_{h,k} \nabla_h \cdot \boldsymbol{\tau}_{h,k} \, \mathrm{d}\boldsymbol{x} + \sum_{\kappa \in \mathcal{T}_h} \int_{\partial\kappa} \widehat{u}_\kappa \boldsymbol{n}_\kappa \cdot \boldsymbol{\tau}_{h,k} \, \mathrm{d}s,$$

$$\int_\Omega \boldsymbol{\chi}_{h,k} \cdot \nabla_h v_{h,k} \,\mathrm{d}\boldsymbol{x} = \int_\Omega f v_{h,k} \,\mathrm{d}\boldsymbol{x} + \sum_{\kappa \in \mathcal{T}_h} \int_{\partial\kappa} \widehat{\boldsymbol{\chi}}_\kappa \cdot \boldsymbol{n}_\kappa \,\mathrm{d}s,$$

for all $\boldsymbol{\tau}_{h,k} \in \boldsymbol{\Sigma}(\mathcal{T}_h, \boldsymbol{k})$ and $v_{h,k} \in V(\mathcal{T}_h, \boldsymbol{k})$, where ∇_h is the elementwise gradient operator. Applying (2.3) gives

$$\begin{aligned}\int_\Omega \boldsymbol{\chi}_{h,k} \cdot \boldsymbol{\tau}_{h,k} \,\mathrm{d}\boldsymbol{x} = &- \int_\Omega u_{h,k} \nabla_h \cdot \boldsymbol{\tau}_{h,k} \,\mathrm{d}\boldsymbol{x} \\ &+ \sum_{F \in \mathcal{F}_h} \int_F [\![\widehat{u}]\!] \cdot \{\!\{\boldsymbol{\tau}_{h,k}\}\!\} \,\mathrm{d}s + \sum_{F \in \mathcal{F}_h^{\mathcal{I}}} \int_F \{\!\{\widehat{u}\}\!\} [\![\boldsymbol{\tau}_{h,k}]\!] \,\mathrm{d}s, \qquad (2.7)\end{aligned}$$

$$\int_\Omega \boldsymbol{\chi}_{h,k} \cdot \nabla_h v_{h,k} \,\mathrm{d}\boldsymbol{x} + \sum_{F \in \mathcal{F}_h} \int_F \{\!\{\widehat{\boldsymbol{\chi}}\}\!\} \cdot [\![v_{h,k}]\!] \,\mathrm{d}s - \sum_{F \in \mathcal{F}_h^{\mathcal{I}}} \{\!\{v_{h,k}\}\!\} [\![\widehat{\boldsymbol{\chi}}]\!] = \int_\Omega f v_{h,k} \,\mathrm{d}\boldsymbol{x}, \qquad (2.8)$$

for all $\boldsymbol{\tau}_{h,k} \in \boldsymbol{\Sigma}(\mathcal{T}_h, \boldsymbol{k})$ and $v_{h,k} \in V(\mathcal{T}_h, \boldsymbol{k})$. We note that by integration by parts, summation over all $\kappa \in \mathcal{T}_h$ and (2.3) that the following identity is derived

$$\begin{aligned}-\int_\Omega u_{h,k} \nabla_h \cdot \boldsymbol{\tau}_{h,k} \,\mathrm{d}\boldsymbol{x} = &\int_\Omega \boldsymbol{\tau}_{h,k} \cdot \nabla_h u_{h,k} \,\mathrm{d}\boldsymbol{x} \\ &- \sum_{F \in \mathcal{F}_h} \int_F [\![u_{h,k}]\!] \cdot \{\!\{\boldsymbol{\tau}_{h,k}\}\!\} \,\mathrm{d}s - \sum_{F \in \mathcal{F}_h^{\mathcal{I}}} \int_F \{\!\{u_{h,k}\}\!\} [\![\boldsymbol{\tau}_{h,k}]\!] \,\mathrm{d}s.\end{aligned}$$

By substituting this into (2.7) gives

$$\begin{aligned}\int_\Omega \boldsymbol{\chi}_{h,k} \cdot \boldsymbol{\tau}_{h,k} \,\mathrm{d}\boldsymbol{x} = &\int_\Omega \boldsymbol{\tau}_{h,k} \cdot \nabla_h u_{h,k} \,\mathrm{d}\boldsymbol{x} \\ &+ \sum_{F \in \mathcal{F}_h} \int_F [\![\widehat{u} - u_{h,k}]\!] \cdot \{\!\{\boldsymbol{\tau}_{h,k}\}\!\} \,\mathrm{d}s + \sum_{F \in \mathcal{F}_h^{\mathcal{I}}} \int_F \{\!\{\widehat{u} - u_{h,k}\}\!\} [\![\boldsymbol{\tau}_{h,k}]\!] \,\mathrm{d}s\end{aligned}$$

for all $\boldsymbol{\tau}_{h,k} \in \boldsymbol{\Sigma}(\mathcal{T}_h, \boldsymbol{k})$. Finally, setting $\boldsymbol{\tau}_{h,k} = \nabla_h v_{h,k}$ and substituting into (2.8) gives the *primal formulation*

$$\begin{aligned}\int_\Omega \nabla_h u_{h,k} \cdot \nabla_h v_{h,k} \,\mathrm{d}\boldsymbol{x} + &\sum_{F \in \mathcal{F}_h} \int_F \left([\![\widehat{u} - u_{h,k}]\!] \cdot \{\!\{\nabla_h v_{h,k}\}\!\} - \{\!\{\widehat{\boldsymbol{\chi}}\}\!\} \cdot [\![v_{h,k}]\!] \right) \mathrm{d}s \\ &+ \sum_{F \in \mathcal{F}_h} \int_F \left(\{\!\{\widehat{u} - u_{h,k}\}\!\} [\![\nabla_h v_{h,k}]\!] - [\![\widehat{\boldsymbol{\chi}}]\!] \{\!\{v_{h,k}\}\!\} \right) \mathrm{d}s = \int_\Omega f v_{h,k} \,\mathrm{d}\boldsymbol{x}.\end{aligned}$$

For a generic IP scheme, which covers IIP, SIP and NIP, we select

$$\widehat{u} = \begin{cases} \{\!\{u_{h,k}\}\!\} + \frac{1}{2}(1+\theta)[\![u_{h,k}]\!] \cdot \boldsymbol{n}_\kappa, & \text{on } F \in \mathcal{F}_h^{\mathcal{I}}, \\ (1+\theta)u_{h,k}, & \text{on } F \in \mathcal{F}_h^{\mathcal{B}}, \end{cases}$$

and

$$\widehat{\boldsymbol{\chi}} = \begin{cases} \{\!\{\nabla_h u_{h,k}\}\!\} - \sigma_{h,k}[\![u_{h,k}]\!], & \text{on } F \in \mathcal{F}_h^{\mathcal{I}}, \\ \nabla_h u_{h,k} - \sigma_{h,k} u_{h,k}\boldsymbol{n}, & \text{on } F \in \mathcal{F}_h^{\mathcal{B}}, \end{cases}$$

where $\theta \in [-1, 1]$ and $\sigma_{h,k} := \gamma k_F^2 h_F^{-1}$, with a positive constant γ, is the *interior penalty parameter*. Elementary manipulations results in the IP formulation: find $u_{h,k} \in V(\mathcal{T}_h, \boldsymbol{k})$ such that

$$A_{h,k}(u_{h,k}, v_{h,k}) = \int_\Omega f v_{h,k} \,\mathrm{d}\boldsymbol{x}, \tag{2.9}$$

for all $v_{h,k} \in V(\mathcal{T}_h, \boldsymbol{k})$, where

$$A_{h,k}(u, v) = \sum_{\kappa \in \mathcal{T}_h} \int_\kappa \nabla u \cdot \nabla v \,\mathrm{d}\boldsymbol{x} - \sum_{F \in \mathcal{F}_h} \int_F \{\!\{\nabla_h u\}\!\} \cdot [\![v]\!] \,\mathrm{d}s + \theta \sum_{F \in \mathcal{F}_h} \int_F \{\!\{\nabla_h v\}\!\} \cdot [\![u]\!] \,\mathrm{d}s + \sum_{F \in \mathcal{F}_h} \int_F \sigma_{h,k} [\![u]\!] \cdot [\![v]\!] \,\mathrm{d}s.$$

Remark 2.1. We note that the formulation corresponds to the symmetric interior penalty (SIP) method when $\theta = -1$, the nonsymmetric interior penalty (NIP) method when $\theta = 1$ and the incomplete interior penalty method (IIP) when $\theta = 0$.

By defining the *energy norm*,

$$\|v\|_{h,k}^2 = \|\nabla_h v\|_{L^2(\Omega)}^2 + \sum_{F \in \mathcal{F}_h} \int_F \sigma_{h,k} |[\![v]\!]|^2 \,\mathrm{d}s,$$

for v on the finite element space $V(\mathcal{T}_h, \boldsymbol{k})$ we can show that $A_{h,k}(\cdot, \cdot)$ and the right-hand side of (2.9) satisfy the conditions of the Lax-Milgram theorem providing $\gamma > \gamma_{\min}$, where $\gamma_{\min}$ is a positive constant; cf. Stamm & Wihler [161], Wihler *et al.* [175]. Therefore, there exists a unique solution $u_{h,k} \in V(\mathcal{T}_h, \boldsymbol{k})$ to (2.9).

2.2.2 *A Priori* Error Analysis

In this section, we state the *a priori* error bound for the standard IP DGFEM approximation (2.9) of the problem (2.5)–(2.6).

Theorem 2.2. *Assuming that the analytical solution u of (2.5)–(2.6) satisfies the conditions that $u \in H_0^1(\Omega)$ and $u|_\kappa \in H^{s_\kappa}(\kappa)$, $s_\kappa \geq 2$, for $\kappa \in \mathcal{T}_h$. Then, the solution $u_{h,k} \in V(\mathcal{T}_h, \boldsymbol{k})$ of (2.9) satisfies the error bound*

$$\|u - u_{h,k}\|_{h,k}^2 \leq C \sum_{\kappa \in \mathcal{T}_h} \frac{h_\kappa^{2r_\kappa - 2}}{k_\kappa^{2s_\kappa - 2}} \|u\|_{H^{s_\kappa}(\kappa)}^2 ,$$

with $1 \leq r_\kappa \leq \min(k_\kappa + 1, s_\kappa)$, $k_\kappa \geq 1$, for $\kappa \in \mathcal{T}_h$ and C is a positive constant independent of u, $\boldsymbol{h}$ and $\boldsymbol{k}$, but depends on the constants ρ_1 and ρ_2 from (2.1) and (2.2), respectively.

Proof. See Stamm & Wihler [161]. □

Remark 2.2. As noted by Stamm & Wihler [161] this theorem has optimal k convergence due to the homogeneous boundary conditions. However, for inhomogeneous boundary conditions only a suboptimal k convergence of $\mathcal{O}(1/k_\kappa^{2s_\kappa - 3})$ can be shown to be sharp, cf. Georgoulis *et al.* [94].

As can be seen, as the value of the norm of u is fixed, the bound converges towards zero as $h \to 0$ or $k \to \infty$, i.e. as the mesh and polynomial degree are refined. As the bound converges to zero it indicates that the error in the numerical solution must also converge to zero.

2.2.3 *A Posteriori* Error Analysis

In this section, we state the energy norm *a posteriori* error bound for the standard IP DGFEM approximation (2.9) of the problem (2.5)–(2.6).

Theorem 2.3. *Let Π_{κ,k_κ} be the local L^2-projector onto the space $\mathcal{S}_{k_\kappa - 1}(\kappa)$, $u \in H_0^1(\Omega)$ be the analytical solution to the problem (2.5)–(2.6) and $u_{h,k} \in V(\mathcal{T}_h, \boldsymbol{k})$ be its DGFEM approxima-*

tion obtained from (2.9)*; then, the following hp-version* a posteriori *error bound holds:*

$$\|u - u_{h,k}\|_{\mathrm{DG}} \leq C \left(\sum_{\kappa \in \mathcal{T}_h} \eta_\kappa^2 + h_\kappa^2 k_\kappa^{-1} \|f - \Pi_{\kappa,k_\kappa} f\|_{L^2(\kappa)}^2 \right)^{1/2},$$

where the local error indicators η_κ, $\kappa \in \mathcal{T}_h$, *are defined by*

$$\eta_\kappa^2 = h_\kappa^2 k_\kappa^{-2} \|\Pi_{\kappa,k_\kappa} f + \triangle u_{h,k}\|_{L^2(\kappa)}^2 + h_\kappa k_\kappa^{-1} \|[\![\nabla_h u_{h,k}]\!]\|_{L^2(\partial\kappa\setminus\Gamma)}^2 + \gamma h_\kappa^{-1} k_\kappa^2 \left\| \underline{[\![u_{h,k}]\!]} \right\|_{L^2(\partial\kappa)}^2.$$

Here, the constant $C > 0$ is independent of $\boldsymbol{h}$, the polynomial degree vector $\boldsymbol{k}$ and the parameter γ and only depends on the shape-regularity of the mesh and the constants ρ_1 and ρ_2 from (2.1) *and* (2.2)*, respectively.*

Proof. See Houston *et al.* [124] for the proof for the SIP formulation (when $\theta = -1$). Proof for the general formulation follows analogously. □

We note that the *a posteriori* estimate provides a bound for the error in terms of computable quantities. We can also see that the error bound is split into *local error indicators* for each element in the mesh. These can be used by an automatic mesh refinement strategy to estimate the elements that contribute the most to the error.

This completes are summary of the DGFEM for Poisson's equation. In the next chapter we start the analysis of the two-grid method for the DGFEM of a quasilinear elliptic problem.

CHAPTER 3

Two-Grid hp-Version Discontinuous Galerkin Finite Element Methods for Second-Order Quasilinear Elliptic PDEs

In this chapter we study the *a priori* and *a posteriori* error analysis, with respect to a mesh-dependent energy norm, of the hp-version of the so-called two-grid interior penalty (IP) DGFEM for the second order quasilinear elliptic PDE:

$$-\nabla \cdot (\mu(\boldsymbol{x}, |\nabla u|)\nabla u) = f(\boldsymbol{x}) \qquad \text{in } \Omega, \tag{3.1}$$

$$u = 0 \qquad \text{on } \Gamma, \tag{3.2}$$

where $\Omega \subset \mathbb{R}^d$, $d = 2, 3$, is a bounded polygonal Lipschitz domain with boundary Γ and $f \in L^2(\Omega)$. The work in this chapter forms the basis of the two published articles [64, 66].

Assumption A. Here, we assume that for the nonlinearity $\mu \in C^0(\bar{\Omega} \times [0, \infty))$ there exists positive constants m_μ and M_μ such that the following monotonicity property is satisfied:

$$m_\mu(t - s) \leq \mu(\boldsymbol{x}, t)t - \mu(\boldsymbol{x}, s)s \leq M_\mu(t - s), \qquad \text{for all } t \geq s \geq 0, \quad \boldsymbol{x} \in \bar{\Omega}. \tag{3.3}$$

From Liu & Barrett [136, Lemma 2.1] we note that, as μ satisfies (3.3), there exists

constants C_1 and C_2, $C_1 \geq C_2 > 0$, such that for all vectors $\boldsymbol{v}, \boldsymbol{w} \in \mathbb{R}^d$ and all $\boldsymbol{x} \in \bar{\Omega}$,

$$|\mu(\boldsymbol{x}, |\boldsymbol{v}|)\boldsymbol{v} - \mu(\boldsymbol{x}, |\boldsymbol{w}|)\boldsymbol{w}| \leq C_1|\boldsymbol{v} - \boldsymbol{w}|, \tag{3.4}$$

$$C_2|\boldsymbol{v} - \boldsymbol{w}|^2 \leq (\mu(\boldsymbol{x}, |\boldsymbol{v}|)\boldsymbol{v} - \mu(\boldsymbol{x}, |\boldsymbol{w}|)\boldsymbol{w}) \cdot (\boldsymbol{v} - \boldsymbol{w}). \tag{3.5}$$

By setting $s = 0$ in (3.3) we deduce the following bound on μ:

$$m_\mu \leq \mu(\boldsymbol{x}, t) \leq M_\mu, \qquad t \geq 0, \qquad \boldsymbol{x} \in \bar{\Omega}. \tag{3.6}$$

For ease of notation we shall suppress the dependence of μ on $\boldsymbol{x}$ and write $\mu(t)$ instead of $\mu(\boldsymbol{x}, t)$. We note that many of the nonlinearities that arise in continuum mechanics, such as the Carreau law $\mu(t) = k_\infty + (k_0 - k_\infty)(1 + \lambda t^2)^{(\vartheta-2)/2}$ with $k_0 > k_\infty > 0$ and $\vartheta \in (1, 2]$, meet the above assumptions.

In this chapter we consider a two-grid IP DGFEM approximation to (3.1)–(3.2), based on solving the nonlinear problem on a coarse mesh and then using this solution to linearise the problem, passing this coarse solution as the argument to the nonlinear coefficient μ, on a finer mesh. In Chapter 5 we consider a different approximation, whereby we employ a single step of a Newton solver on the fine mesh, cf. Axelsson & Layton [10], Xu [180, Section 5.2], using the coarse grid solution as the initial guess. Before considering these approximations we state for comparison the *standard* IP DGFEM approximation to (3.1)–(3.2) in Section 3.1. In this chapter we only study the theoretical error bounds for the method; numerical experiments are presented in Chapter 4.

Using the notation from Section 2.1.2, we consider two partitions $\mathcal{T}_h$ and $\mathcal{T}_H$ of the computational domain Ω, of granularity h and H, respectively. Here, we refer to $\mathcal{T}_h$ and $\mathcal{T}_H$ as the fine and coarse mesh partitions of Ω, respectively. Moreover, to each mesh $\mathcal{T}_h$ and $\mathcal{T}_H$, we associate corresponding polynomial degree distributions $\boldsymbol{k} = \{k_\kappa : \kappa \in \mathcal{T}_h\}$ and $\boldsymbol{K} = \{K_\kappa : \kappa \in \mathcal{T}_H\}$, respectively.

Assumption B. In particular, we assume that $\mathcal{T}_h$ and $\mathcal{T}_H$ are nested in the sense that, for any $\kappa_h \in \mathcal{T}_h$ there exists an element $\kappa_H \in \mathcal{T}_H$ such that $\bar{\kappa}_h \subseteq \bar{\kappa}_H$. We also enforce the

polynomial degree distributions to satisfy the condition that $k_{\kappa_h} \geq K_{\kappa_H}$ for $\kappa_h \in \mathcal{T}_h$ and the associated $\kappa_H \in \mathcal{T}_H$, such that $\bar{\kappa}_h \subseteq \bar{\kappa}_H$.

Given $\mathcal{T}_h$, $\boldsymbol{k}$, $\mathcal{T}_H$ and $\boldsymbol{K}$ we construct the fine hp-finite element space

$$V(\mathcal{T}_h, \boldsymbol{k}) = \left\{ v \in L^2(\Omega) : v|_\kappa \circ T_\kappa \in \mathcal{S}_{k_\kappa}(\widehat{\kappa}), \kappa \in \mathcal{T}_h \right\}; \tag{3.7}$$

the coarse hp-finite element space $V(\mathcal{T}_H, \boldsymbol{K})$ is defined analogously, and satisfies the condition $V(\mathcal{T}_H, \boldsymbol{K}) \subseteq V(\mathcal{T}_h, \boldsymbol{k})$.

3.1 Standard hp-Version IP DGFEM

In this section we first consider a *standard* IP DGFEM for the numerical approximation of the problem (3.1)–(3.2), cf. Gudi *et al.* [101], Houston *et al.* [122, 125]. To this end, on the (fine) mesh $\mathcal{T}_h$ partition of Ω, together with the corresponding polynomial degree vector $\boldsymbol{k}$, the standard IP DGFEM is defined as follows: find $u_{h,k} \in V(\mathcal{T}_h, \boldsymbol{k})$ such that

$$A_{h,k}(u_{h,k}; u_{h,k}, v_{h,k}) = F_{h,k}(v_{h,k}) \tag{3.8}$$

for all $v_{h,k} \in V(\mathcal{T}_h, \boldsymbol{k})$, where

$$\begin{aligned} A_{h,k}(\psi; u, v) = &\sum_{\kappa \in \mathcal{T}_h} \int_\kappa \mu(|\nabla \psi|) \nabla u \cdot \nabla v \, \mathrm{d}\boldsymbol{x} - \sum_{F \in \mathcal{F}_h} \int_F \{\!\{ \mu(|\nabla_h \psi|) \nabla_h u \}\!\} \cdot [\![v]\!] \, \mathrm{d}s \\ &+ \theta \sum_{F \in \mathcal{F}_h} \int_F \{\!\{ \mu(h_F^{-1} |[\![\psi]\!]|) \nabla_h v \}\!\} \cdot [\![u]\!] \, \mathrm{d}s + \sum_{F \in \mathcal{F}_h} \int_F \sigma_{h,k} [\![u]\!] \cdot [\![v]\!] \, \mathrm{d}s, \\ F_{h,k}(v) = &\sum_{\kappa \in \mathcal{T}_h} \int_\kappa f v \, \mathrm{d}\boldsymbol{x}, \end{aligned}$$

and ∇_h is used to denote the broken gradient operator, defined elementwise. Here,

$$\sigma_{h,k} := \gamma \frac{k_F^2}{h_F}$$

is the *interior penalty parameter*, where $\gamma > 0$ is a constant, and $\theta \in [-1, 1]$. We note that, due to the condition on the nonlinearity (3.3), the interior penalty stabilisation may

be selected independent of $\mu(\cdot)$, provided the penalty parameter is chosen sufficiently large (independent of local element sizes and polynomial degrees) such that it is greater than a constant $\gamma_{\min}$, dependent on m_μ and M_μ, cf. Lemma 3.1 and Remark 3.3 below; see, also, Gudi *et al.* [101], Houston *et al.* [122], for example.

Remark 3.1. We note that the formulation (3.8) corresponds to the symmetric interior penalty (SIP) method when $\theta = -1$, the nonsymmetric interior penalty (NIP) method when $\theta = 1$ and the incomplete interior penalty method (IIP) when $\theta = 0$.

Existence and uniqueness of the solution $u_{h,k}$ for this formulation is proven in Houston *et al.* [122]; cf. Gudi *et al.* [101].

Remark 3.2. In the case of an inhomogeneous boundary condition $u = g$ on Γ, the right-hand side linear functional $F_{h,k}(\cdot)$ must be replaced by

$$F_{h,k}(v) = \sum_{\kappa\in\mathcal{T}_h}\int_\kappa fv\,\mathrm{d}\boldsymbol{x} + \sum_{F\in\mathcal{F}_h^{\mathcal{B}}}\int_F \sigma_{h,k}gv\,\mathrm{d}s$$

and the third term in the semilinear form $A_{h,k}$ is replaced by

$$\theta\sum_{F\in\mathcal{F}_h^{\mathcal{I}}}\int_F \{\!\{\mu(h_F^{-1}|[\![\psi]\!]|)\nabla_h v\}\!\}\cdot[\![u]\!]\,\mathrm{d}s + \theta\sum_{F\in\mathcal{F}_h^{\mathcal{B}}}\int_F \mu(h_F^{-1}|\psi-g|)\nabla_h v\cdot\boldsymbol{n}(u-g)\,\mathrm{d}s;$$

cf. Houston *et al.* [122]

Introducing the *energy norm*

$$\|v\|_{h,k}^2 = \|\nabla_h v\|_{L^2(\Omega)}^2 + \sum_{F\in\mathcal{F}_h}\int_F \sigma_{h,k}|[\![v]\!]|^2\,\mathrm{d}s, \tag{3.9}$$

on the class of spaces $H^1(\Omega) + V(\mathcal{T}_h,\boldsymbol{k})$, the semilinear form $A_{h,k}(\psi;\cdot,\cdot)$ is coercive, in the sense that the following lemma holds for sufficiently large γ.

Lemma 3.1. *There exists a positive constant $\gamma_{\min}$, such that for any $\gamma \geq \gamma_{\min}$, there exists a coercivity constant $C_C = C_C(m_\mu, M_\mu, C_T, \rho_1, \rho_2) > 0$, independent of $\boldsymbol{h}$ and $\boldsymbol{k}$, such that for all $\psi, v \in V(\mathcal{T}_h,\boldsymbol{k})$.*

$$A_{h,k}(\psi; v, v) \geq C_C\,\|v\|_{h,k}^2\,.$$

Proof. By application of (3.6), Lemma 2.1 and the arithmetic-geometric mean inequality, $2ab \leq \varepsilon a^2 + \varepsilon^{-1}b^2$ with $\varepsilon = \delta\sigma_{h,k}^{-1}$ and $\delta > 1$, we have, noting $\theta^2 \leq 1$, that

$$\begin{aligned}
A_{h,k}(\psi; v, v) &= \sum_{\kappa\in\mathcal{T}_h}\int_\kappa \mu(|\nabla\psi|)|\nabla v|^2\,\mathrm{d}\boldsymbol{x} - \sum_{F\in\mathcal{F}_h}\int_F \{\!\{\mu(|\nabla_h\psi|)\nabla v\}\!\}\cdot[\![v]\!]\,\mathrm{d}s \\
&\quad + \theta\sum_{F\in\mathcal{F}_h}\int_F \{\!\{\mu(h_F^{-1}|[\![\psi]\!]|)\nabla_h v\}\!\}\cdot[\![v]\!]\,\mathrm{d}s + \sum_{F\in\mathcal{F}_h}\int_F \sigma_{h,k}|[\![v]\!]|^2\,\mathrm{d}s \\
&\geq \sum_{\kappa\in\mathcal{T}_h}\int_\kappa \mu(|\nabla\psi|)|\nabla v|^2\,\mathrm{d}\boldsymbol{x} + \sum_{F\in\mathcal{F}_h}\int_F \sigma_{h,k}|[\![v]\!]|^2\,\mathrm{d}s - \sum_{F\in\mathcal{F}_h}\int_F \varepsilon^{-1}|[\![v]\!]|^2\,\mathrm{d}s \\
&\quad - \sum_{F\in\mathcal{F}_h}\int_F \frac{\varepsilon}{2}\left(|\{\!\{\mu(|\nabla_h\psi|)\nabla_h v\}\!\}|^2 + \theta^2|\{\!\{\mu(h_F^{-1}|[\![\psi]\!]|)\nabla_h v\}\!\}|^2\right)\,\mathrm{d}s \\
&\geq m_\mu\sum_{\kappa\in\mathcal{T}_h}\|\nabla v\|^2_{L^2(\kappa)} + (1-\delta^{-1})\sum_{F\in\mathcal{F}_h}\int_F \sigma_{h,k}|[\![v]\!]|^2\,\mathrm{d}s \\
&\quad - M_\mu^2\delta\gamma^{-1}\sum_{F\in\mathcal{F}_h}\int_F k_\kappa^{-2}h_F|\{\!\{\nabla_h v\}\!\}|^2\,\mathrm{d}s \\
&\geq \min(m_\mu - C_T M_\mu^2\delta\gamma^{-1}, 1-\delta^{-1})\,\|v\|^2_{h,k}\,.
\end{aligned}$$

Thereby, the statement of the lemma immediately follows, provided $\gamma > C_T M_\mu^2\delta m_\mu^{-1}$, with δ sufficiently large. □

Remark 3.3. From the proof of Lemma 3.1, we observe that the requirement on the parameter γ appearing in the definition of $\sigma_{h,k}$ is that $\gamma > C_T M_\mu^2\delta m_\mu^{-1}$. Thereby, a reduction in the magnitude of the constant m_μ appearing in the lower bound (3.3) leads to a corresponding increase in the minimal value of γ needed to guarantee coercivity.

3.1.1 *A Priori* Error Bound

We recall the following *a priori* error bound for the standard IP DGFEM approximation (3.8) of the quasilinear problem (3.1)–(3.2).

Lemma 3.2. *Assuming that $u \in C^1(\Omega)$ and $u|_\kappa \in H^{s_\kappa}(\kappa)$, $s_\kappa \geq 2$, for $\kappa \in \mathcal{T}_h$ then the solution $u_{h,k} \in V(\mathcal{T}_h, \boldsymbol{k})$ of (3.8) satisfies the error bound*

$$\|u - u_{h,k}\|^2_{h,k} \leq C_3\sum_{\kappa\in\mathcal{T}_h}\frac{h_\kappa^{2r_\kappa-2}}{k_\kappa^{2s_\kappa-3}}\,\|u\|^2_{H^{s_\kappa}(\kappa)}\,,$$

with $1 \leq r_\kappa \leq \min(k_\kappa + 1, s_\kappa)$, $k_\kappa \geq 1$, *for* $\kappa \in \mathcal{T}_h$ *and* C_3 *is a positive constant independent of* u, $\boldsymbol{h}$ *and* $\boldsymbol{k}$, *but depends on the constants* ρ_1 *and* ρ_2 *from* (2.1) *and* (2.2), *respectively, as well as the constants* m_μ, M_μ, C_1 *and* C_2 *from the monotonicity properties of* $\mu(\cdot)$.

Proof. See Houston *et al.* [122]. □

3.2 hp-Version Two-Grid DGFEM

In this section, we now introduce the hp-version of the two-grid algorithm [36, Algorithm 1] for the IP DGFEM discretisation of (3.1)–(3.2):

1. (Nonlinear solve) Compute the coarse grid approximation $u_{H,K} \in V(\mathcal{T}_H, \boldsymbol{K})$ such that

$$A_{H,K}(u_{H,K}; u_{H,K}, v_{H,K}) = F_{H,K}(v_{H,K}) \tag{3.10}$$

   for all $v_{H,K} \in V(\mathcal{T}_H, \boldsymbol{K})$.

2. (Linear solve) Determine the fine grid solution $u_{2G} \in V(\mathcal{T}_h, \boldsymbol{k})$ such that

$$A_{h,k}(u_{H,K}; u_{2G}, v_{h,k}) = F_{h,k}(v_{h,k}) \tag{3.11}$$

   for all $v_{h,k} \in V(\mathcal{T}_h, \boldsymbol{k})$.

Existence and uniqueness of the solution $u_{H,K}$ for this formulation follows from the existence and uniqueness of the formulation (3.8), cf. Gudi *et al.* [101], Houston *et al.* [122]. The formulation (3.11) is an interior penalty discretisation of a linear elliptic PDE, where the coefficient $\mu(|\nabla_h u_{H,K}|)$ is a known function; thereby, the existence and uniqueness of the solution u_{2G} follows immediately, cf., for example, Stamm & Wihler [161], Wihler *et al.* [175].

3.3 *A Priori* Error Bound

In this section, we develop the *a priori* error analysis of the two-grid IP DGFEM defined by (3.10)–(3.11). We note that the standard *a priori* error bound, Lemma 3.2, also clearly holds for the two-grid coarse solution $u_{H,K}$ defined in (3.10) with the energy norm

$\|\cdot\|_{h,k}$ replaced by $\|\cdot\|_{H,K}$ and similarly the mesh size and polynomial degrees h_κ and k_κ replaced by H_κ and K_κ, respectively. By employing this bound we can now deduce the following error bound for the two-grid approximation defined in (3.10)–(3.11).

Theorem 3.3. *Assuming $u \in C^1(\Omega)$, $u|_\kappa \in H^{s_\kappa}(\kappa)$, $s_\kappa \geq 2$, for $\kappa \in \mathcal{T}_h$ and $u|_\kappa \in H^{S_\kappa}(\kappa)$, $S_\kappa \geq 2$, for $\kappa \in \mathcal{T}_H$ then the solution $u_{2G} \in V(\mathcal{T}_h, \boldsymbol{k})$ of (3.11) satisfies the error bounds*

$$\|u_{h,k} - u_{2G}\|_{h,k}^2 \leq C_4 \sum_{\kappa \in \mathcal{T}_H} \frac{H_\kappa^{2R_\kappa - 2}}{K_\kappa^{2S_\kappa - 3}} \|u\|_{H^{S_\kappa}(\kappa)}^2 , \tag{3.12}$$

$$\|u - u_{2G}\|_{h,k}^2 \leq 2C_3 \sum_{\kappa \in \mathcal{T}_h} \frac{h_\kappa^{2r_\kappa - 2}}{k_\kappa^{2s_\kappa - 3}} \|u\|_{H^{s_\kappa}(\kappa)}^2 + 2C_4 \sum_{\kappa \in \mathcal{T}_H} \frac{H_\kappa^{2R_\kappa - 2}}{K_\kappa^{2S_\kappa - 3}} \|u\|_{H^{S_\kappa}(\kappa)}^2 , \tag{3.13}$$

with $1 \leq r_\kappa \leq \min(k_\kappa + 1, s_\kappa)$, $k_\kappa \geq 1$, for $\kappa \in \mathcal{T}_h$, $1 \leq R_\kappa \leq \min(K_\kappa + 1, S_\kappa)$, $K_\kappa \geq 1$, for $\kappa \in \mathcal{T}_H$ and C_3 and C_4 are positive constants independent of u, $\boldsymbol{h}$, $\boldsymbol{H}$, $\boldsymbol{k}$ and $\boldsymbol{K}$, but dependent on the constants ρ_1 and ρ_2 from (2.1) and (2.2), respectively, as well as the constants m_μ, M_μ, C_1 and C_2 from the monotonicity properties of $\mu(\cdot)$.

Proof. By application of the triangle inequality, we get

$$\|u - u_{2G}\|_{h,k}^2 \leq 2\|u - u_{h,k}\|_{h,k}^2 + 2\|u_{2G} - u_{h,k}\|_{h,k}^2 . \tag{3.14}$$

We note that the first term on the right-hand side of (3.14) may be bounded by employing Lemma 3.2. Let us now deal with the second term; to this end, from (3.8) and (3.11) we have that

$$A_{h,k}(u_{H,K}; u_{2G}, v_{h,k}) = A_{h,k}(u_{h,k}; u_{h,k}, v_{h,k})$$

for all $v_{h,k}$ in $V(\mathcal{T}_h, \boldsymbol{k})$. Let $\phi = u_{2G} - u_{h,k} \in V(\mathcal{T}_h, \boldsymbol{k})$; then from Lemma 3.1, we get

$$\begin{aligned} C_C \|u_{2G} - u_{h,k}\|_{h,k}^2 &\leq A_{h,k}(u_{H,K}; u_{2G} - u_{h,k}, \phi) \\ &= A_{h,k}(u_{H,K}; u_{2G}, \phi) - A_{h,k}(u_{H,K}; u_{h,k}, \phi) \\ &= A_{h,k}(u_{h,k}; u_{h,k}, \phi) - A_{h,k}(u_{H,K}; u_{h,k}, \phi) \\ &\equiv T_1 + T_2 + T_3, \end{aligned} \tag{3.15}$$

where we define

$$T_1 = \sum_{\kappa\in\mathcal{T}_h}\int_\kappa (\mu(|\nabla u_{h,k}|) - \mu(|\nabla u_{H,K}|))\nabla u_{h,k}\cdot\nabla\phi\,\mathrm{d}\boldsymbol{x},$$
$$T_2 = -\sum_{F\in\mathcal{F}_h}\int_F \{\!\{(\mu(|\nabla_h u_{h,k}|) - \mu(|\nabla_h u_{H,K}|))\nabla_h u_{h,k}\}\!\}\cdot[\![\phi]\!]\,\mathrm{d}s,$$
$$T_3 = \theta\sum_{F\in\mathcal{F}_h}\int_F \{\!\{(\mu(h_F^{-1}|[\![u_{h,k}]\!]|) - \mu(h_F^{-1}|[\![u_{H,K}]\!]|))\nabla_h\phi\}\!\}\cdot[\![u_{h,k}]\!]\,\mathrm{d}s.$$

To bound term T_1, we employ the triangle inequality, (3.4), (3.6) and Lemma 3.2; thereby, we deduce that

$$\begin{aligned}
|T_1| &\le \sum_{\kappa\in\mathcal{T}_h}\int_\kappa |\mu(|\nabla u_{h,k}|)\nabla u_{h,k} - \mu(|\nabla u_{H,K}|)\nabla u_{H,K}||\nabla\phi|\,\mathrm{d}\boldsymbol{x}\\
&\quad + \sum_{\kappa\in\mathcal{T}_h}\int_\kappa |\mu(|\nabla u_{H,K}|)\nabla\left(u_{H,K}-u_{h,k}\right)||\nabla\phi|\,\mathrm{d}\boldsymbol{x}\\
&\le (C_1+M_\mu)\sum_{\kappa\in\mathcal{T}_h}\int_\kappa |\nabla\left(u_{h,k}-u_{H,K}\right)||\nabla\phi|\,\mathrm{d}\boldsymbol{x}\\
&\le (C_1+M_\mu)\,\|\nabla_h\phi\|_{L^2(\Omega)}\\
&\quad\times\left\{\left(\sum_{\kappa\in\mathcal{T}_h}\|\nabla(u-u_{h,k})\|^2_{L^2(\kappa)}\right)^{1/2} + \left(\sum_{\kappa\in\mathcal{T}_H}\|\nabla(u-u_{H,K})\|^2_{L^2(\kappa)}\right)^{1/2}\right\}\\
&\le (C_1+M_\mu)\,C_3^{1/2}\,\|\phi\|_{h,k}\\
&\quad\times\left\{\left(\sum_{\kappa\in\mathcal{T}_h}\frac{h_\kappa^{2r_\kappa-2}}{k_\kappa^{2s_\kappa-3}}\,\|u\|^2_{H^{s_\kappa}(\kappa)}\right)^{1/2} + \left(\sum_{\kappa\in\mathcal{T}_H}\frac{H_\kappa^{2R_\kappa-2}}{K_\kappa^{2S_\kappa-3}}\,\|u\|^2_{H^{S_\kappa}(\kappa)}\right)^{1/2}\right\}.
\end{aligned}\tag{3.16}$$

Proceeding in an analogous manner for term T_2, we get that

$$\begin{aligned}
|T_2| &\le \sum_{F\in\mathcal{F}_h}\int_F \{\!\{|\mu(|\nabla_h u_{h,k}|)\nabla_h u_{h,k} - \mu(|\nabla_h u_{H,K}|)\nabla_h u_{H,K}|\}\!\}|[\![\phi]\!]|\,\mathrm{d}s\\
&\quad + \sum_{F\in\mathcal{F}_h}\int_F \{\!\{|\mu(|\nabla_h u_{H,K}|)\nabla_h\left(u_{H,K}-u_{h,k}\right)|\}\!\}|[\![\phi]\!]|\,\mathrm{d}s\\
&\le (C_1+M_\mu)\sum_{F\in\mathcal{F}_h}\int_F \{\!\{|\nabla_h\left(u_{h,k}-u_{H,K}\right)|\}\!\}\cdot|[\![\phi]\!]|\,\mathrm{d}s,
\end{aligned}$$

$$|T_2| \leq (C_1 + M_\mu) \left\{ \left(\sum_{F \in \mathcal{F}_h} \sigma_{h,k}^{-1} \|\{\!|\nabla_h(u - u_{h,k})|\!\}\|_{L^2(F)}^2 \right)^{1/2} + \left(\sum_{F \in \mathcal{F}_h} \sigma_{h,k}^{-1} \|\{\!|\nabla_h(u - u_{H,K})|\!\}\|_{L^2(F)}^2 \right)^{1/2} \right\} \left(\sum_{F \in \mathcal{F}_h} \int_F \sigma_{h,k} |[\![\phi]\!]|^2 \, \mathrm{d}s \right)^{1/2}.$$

Applying Lemma 2.1 and Lemma 3.2 gives

$$\begin{aligned} |T_2| &\leq (C_1 + M_\mu) \, C_T^{1/2} \gamma^{-1/2} \, \|\phi\|_{h,k} \\ &\quad \times \left\{ \left(\sum_{\kappa \in \mathcal{T}_h} \|\nabla(u - u_{h,k})\|_{L^2(\kappa)}^2 \right)^{1/2} + \left(\sum_{\kappa \in \mathcal{T}_h} \|\nabla(u - u_{H,K})\|_{L^2(\kappa)}^2 \right)^{1/2} \right\} \\ &\leq (C_1 + M_\mu) \, C_3^{1/2} C_T^{1/2} \gamma^{-1/2} \, \|\phi\|_{h,k} \\ &\quad \times \left\{ \left(\sum_{\kappa \in \mathcal{T}_h} \frac{h_\kappa^{2r_\kappa - 2}}{k_\kappa^{2s_\kappa - 3}} \|u\|_{H^{s_\kappa}(\kappa)}^2 \right)^{1/2} + \left(\sum_{\kappa \in \mathcal{T}_H} \frac{H_\kappa^{2R_\kappa - 2}}{K_\kappa^{2K_\kappa - 3}} \|u\|_{H^{S_\kappa}(\kappa)}^2 \right)^{1/2} \right\}. \end{aligned} \tag{3.17}$$

We now consider the term T_3:

$$\begin{aligned} |T_3| &\leq \sum_{F \in \mathcal{F}_h} \int_F \{\!|\left(\mu(h_F^{-1}|[\![u_{h,k}]\!]|) - \mu(h_F^{-1}|[\![u_{H,K}]\!]|)\right) \nabla_h \phi|\!\}|[\![u_{h,k}]\!]| \, \mathrm{d}s \\ &\leq \sum_{F \in \mathcal{F}_h} \left\| \mu(h_F^{-1}|[\![u_{h,k}]\!]|) - \mu(h_F^{-1}|[\![u_{H,K}]\!]|) \right\|_{L^\infty(F)} \|\{\!|\nabla_h \phi|\!\}\|_{L^2(F)} \, \|[\![u_{h,k}]\!]\|_{L^2(F)}. \end{aligned}$$

We note that from inequality (3.6), we have

$$\begin{aligned} &\left\| \mu(h_F^{-1}|[\![u_{h,k}]\!]|) - \mu(h_F^{-1}|[\![u_{H,K}]\!]|) \right\|_{L^\infty(F)} \\ &\qquad \leq \left\| \mu(h_k^{-1}|[\![u_{h,k}]\!]|) \right\|_{L^\infty(F)} + \left\| \mu(h_k^{-1}|[\![u_{H,K}]\!]|) \right\|_{L^\infty(F)} \leq 2M_\mu. \end{aligned}$$

Since $u \in H_0^1(\Omega)$, we note that $|[\![u - u_{h,k}]\!]| = |[\![u_{h,k}]\!]|$; thereby,

$$|T_3| \leq 2M_\mu \left(\sum_{F \in \mathcal{F}_h} \sigma_{h,k}^{-1} \|\{\!|\nabla_h \phi|\!\}\|_{L^2(F)}^2 \right)^{1/2} \left(\sum_{F \in \mathcal{F}_h} \int_F \sigma_{h,k} |[\![u - u_{h,k}]\!]|^2 \, \mathrm{d}s \right)^{1/2}.$$

Applying Lemma 2.1 and Lemma 3.2 completes the bound for this term:

$$|T_3| \leq 2M_\mu C_T^{1/2}\gamma^{-1/2}\left(\sum_{\kappa\in\mathcal{T}_h}\|\nabla\phi\|^2_{L^2(\kappa)}\right)^{1/2}\|u-u_{h,k}\|_{h,k}$$
$$\leq 2M_\mu C_3^{1/2}C_T^{1/2}\gamma^{-1/2}\|\phi\|_{h,k}\left(\sum_{\kappa\in\mathcal{T}_h}\frac{h_\kappa^{2r_k-2}}{k_\kappa^{2s_\kappa-3}}\|u\|^2_{H^{s_\kappa}(\kappa)}\right)^{1/2}. \tag{3.18}$$

Inserting (3.16)–(3.18) into (3.15) and dividing both sides by $\|\phi\|_{h,k}$ gives

$$\|u_{2G}-u_{h,k}\|_{h,k} \leq \frac{C_4^{1/2}}{2}\left\{\left(\sum_{\kappa\in\mathcal{T}_h}\frac{h_\kappa^{2r_\kappa-2}}{k_\kappa^{2s_\kappa-3}}\|u\|^2_{H^{s_\kappa}(\kappa)}\right)^{1/2}+\left(\sum_{\kappa\in\mathcal{T}_H}\frac{H_\kappa^{2R_\kappa-2}}{K_\kappa^{2S_\kappa-3}}\|u\|^2_{H^{S_\kappa}(\kappa)}\right)^{1/2}\right\}.$$

Noting that $V(\mathcal{T}_H,\boldsymbol{K})\subseteq V(\mathcal{T}_h,\boldsymbol{k})$, we deduce that

$$\|u_{2G}-u_{h,k}\|_{h,k} \leq C_4^{1/2}\left(\sum_{\kappa\in\mathcal{T}_H}\frac{H_\kappa^{2R_\kappa-2}}{K_\kappa^{2S_\kappa-3}}\|u\|^2_{H^{S_\kappa}(\kappa)}\right)^{1/2},$$

which gives (3.12).

Exploiting this inequality to bound the second term on the right-hand side of (3.14) and applying Lemma 3.2 to bound the first term, we deduce (3.13). □

Remark 3.4. We note that due to the dependence of the nonlinear coefficient μ on $|\nabla u|$, the error bound derived in Theorem 3.3 indicates that the mesh and polynomial distribution of both the fine and coarse finite element spaces $V(\mathcal{T}_h,\boldsymbol{k})$ and $V(\mathcal{T}_H,\boldsymbol{K})$, respectively, should grow at roughly the same rate, albeit the constants C_3 and C_4 present in the error bound being of differing sizes. Numerical experiments demonstrating the optimality of these theoretical bounds are given in Chapter 4. We stress that this theoretical result by no means requires that $V(\mathcal{T}_h,\boldsymbol{k})$ and $V(\mathcal{T}_H,\boldsymbol{K})$ should be of the same dimension, but simply that the mesh-size and polynomial degree distributions should be enriched at roughly the same rate. This is analogous to the corresponding results for Schwarz-type preconditioners: to ensure scalability of the preconditioner, in the sense that the number of iterations required to achieve convergence is uniform, the coarse

and fine meshes (in the case of an h-version method) must be refined at roughly the same rate, cf. Antonietti & Ayuso [5], for example. Indeed, in Chapter 4 we shall observe that there is indeed quite an offset between the dimension of the fine and coarse finite element spaces.

Remark 3.5. As noted in Remark 3.4, Theorem 3.3 indicates that the mesh and polynomial distribution of both the fine and coarse finite element spaces $V(\mathcal{T}_h, \boldsymbol{k})$ and $V(\mathcal{T}_H, \boldsymbol{K})$, respectively, should grow at roughly the same rate. This is in contrast to the h-version *a priori* error analysis undertaken in Bi & Ginting [36] in the case when $\mu = \mu(u)$. Indeed, in that setting, by using a suitable duality argument (e.g., in convex domains) in order to optimally bound the resulting L^2-terms, it is shown that for convergence, the coarse and fine mesh sizes H and h, respectively, should satisfy $H = \mathcal{O}(\sqrt{h})$, when the polynomial degree is (uniformly) set equal to one. In Chapter 5 we develop an alternative two-grid IP DGFEM to the one proposed in this section, cf. (3.10)–(3.11), based on employing an incomplete Newton iteration on the fine finite element space $V(\mathcal{T}_h, \boldsymbol{k})$, which results in an improved convergence rate.

3.4 *A Posteriori* Error Bound

In this section, we develop the *a posteriori* error analysis of the two-grid IP DGFEM defined by (3.10)–(3.11). To this end, let us denote by Π_{κ,k_κ} the L^2-projection onto $V(\mathcal{T}_h, \boldsymbol{k})$. Then, we state the following upper bound.

Theorem 3.4. *Let $u \in H_0^1(\Omega)$ be the analytical solution of (3.1)-(3.2), $u_{H,K} \in V(\mathcal{T}_H, \boldsymbol{K})$ the numerical approximation obtained from (3.10) and $u_{2G} \in V(\mathcal{T}_h, \boldsymbol{k})$ the numerical approximation computed from (3.11); then, the following hp-a posteriori error bound holds*

$$\|u - u_{2G}\|_{h,k} \leq C_5 \left(\sum_{\kappa \in \mathcal{T}_h} \left(\eta_\kappa^2 + \xi_\kappa^2\right) + \sum_{\kappa \in \mathcal{T}_h} h_\kappa^2 k_\kappa^{-2} \|f - \Pi_{\kappa,k_\kappa} f\|_{L^2(\kappa)}^2 \right)^{1/2}, \tag{3.19}$$

with a constant $C_5 > 0$, which is independent of $\boldsymbol{h}$, $\boldsymbol{H}$, $\boldsymbol{k}$ and $\boldsymbol{K}$. Here, for $\kappa \in \mathcal{T}_h$, the local

fine grid error indicators η_κ *are defined by*

$$\begin{aligned}\eta_\kappa^2 = h_\kappa^2 k_\kappa^{-2} \left\| \Pi_{\kappa,k_\kappa} f + \nabla \cdot (\mu(|\nabla u_{H,K}|)\nabla u_{2G}) \right\|_{L^2(\kappa)}^2 \\ + h_\kappa k_\kappa^{-1} \left\| [\![\mu(|\nabla u_{H,K}|)\nabla u_{2G}]\!] \right\|_{L^2(\partial\kappa\setminus\Gamma)}^2 + \gamma^2 h_\kappa^{-1} k_\kappa^3 \left\| [\![u_{2G}]\!] \right\|_{L^2(\partial\kappa)}^2\end{aligned} \tag{3.20}$$

and the local two-grid error indicators ξ_κ *are defined, for all* $\kappa \in \mathcal{T}_h$*, as*

$$\xi_\kappa^2 = \left\| (\mu(|\nabla u_{H,K}|) - \mu(|\nabla u_{2G}|))\nabla u_{2G} \right\|_{L^2(\kappa)}^2 . \tag{3.21}$$

Remark 3.6. We refer to η_κ as the local fine grid error indicators, since they are analogous to the corresponding error indicators present in the *a posteriori* error bounds derived for the standard IP DGFEM applied to both the linear Poisson and quasilinear problems, cf. Houston *et al.* [124, 125], respectively. On the other hand, the local error indicators ξ_κ stem from the exploitation of the two-grid approach. With this in mind, we refer to ξ_κ as the local two-grid error indicators; they effectively model the error generated by approximating the nonlinearity on the fine grid with the coarse grid solution.

Remark 3.7. We note that the third term in the local two-grid error indicator η_κ defined in (3.20) is suboptimal with respect to the polynomial degree. This suboptimality results from the fact that due to the possible presence of hanging nodes in $\mathcal{T}_h$, a non-conforming interpolant is used in the proof of Theorem 3.4. For conforming meshes, a conforming *hp*-version interpolant may be employed, which removes this suboptimality; see Houston *et al.* [125, Remark 3.3] for details.

Remark 3.8. In the case of an inhomogeneous boundary condition $u = g \in H^{1/2}(\Gamma)$ on Γ, the third term in the local error indicators η_κ is replaced by

$$\gamma^2 h_\kappa^{-1} k_\kappa^3 \left\| [\![u_{2G}]\!] \right\|_{L^2(\partial\kappa\setminus\Gamma)}^2 + \gamma^2 h_\kappa^{-1} k_\kappa^3 \left\| u_{2G} - g_h \right\|_{L^2(\partial\kappa\cap\Gamma)}^2 ,$$

where g_h is a piecewise polynomial approximation to the boundary function g; in this setting additional data-oscillation terms also arise, see Houston *et al.* [124] for details.

Remark 3.9. We remark that local lower bounds for the right-hand side of (3.19), i.e., the

efficiency of the proposed error indicator, can be proved by adding the term

$$E^2 := \sum_{\kappa\in\mathcal{T}_h} \|\mu(|\nabla u|)\nabla u - \mu(|\nabla u_{H,K}|)\nabla u_{2G}\|^2_{L^2(\kappa)}$$

to the norm $\|u - u_{2G}\|^2_{h,k}$. Then, by applying (3.4) we have

$$\begin{aligned} E^2 &\leq 2\sum_{\kappa\in\mathcal{T}_h} \xi_\kappa^2 + 2\sum_{\kappa\in\mathcal{T}_h} \|\mu(|\nabla u|)\nabla u - \mu(|\nabla u_{2G}|)\nabla u_{2G}\|^2_{L^2(\kappa)} \\ &\leq 2\sum_{\kappa\in\mathcal{T}_h} \xi_\kappa^2 + 2C_1^2 \sum_{\kappa\in\mathcal{T}_h} \|\nabla u - \nabla u_{2G}\|^2_{L^2(\kappa)} \\ &\leq 2\sum_{\kappa\in\mathcal{T}_h} \xi_\kappa^2 + 2C_1^2 \|u - u_{2G}\|^2_{h,k}, \end{aligned}$$

and, therefore, we obtain (3.19) with the left-hand side of the inequality replaced by $\left(\|u - u_{2G}\|_{h,k} + E^2\right)^{1/2}$, and a different constant $\widetilde{C}_5$. Furthermore, in order to obtain lower bounds on the error, the fine grid indicators η_κ can be estimated in terms of the local error by proceeding along the lines of Houston *et al.* [125]. Finally, in order to bound the two-grid error indicators, we use again (3.4) to infer that

$$\begin{aligned} \xi_\kappa &\leq \|\mu(|\nabla u_{H,K}|)\nabla u_{2G} - \mu(|\nabla u|)\nabla u\|_{L^2(\kappa)} + \|\mu(|\nabla u|)\nabla u - \mu(|\nabla u_{2G}|)\nabla u_{2G}\|_{L^2(\kappa)} \\ &\leq \|\mu(|\nabla u_{H,K}|)\nabla u_{2G} - \mu(|\nabla u|)\nabla u\|_{L^2(\kappa)} + C_1 \|\nabla u - \nabla u_{2G}\|_{L^2(\kappa)}. \end{aligned}$$

3.4.1 DG Decomposition

The proof of this error bound is based on a generalisation of the proof of the corresponding *a posteriori* bound for the standard hp-version IP DGFEM for second-order quasilinear elliptic PDEs; see Houston *et al.* [125] for details. Given that the fine mesh partition $\mathcal{T}_h$ of Ω may contain hanging nodes, we note we can create a 1-irregular auxiliary mesh $\mathcal{T}_{\widetilde{h}}$ as outlined in Section 2.1.2. We denote by $V(\mathcal{T}_{\widetilde{h}}, \widetilde{\boldsymbol{k}})$ the corresponding DGFEM finite element space with elemental diameter vector $\widetilde{\boldsymbol{h}}$, and polynomial degree vector $\widetilde{\boldsymbol{k}}$ defined by $\widetilde{k}_{\widetilde{\kappa}} = k_\kappa$ for any $\widetilde{\kappa} \in \mathcal{T}_{\widetilde{h}}$ with $\widetilde{\kappa} \subseteq \kappa$, $\kappa \in \mathcal{T}_h$. We note that $V(\mathcal{T}_h, \boldsymbol{k}) \subseteq V(\mathcal{T}_{\widetilde{h}}, \widetilde{\boldsymbol{k}})$ and due to the assumptions in Section 2.1.2, the DGFEM norms

$\|\cdot\|_{h,k}$ and $\|\cdot\|_{\widetilde{h},\widetilde{k}}$ corresponding to the spaces $V(\mathcal{T}_h,\boldsymbol{k})$ and $V(\mathcal{T}_{\widetilde{h}},\widetilde{\boldsymbol{k}})$, respectively, are equivalent on $V(\mathcal{T}_h,\boldsymbol{k})$; in particular there exists positive constants N_1 and N_2, independent of $\boldsymbol{h}$, $\widetilde{\boldsymbol{h}}$, $\boldsymbol{k}$ and $\widetilde{\boldsymbol{k}}$, such that

$$N_1 \sum_{F\in\mathcal{F}_h} \int_F \sigma_{h,k}|[\![v]\!]|^2 \,\mathrm{d}s \leq \sum_{\widetilde{F}\in\mathcal{F}_{\widetilde{h}}} \int_{\widetilde{F}} \sigma_{\widetilde{h},\widetilde{k}}|[\![v]\!]|^2 \,\mathrm{d}s \leq N_2 \sum_{F\in\mathcal{F}_h} \int_F \sigma_{h,k}|[\![v]\!]|^2 \,\mathrm{d}s \tag{3.22}$$

for all $v\in V(\mathcal{T}_h,\boldsymbol{k})$; cf. Houston *et al.* [125], Zhu [181], Zhu & Schötzau [182]. Here, $\mathcal{F}_{\widetilde{h}}$ denotes the set of all faces in $\mathcal{T}_{\widetilde{h}}$ and $\sigma_{\widetilde{h},\widetilde{k}}$ is the discontinuous penalisation parameter on $V(\mathcal{T}_{\widetilde{h}},\widetilde{\boldsymbol{k}})$, which is defined analogously to $\sigma_{h,k}$ on $V(\mathcal{T}_h,\boldsymbol{k})$.

An important step in our analysis is the decomposition of the DGFEM space $V(\mathcal{T}_{\widetilde{h}},\widetilde{\boldsymbol{k}})$ into two orthogonal subspaces, cf. Karakashian & Pascal [131]: a conforming part $\left[V(\mathcal{T}_{\widetilde{h}},\widetilde{\boldsymbol{k}})\right]^c = V(\mathcal{T}_{\widetilde{h}},\widetilde{\boldsymbol{k}})\cap H_0^1(\Omega)$, and a nonconforming part $\left[V(\mathcal{T}_{\widetilde{h}},\widetilde{\boldsymbol{k}})\right]^\perp$ defined as the orthogonal complement of $\left[V(\mathcal{T}_{\widetilde{h}},\widetilde{\boldsymbol{k}})\right]^c$ in $V(\mathcal{T}_{\widetilde{h}},\widetilde{\boldsymbol{k}})$ with respect to the DGFEM energy inner product $(\cdot,\cdot)_{\widetilde{h},\widetilde{k}}$ (inducing the DGFEM energy norm $\|\cdot\|_{\widetilde{h},\widetilde{k}}$), i.e.,

$$V(\mathcal{T}_{\widetilde{h}},\widetilde{\boldsymbol{k}}) = \left[V(\mathcal{T}_{\widetilde{h}},\widetilde{\boldsymbol{k}})\right]^c \oplus_{\|\cdot\|_{\widetilde{h},\widetilde{k}}} \left[V(\mathcal{T}_{\widetilde{h}},\widetilde{\boldsymbol{k}})\right]^\perp.$$

Based on this setting, the DGFEM solution u_{2G} obtained by (3.10)–(3.11) may be split accordingly,

$$u_{2G} = u_{2G}^c + u_{2G}^\perp, \tag{3.23}$$

where $u_{2G}^c \in \left[V(\mathcal{T}_{\widetilde{h}},\widetilde{\boldsymbol{k}})\right]^c$ and $u_{2G}^\perp \in \left[V(\mathcal{T}_{\widetilde{h}},\widetilde{\boldsymbol{k}})\right]^\perp$. We can define the error in the solution obtained by (3.10)–(3.11) as

$$e_{2G} = u - u_{2G},$$

and let

$$e_{2G}^c = u - u_{2G}^c \in H_0^1(\Omega). \tag{3.24}$$

3.4.2 Auxiliary Results

In order to prove Theorem 3.4 we first state the following auxiliary results.

Lemma 3.5. *With $u_{2G}^{\perp}$ and e_{2G}^{c} defined by (3.23) and (3.24), respectively, the following bounds hold:*

$$\left\|u_{2G}^{\perp}\right\|_{\widetilde{h},k} \leq D_1 \left(\sum_{F\in\mathcal{F}_h}\int_F \sigma_{h,k}|[\![u_{2G}]\!]|^2\,\mathrm{d}s\right)^{1/2}, \qquad \|e_{2G}^{c}\|_{h,k} \leq D_2\,\|e_{2G}\|_{h,k}\,,$$

where the constants $D_1, D_2 > 0$ are independent of γ, $\boldsymbol{h}$ and $\boldsymbol{k}$, but depends only on the shape regularity of $\mathcal{T}_h$ and the constants ρ_1 and ρ_2 in (2.1) and (2.2), respectively.

Proof. This proof follows in an analogous manner to the proof of Zhu & Schötzau [182, Lemma 4.6] and Zhu *et al.* [183, Lemma 4.1] for the case when $d = 2, 3$, respectively; cf. Houston *et al.* [125, Corollary 3.6]. □

We now state the following result from Houston *et al.* [125, Lemma 3.7]

Lemma 3.6. *For any $v \in H_0^1(\Omega)$, there exists a function $v_{h,k} \in V(\mathcal{T}_h, \boldsymbol{k})$ such that*

$$h_\kappa^{-2}k_\kappa^2\,\|v - v_{h,k}\|_{L^2(\kappa)}^2 + \|\nabla(v - v_{h,k})\|_{L^2(\kappa)}^2 + h_\kappa^{-1}k_\kappa\,\|v - v_{h,k}\|_{L^2(\partial\kappa)}^2 \leq C_I\,\|\nabla v\|_{L^2(\kappa)}^2\,,$$

for any $\kappa \in \mathcal{T}_h$, with a constant $C_I > 0$, independent on $\boldsymbol{h}$ and $\boldsymbol{k}$ but dependent on the shape regularity of the mesh and the constants ρ_1 and ρ_2 from (2.1) and (2.2), respectively.

Proof. See Houston *et al.* [125, Lemma 3.7]. □

3.4.3 Proof of Theorem 3.4

We can now apply these results to prove Theorem 3.4. We start by exploiting inequality (3.5) to yield that

$$\begin{aligned} C_2\,\|e_{2G}\|_{h,k}^2 &= C_2\left(\sum_{\widetilde{\kappa}\in\mathcal{T}_{\widetilde{h}}}\int_{\widetilde{\kappa}}|\nabla(u - u_{2G})|^2\,\mathrm{d}\boldsymbol{x} + \sum_{F\in\mathcal{F}_h}\int_F \sigma_{h,k}|[\![e_{2G}]\!]|^2\,\mathrm{d}s\right) \\ &\leq \sum_{\widetilde{\kappa}\in\mathcal{T}_{\widetilde{h}}}\int_{\widetilde{\kappa}}(\mu(|\nabla u|)\nabla u - \mu(|\nabla u_{2G}|)\nabla u_{2G})\cdot\nabla e_{2G}\,\mathrm{d}\boldsymbol{x} \\ &\quad + C_2\sum_{F\in\mathcal{F}_h}\int_F \sigma_{h,k}|[\![e_{2G}]\!]|^2\,\mathrm{d}s. \end{aligned}$$

Here, we point out that the volume integrals appearing in the above equation are defined over the auxiliary mesh $\mathcal{T}_{\widetilde{h}}$, while the face integral terms are defined over the skeleton of the original (fine) mesh $\mathcal{T}_h$, cf. Houston *et al.* [125]. By noticing that $e_{2G} = e_{2G}^c - u_{2G}^\perp$, we split the right-hand side of this inequality into the following four parts

$$C_2 \, \|e_{2G}\|_{h,k}^2 \leq |T_1| + |T_2| + |T_3| + |T_4|, \tag{3.25}$$

where

$$\begin{aligned}
T_1 &= \sum_{\widetilde{\kappa} \in \mathcal{T}_{\widetilde{h}}} \int_{\widetilde{\kappa}} (\mu(|\nabla u|)\nabla u - \mu(|\nabla u_{H,K}|)\nabla u_{2G}) \cdot \nabla e_{2G}^c \, \mathrm{d}\boldsymbol{x}, \\
T_2 &= -\sum_{\widetilde{\kappa} \in \mathcal{T}_{\widetilde{h}}} \int_{\widetilde{\kappa}} (\mu(|\nabla u|)\nabla u - \mu(|\nabla u_{2G}|)\nabla u_{2G}) \cdot \nabla u_{2G}^\perp \, \mathrm{d}\boldsymbol{x}, \\
T_3 &= C_2 \sum_{F \in \mathcal{F}_h} \int_F \sigma_{h,k} |[\![e_{2G}]\!]|^2 \, \mathrm{d}s, \\
T_4 &= \sum_{\widetilde{\kappa} \in \mathcal{T}_{\widetilde{h}}} \int_{\widetilde{\kappa}} (\mu(|\nabla u_{H,K}|)\nabla u_{2G} - \mu(|\nabla u_{2G}|)\nabla u_{2G}) \cdot \nabla e_{2G}^c \, \mathrm{d}\boldsymbol{x}.
\end{aligned}$$

Here, $e_{2G}^c \in H_0^1(\Omega)$ and $u_{2G}^\perp \in \left[V(\mathcal{T}_{\widetilde{h}}, \widetilde{\boldsymbol{k}})\right]^\perp$ are defined by (3.24) and (3.23), respectively.

We note that T_1, T_2 and T_3 are analogous to the corresponding terms that arise in the *a posteriori* error analysis of the standard IP DGFEM discretisation of (3.1)–(3.2), cf. Houston *et al.* [125]. We outline the proof of these three terms briefly for reference.

Term T_1

Noting that the sum of the volume integrals on the fine mesh are equivalent to the sum of the volume integrals on the auxillary mesh; then, using integration by parts we obtain

$$\begin{aligned}
T_1 &= -\sum_{\kappa \in \mathcal{T}_h} \int_\kappa \nabla \cdot (\mu(|\nabla u|)\nabla u) e_{2G}^c \, \mathrm{d}\boldsymbol{x} - \sum_{\kappa \in \mathcal{T}_h} \int_\kappa \mu(|\nabla u_{H,K}|)\nabla u_{2G} \cdot \nabla e_{2G}^c \, \mathrm{d}\boldsymbol{x} \\
&= \sum_{\kappa \in \mathcal{T}_h} \int_\kappa f e_{2G}^c \, \mathrm{d}\boldsymbol{x} - \sum_{\kappa \in \mathcal{T}_h} \int_\kappa \mu(|\nabla u_{H,K}|)\nabla u_{2G} \cdot \nabla e_{2G}^c \, \mathrm{d}\boldsymbol{x}.
\end{aligned}$$

Letting $v_{h,k} \in V(\mathcal{T}_h, \boldsymbol{k})$ be the elementwise interpolant of e^c_{2G} satisfying Lemma 3.6 then by (3.11), integration by parts and the fact that $[\![e^c_{2G}]\!] = 0$, since $e^c_{2G} \in H^1_0(\Omega)$, it follows that

$$\begin{aligned}
T_1 = &\sum_{\kappa\in\mathcal{T}_h}\int_\kappa \left(f + \nabla\cdot(\mu(|\nabla u_{H,K}|)\nabla u_{2G})\right)(e^c_{2G} - v_{h,k})\,\mathrm{d}\boldsymbol{x}\\
&- \sum_{\kappa\in\mathcal{T}_h}\int_{\partial\kappa} ((\mu(|\nabla u_{H,K}|)\nabla u_{2G})\cdot\boldsymbol{n}_\kappa)(e^c_{2G} - v_{h,k})\,\mathrm{d}s\\
&- \sum_{F\in\mathcal{F}_h}\int_F \{\!\{\mu(|\nabla_h u_{H,K}|)\nabla_h u_{2G}\}\!\}[\![v_{h,k}]\!]\,\mathrm{d}s\\
&+ \theta\sum_{F\in\mathcal{F}_h}\int_F \{\!\{\mu(h_F^{-1}|[\![u_{H,K}]\!]|)\nabla_h v_{h,k}\}\!\}\{\!\{u_{2G}\}\!\}\,\mathrm{d}s + \sum_{F\in\mathcal{F}_h}\int_F \sigma_{h,k}[\![u_{2G}]\!][\![v_{h,k}]\!]\,\mathrm{d}s.
\end{aligned}$$

By applying (2.3)

$$\begin{aligned}
T_1 = &\sum_{\kappa\in\mathcal{T}_h}\int_\kappa \left(f + \nabla\cdot(\mu(|\nabla u_{H,K}|)\nabla u_{2G})\right)(e^c_{2G} - v_{h,k})\,\mathrm{d}\boldsymbol{x}\\
&- \sum_{F\in\mathcal{F}_h^{\mathcal{I}}}\int_F [\![\mu(|\nabla u_{H,K}|)\nabla u_{2G}]\!]\{\!\{e^c_{2G} - v_{h,k}\}\!\}\,\mathrm{d}s\\
&+ \theta\sum_{F\in\mathcal{F}_h}\int_F \{\!\{\mu(h_F^{-1}|[\![u_{H,K}]\!]|)\nabla_h v_{h,k}\}\!\}[\![u_{2G}]\!]\,\mathrm{d}s + \sum_{F\in\mathcal{F}_h}\int_F \sigma_{h,k}[\![u_{2G}]\!][\![v_{h,k}]\!]\,\mathrm{d}s.
\end{aligned} \tag{3.26}$$

Using (3.6), Lemma 2.1, Lemma 3.6 and noting that $\gamma \geq 1$ we get that

$$\begin{aligned}
T_1 \leq &\left(\sum_{\kappa\in\mathcal{T}_h}\frac{h_\kappa^2}{k_\kappa^2}\|f + \nabla\cdot(\mu(|\nabla u_{H,K}|)\nabla u_{2G}\|^2_{L^2(\kappa)}\right)^{1/2}\left(\sum_{\kappa\in\mathcal{T}_h}\frac{k_\kappa^2}{h_\kappa^2}\|e^c_{2G} - v_{h,k}\|^2_{L^2(\kappa)}\right)^{1/2}\\
&+ \frac{1}{2}\left(\sum_{\kappa\in\mathcal{T}_h}\frac{h_\kappa}{k_\kappa}\|[\![\mu(|\nabla u_{H,K}|)\nabla u_{2G}]\!]\|^2_{L^2(\partial\kappa\setminus\Gamma)}\right)^{1/2}\left(\sum_{\kappa\in\mathcal{T}_h}\frac{k_\kappa}{h_\kappa}\|e^c_{2G} - v_{h,k}\|^2_{L^2(\partial\kappa)}\right)^{1/2}\\
&+ M_\mu C_T^{1/2}(C_I+1)^{1/2}|\theta|\left(\sum_{F\in\mathcal{F}_h}\int_F \sigma_{h,k}|[\![u_{2G}]\!]|^2\,\mathrm{d}s\right)^{1/2}\left(\sum_{\kappa\in\mathcal{T}_h}\|\nabla e^c_{2G}\|^2_{L^2(\kappa)}\right)^{1/2}\\
&+ C\gamma^{1/2}\left(\sum_{F\in\mathcal{F}_h}\int_F \sigma_{h,k}k_F|[\![u_{2G}]\!]|^2\,\mathrm{d}s\right)^{1/2}\left(\sum_{\kappa\in\mathcal{T}_h}\frac{k_\kappa}{h_\kappa}\|e^c_{2G} - v_{h,k}\|^2_{L^2(\partial\kappa)}\right)^{1/2}.
\end{aligned}$$

Applying Lemma 3.6, again, the triangle inequality and using the fact that $\gamma \geq 1 \geq |\theta| \geq 0$, along with Lemma 3.5, results in the fact that

$$|T_1| \leq C \left(\sum_{\kappa \in \mathcal{T}_h} \eta_\kappa^2 + \sum_{\kappa \in \mathcal{T}_h} h_\kappa^2 k_\kappa^{-2} \left\| f - \Pi_{\kappa,k_\kappa} f \right\|_{L^2(\kappa)}^2 \right)^{1/2} \|e_{2G}\|_{h,k} \,. \tag{3.27}$$

Term T_2

To bound T_2, we use (3.4) yielding that

$$T_2 \leq C_1 \sum_{\widetilde{\kappa} \in \mathcal{T}_{\widetilde{h}}} \int_{\widetilde{\kappa}} |\nabla e_{2G}| |\nabla u_{2G}^{\perp}| \, \mathrm{d}\boldsymbol{x} \leq C_1 \left(\sum_{\widetilde{\kappa} \in \mathcal{T}_{\widetilde{h}}} \|\nabla e_{2G}\|_{L^2(\widetilde{K})}^2 \right)^{1/2} \left(\sum_{\widetilde{\kappa} \in \mathcal{T}_{\widetilde{h}}} \left\| \nabla u_{2G}^{\perp} \right\|_{L^2(\widetilde{K})}^2 \right)^{1/2}$$

Hence, we have by applying Lemma 3.5 and noting that $\gamma \geq 1$

$$\begin{aligned} T_2 \leq C_1 \|e_{2G}\|_{h,k} \left\| u_{2G}^{\perp} \right\|_{\widetilde{h},k} &\leq C_1 D_1 \|e_{2G}\|_{h,k} \left(\sum_{F \in \mathcal{F}_h} \int_F \sigma_{h,k} |[\![u_{2G}]\!]|^2 \, \mathrm{d}s \right)^{1/2} \\ &\leq C C_1 D_1 \|e_{2G}\|_{h,k} \left(\gamma \sum_{\kappa \in \mathcal{T}_h} h_\kappa^{-1} k_\kappa^2 \, \|[\![u_{2G}]\!]\|_{L^2(\partial\kappa)}^2 \right)^{1/2} \\ &\leq C C_1 D_1 \|e_{2G}\|_{h,k} \left(\sum_{\kappa \in \mathcal{T}_h} \eta_\kappa^2 \right)^{1/2} . \end{aligned} \tag{3.28}$$

Term T_3

Noting that since $u \in H_0^1(\Omega)$ we have $[\![u]\!] = 0$, and hence $[\![e_{2G}]\!] = [\![u_{2G}]\!]$; thereby,

$$\begin{aligned} T_3 &\leq C_2 \left(\sum_{F \in \mathcal{F}_h} \int_F \sigma_{h,k} |[\![e_{2G}]\!]| \, \mathrm{d}s \right)^{1/2} \left(\sum_{F \in \mathcal{F}_h} \int_F \sigma_{h,k} |[\![u_{2G}]\!]| \, \mathrm{d}s \right)^{1/2} \\ &\leq C C_2 \|e_{2G}\|_{h,k} \left(\gamma \sum_{\kappa \in \mathcal{T}_h} h_\kappa^{-1} k_\kappa^2 \, \|[\![u_{2G}]\!]\|_{L^2(\partial\kappa)}^2 \right)^{1/2} \\ &\leq C C_2 \|e_{2G}\|_{h,k} \left(\sum_{\kappa \in \mathcal{T}_h} \eta_\kappa^2 \right)^{1/2} . \end{aligned} \tag{3.29}$$

Term T_4

We now consider the term T_4

$$T_4 \leq \sum_{\kappa\in\mathcal{T}_h} \|(\mu(|\nabla u_{H,K}|) - \mu(|\nabla u_{2G}|))\nabla u_{2G}\|_{L^2(\kappa)} \|\nabla e^c_{2G}\|_{L^2(\kappa)} \leq \left(\sum_{\kappa\in\mathcal{T}_h} \xi^2_\kappa\right)^{1/2} \|e^c_{2G}\|_{h,k}\,.$$

Thereby, applying Lemma 3.5, gives

$$T_4 \leq D_2 \left(\sum_{\kappa\in\mathcal{T}_h} \xi^2_\kappa\right)^{1/2} \|e_{2G}\|_{h,k}\,. \tag{3.30}$$

Combining T_1–T_4

Inserting (3.27)–(3.30) into (3.25), and dividing both sides by $\|e_{2G}\|_{h,k}$ gives

$$C_2\,\|e_{2G}\|_{h,k} \leq C\left(\sum_{\kappa\in\mathcal{T}_h} \eta^2_\kappa + \sum_{\kappa\in\mathcal{T}_h} h^2_\kappa k^{-2}_\kappa \|f - \Pi_{\kappa,k_\kappa} f\|^2_{L^2(\kappa)}\right)^{1/2} + D_2\left(\sum_{\kappa\in\mathcal{T}_h} \xi^2_\kappa\right)^{1/2}.$$

Using the Cauchy–Schwarz inequality completes the proof of Theorem 3.4. □

3.5 Summary

In this chapter, we have studied the so-called two-grid numerical approximation of a quasilinear elliptic problem of strongly monotone type by means of hp-interior penalty discontinuous Galerkin methods. We have derived both *a priori* and *a posteriori* bounds on the error with respect to the discontinuous Galerkin energy norm (3.9). In the next chapter we perform numerical experiments to validate these two error bounds and discuss the use of the error indicators from Theorem 3.4 to construct an hp-adaptive mesh refinement algorithm for the proposed two-grid method.

CHAPTER 4

Computational Implementation and Numerical Experiments

In Section 4.1 and Section 4.3 of this chapter we perform numerical experiments to validate the *a priori* and *a posteriori* error bounds, respectively, for the two-grid method for the second order quasilinear elliptic PDE (3.1)–(3.2) from Chapter 3. In the later case we develop an automatic hp-adaptive mesh refinement algorithm to refine both the coarse and fine mesh based on the local error indicators defined in Theorem 3.4; to this end, in Section 4.2, we outline two potential adaptive algorithms for two-grid mesh refinement.

4.1 Validation of *A Priori* Error Bounds

In this section, we present numerical experiments to confirm the *a priori* error bounds for the two-grid method for the second order quasilinear elliptic PDE (3.1)–(3.2) outlined in Theorem 3.3. To this end, we let $\Omega = (0,1)^2 \subset \mathbb{R}^2$ be the unit square, and define the nonlinear coefficient as

$$\mu(|\nabla u|) = 2 + \frac{1}{1+|\nabla u|}. \tag{4.1}$$

Furthermore, we select the right-hand forcing function f so that the analytical solution to (3.1)–(3.2) is given by

$$u(x,y) = x(1-x)y(1-y)(1-2y)\mathrm{e}^{-20(2x-1)^2}. \tag{4.2}$$

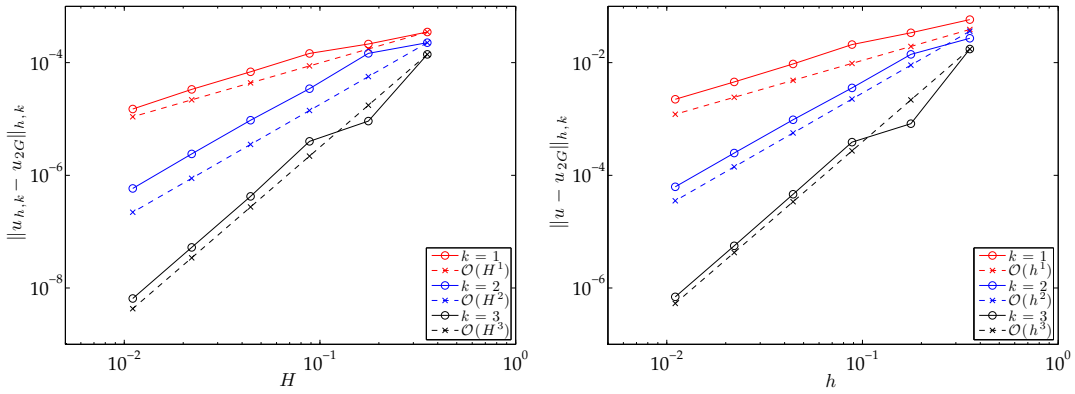

Figure 4.1: (a) Plot of $\|u_{h,k} - u_{2G}\|_{h,k}$ against H, for a fixed fine mesh; (b) Plot of $\|u - u_{2G}\|_{h,k}$ against h as both the fine and coarse meshes are uniformly refined, with $h = H/2$.

Firstly, we consider the case when the fine mesh $\mathcal{T}_h$ is fixed as a 256×256 uniform square mesh and the coarse grid is uniformly refined. In Figure 4.1(a) we plot $\|u_{h,k} - u_{2G}\|_{h,k}$ against H in the case when the coarse and fine polynomial degrees $\boldsymbol{K}$ and $\boldsymbol{k}$, respectively, are both uniform and equal, i.e., $K_\kappa = k$ for all $\kappa \in \mathcal{T}_H$ and $k_\kappa = k$ for all $\kappa \in \mathcal{T}_h$; here, we consider the cases when $k = 1, 2, 3$. We clearly observe that the error $\|u_{h,k} - u_{2G}\|_{h,k}$ converges to zero at the rate $\mathcal{O}(H^k)$, as H tends to zero, for each fixed polynomial degree, which is in full agreement with (3.12).

Secondly, we note from (3.13), cf. Remark 3.4, that an optimal convergence rate should be obtained when $h = \mathcal{O}(H)$; hence, we now consider the case when the fine and coarse meshes are both simultaneously refined together. To this end, we again consider the case when $\boldsymbol{K}$ and $\boldsymbol{k}$ are both uniform and equal, and consider a sequence of uniformly refined meshes, such that $h = H/2$. From Figure 4.1(b), we observe that $\|u - u_{2G}\|_{h,k}$ convergences to zero at the rate $\mathcal{O}(h^k)$, as h tends to zero, for each fixed polynomial degree; this confirms (3.13).

4.2 Two-Grid hp-Adaptive Mesh Refinement Algorithm

For the standard IP DGFEM discretisation of the quasilinear problem (3.1)–(3.2), the mesh may be automatically constructed using the hp-adaptive refinement algorithm outlined in Houston *et al.* [125]. In that setting, the local error indicators are defined in

an analogous way to η_κ given in (3.20), with $u_{H,K}$ and u_{2G} both replaced by $u_{h,k}$. In the context of the two-grid IP DGFEM discretisation defined by (3.10)–(3.11), it is necessary to refine both the fine and coarse meshes, together with their corresponding polynomial degree vectors, in order to decrease the error between u and u_{2G} with respect to the energy norm $\|\cdot\|_{h,k}$.

To this end, we first note that, from Theorem 3.4, we have for each fine element $\kappa \in \mathcal{T}_h$ a local fine grid error indicator η_κ and a local two-grid error indicator ξ_κ. As noted above, cf. also Chapter 3, the local fine grid error indicator η_κ is analogous to the one that arises within the analysis of the standard IP DGFEM discretisation. With this in mind, η_κ represents the error arising from the linear fine grid solve defined in (3.11), while the local two-grid error indicator ξ_κ represents the error stemming from the approximation of the nonlinear coefficient $\mu(|\nabla u_{h,k}|)$ on the fine mesh $\mathcal{T}_h$ by the same quantity evaluated with respect to the coarse grid solution $u_{H,K}$, i.e., the error committed by replacing $\mu(|\nabla u_{h,k}|)$ by $\mu(|\nabla u_{H,K}|)$. With this observation, we design the fine finite element space $V(\mathcal{T}_h, \boldsymbol{k})$ by employing the local fine grid error indicators (3.20), while the coarse finite element space $V(\mathcal{T}_H, \boldsymbol{K})$ is constructed in such a manner as to control the size of the local two-grid error indicators (3.21).

Assuming we have a method for selecting the elements to refine in the fine and coarse grid based on η_κ and ξ_κ, respectively, we can then devise the following general hp-refinement algorithm for the proposed two-grid method.

Algorithm 4.1. *The finite element spaces $V(\mathcal{T}_h, \boldsymbol{k})$ and $V(\mathcal{T}_H, \boldsymbol{K})$ are constructed, based on employing the following algorithm.*

1. *Initial step: Select the initial coarse and fine meshes $\mathcal{T}_H$ and $\mathcal{T}_h$, as well as the initial coarse and fine polynomial degree distributions $\boldsymbol{K}$ and $\boldsymbol{k}$, respectively, in such a manner that the resulting coarse and fine hp-finite element spaces $V(\mathcal{T}_H, \boldsymbol{K})$ and $V(\mathcal{T}_h, \boldsymbol{k})$, respectively, satisfy the condition: $V(\mathcal{T}_H, \boldsymbol{K}) \subseteq V(\mathcal{T}_h, \boldsymbol{k})$.*

2. *Select elements in $\mathcal{T}_h$ and $\mathcal{T}_H$ for refinement/derefinement, based on the local fine grid error indicators η_κ and the local two-grid error indicators ξ_κ from (3.20) and (3.21),*

respectively.

3. *For elements marked for refinement in the fine and coarse mesh, determine whether to perform h- or p-refinement; see, for example, Fankhauser* et al. *[83], Houston & Süli [116], Mitchell & McClain [142, 143], Wihler [172, 173].*

4. *Perform mesh smoothing to ensure:*

   - *For all $\kappa \in \mathcal{T}_h$ there exists a coarse mesh element $\kappa_H \in \mathcal{T}_H$ such that $\kappa \subseteq \kappa_H$;*
   - *For all $\kappa \in \mathcal{T}_h$ and $\kappa_H \in \mathcal{T}_H$, where $\kappa \subseteq \kappa_H$, that $K_{\kappa_H} \leq k_\kappa$.*

   In this thesis we perform h-refinement on the fine mesh $\mathcal{T}_h$ and p-derefinement on the coarse mesh $\mathcal{T}_H$ where necessary.

Remark 4.1. For the purposes of the numerical experiments in the following section we start the two-grid hp-adaptive algorithm with $V(\mathcal{T}_H, \boldsymbol{K}) = V(\mathcal{T}_h, \boldsymbol{k})$ in Step 1 above.

In order to employ this algorithm we need a strategy to select elements in $\mathcal{T}_h$ and $\mathcal{T}_H$ for refinement/derefinement, cf. Step 2 above. In this chapter we propose two different methods.

4.2.1 Strategy One - Independent Fine and Coarse Grid Refinement

We base the first refinement strategy on the principal that we want the local two-grid error indicators to always be less than the local fine grid error indicators. We refine the fine grid as for a standard method, using the local fine grid error indicators η_κ, and then refine the coarse grid wherever $\xi_\kappa \gtrsim \eta_\kappa$; cf. Figure 4.2 for a graphical demonstration of the refinement routine.

Algorithm 4.2. *Elements in the coarse and fine meshes $\mathcal{T}_h$ and $\mathcal{T}_H$, respectively, are selected for refinement/derefinement based on employing the following algorithm.*

1. *Select fine grid elements: Using the fine grid error indicators η_κ from (3.20), apply a standard refinement strategy to mark fine grid elements with a comparatively large error contribution for refinement, e.g. using the fixed fraction refinement strategy.*

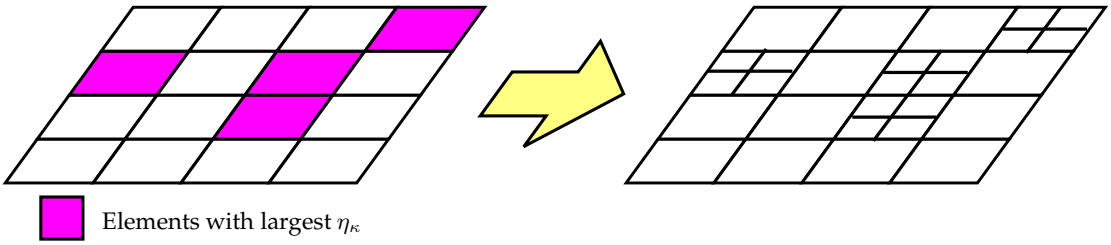

(a) Fine Grid

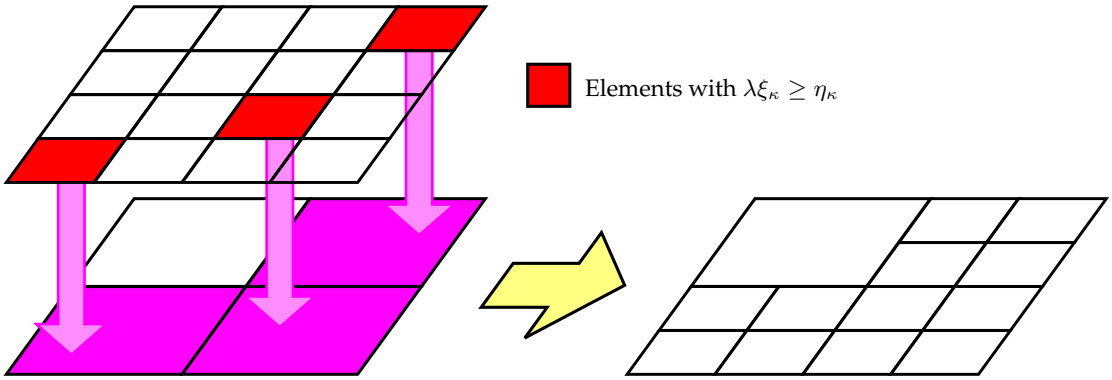

(b) Coarse Grid

Figure 4.2: One step of the Algorithm 4.2 refinement strategy, demonstrating how the fine (a) and coarse (b) meshes are refined independently for h-refinement; we note p-refinement works in an analogous manner.

2. *Select coarse grid elements: for a fixed constant steering parameter* $0 \leq \lambda < \infty$*, for each element* $\kappa \in \mathcal{T}_h$*, if* $\lambda\xi_\kappa \geq \eta_\kappa$ *then mark for refinement the coarse element* $\kappa_H \in \mathcal{T}_H$ *where* $\kappa \subseteq \kappa_H$*.*

Remark 4.2. We note that the algorithm allows the steering parameter λ to be zero. In this situation no coarse mesh refinement will be performed and hence the algorithm will only refine the fine mesh.

4.2.2 Strategy Two - Linked Fine and Coarse Grid Refinement

An issue with the refinement strategy outlined in the previous section is that it always performs coarse refinement if the local two-grid error indicator is larger than the local fine grid error indicator, regardless of how much this error contributes to the total error. As an example, if the local two-grid error indicator ξ_κ on one element κ is greater than the local fine grid error indicator η_κ on κ, but ξ_κ is several orders of magnitude lower than the error indicators on the other elements present in the mesh $\mathcal{T}_h$ it will

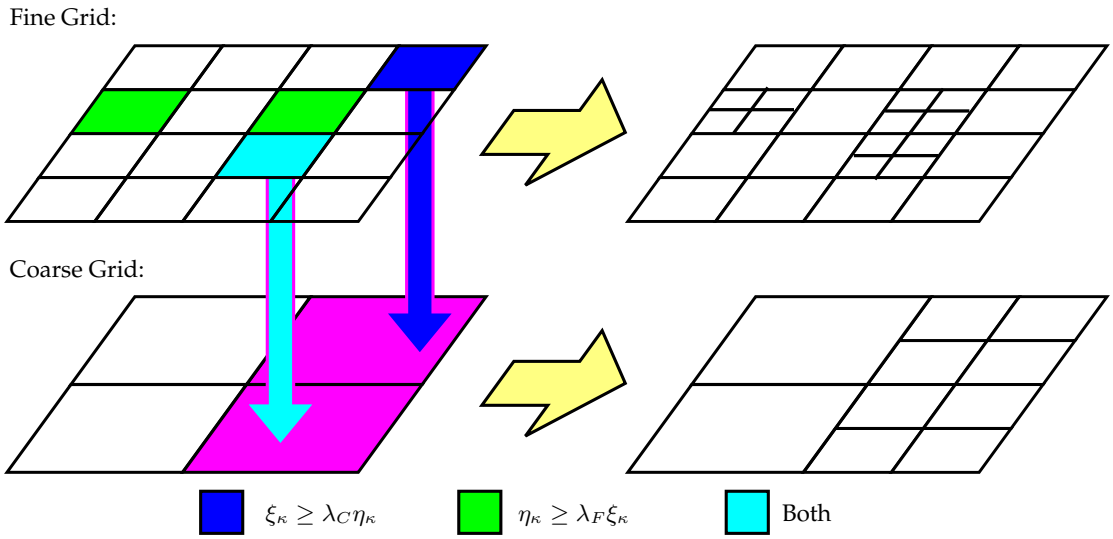

Figure 4.3: One step of the Algorithm 4.3 refinement strategy, demonstrating how the elements selected for possible refinement based on $\eta_\kappa + \xi_\kappa$ in the fine grid are used to decide on how to perform fine and coarse mesh h-refinement; we note p-refinement works analogously.

still be refined, which will probably result in a minimal reduction of the overall error. The second strategy we propose, therefore, only considers elements based on the total local error indicator $(\eta_\kappa + \xi_\kappa)$ and then decides whether to perform coarse or fine refinement based on if the local two-grid error indicator or the local fine grid error indicator, respectively, is largest; cf. Figure 4.3 for a graphical demonstration of the refinement routine.

Algorithm 4.3. *Elements in the coarse and fine meshes $\mathcal{T}_h$ and $\mathcal{T}_H$, respectively, are selected for refinement/derefinement based on employing the following algorithm.*

1. *Determine the sets $\mathfrak{R}(\mathcal{T}_h) \subseteq \mathcal{T}_h$ and $\mathfrak{D}(\mathcal{T}_h) \subseteq \mathcal{T}_h$ of fine elements to be (potentially) refined/derefined, respectively, based on the size of $\eta_\kappa + \xi_\kappa$ using a standard refinement algorithm, e.g., the fixed fraction refinement strategy.*

2. *For all elements selected for derefinement decide whether to perform derefinement of the fine or coarse mesh: for all $\kappa \in \mathfrak{D}(\mathcal{T}_h)$*

   - *if $\lambda_F \xi_\kappa \leq \eta_\kappa$ derefine the coarse element $\kappa_H \in \mathcal{T}_H$, where $\kappa \subseteq \kappa_H$, and*
   - *if $\lambda_C \eta_\kappa \leq \xi_\kappa$ derefine the fine element κ.*

3. *For all elements selected for refinement decide whether to perform refinement of the fine or coarse mesh: for all* $\kappa \in \mathfrak{R}(\mathcal{T}_h)$

   - *if* $\lambda_F \xi_\kappa \leq \eta_\kappa$ *refine the fine element* κ *and*
   - *if* $\lambda_C \eta_\kappa \leq \xi_\kappa$ *refine the coarse element* $\kappa_H \in \mathcal{T}_H$*, where* $\kappa \subseteq \kappa_H$*.*

Here, $\lambda_F, \lambda_C \in (0, \infty)$ *are steering parameters selected such that* $\lambda_F \lambda_C \leq 1$*.*

Remark 4.3. We note that it is possible for a coarse element $\kappa_H \in \mathcal{T}_H$ to be marked for both refinement and derefinement. When this occurs the coarse element is refined, as refinement should take precedence over derefinement.

Proposition 4.1. *For all elements* $\kappa \in \mathfrak{R}(\mathcal{T}_h)$ *either the fine element* $\kappa \in \mathcal{T}_h$ *or the coarse element* $\kappa_H \in \mathcal{T}_H$*, where* $\kappa \subseteq \kappa_H$*, will be marked for refinement.*

Proof. To prove this statement it is sufficient to show that either $p(\kappa) : \lambda_F \xi_\kappa \leq \eta_\kappa$ or $q(\kappa) : \lambda_C \eta_\kappa \leq \xi_\kappa$ is true for all $\kappa \in \mathcal{T}_h$. For any $\kappa \in \mathcal{T}_h$, if $p(\kappa)$ is true then $p(\kappa) \vee q(\kappa)$ is true by definition; hence, it is only necessary to prove that $q(\kappa)$ is true if $p(\kappa)$ is false. As $q(\kappa)$ is false and $\lambda_F \lambda_C \leq 1$ then

$$\lambda_F \xi_\kappa > \eta_\kappa \geq \lambda_F \lambda_C \eta_\kappa.$$

Dividing through by $\lambda_F > 0$ gives that $\xi_\kappa \geq \lambda_C \eta_\kappa$; hence, $q(\kappa)$ is true if $p(\kappa)$ is false. □

Remark 4.4. We note that although a similar result exists for the derefinement of elements $\kappa \in \mathfrak{D}(\mathcal{T}_h)$ it is possible for no element to be derefined for an element $\kappa \in \mathfrak{D}(\mathcal{T}_h)$ due to Remark 4.3.

4.3 Adaptive Numerical Experiments

In this section, we present a series of numerical experiments in two- and three-dimensional space to demonstrate the performance of the *a posteriori* error bound derived in Theorem 3.4 and the two hp-adaptive mesh refinement strategies outlined in Section 4.2. We set the interior penalty parameter constant γ to 10, the steering

parameter λ from Algorithm 4.2 to 1 and the steering parameters λ_F and λ_C from Algorithm 4.2 both to 1 for all experiments. Throughout this section we compute the numerical solutions with $\theta = 0$, i.e. we employ the IIP scheme. The nonlinear equations, cf. (3.10), are solved by employing a damped Newton method [147, Section 14.4] until the 2-norm of the residual $F_{H,K}(v_{H,K}) - A_{H,K}(u_{H,K}; u_{H,K}, v_{H,K})$ reaches a specific tolerance (1.0×10^{-8}). The solution of the resulting set of linear equations, emanating from either the fine mesh or at each step of the iterative nonlinear solver, was computed using either the direct Multifrontal Massively Parallel Solver (MUMPS) solver, see Amestoy *et al.* [2, 3, 4], for two-dimensional problems or an ILU preconditioned GMRES algorithm, see Saad & Schultz [153], for the three-dimensional problem. We also calculate the error bound stated in Theorem 3.4, cf. (3.19), by setting the constant C_5 equal to 1; cf. Becker *et al.* [26], Houston *et al.* [125]. In general this constant must be determined numerically from the underlying problem to ensure the reliability of the error estimator, cf. Eriksson *et al.* [82]. We note that for the marking strategy required by the mesh refinement strategy we employ a fixed fraction strategy, where the refinement and derefinement fractions are set to 25% and 5%, respectively.

For each example, as well as solving using the two-grid method, we compute the standard IP DGFEM formulation (3.8) for comparison using a standard fixed fraction strategy with refinement and derefinement fractions set to 25% and 5%, respectively. In order to determine the improvement in the computation time from using the two-grid method over the standard IP DGFEM, both algorithms were timed, on the same computer, using the FORTRAN `cpu_time` function [141, Section 8.16.2], which times purely the amount of CPU time and is, therefore, unaffected by other processes on the computer.

4.3.1 Example 1: 2D Smooth Analytical Solution

In this example, we repeat the first numerical experiment from Houston *et al.* [125, Section 4.1]. Therefore, we let Ω be the unit square $(0,1)^2 \subset \mathbb{R}^2$ and use the nonlinear coefficient defined in (4.1). We select the right-hand forcing function f so that the

analytical solution to (3.1)–(3.2) is given by (4.2).

In Figure 4.4(a) we present a comparison of the actual error measured in terms of the energy norm versus the square root of the number of degrees of freedom in the fine mesh finite element space $V(\mathcal{T}_h, \boldsymbol{k})$ for both the standard DGFEM formulation (3.8), together with the two-grid IP DGFEM (3.10)–(3.11) based on employing the first and second refinement strategies outlined in Algorithm 4.2 and Algorithm 4.3, respectively. In this figure we perform both h- and hp-adaptive mesh refinement for all schemes. Here, we can see that, for the problem at hand, the true error in the two-grid IP DGFEM is only marginally worse than the corresponding quantity for the standard IP DGFEM, when the same number of degrees of freedom in the two-grid fine mesh, as in the mesh for the standard IP DGFEM, are used. We also notice that the two different refinement strategies result in similar convergence rates. Although the two-grid IP DGFEM gives a slightly worse error than the standard IP DGFEM, for a fixed number of fine mesh degrees of freedom, we note that the two-grid algorithm only performs the expensive nonlinear solve on a coarser grid which possesses far less degrees of freedom than the standard IP DGFEM. Indeed, in Figure 4.4(b) we compare, at each iteration of the automatic two-grid mesh refinement algorithm, the number of degrees of freedom used in both the coarse and fine finite element spaces. We note here that the second refinement strategy has slightly more fine/less coarse degrees of freedom compared to the first refinement strategy. As can be seen, there are considerable less degrees of freedom on the coarse grid and, therefore, we would expect the two-grid solver to be computationally less expensive.

In order to validate this, we plot the magnitude of the true error, measured in the DGFEM norm, for both the standard and two-grid methods, when both h- and hp-adaptive mesh refinement has been employed, compared to the cumulative CPU time required for the calculation of each numerical solution in Figure 4.5. This figure clearly illustrates the superiority of employing the two-grid variant of the IP DGFEM for this problem. Indeed, for a given fixed accuracy, the two-grid IP DGFEM requires around an order of magnitude less CPU time to compute the numerical approximation to u,

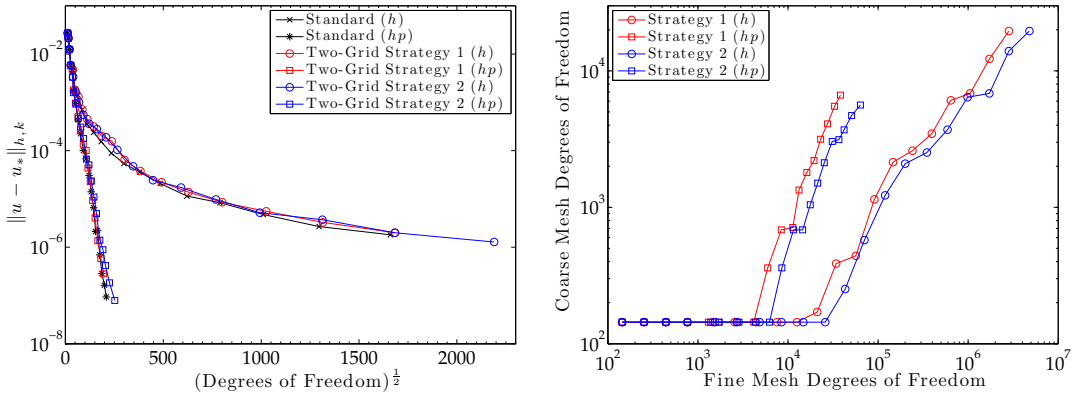

(a) *(b)*

Figure 4.4: Example 1. (a) Comparison of the error in the DG norm, for both the standard ($u_* = u_{h,k}$) and two-grid methods ($u_* = u_{2G}$), with respect to the number of degrees of freedom; (b) Comparison of number of degrees of freedom in the coarse and fine mesh at each iteration.

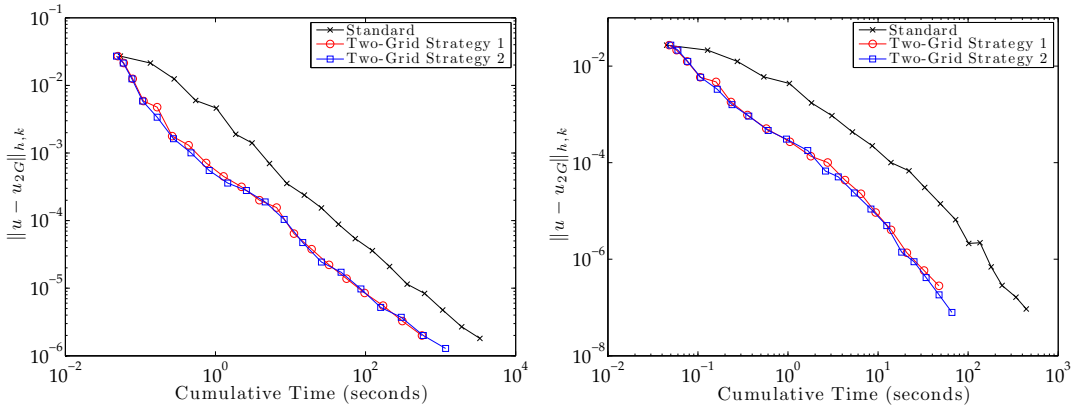

(a) h-refinement *(b) hp*-refinement

Figure 4.5: Example 1. Cumulative CPU timing of both the standard ($u_* = u_{h,k}$) and two-grid ($u_* = u_{2G}$) solvers compared to the error in the DG norm: (a) h-refinement; (b) hp-refinement.

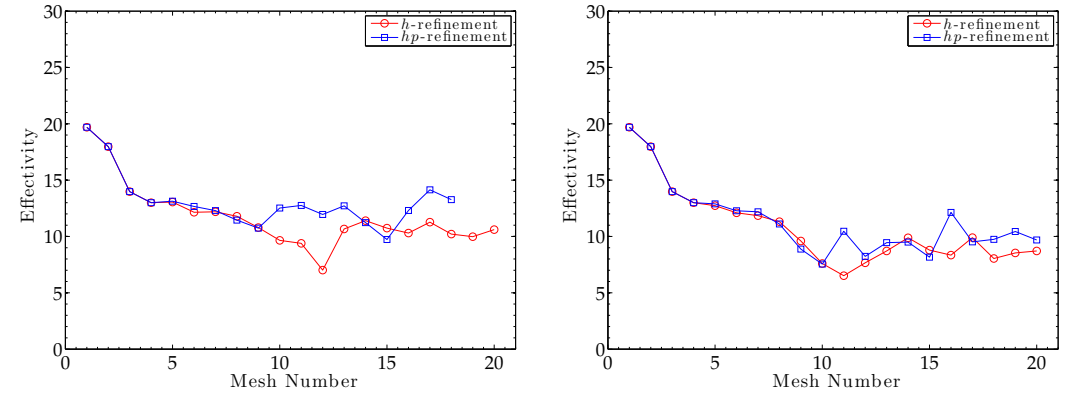

(a) Algorithm 4.2 *(b)* Algorithm 4.3

Figure 4.6: Example 1. Effectivity of the h- and hp-refinement using the two-grid method for the refinement strategies: (a) Algorithm 4.2; (b) Algorithm 4.3.

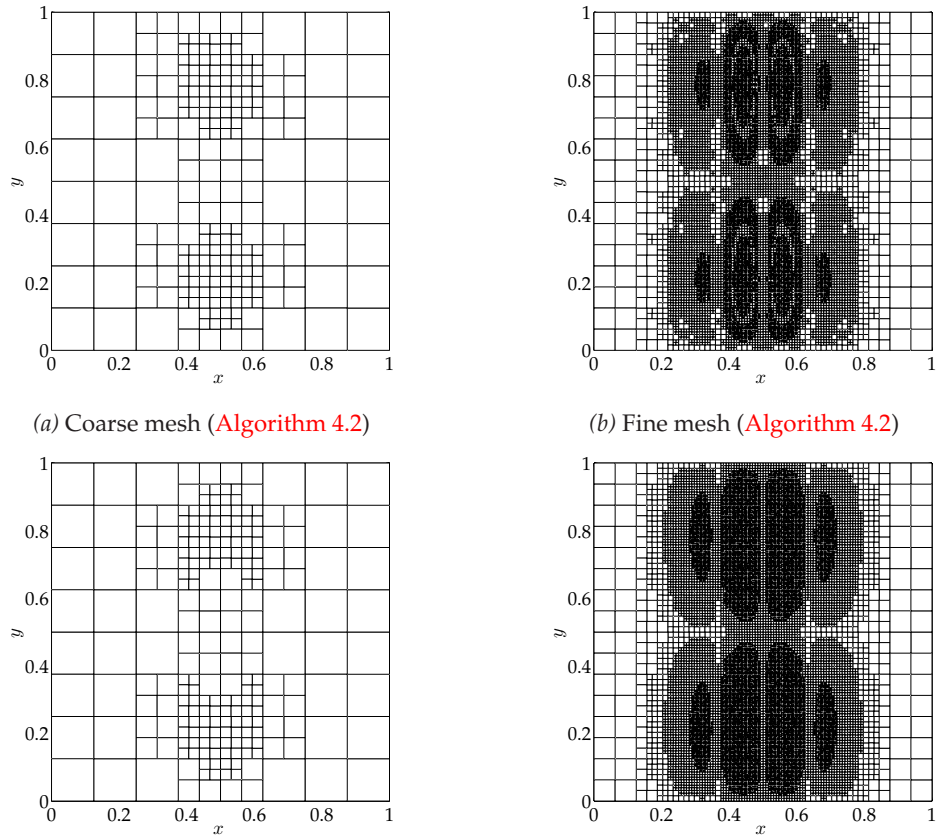

(a) Coarse mesh (Algorithm 4.2)

(b) Fine mesh (Algorithm 4.2)

(c) Coarse mesh (Algorithm 4.3)

(d) Fine mesh (Algorithm 4.3)

Figure 4.7: Example 1. Meshes after 13 h-refinements.

compared to the standard IP DGFEM. We note also that the two refinement strategies give similar results, although the second refinement strategy gives a slight improvement.

Finally, in order to validate the error bound derived in (3.4) we divide the computed error bound by the norm of the true error to derive the effectivity indices. We plot these indices in Figure 4.6(a) and Figure 4.6(b) for the first and second refinement strategies, respectively. We note that from this graph we can see that the error bound overestimates the true error by a roughly consistent amount for both h- and hp-refinement, in the sense that the effectivity indices are roughly constant; indeed, here, the effectivity indices are around 13.

In Figure 4.7 we present the fine and coarse h-refinement meshes after 13 mesh refinements, for both refinement strategies. All the fine grid refinement occurs around the

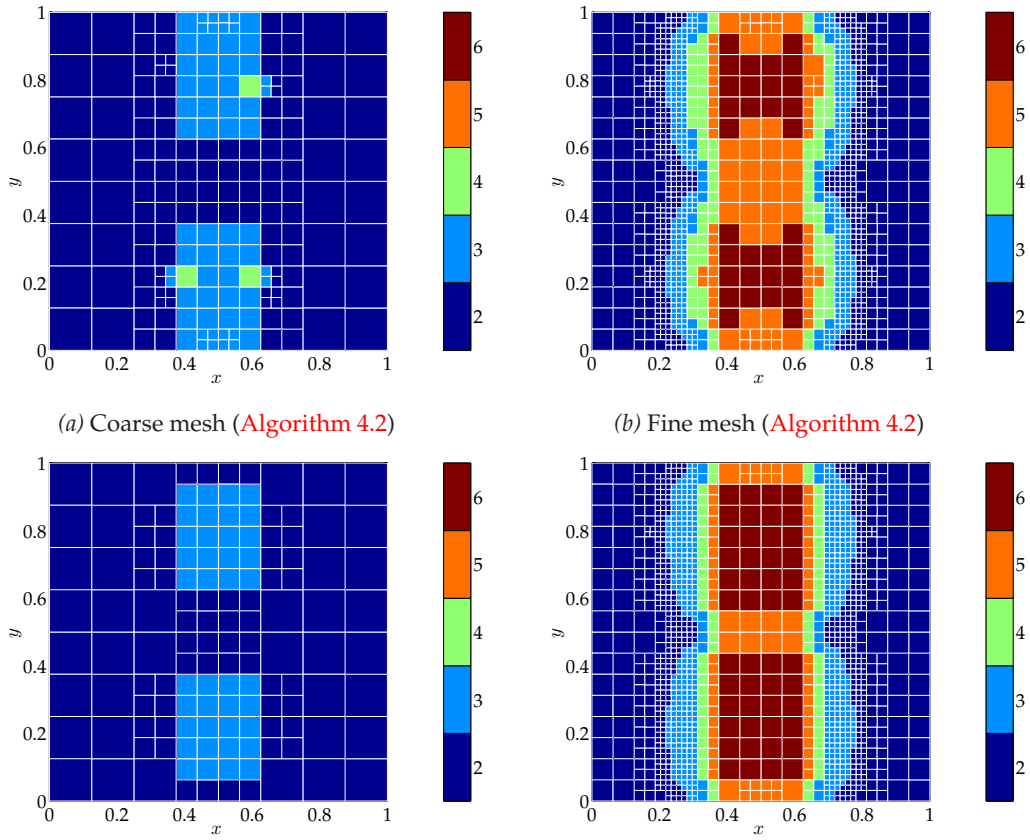

(a) Coarse mesh (Algorithm 4.2)

(b) Fine mesh (Algorithm 4.2)

(c) Coarse mesh (Algorithm 4.3)

(d) Fine mesh (Algorithm 4.3)

Figure 4.8: Example 1. Meshes after 13 hp-refinements.

interior and bases of the exponential 'hills' in the analytical solution, as would occur for the standard IP DGFEM. Notice that only a small amount of refinement has occurred in the corresponding elements in the coarse mesh, namely, wherever ξ_κ is expected to be large. We also note that the coarse mesh for both refinement strategies are very similar; whereas, the fine mesh is more refined when utilising the second refinement strategy in comparison to the first. Figure 4.8 shows, for both refinement strategies, the fine and coarse hp-refined meshes after 13 mesh refinements, where the colour bar indicates the polynomial degree. In the fine mesh the h-refinement occurs mostly around the base of the hills with p-refinement in the interior of the hills, cf. also the coarse grid. We note that when employing the second refinement strategy, the coarse mesh is slightly less refined and the fine mesh slighlty more refined, when compared to the corresponding meshes computed based on exploiting the first refinement strategy.

4.3.2 Example 2: 2D Singular Solution

In this example, we repeat the second experiment from Houston *et al.* [125, Section 4.2]. Thereby, we let Ω denote the L-shaped domain $(-1,1)^2 \setminus [0,1) \times (-1,0] \subset \mathbb{R}^2$ and select the nonlinearity to be

$$\mu(\boldsymbol{x}, |\nabla u|) = 1 + \mathrm{e}^{-|\nabla u|^2}.$$

By writing (r, φ) to denote the system of polar coordinates, we choose the forcing function f and an inhomogeneous boundary condition such that the analytical solution to (3.1)–(3.2) is

$$u(r, \varphi) = r^{2/3} \sin\left(\frac{2}{3}\varphi\right).$$

Note that u is analytic in $\bar{\Omega} \setminus \{\mathbf{0}\}$, but ∇u is singular at the origin.

In Figure 4.9(a), we again present a comparison of the actual error measured in terms of the energy norm versus the third root of the number of degrees of freedom in the finite element space $V(\mathcal{T}_h, \boldsymbol{k})$ for both the standard IP DGFEM formulation (3.8), together with the two-grid IP DGFEM (3.10)–(3.11) based on employing the first and second refinement strategies from Algorithm 4.2 and Algorithm 4.3, respectively. We employ both h- and hp-adaptive mesh refinement for all schemes. For this problem the true error in the two-grid IP DGFEM is very similar to the corresponding quantity for the standard IP DGFEM, when the same number of degrees of freedom in the two-grid fine mesh, as in the mesh for the standard IP DGFEM, are employed. We can see from Figure 4.9(b), which shows the number of degrees of freedom on the coarse grid compared to the number of degrees of freedom on the fine mesh at each iteration of the automatic mesh refinement algorithm, using the first and second refinement strategies, that there are considerable less degrees of freedom on the coarse grid and, thereby, we would again expect the two-grid solver to be computationally less expensive. We note again that the second refinement strategy has slightly more fine/less coarse degrees of freedom compared to the first refinement strategy.

In Figure 4.10 we plot the cumulative CPU time taken by the standard and the two-

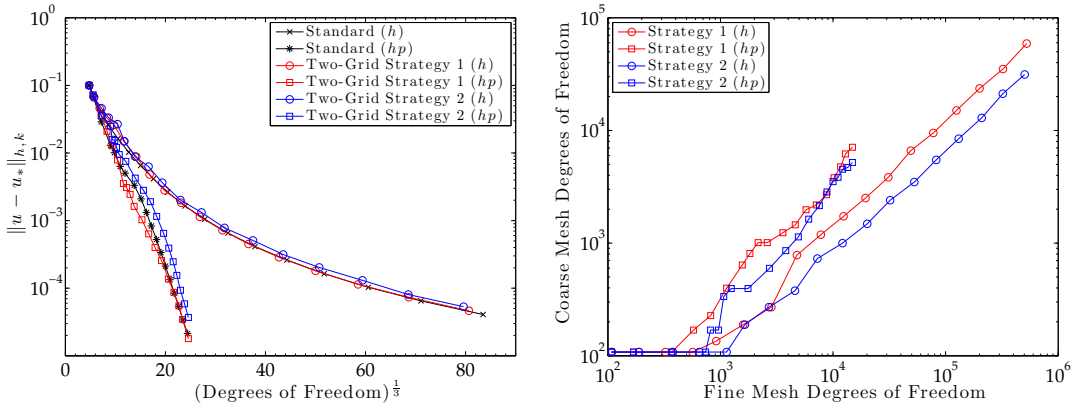

(a) *(b)*

Figure 4.9: Example 2. (a) Comparison of the error in the DG norm, for both the standard ($u_* = u_{h,k}$) and two-grid methods ($u_* = u_{2G}$), with respect to the number of degrees of freedom; (b) Comparison of number of degrees of freedom in the coarse and fine mesh at each iteration.

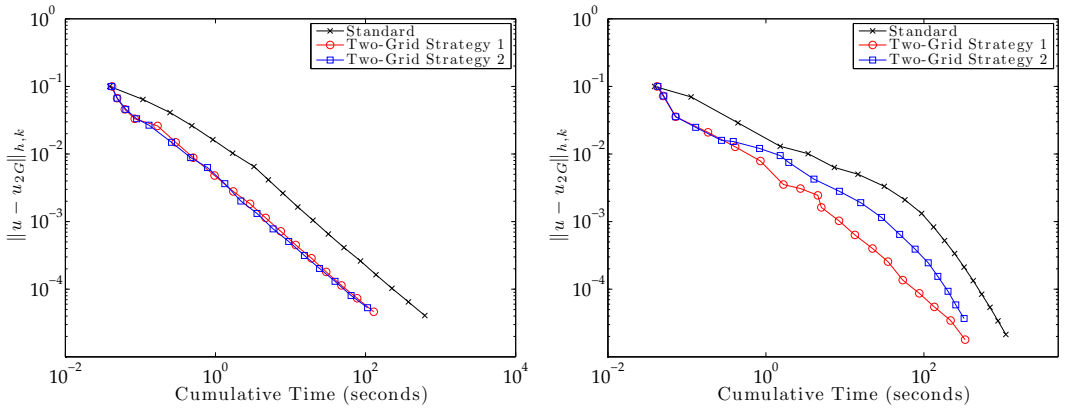

(a) h-refinement *(b)* hp-refinement

Figure 4.10: Example 2. Cumulative CPU timing of the standard ($u_* = u_{h,k}$) and two-grid ($u_* = u_{2G}$) solvers compared to the error in the DG norm: (a) h-refinement; (b) hp-refinement.

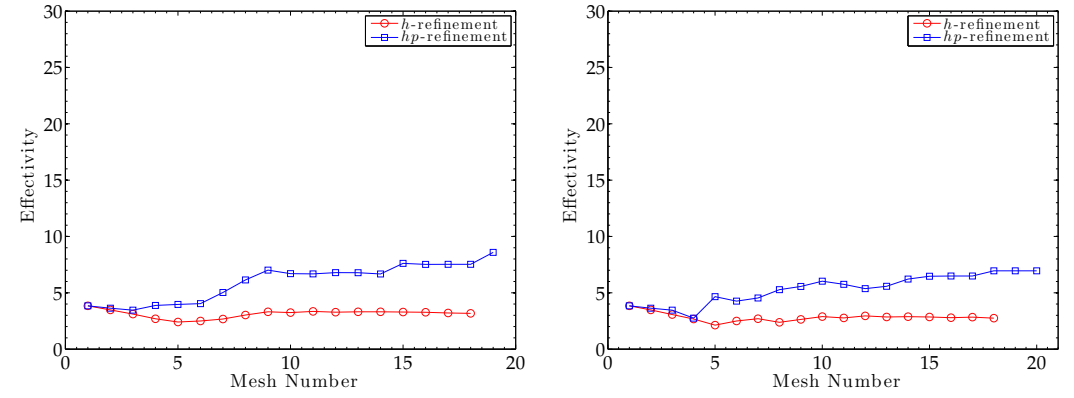

(a) Algorithm 4.2 *(b)* Algorithm 4.3

Figure 4.11: Example 2. Effectivity of the h- and hp-refinement using the two-grid method with the refinement strategies: (a) Algorithm 4.2; (b) Algorithm 4.3.

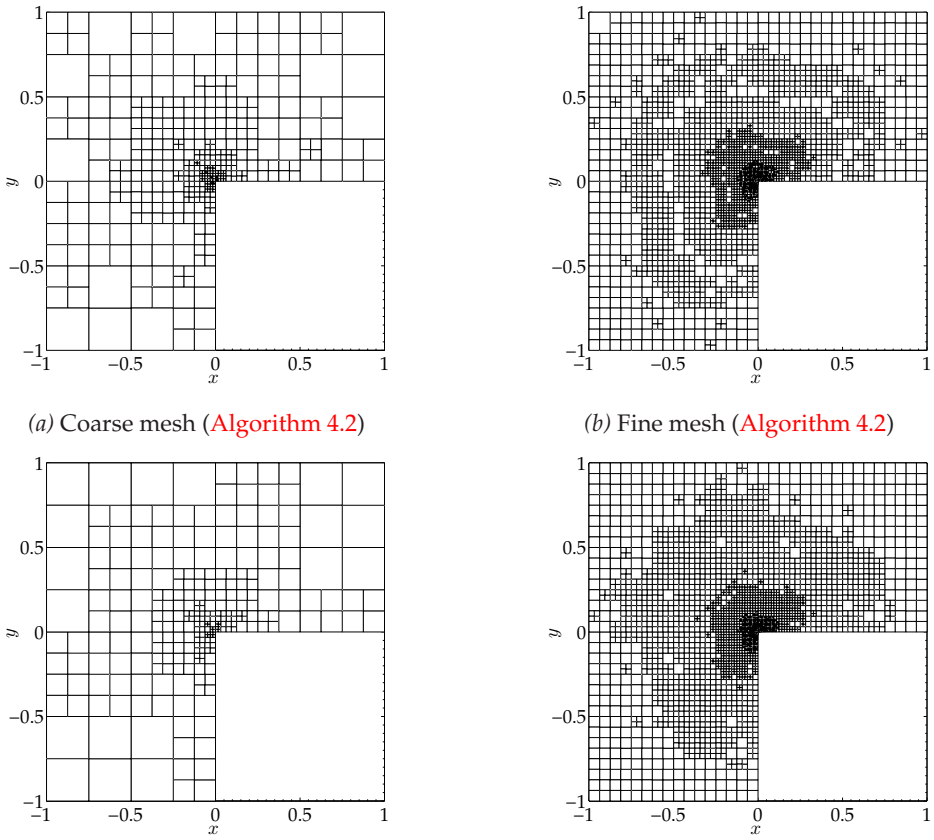

(a) Coarse mesh (Algorithm 4.2)

(b) Fine mesh (Algorithm 4.2)

(c) Coarse mesh (Algorithm 4.3)

(d) Fine mesh (Algorithm 4.3)

Figure 4.12: Example 2. Meshes after 11 h-adaptive mesh refinements.

grid method based on employing both refinement strategies, which is compared to the actual error, for both h– and hp-refinement strategies. Here, we see that for h-refinement, both refinement strategies of the two-grid IP DGFEM result in an error that is roughly a constant amount lower than the error in the standard method, for the same computation time. For hp-refinement, we note that the first refinement scheme offers a significant improvement over all meshes; whereas, the second refinement scheme produces less improvement during the refinement steps, but appears to be converging to the same computation time reduction by the end of the sequence of mesh refinements.

We plot the effectivity indices of both the h– and hp–refinement for both refinement strategies in Figure 4.11. Here we observe that in each case the effectivity indices tend towards a constant as the mesh is refined, although we note a higher constant for hp-refinement compared to h-refinement.

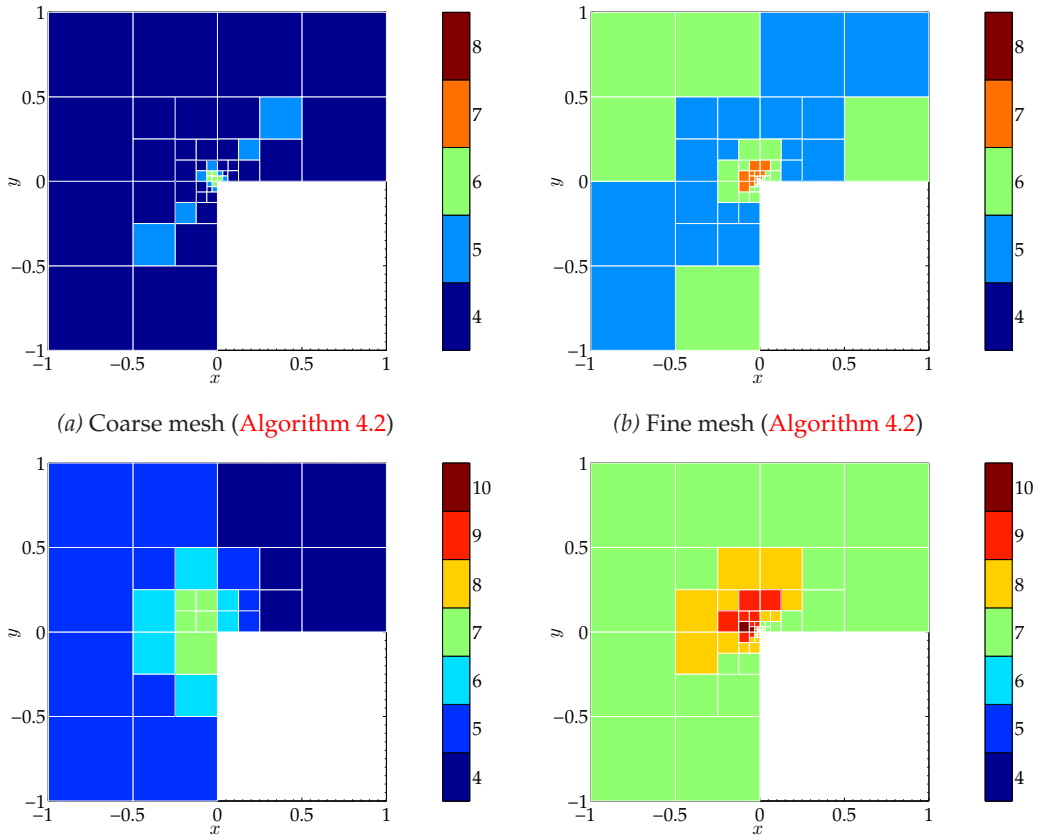

(a) Coarse mesh (Algorithm 4.2)

(b) Fine mesh (Algorithm 4.2)

(c) Coarse mesh (Algorithm 4.3)

(d) Fine mesh (Algorithm 4.3)

Figure 4.13: Example 2. Meshes after 11 hp-adaptive mesh refinements.

In Figure 4.12 we show the fine and coarse h-refinement meshes after 11 mesh refinements, for both refinement strategies. We note that the mesh refinement is concentrated around the singularity at the origin, as we would expect, for both the fine and coarse meshes employing both refinement strategies. In the hp-refinement case, cf. Figure 4.13, the h-refinement occurs mostly around the origin with high p-refinement in the rest of the domain. We note that the two schemes have chosen radically different refinements. The first strategy has performed far less p-refinement on the mesh as a whole with slightly more on the $x = y$ diagonal; whereas, the second strategy has focused it's p-refinement to the immediate top-right of the singularity, as would be expected, cf. Wihler *et al.* [175], but performed much less h-refinement around the origin in the coarse mesh compared to the first refinement strategy.

4.3.3 Example 3: 3D Singular Solution

In this section we let Ω be the Fichera corner $(-1,1)^3 \setminus [0,1)^3 \subset \mathbb{R}^3$, use the nonlinearity (4.1) from the first example and select f and suitable inhomogeneous boundary conditions such that the analytical solution to (3.1)–(3.2) is

$$u(x,y,z) = (x^2+y^2+z^2)^{q/2},$$

where $q \in \mathbb{R}$. From Beilina *et al.* [27] we note that for $q > -1/2$ the solution satisfies $u \in H^1(\Omega)$; in this case we select $q = -1/4$ as in Zhu *et al.* [183]. We note that this gives a singularity at the re-entrant corner (the origin).

In Figure 4.14(a), we again present a comparison of the actual error measured in terms of the energy norm versus the fourth root [183] of the number of degrees of freedom in the finite element space $V(\mathcal{T}_h, \boldsymbol{k})$ for both the standard IP DGFEM formulation (3.8), together with the two-grid IP DGFEM (3.10)–(3.11), based on employing both refinement strategies from Algorithm 4.2 and Algorithm 4.3. Here, we can see that for this problem the true error for both refinement strategies in the two-grid IP DGFEM is almost identical to the corresponding quantity for the standard IP DGFEM when the same number of degrees of freedom in the two-grid fine mesh is employed as in the mesh for the standard IP DGFEM. From Figure 4.14(b), which shows the number of degrees of freedom on the coarse grid compared to the number of degrees of freedom on the fine mesh at each iteration of the automatic mesh refinement algorithm for both refinement strategies, we can see that the two-grid solver uses significantly less degrees of freedom on the coarse grid than on the fine mesh.

From the comparison of the cumulative CPU timings with the actual error in the DGFEM norm, Figure 4.16, we observe a significant time improvement for both h- and hp-refinement strategies by using the two-grid method. In particular, for a given fixed accuracy, the two-grid IP DGFEM requires around an order of magnitude less CPU time to compute the numerical approximation to u, compared to the standard IP DGFEM. We note that both refinement strategies perform similarly, with the refinement

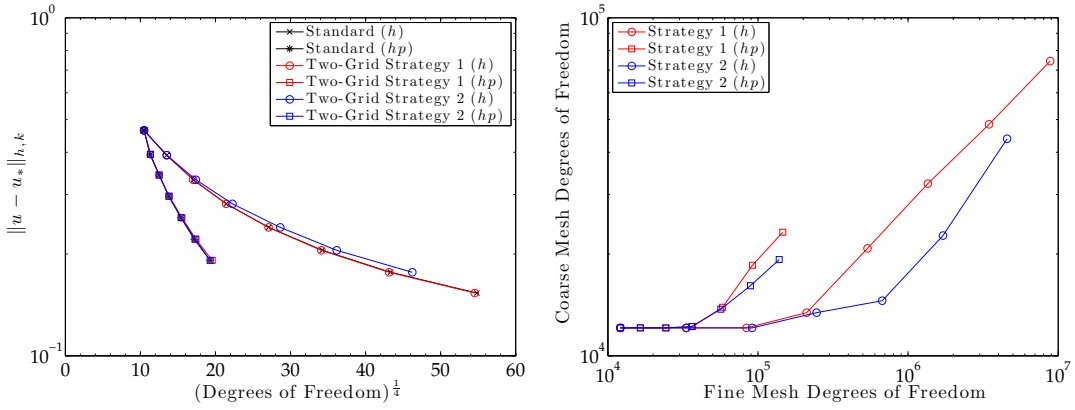

(a) *(b)*

Figure 4.14: Example 3. (a) Comparison of the error in the DG norm, for both the standard ($u_* = u_{h,k}$) and two-grid methods ($u_* = u_{2G}$), with respect to the number of degrees of freedom; (b) Comparison of number of degrees of freedom in the coarse and fine mesh at each iteration.

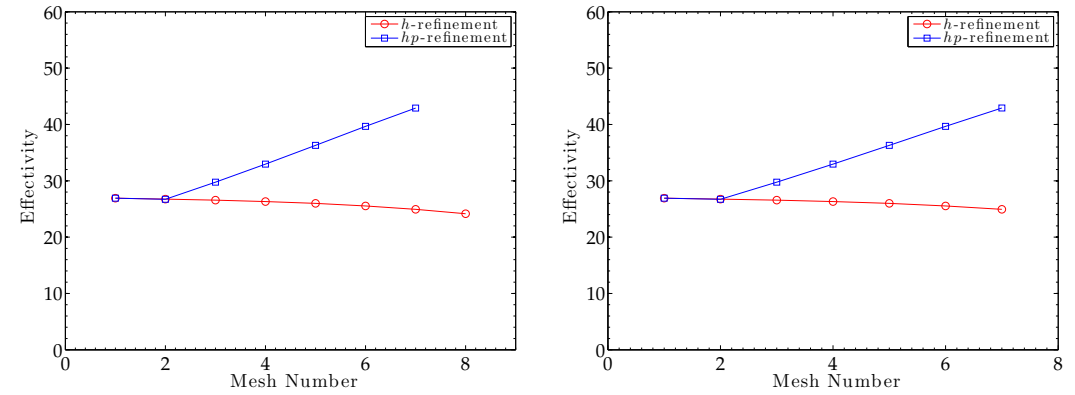

(a) Algorithm 4.2 *(b)* Algorithm 4.3

Figure 4.15: Example 3. Effectivity of the h- and hp-refinement using the two-grid method with the refinement strategies: (a) Algorithm 4.2; (b) Algorithm 4.3.

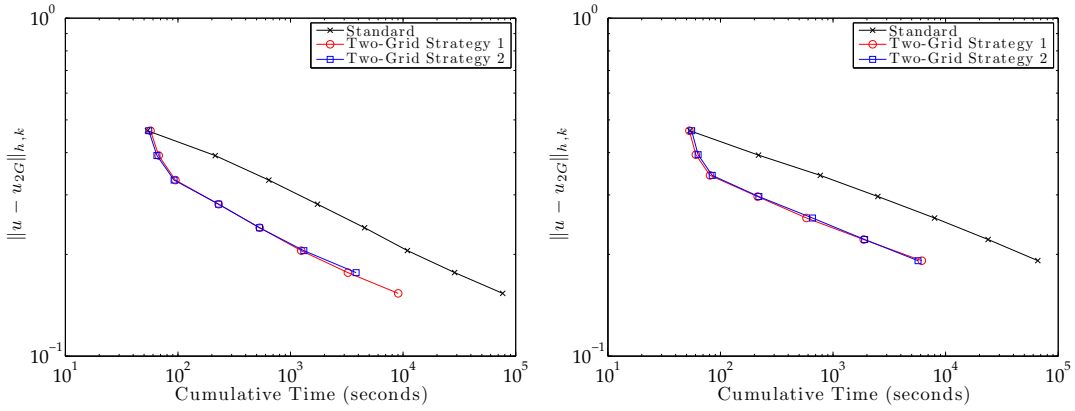

(a) h-Refinement *(b)* hp-Refinement

Figure 4.16: Example 3. Cumulative CPU timing of the standard ($u_* = u_{h,k}$) and two-grid ($u_* = u_{2G}$) solvers compared to the error in the DG norm: (a) h-refinement; (b) hp-refinement.

strategy from Algorithm 4.2 performing fractionally better for h-refinement and the refinement strategy from Algorithm 4.3 performing fractionally better for hp-refinement.

From Figure 4.15, we can see that the effectivity indices of the h-refinement strategy are roughly constant, for both refinement strategies, suggesting that the error bound constantly overestimates the error. For the hp–refinement strategy, we note that the effectivity index seems to rise as refinement occurs; we point out that similar behaviour was observed in Zhu *et al.* [183] for the numerical approximation of the Poisson equation posed in the same Fichera corner domain. The increase in the effectivity index may be due to being in a pre-asymptotic region.

Figure 4.17 shows the fine and coarse meshes after 5 h-refinements for both refinement strategies. We can see that both the fine and coarse grid refinement is fairly uniform but concentrated around the singularity at the origin; we also note that the coarse grid mesh is less refined than the fine mesh, as we would expect. Algorithm 4.3 appears to be slightly less refined in the coarse mesh but slightly more in the fine compared to the refinement based on Algorithm 4.2. The fine and coarse meshes after 6 hp–mesh refinements are shown in Figure 4.18. Here, we see that around the singularity at the origin both the fine and coarse meshes have mostly h-refinement with p-refinement occurring away from this area. Again we can see that both the coarse and fine meshes have been refined in a similar manner, with the coarse mesh just being less refined than the fine mesh. This time we note that both refinement strategies perform almost identical h-refinements but that Algorithm 4.3 performs slightly less p-refinement in both meshes.

4.4 Summary

In this chapter, we have proposed a mesh refinement algorithm, together with two different mesh refinement strategies, to perform hp-adaptive mesh refinement for the proposed two-grid method. This refinement strategy has been implemented in order to validate the analysis from Chapter 3 for a strongly monotone quasilinear PDE. We note that the two different marking strategies appear to give rise to similar results for the

(a) Coarse mesh (Algorithm 4.2) *(b)* Fine mesh (Algorithm 4.2) *(c)* Coarse mesh (Algorithm 4.3) *(d)* Fine mesh (Algorithm 4.3)

(e) Coarse mesh 3-slice (Algorithm 4.2) *(f)* Fine mesh 3-slice (Algorithm 4.2) *(g)* Coarse mesh 3-slice (Algorithm 4.3) *(h)* Fine mesh 3-slice (Algorithm 4.3)

Figure 4.17: Example 3. Meshes after 5 h-adaptive mesh refinements.

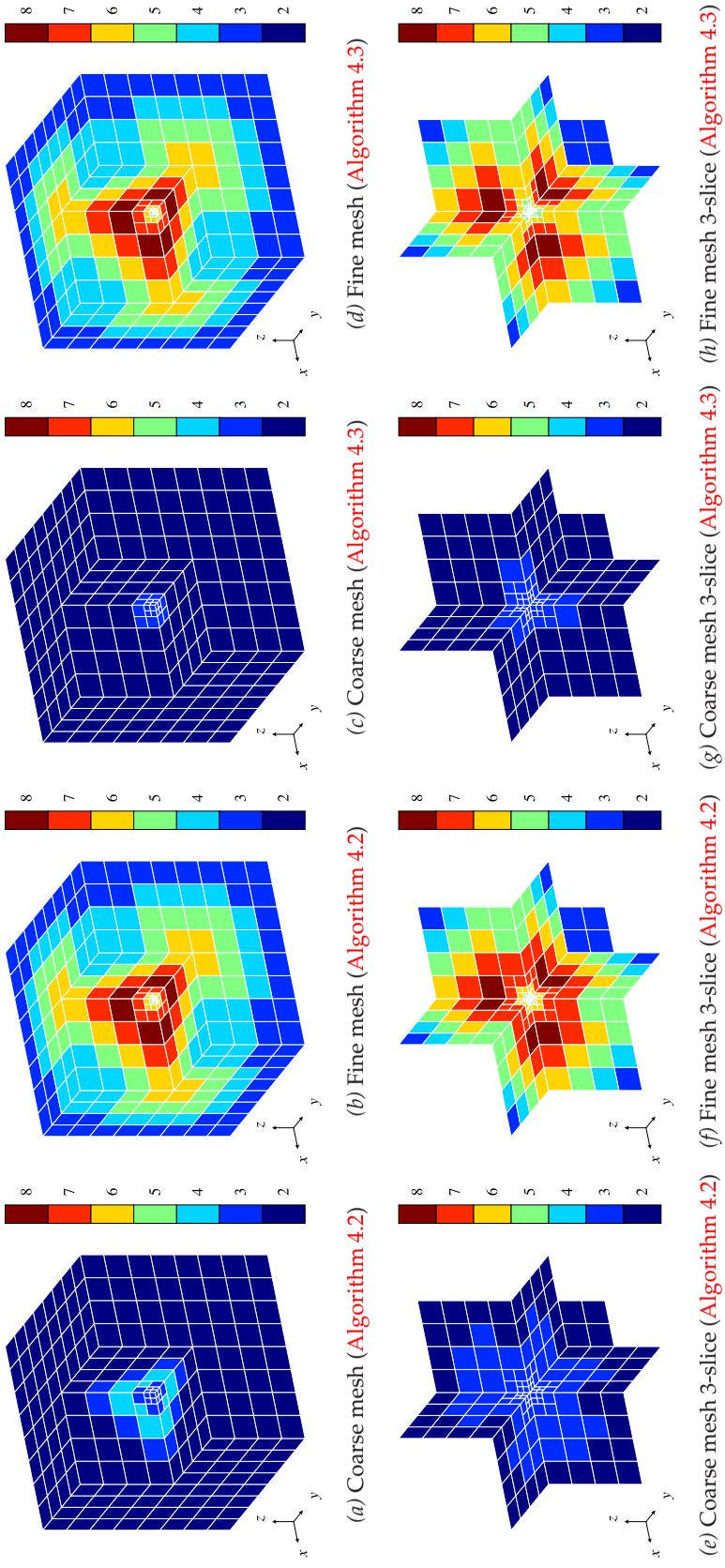

(a) Coarse mesh (Algorithm 4.2) *(b)* Fine mesh (Algorithm 4.2) *(c)* Coarse mesh (Algorithm 4.3) *(d)* Fine mesh (Algorithm 4.3)

(e) Coarse mesh 3-slice (Algorithm 4.2) *(f)* Fine mesh 3-slice (Algorithm 4.2) *(g)* Coarse mesh 3-slice (Algorithm 4.3) *(h)* Fine mesh 3-slice (Algorithm 4.3)

Figure 4.18: Example 3. Meshes after 6 *hp*-adaptive mesh refinements.

problems considered in this chapter. We have also performed numerical experiments to validate the *a priori* error bounds.

With the given framework for adaptive mesh refinement, in the next chapter we develop an alternative two-grid formulation for the strongly monotone quasilinear PDE (3.1)–(3.2) based on employing a single iteration of a Newton solver.

CHAPTER 5

hp-Version Two-Grid DGFEM for Second-Order Quasilinear Elliptic PDEs Based on a Single Newton Iteration

In this chapter we now introduce an alternative hp-version two-grid IP DGFEM based on a single Newton iteration step, cf. Axelsson & Layton [10], Xu [180, Section 5.2], for the second-order quasilinear PDE:

$$-\nabla \cdot (\mu(\boldsymbol{x}, |\nabla u|)\nabla u) = f(\boldsymbol{x}) \qquad \text{in } \Omega, \tag{5.1}$$

$$u = 0 \qquad \text{on } \Gamma, \tag{5.2}$$

where $\Omega \subset \mathbb{R}^d$, $d = 2, 3$ is a bounded polygonal Lipschitz domain with boundary Γ and $f \in L^2(\Omega)$; cf. (3.1)–(3.2). We note that the contents of this chapter has been published in the conference proceedings [63].

Assumption C. Here, we assume that for the nonlinearity $\mu \in C^2(\bar{\Omega} \times [0, \infty))$ there exists positive constants m_μ and M_μ such that

$$m_\mu(t - s) \leq \mu(\boldsymbol{x}, t)t - \mu(\boldsymbol{x}, s)s \leq M_\mu(t - s), \qquad t \geq s \geq 0, \quad \boldsymbol{x} \in \bar{\Omega}.$$

Remark 5.1. We note that here it is necessary to assume a higher regularity on the nonlinearity μ than in Chapter 3, cf. Assumption A.

For ease of notation we shall suppress the dependence of μ on $\boldsymbol{x}$ and write $\mu(t)$ instead of $\mu(\boldsymbol{x}, t)$. As in Chapter 3 we use the notation from Section 2.1.2 to consider the fine $\mathcal{T}_h$ and coarse $\mathcal{T}_H$ partitions of the computational domain Ω, of granularity h and H, respectively. We again associate the corresponding polynomial degree distributions $\boldsymbol{k} = \{k_\kappa : \kappa \in \mathcal{T}_h\}$ and $\boldsymbol{K} = \{K_\kappa : \kappa \in \mathcal{T}_H\}$ and assume that Assumption B holds. Given $\mathcal{T}_h$, $\boldsymbol{k}$, $\mathcal{T}_H$ and $\boldsymbol{K}$ we construct the fine and coarse hp-finite element spaces $V(\mathcal{T}_h, \boldsymbol{k})$ and $V(\mathcal{T}_H, \boldsymbol{K})$, respectively, which satisfies $V(\mathcal{T}_H, \boldsymbol{K}) \subseteq V(\mathcal{T}_h, \boldsymbol{k})$.

5.1 hp-Version Two-Grid DGFEM

In this section we state the two-grid IP DGFEM discretisation of (5.1)–(5.2) based on employing a single Newton iteration:

1. Compute the coarse grid approximation $u_{H,K} \in V(\mathcal{T}_H, \boldsymbol{K})$ such that

$$A_{H,K}(u_{H,K}, v_{H,K}) = F_{H,K}(v_{H,K}) \tag{5.3}$$

   for all $v_{H,K} \in V(\mathcal{T}_H, \boldsymbol{K})$.

2. Determine the fine grid solution $u_{2G} \in V(\mathcal{T}_h, \boldsymbol{k})$ such that

$$A'_{h,k}[u_{H,K}](u_{2G}, v_{h,k}) = A'_{h,k}[u_{H,K}](u_{H,K}, v_{h,k}) - A_{h,k}(u_{H,K}, v_{h,k}) + F_{h,k}(v_{h,k}) \tag{5.4}$$

   for all $v_{h,k} \in V(\mathcal{T}_h, \boldsymbol{k})$.

Here,

$$\begin{aligned} A_{h,k}(u,v) = &\sum_{\kappa\in\mathcal{T}_h}\int_\kappa \mu(|\nabla u|)\nabla u\cdot\nabla v\,\mathrm{d}\boldsymbol{x} - \sum_{F\in\mathcal{F}_h}\int_F \{\!\{\mu(|\nabla_h u|)\nabla_h u\}\!\}\cdot[\![v]\!]\,\mathrm{d}s \\ &+\theta\sum_{F\in\mathcal{F}_h}\int_F \{\!\{\mu(h_F^{-1}|[\![u]\!]|)\nabla_h v\}\!\}\cdot[\![u]\!]\,\mathrm{d}s + \sum_{F\in\mathcal{F}_h}\int_F \sigma_{h,k}[\![u]\!]\cdot[\![v]\!]\,\mathrm{d}s, \\ F_{h,k}(v) = &\sum_{\kappa\in\mathcal{T}_h}\int_\kappa f v\,\mathrm{d}\boldsymbol{x}, \end{aligned}$$

∇_h denotes the elementwise gradient operator and $A'_{h,k}[u](\cdot, v)$ denotes the Fréchet derivative of $u \to A_{h,k}(u, v)$, for fixed v, evaluated at u; thereby, given ϕ we have

$$A'_{h,k}[u](\phi, v) = \lim_{t \to 0} \frac{A_{h,k}(u + t\phi, v) - A_{h,k}(u, v)}{t}.$$

Here, $\theta \in [-1, 1]$ and the *interior penalty parameter* $\sigma_{h,k}$ is defined as $\sigma_{h,k} := \gamma k_F^2 h_F^{-1}$, where $\gamma > 0$ is a constant.

Lemma 5.1. *The semilinear form $A_{h,k}(\cdot, \cdot)$ is strongly monotone in the sense that, there exists a constant $\gamma_{\min} > 0$, such that for any $\gamma \geq \gamma_{\min}$*

$$A_{h,k}(w_1, w_1 - w_2) - A_{h,k}(w_2, w_1 - w_2) \geq C_m \|w_1 - w_2\|_{h,k}^2$$

for all $w_1, w_2 \in V(\mathcal{T}_h, \boldsymbol{k})$, where C_m is a positive constant, independent of the discretisation parameters.

Proof. See Houston *et al.* [122, Lemma 2.3]. □

We note that due to the fact that $A_{h,k}(\cdot, \cdot)$ is strongly monotone the following coercivity result holds for the bilinear form $A'_{h,k}[\,\cdot\,](\cdot, \cdot)$.

Corollary 5.2. *Under the assumptions on μ, there exists a constant $\gamma_{\min} > 0$, such that for any $\gamma \geq \gamma_{\min}$*

$$A'_{h,k}[u](v, v) \geq C_m \|v\|_{h,k}^2$$

for all $u, v \in V(\mathcal{T}_h, \boldsymbol{k})$, where C_m is a positive constant, independent of the discretisation parameters.

Proof. Setting $w_1 = u + tv$ and $w_2 = u$ in Lemma 5.1, $u, v \in V(\mathcal{T}_h, \boldsymbol{k})$, $t > 0$:

$$A_{h,k}(u + tv, tv) - A_{h,k}(u, tv) \geq C_m \|tv\|_{h,k}^2 .$$

Thereby,

$$\frac{A_{h,k}(u + tv, v) - A_{h,k}(u, v)}{t} \geq C_m \|v\|_{h,k}^2 ;$$

taking the limit as $t \to 0$, we deduce the statement of the Lemma. □

Remark 5.2. For simplicity of presentation, throughout the rest of this chapter we shall only consider the incomplete IP variation of the DGFEM, i.e., when $\theta = 0$.

5.2 *A Priori* Error Analysis

In this section, we derive an *a priori* error bound for the two-grid IP DGFEM defined by (5.3)–(5.4). We note, again, that the standard *a priori* error bound, Lemma 3.2, also clearly holds for the two-grid coarse solution $u_{H,K}$ defined in (5.3). For simplicity of presentation, in this section we consider a quasiuniform mesh with size h with a uniform polynomial degree k on all elements. We can now deduce the following error bound for the two-grid approximation defined in (5.3)–(5.4).

Theorem 5.3. *Assuming that* $u \in C^1(\Omega)$, $\nabla u \in [L^\infty(\Omega)]^d$ *and* $u \in H^s(\Omega)$, $s \geq 2$, *the solution* $u_{2G} \in V(\mathcal{T}_h, \boldsymbol{k})$ *of* (5.4) *satisfies*

$$\|u_{h,k} - u_{2G}\|_{h,k} \leq C_6 \frac{k^{7/2}}{h} \frac{H^{2R-2}}{K^{2s-3}} \|u\|^2_{H^s(\Omega)}\,, \tag{5.5}$$

$$\|u - u_{2G}\|_{h,k} \leq C_3^{1/2} \frac{h^{r-1}}{k^{s-3/2}} \|u\|_{H^s(\Omega)} + C_6 \frac{k^{7/2}}{h} \frac{H^{2R-2}}{K^{2s-3}} \|u\|^2_{H^s(\Omega)}\,, \tag{5.6}$$

with $1 \leq r \leq \min(k+1, s)$, $k \geq 1$ *and* $1 \leq R \leq \min(K+1, s)$, $K \geq 1$, *where* C_3, C_6 *are positive constants independent of* u, $\boldsymbol{h}$, $\boldsymbol{H}$, $\boldsymbol{k}$, $\boldsymbol{K}$, *but dependent on the constants* m_μ, M_μ, C_1 *and* C_2 *from the monotonicity properties of* $\mu(\cdot)$.

Remark 5.3. It is possible to produce a bound for non-uniform meshes; however, a reduced optimality in the bound for Lemma 5.6 below results in the *a priori* bound

$$\|u_{h,k} - u_{2G}\|_{h,k} \leq C_6 \frac{k^4_{\max} H_{\max}}{h_{\min} K^{1/2}_{\min}} \sum_{\kappa \in \mathcal{T}_h} \frac{H_\kappa^{2R_\kappa - 2}}{K_\kappa^{2S_\kappa - 3}} \|u\|^2_{H^{S_\kappa}(\Omega)}\,,$$

and a similar second bound obtained via the triangle inequality. Here, $h_{\min}$ and $H_{\max}$ are the minimum and maximum element diameters, respectively, of the fine and coarse mesh, respectively, and $K_{\min}$ is the minimum polynomial degree on the coarse mesh.

5.2.1 Auxiliary Results

In order to prove Theorem 5.3 we first state the following auxiliary results.

Lemma 5.4. *For a function $v \in V(\mathcal{T}_h, \boldsymbol{k})$ we have the inverse inequality*

$$\|v\|_{L^4(\Omega)} \leq C_L k h^{-1/2} \|v\|_{L^2(\Omega)},$$

where C_L is a positive constant, independent of the discretisation parameters.

Proof. Given $\kappa \in \mathcal{T}_h$, employing standard inverse inequalities, see Schwab [158], gives

$$\int_\kappa |v|^4 \, \mathrm{d}\boldsymbol{x} \leq \|v\|^2_{L^\infty(\kappa)} \|v\|^2_{L^2(\kappa)} \leq C k^4 h^{-2} \|v\|^2_{L^2(\kappa)} \|v\|^2_{L^2(\kappa)} = C k^4 h^{-2} \|v\|^4_{L^2(\kappa)}.$$

Summing over $\kappa \in \mathcal{T}_h$, employing the inequality $\sum_{i=1}^n a_i \leq \left(\sum_{i=1}^n \sqrt{a_i}\right)^2$, $a_i \geq 0$, $i = 1, \ldots, n$, and taking the fourth root of both sides, completes the proof. □

Lemma 5.5. *For any $v, w, \phi \in V(\mathcal{T}_h, \boldsymbol{k})$,*

$$A_{h,k}(w, \phi) = A_{h,k}(v, \phi) + A'_{h,k}[v](w - v, \phi) + \mathcal{Q}(v, w, \phi), \tag{5.7}$$

where the remainder $\mathcal{Q}$ satisfies

$$|\mathcal{Q}(v, w, \phi)| \leq C_{\mathcal{Q}} k^2 h^{-1} \left(1 + \|\nabla w\|_{L^\infty(\Omega)} + \|\nabla v\|_{L^\infty(\Omega)}\right) \|\nabla(w - v)\|^2_{h,k} \|\nabla \phi\|_{h,k}$$

and $C_{\mathcal{Q}}$ is a positive constant, independent of the discretisation parameters.

Proof. We follow the proof outlined by Xu [180, Lemma 3.1]; to this end, setting $\xi(t) = v + t(w - v)$ and $\eta(t) = A_{h,k}(\xi(t), \phi)$, we note that the first equation follows from the identity

$$\eta(1) = \eta(0) + \eta'(0) + \int_0^1 \eta''(t)(1 - t) \, \mathrm{d}t,$$

where $\mathcal{Q}(v,w,\phi) = \int_0^1 \eta''(t)(1-t)\,\mathrm{d}t$ and $\eta''(t) = A''_{h,k}[\xi(t)](w-v,w-v,\phi)$. Thereby,

$$\begin{aligned}
\mathcal{Q}(v,w,\phi) &= 2\int_0^1 (1-t)\int_\Omega \mu'_{\nabla u}(|\nabla\xi(t)|)\cdot\nabla(w-v)\nabla(w-v)\cdot\nabla\phi\,\mathrm{d}\boldsymbol{x}\,\mathrm{d}t \\
&\quad + \int_0^1 (1-t)\int_\Omega \mu''_{\nabla u}(|\nabla\xi(t)|)|\nabla(w-v)|^2\nabla\xi(t)\cdot\nabla\phi\,\mathrm{d}\boldsymbol{x}\,\mathrm{d}t \\
&\quad - 2\int_0^1 (1-t)\sum_{F\in\mathcal{F}_h}\int_e \{\!\{\mu'_{\nabla u}(|\nabla\xi(t)|)\cdot\nabla(w-v)\nabla(w-v)\}\!\}\cdot[\![\phi]\!]\,\mathrm{d}s\,\mathrm{d}t \\
&\quad - \int_0^1 (1-t)\sum_{F\in\mathcal{F}_h}\int_e \{\!\{\mu''_{\nabla u}(|\nabla\xi(t)|)|\nabla(w-v)|^2\nabla\xi(t)\}\!\}\cdot[\![\phi]\!]\,\mathrm{d}s\,\mathrm{d}t \\
&\equiv T_1+T_2+T_3+T_4,
\end{aligned}$$

where

$$\begin{aligned}
T_1 &= 2\int_0^1 (1-t)\int_\Omega \mu'_{\nabla u}(|\nabla\xi(t)|)\cdot\nabla(w-v)\nabla(w-v)\cdot\nabla\phi\,\mathrm{d}\boldsymbol{x}\,\mathrm{d}t, \\
T_2 &= \int_0^1 (1-t)\int_\Omega \mu''_{\nabla u}(|\nabla\xi(t)|)|\nabla(w-v)|^2\nabla\xi(t)\cdot\nabla\phi\,\mathrm{d}\boldsymbol{x}\,\mathrm{d}t, \\
T_3 &= -2\int_0^1 (1-t)\sum_{F\in\mathcal{F}_h}\int_F \{\!\{\mu'_{\nabla u}(|\nabla\xi(t)|)\cdot\nabla(w-v)\nabla(w-v)\}\!\}\cdot[\![\phi]\!]\,\mathrm{d}s\,\mathrm{d}t, \\
T_4 &= -\int_0^1 (1-t)\sum_{F\in\mathcal{F}_h}\int_F \{\!\{\mu''_{\nabla u}(|\nabla\xi(t)|)|\nabla(w-v)|^2\nabla\xi(t)\}\!\}\cdot[\![\phi]\!]\,\mathrm{d}s\,\mathrm{d}t.
\end{aligned}$$

Here, $\mu'_{\nabla u}(|\cdot|)$ and $\mu''_{\nabla u}(|\cdot|)$ denote the first and second derivatives of $\mu(|\cdot|)$, respectively.

First consider T_1: given that $\mu \in C^2(\bar{\Omega}\times[0,\infty))$, Lemma 5.4 gives

$$T_1 \le C\,\|\nabla(w-v)\|^2_{L^4(\Omega)}\,\|\nabla\phi\|_{L^2(\Omega)} \le Ck^2h^{-1}\,\|\nabla(w-v)\|^2_{L^2(\Omega)}\,\|\nabla\phi\|_{L^2(\Omega)}.$$

Secondly, term T_2 is bounded in an analogous fashion as follows:

$$\begin{aligned}
T_2 &\le C\left(\|\nabla w\|_{L^\infty(\Omega)} + \|\nabla v\|_{L^\infty(\Omega)}\right)\|\nabla(w-v)\|^2_{L^4(\Omega)}\,\|\nabla\phi\|_{L^2(\Omega)} \\
&\le C\left(\|\nabla w\|_{L^\infty(\Omega)} + \|\nabla v\|_{L^\infty(\Omega)}\right)k^2h^{-1}\,\|\nabla(w-v)\|^2_{L^2(\Omega)}\,\|\nabla\phi\|_{L^2(\Omega)}.
\end{aligned}$$

Term T_3 is bounded via Lemma 2.1 and Lemma 5.4:

$$\begin{aligned} T_3 &\leq C\gamma^{1/2} \left(\sum_{F\in\mathcal{F}_h} h_F k_F^{-2} \left\| \{\!\{ |\nabla(w-v)|^2 \}\!\} \right\|_{L^2(F)}^2 \right)^{1/2} \left(\sum_{F\in\mathcal{F}_h} \int_F \gamma k_F^2 h_F^{-1} |[\![\phi]\!]|^2 \,\mathrm{d}s \right)^{1/2} \\ &\leq C \left\| \nabla(w-v) \right\|_{L^4(\Omega)}^2 \left\| \phi \right\|_{h,k} \\ &\leq Ck^2 h^{-1} \left\| \nabla(w-v) \right\|_{L^2(\Omega)}^2 \left\| \phi \right\|_{h,k}. \end{aligned}$$

We can bound T_4 in an analogous manner as follows:

$$\begin{aligned} T_4 &\leq C\gamma^{1/2} \left(\sum_{F\in\mathcal{F}_h} h_F k_F^{-2} \left\| \{\!\{ |\nabla(w-v)|^2 |\nabla w| \}\!\} \right\|_{L^2(F)}^2 \right)^{1/2} \left(\sum_{F\in\mathcal{F}_h} \int_F \gamma k^2 h^{-1} |[\![\phi]\!]|^2 \,\mathrm{d}s \right)^{1/2} \\ &\quad + C\gamma^{1/2} \left\{ \sum_{F\in\mathcal{F}_h} h_F k_F^{-2} \left\| \{\!\{ |\nabla(w-v)|^2 |\nabla v| \}\!\} \right\|_{L^2(F)}^2 \right)^{1/2} \left(\sum_{F\in\mathcal{F}_h} \int_F \gamma k^2 h^{-1} |[\![\phi]\!]|^2 \,\mathrm{d}s \right)^{1/2} \\ &\leq C \left(\left\| \nabla w \right\|_{L^\infty(\Omega)} + \left\| \nabla v \right\|_{L^\infty(\Omega)} \right) \left\| \nabla(w-v) \right\|_{L^4(\Omega)}^2 \left\| \phi \right\|_{h,k} \\ &\leq Ck^2 h^{-1} \left(\left\| \nabla w \right\|_{L^\infty(\Omega)} + \left\| \nabla v \right\|_{L^\infty(\Omega)} \right) \left\| \nabla(w-v) \right\|_{L^2(\Omega)}^2 \left\| \phi \right\|_{h,k}. \end{aligned}$$

Combining these bounds for terms T_1, T_2, T_3 and T_4 completes the proof. □

Lemma 5.6. *Let $u \in H^2(\Omega)$ be the analytical solution of (3.1), such that $\nabla u \in [L^\infty(\Omega)]^d$, and $u_{h,k} \in V(\mathcal{T}_h, \boldsymbol{k})$ be the IP DGFEM defined by (3.8), we have that*

$$\left\| \nabla u_{h,k} \right\|_{L^\infty(\Omega)} \leq C_\infty k^{3/2},$$

where C_∞ is a positive constant, independent of the discretisation parameters.

Proof. Writing Π_{κ,k_κ} to denote the projection operator onto the finite element space $V(\mathcal{T}_h, \boldsymbol{k})$ defined in Babuška & Suri [12], we have that

$$\left\| u - \Pi_{\kappa,k_\kappa} u \right\|_{H^q(\Omega)} \leq C \frac{h^{2-q}}{k^{2-q}} \left\| u \right\|_{H^2(\Omega)}, \qquad \left\| \nabla(u - \Pi_{\kappa,k_\kappa} u) \right\|_{L^\infty(\Omega)} \leq C \left\| u \right\|_{H^2(\Omega)},$$

for all $q \leq 2$. Exploiting these bounds, standard inverse inequalities [158] and the *a*

priori bound for the IP DGFEM, Lemma 3.2, gives

$$\begin{aligned}
\|\nabla u_{h,k}\|_{L^\infty(\Omega)} &\leq \|\nabla(u_{h,k} - \Pi_{\kappa,k_\kappa} u)\|_{L^\infty(\Omega)} + \|\nabla(\Pi_{\kappa,k_\kappa} u)\|_{L^\infty(\Omega)} \\
&\leq Ck^2 h^{-1} \|\nabla(u_{h,k} - \Pi_{\kappa,k_\kappa} u)\|_{L^2(\Omega)} \\
&\quad + \|\nabla(u - \Pi_{\kappa,k_\kappa} u)\|_{L^\infty(\Omega)} + \|\nabla u\|_{L^\infty(\Omega)} \\
&\leq C\Big\{ k^2 h^{-1} \Big(\|u - u_{h,k}\|_{h,k} + \|\nabla(u - \Pi_{\kappa,k_\kappa} u)\|_{L^2(\Omega)} \Big) \\
&\qquad + \|u\|_{H^2(\Omega)} + \|\nabla u\|_{L^\infty(\Omega)} \Big\} \\
&\leq Ck^{3/2} \Big(\|u\|_{H^2(\Omega)} + \|\nabla u\|_{L^\infty(\Omega)} \Big).
\end{aligned}$$

Since $u \in H^2(\Omega)$ and $\nabla u \in [L^\infty(\Omega)]^d$, the quantities $\|u\|_{H^2(\Omega)}$ and $\|\nabla u\|_{L^\infty(\Omega)}$ are both bounded uniformly by a constant; this then completes the proof. □

5.2.2 Proof of Theorem 5.3

We now exploit the above results to prove Theorem 5.3. For the first bound (5.5), we employ Corollary 5.2, (3.8), (5.4) and (5.7); thereby, with $\phi = u_{h,k} - u_{2G}$, we deduce that

$$\begin{aligned}
C_m \|u_{h,k} - u_{2G}\|_{h,k}^2 &\leq A'_{h,k}[u_{H,K}](u_{h,k} - u_{2G}, \phi) \\
&= A'_{h,k}[u_{H,K}](u_{h,k} - u_{H,K}, \phi) + A'_{h,k}[u_{H,K}](u_{H,K} - u_{2G}, \phi) \\
&= A'_{h,k}[u_{H,K}](u_{h,k} - u_{H,K}, \phi) + A_{h,k}(u_{H,K}, \phi) - F_{h,k}(\phi) \\
&= A'_{h,k}[u_{H,K}](u_{h,k} - u_{H,K}, \phi) + A_{h,k}(u_{H,K}, \phi) - A_{h,k}(u_{h,k}, \phi) \\
&= -\mathcal{Q}(u_{H,K}, u_{h,k}, \phi).
\end{aligned}$$

Applying Lemma 5.5, Lemma 5.6, noting that $k^{3/2} \geq K^{3/2} \geq 1$, and the *a priori* bound for the standard IP DGFEM, cf. Lemma 3.2, gives

$$\begin{aligned}
\|u_{h,k} - u_{2G}\|_{h,k} &\leq Ck^2 h^{-1} \Big(1 + \|\nabla u_{h,k}\|_{L^\infty(\Omega)} + \|\nabla u_{H,K}\|_{L^\infty(\Omega)} \Big) \|u_{h,k} - u_{H,K}\|_{h,k}^2 \\
&\leq Ck^2 h^{-1} \Big(1 + k^{3/2} + K^{3/2} \Big) \Big(\|u - u_{h,k}\|_{h,k}^2 + \|u - u_{H,K}\|_{h,k}^2 \Big) \\
&\leq Ck^{7/2} h^{-1} \left(\frac{h^{2r-2}}{k^{2s-3}} \|u\|_{H^s(\Omega)}^2 + \frac{H^{2R-2}}{K^{2s-3}} \|u\|_{H^s(\Omega)}^2 \right).
\end{aligned}$$

Noting that $h \leq H$ and $k \geq K$ completes the proof of the first bound (5.5). To prove the second inequality (5.6), we first employ the triangle inequality

$$\|u - u_{2G}\|_{h,k} \leq \|u - u_{h,k}\|_{h,k} + \|u_{h,k} - u_{2G}\|_{h,k} .$$

Thereby, applying Lemma 3.2, together with the bound (5.5), completes the proof of Theorem 5.3.

5.3 *A Posteriori* Error Analysis

In this section, we state and prove an *a posteriori* error bound for the two-grid IP DGFEM defined by (5.3)–(5.4). Let us denote by Π_{κ,k_κ} the L^2-projection onto $V(\mathcal{T}_h, \boldsymbol{k})$. Then, we state the following upper bound.

Theorem 5.7. *Let $u \in H_0^1(\Omega)$ be the analytical solution of (3.1)–(3.2), $u_{H,K} \in V(\mathcal{T}_H, \boldsymbol{K})$ and $u_{2G} \in V(\mathcal{T}_h, \boldsymbol{k})$ the numerical approximations obtained from (5.3) and (5.4), respectively; then, the following hp-*a posteriori *error bound holds*

$$\|u - u_{2G}\|_{h,k} \leq C_7 \left(\sum_{\kappa \in \mathcal{T}_h} \left(\eta_\kappa^2 + \xi_\kappa^2\right) + \sum_{\kappa \in \mathcal{T}_h} h_\kappa^2 k_\kappa^{-2} \|f - \Pi_{\kappa,k_\kappa} f\|_{L^2(\kappa)}^2 \right)^{1/2}, \tag{5.8}$$

with a constant $C_7 > 0$, which is independent of $\boldsymbol{h}$, $\boldsymbol{H}$, $\boldsymbol{k}$ and $\boldsymbol{K}$. Here, for $\kappa \in \mathcal{T}_h$,

$$\begin{aligned}
\eta_\kappa^2 &= h_\kappa^2 k_\kappa^{-2} \|\Pi_{\kappa,k_\kappa} f + \nabla \cdot (\mu(|\nabla u_{H,K}|)\nabla u_{2G})\|_{L^2(\kappa)}^2 \\
&\quad + h_\kappa k_\kappa^{-1} \|[\![\mu(|\nabla u_{H,K}|)\nabla u_{2G}]\!]\|_{L^2(\partial\kappa\setminus\Gamma)}^2 + \gamma^2 h_\kappa^{-1} k_\kappa^3 \|[\![u_{2G}]\!]\|_{L^2(\partial\kappa)}^2 , \\
\xi_\kappa^2 &= \|(\mu(|\nabla u_{H,K}|) - \mu(|\nabla u_{2G}|))\nabla u_{2G}\|_{L^2(\kappa)}^2 \\
&\quad + \left\| \left(\mu'_{\nabla u}(|\nabla u_{H,K}|) \cdot (\nabla u_{2G} - \nabla u_{H,K})\right) \nabla u_{H,K} \right\|_{L^2(\kappa)}^2 \\
&\quad + h_\kappa k_\kappa^{-1} \left\| \left(\mu'_{\nabla u}(|\nabla u_{H,K}|) \cdot (\nabla u_{2G} - \nabla u_{H,K})\right) \nabla u_{H,K} \right\|_{L^2(\partial\kappa)}^2 ,
\end{aligned}$$

and Π_{κ,k_κ} denotes the (elementwise) L^2-projection onto $V(\mathcal{T}_h, \boldsymbol{k})$.

5.3.1 Proof of Theorem 5.7

The proof of this theorem follows in an analogous manner to the proof for the *a posteriori* bound, Theorem 3.4, of the two-grid method from Chapter 3; cf. Section 3.4. We note that as the fine mesh partition $\mathcal{T}_h$ of Ω may contain hanging nodes, we create an 1-irregular auxiliary mesh $\mathcal{T}_{\widetilde{h}}$, as outlined in Section 2.1.2, with corresponding DGFEM finite element space $V(\mathcal{T}_{\widetilde{h}}, \widetilde{\boldsymbol{k}})$ and polynomial degree vector $\widetilde{\boldsymbol{k}}$ such that $V(\mathcal{T}_h, \boldsymbol{k}) \subseteq V(\mathcal{T}_{\widetilde{h}}, \widetilde{\boldsymbol{k}})$; cf. Section 3.4.1.

As in Section 3.4.1 we decompose the DGFEM space $V(\mathcal{T}_{\widetilde{h}}, \widetilde{\boldsymbol{k}})$ into two orthogonal subspaces, cf. Karakashian & Pascal [131]: a conforming part $\left[V(\mathcal{T}_{\widetilde{h}}, \widetilde{\boldsymbol{k}})\right]^c = V(\mathcal{T}_{\widetilde{h}}, \widetilde{\boldsymbol{k}}) \cap H_0^1(\Omega)$, and a nonconforming part $\left[V(\mathcal{T}_{\widetilde{h}}, \widetilde{\boldsymbol{k}})\right]^\perp$ defined as the orthogonal complement of $\left[V(\mathcal{T}_{\widetilde{h}}, \widetilde{\boldsymbol{k}})\right]^c$ in $V(\mathcal{T}_{\widetilde{h}}, \widetilde{\boldsymbol{k}})$. The DGFEM solution u_{2G} obtained by (5.3)–(5.4) is split accordingly,

$$u_{2G} = u_{2G}^c + u_{2G}^\perp,$$

where $u_{2G}^c \in \left[V(\mathcal{T}_{\widetilde{h}}, \widetilde{\boldsymbol{k}})\right]^c$ and $u_{2G}^\perp \in \left[V(\mathcal{T}_{\widetilde{h}}, \widetilde{\boldsymbol{k}})\right]^\perp$. We can define the error in the solution obtained by (5.3)–(5.4) as

$$e_{2G} = u - u_{2G},$$

and let

$$e_{2G}^c = u - u_{2G}^c \in H_0^1(\Omega).$$

From the definition of the norm and applying (3.5) we have that

$$C_2 \left\| e_{2G} \right\|_{h,k}^2 \leq |T_1| + |T_2| + |T_3| + |T_4|, \tag{5.9}$$

where

$$T_1 = \sum_{\widetilde{\kappa} \in \mathcal{T}_{\widetilde{h}}} \int_{\widetilde{\kappa}} (\mu(|\nabla u|)\nabla u - \mu(|\nabla u_{H,K}|)\nabla u_{2G}) \cdot \nabla e_{2G}^c \, \mathrm{d}\boldsymbol{x},$$

$$T_2 = -\sum_{\widetilde{\kappa} \in \mathcal{T}_{\widetilde{h}}} \int_{\widetilde{\kappa}} (\mu(|\nabla u|)\nabla u - \mu(|\nabla u_{2G}|)\nabla u_{2G}) \cdot \nabla u_{2G}^\perp \, \mathrm{d}\boldsymbol{x}$$

$$T_3 = C_2 \sum_{F\in\mathcal{F}_h} \int_F \sigma_{h,k} |[\![e_{2G}]\!]|^2 \,\mathrm{d}s,$$
$$T_4 = \sum_{\widetilde{\kappa}\in\mathcal{T}_{\widetilde{h}}} \int_{\widetilde{\kappa}} (\mu(|\nabla u_{H,K}|)\nabla u_{2G} - \mu(|\nabla u_{2G}|)\nabla u_{2G}) \cdot \nabla e_{2G}^c \,\mathrm{d}\boldsymbol{x};$$

cf. (3.25).

We first consider the term T_1, noting the equivalence of the integrals on the fine mesh $\mathcal{T}_h$ and the conforming mesh $\mathcal{T}_{\widetilde{h}}$, then by integration by parts:

$$\begin{aligned} T_1 &= -\sum_{\kappa\in\mathcal{T}_h} \int_\kappa \nabla\cdot(\mu(|\nabla u|)\nabla u) e_{2G}^c \,\mathrm{d}\boldsymbol{x} - \sum_{\kappa\in\mathcal{T}_h} \int_\kappa \mu(|\nabla u_{H,K}|)\nabla u_{2G}\cdot\nabla e_{2G}^c \,\mathrm{d}\boldsymbol{x} \\ &= \sum_{\kappa\in\mathcal{T}_h} \int_\kappa f e_{2G}^c \,\mathrm{d}\boldsymbol{x} - \sum_{\kappa\in\mathcal{T}_h} \int_\kappa \mu(|\nabla u_{H,K}|)\nabla u_{2G}\cdot\nabla e_{2G}^c \,\mathrm{d}\boldsymbol{x}. \end{aligned}$$

Letting $v_{h,k} \in V(\mathcal{T}_h, \boldsymbol{k})$ be the elementwise interpolant of e_{2G}^c satisfying Lemma 3.6 then by (2.3), (5.4), integration by parts and the fact that $[\![e_{2G}^c]\!] = 0$, since $e_{2G}^c \in H_0^1(\Omega)$, it follows that

$$\begin{aligned} T_1 &= \sum_{\kappa\in\mathcal{T}_h} \int_\kappa (f + \nabla\cdot(\mu(|\nabla u_{H,K}|)\nabla u_{2G}))\,(e_{2G}^c - v_{h,k}) \,\mathrm{d}\boldsymbol{x} \\ &\quad - \sum_{F\in\mathcal{F}_h^{\mathcal{I}}} \int_F [\![\mu(|\nabla u_{H,K}|)\nabla u_{2G}]\!]\{\!\{e_{2G}^c - v_{h,k}\}\!\} \,\mathrm{d}s + \sum_{F\in\mathcal{F}_h} \int_F \sigma_{h,k}[\![u_{2G}]\!][\![v_{h,k}]\!] \,\mathrm{d}s \\ &\quad + \sum_{\kappa\in\mathcal{T}_h} \int_\kappa \left(\mu'_{\nabla u}(|\nabla u_{H,K}|)\cdot\nabla(u_{2G} - u_{H,K})\right)\nabla u_{H,K}\cdot\nabla v_{h,k} \,\mathrm{d}\boldsymbol{x} \\ &\quad - \sum_{F\in\mathcal{F}_h} \int_F \{\!\{\left(\mu'_{\nabla u}(|\nabla u_{H,K}|)\cdot\nabla(u_{2G} - u_{H,K})\right)\nabla u_{H,K}\}\!\}\cdot[\![v_{h,k}]\!] \,\mathrm{d}s. \end{aligned}$$

We note that this is similar to (3.26), for the case when $\theta = 0$, with the two additional terms

$$\begin{aligned} T_{1,A} \equiv \sum_{\kappa\in\mathcal{T}_h} \int_\kappa &\left(\mu'_{\nabla u}(|\nabla u_{H,K}|)\cdot\nabla(u_{2G} - u_{H,K})\right)\nabla u_{H,K}\cdot\nabla v_{h,k} \,\mathrm{d}\boldsymbol{x} \\ &- \sum_{F\in\mathcal{F}_h} \int_F \{\!\{\left(\mu'_{\nabla u}(|\nabla u_{H,K}|)\cdot\nabla(u_{2G} - u_{H,K})\right)\nabla u_{H,K}\}\!\}\cdot[\![v_{h,k}]\!] \,\mathrm{d}s. \end{aligned}$$

Thereby, we need only to bound two terms, since the other terms can be bound as in Section 3.4.3. We note that by applying the triangle inequality, the Cauchy-Schwarz inequality and the fact that $[\![e^c_{2G}]\!] = 0$ we get

$$|T_{1,A}| \leq \left(\sum_{\kappa \in \mathcal{T}_h} \left\| \left(\mu'_{\nabla u}(|\nabla u_{H,K}|) \cdot \nabla (u_{2G} - u_{H,K}) \right) \nabla u_{H,K} \right\|^2_{L^2(\kappa)} \right)^{1/2} \|\nabla_h v_{h,k}\|_{L^2(\Omega)}$$
$$+ C \left(\sum_{\kappa \in \mathcal{T}_h} \frac{h_\kappa}{k_\kappa} \left\| \{\!\{ \left(\mu'_{\nabla u}(|\nabla u_{H,K}|) \cdot \nabla (u_{2G} - u_{H,K}) \right) \nabla u_{H,K} \}\!\} \right\|^2_{L^2(\partial\kappa)} \right)^{1/2}$$
$$\times \left(\sum_{\kappa \in \mathcal{T}_h} \frac{h_\kappa}{k_\kappa} \|e^c_{2G} - v_{h,k}\|^2_{L^2(\partial\kappa)} \right)^{1/2}.$$

Exploiting Lemma 3.6 and Lemma 3.5 together with the bounds for the remaining terms in T_1, cf. (3.27), yields

$$|T_1| \leq C \left(\sum_{\kappa \in \mathcal{T}_h} (\eta^2_\kappa + \xi^2_\kappa) + \sum_{\kappa \in \mathcal{T}_h} h^2_\kappa k^{-2}_\kappa \|f - \Pi_{\kappa,k_\kappa} f\|^2_{L^2(\kappa)} \right)^{1/2} \|e_{2G}\|_{h,k}. \tag{5.10}$$

We note that the proof of T_2, T_3 and T_4 follows identically to Section 3.4.3. Combining the bounds for T_1, T_2 T_3 and T_4 from (5.10), (3.28), (3.29) and (3.30), respectively, into (5.9) completes the proof. □

5.4 Numerical Experiments

In this section, we perform numerical experiments to validate the *a priori* and *a posteriori* error bounds for the two-grid method for the quasilinear elliptic PDE (5.1)–(5.2) based on a single Newton iteration outlined in Theorem 5.3 and Theorem 5.7, respectively.

5.4.1 Validation of *A Priori* Error Bounds

We first validate the *a priori* bound stated in Theorem 5.3. To this end, we let $\Omega = (0,1)^2 \subset \mathbb{R}^2$ be the unit square, and define the nonlinear coefficient as

$$\mu(|\nabla u|) = 2 + \frac{1}{1 + |\nabla u|}.$$

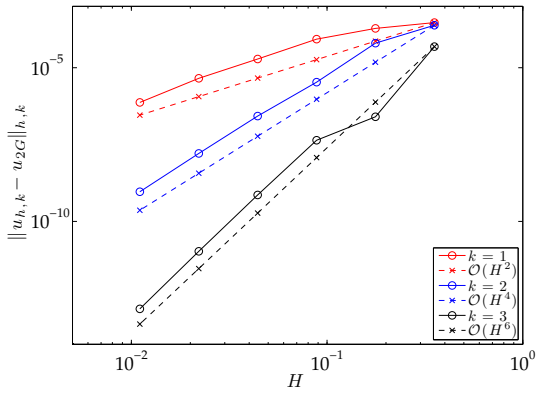

Figure 5.1: Plot of $\|u_{h,k} - u_{2G}\|_{h,k}$ against H, for a fixed fine mesh.

Furthermore, we select the right-hand forcing function f so that the analytical solution to (5.1)–(5.2) is given by

$$u(x, y) = x(1 - x)y(1 - y)(1 - 2y)\mathrm{e}^{-20(2x-1)^2}. \tag{5.11}$$

We consider the case when the fine mesh $\mathcal{T}_h$ is fixed as a 256×256 uniform square mesh and the coarse grid is uniformly refined. In Figure 5.1 we plot $\|u_{h,k} - u_{2G}\|_{h,k}$ against H in the case when the coarse and fine polynomial degrees $\boldsymbol{K}$ and $\boldsymbol{k}$, respectively, are both uniform and equal, i.e., $K_\kappa = k$ for all $\kappa \in \mathcal{T}_H$ and $k_\kappa = k$ for all $\kappa \in \mathcal{T}_h$; here, we consider the cases when $k = 1, 2, 3$. We clearly observe that the error $\|u_{h,k} - u_{2G}\|_{h,k}$ converges to zero at the rate $\mathcal{O}(H^{2k})$, as H tends to zero, for each fixed polynomial degree, which is in full agreement with (5.5). We note that we are unable to computationally verify the second bound (5.6) of Theorem 5.3 as it is not possible to select h and H, such that $V(\mathcal{T}_H, \boldsymbol{K}) \subseteq V(\mathcal{T}_h, \boldsymbol{k})$, so that the two parts of the bound converge at the same rate.

5.4.2 Validation of *A Posteriori* Error Bounds

We now present a series of numerical experiments in two-dimensional space to demonstrate the performance of the *a posteriori* error bound derived in Theorem 5.7. Here, we use the second mesh refinement strategy outlined in Algorithm 4.3 from Section 4.2. We set the interior penalty parameter constant γ to 10, and the steering parameters

λ_F and λ_C from Algorithm 4.3 both to 1 for all experiments. Throughout this section we compute the numerical solutions with $\theta = 0$, i.e. we employ the IIP scheme. The nonlinear equations are solved by employing a damped Newton method [147, Section 14.4]. The solution of the resulting set of linear equations, emanating from either the fine mesh or at each step of the iterative nonlinear solver, was computed using the direct Multifrontal Massively Parallel Solver (MUMPS) solver, see Amestoy *et al.* [2, 3, 4]. We also calculate the error bound stated in Theorem 5.7, cf. (5.8), by setting the constant C_7 equal to 1; cf. Becker *et al.* [26], Houston *et al.* [125].

For each example, as well as solving using the two-grid method based on a single Newton iteration, we also compute the standard IP DGFEM formulation (3.8) for comparison using a standard fixed fraction strategy with refinement and derefinement fractions are set to 25% and 5%, respectively. In order to determine the improvement in the computation time from using the two-grid method over the standard IP DGFEM, both algorithms were timed, on the same computer, using the FORTRAN `cpu_time` function [141, Section 8.16.2], which times purely the amount of CPU time and is, therefore, unaffected by other processes on the computer. We also present, for comparison, the results for the same experiment for the first two-grid method outlined in Chapter 3 using the mesh refinement strategy outlined in Section 4.2; cf. Section 4.3.

Example 1: Smooth Analytical Solution

In this example, we repeat the first numerical experiment from Section 4.3. Therefore, we let Ω be the unit square $(0,1)^2 \subset \mathbb{R}^2$ and use the nonlinear coefficient defined in (4.1). We select the right-hand forcing function f so that the analytical solution to (5.1)–(5.2) is given by (5.11).

In Figure 5.2(a) we present a comparison of the actual error measured in terms of the energy norm versus the square root of the number of degrees of freedom in the fine mesh finite element space $V(\mathcal{T}_h, \boldsymbol{k})$ for the standard DGFEM formulation (3.8), the first two-grid IP DGFEM (3.10)–(3.11) presented in Chapter 3 and the second two-grid IP DGFEM (5.3)–(5.4) outlined in this chapter. In this figure we perform both h- and

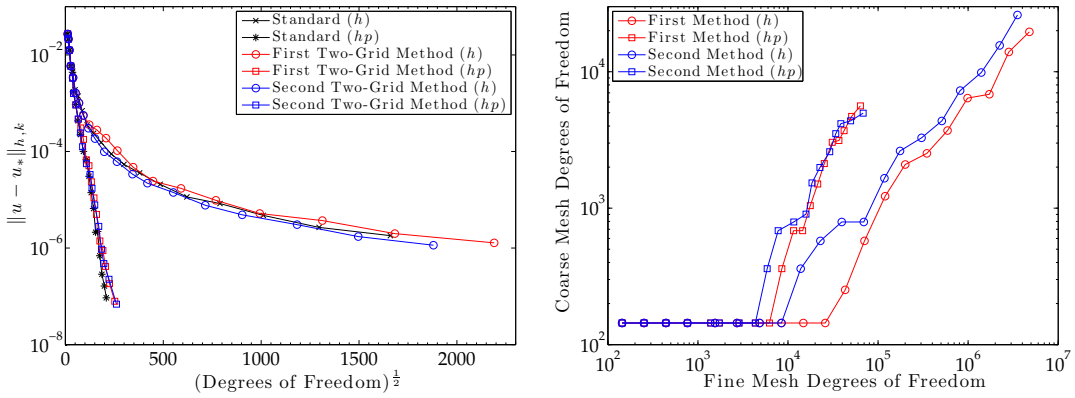

(a) *(b)*

Figure 5.2: Example 1. (a) Comparison of the error in the DG norm, for both the standard ($u_* = u_{h,k}$) and two-grid methods ($u_* = u_{2G}$), with respect to the number of degrees of freedom; (b) Comparison of number of degrees of freedom in the coarse and fine mesh at each iteration.

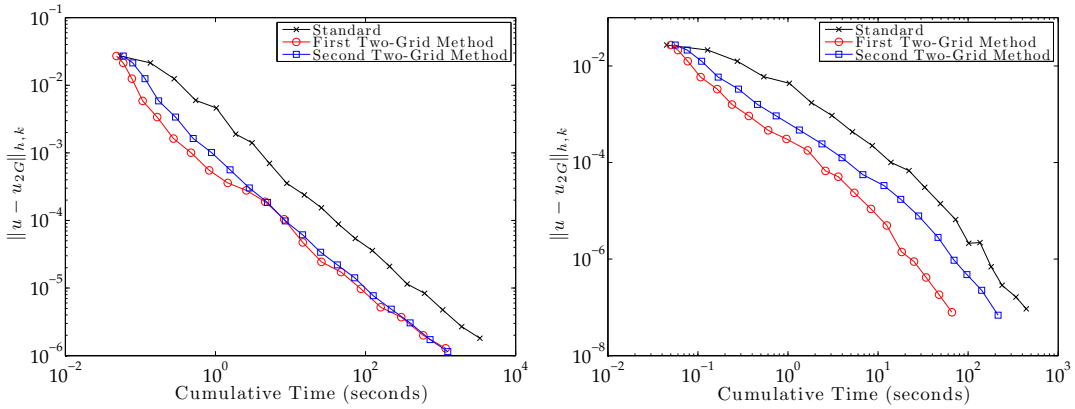

(a) h-refinement *(b) hp*-refinement

Figure 5.3: Example 1. Cumulative CPU timing of both the standard ($u_* = u_{h,k}$) and two-grid ($u_* = u_{2G}$) solvers compared to the error in the DG norm: (a) h-refinement; (b) hp-refinement.

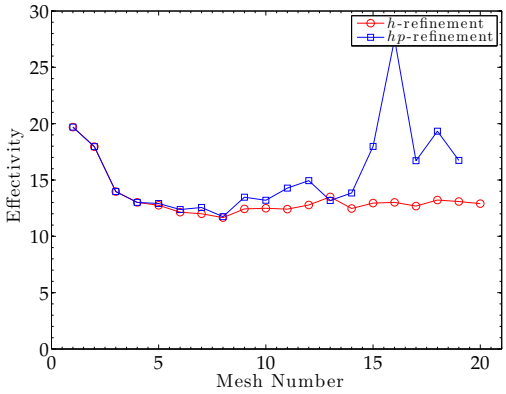

Figure 5.4: Example 1. Effectivity of the h- and hp-refinement using the two-grid method.

hp-adaptive mesh refinement for all schemes. Here, we can see that, for the problem at hand, the true error in the two-grid IP DGFEM based on a single Newton iteration is slightly lower than the first two-grid method and in the case of the h-refinement even slightly better than the standard method, when the same number of degrees of freedom in the two-grid fine mesh as in the mesh for the standard IP DGFEM are used. We note that the two-grid algorithm only performs the expensive nonlinear solve on a coarser grid which possesses far less degrees of freedom than the standard IP DGFEM. Indeed, in Figure 5.2(b) we compare, at each iteration of the automatic two-grid mesh refinement algorithm, the number of degrees of freedom used in both the coarse and fine finite element spaces. We note here that the two-grid method based on a single Newton iteration results in slighty more coarse/less fine degrees of freedom compared to the first two-grid method from Chapter 3. However, there are still considerable less degrees of freedom on the coarse grid and, therefore, we would expect the two-grid solver to be computationally less expensive.

We plot the magnitude of the true error, measured in the DGFEM norm, for the standard method and both two-grid methods, when both h- and hp-adaptive mesh refinement has been employed, compared to the cumulative CPU time required for the calculation of each numerical solution in Figure 5.3. Here, we can see that, for h-refinement the second refinement strategy based on a single Newton iteration is similar to the first two-grid method; however, for hp-refinement it appears to perform worse.

Finally, in order to validate the error bound derived in (5.7) we divide the computed error bound by the norm of the true error to derive the effectivity indices; we plot these indices in Figure 5.4. We note that from this graph we can see that the error bound overestimates the true error by a roughly consistent amount for both h- and hp-refinement, in the sense that the effectivity indices are roughly constant, with the odd exception.

In Figure 5.5 we present the fine and coarse h- and hp-refinement meshes after 13 mesh refinements, for the two-grid method based on a single Newton iteration. We note that we get similar results for the two-grid method based on a single Newton itera-

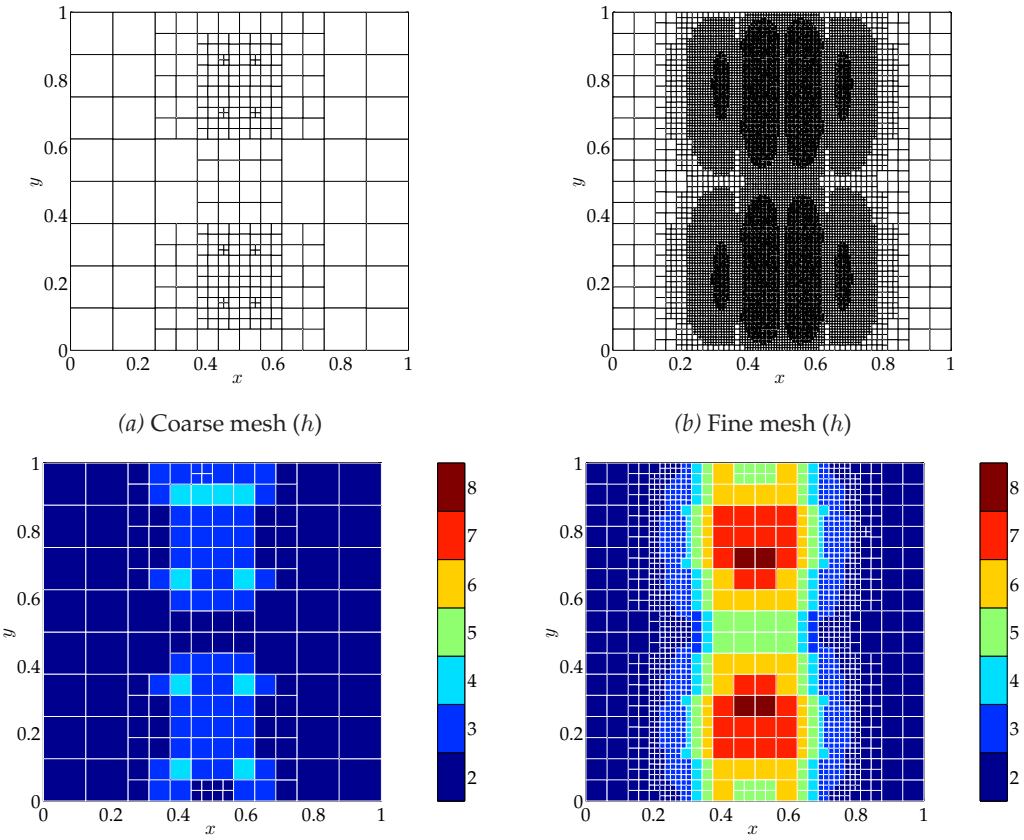

(a) Coarse mesh (h)

(b) Fine mesh (h)

(c) Coarse mesh (hp)

(d) Fine mesh (hp)

Figure 5.5: Example 1. Meshes after 13 h/hp-refinements.

tion as to the first two-grid method outlined in Chapter 3; cf. Figure 4.7 and Figure 4.8. In the h-refinement case all the fine grid refinement occurs around the interior and bases of the exponential 'hills' in the analytical solution with only a small amount of refinement taking place in the corresponding elements in the coarse mesh. In the hp-refinement case the fine mesh the h-refinement occurs mostly around the base of the hills with p-refinement in the interior of the hills, cf. also the coarse grid.

Example 2: Singular Solution

In this example, we repeat the second experiment from Section 4.3. Thereby, we let Ω denote the L-shaped domain $(-1,1)^2 \setminus [0,1) \times (-1,0] \subset \mathbb{R}^2$ and select the nonlinearity to be

$$\mu(\boldsymbol{x}, |\nabla u|) = 1 + \mathrm{e}^{-|\nabla u|^2}.$$

By writing (r, φ) to denote the system of polar coordinates, we choose the forcing function f and an inhomogeneous boundary condition such that the analytical solution to (5.1)–(5.2) is

$$u(r, \varphi) = r^{2/3} \sin\left(\frac{2}{3}\varphi\right).$$

Note that u is analytic in $\bar{\Omega} \setminus \{\mathbf{0}\}$, but ∇u is singular at the origin.

In Figure 5.6(a), we again present a comparison of the actual error measured in terms of the energy norm versus the third root of the number of degrees of freedom in the finite element space $V(\mathcal{T}_h, \boldsymbol{k})$ for the standard IP DGFEM formulation (3.8) and both two-grid IP DGFEM formulations, (3.10)–(3.11) and (5.3)–(5.4). We again note that the second two-grid method based on a single Newton iteration outlined in this chapter appears to give lower errors compared to the first two-grid method from Chapter 3 for the same number of degrees of freedom on the fine mesh and even outperforms the standard method in the h-adaptive case. We can see from Figure 5.6(b), which shows the number of degrees of freedom on the coarse grid compared to the number of degrees of freedom on the fine mesh at each iteration of the automatic mesh refinement algorithm, that the two-grid method outlined in this chapter results, generally, in slightly more coarse/less fine degrees of freedom compared to the first two-grid method.

In Figure 5.7 we plot the cumulative CPU time taken by the standard method and both two-grid methods, which is compared to the actual error, for both h- and hp-refinement strategies. Here, we see that the two methods perform broadly similarly, with the first two-grid method from Chapter 3 resulting in slightly less computation time initially; however, both methods appear to converge to the same computation time as refinement progresses.

We plot the effectivity indices of the two-grid method based on a single Newton iteration in Figure 5.8. Here we observe that in each case the effectivity indices tend towards a constant as the mesh is refined, although we note a higher constant for hp-refinement compared to h-refinement.

In Figure 5.9 we show the fine and coarse h- and hp-refinement meshes after 11

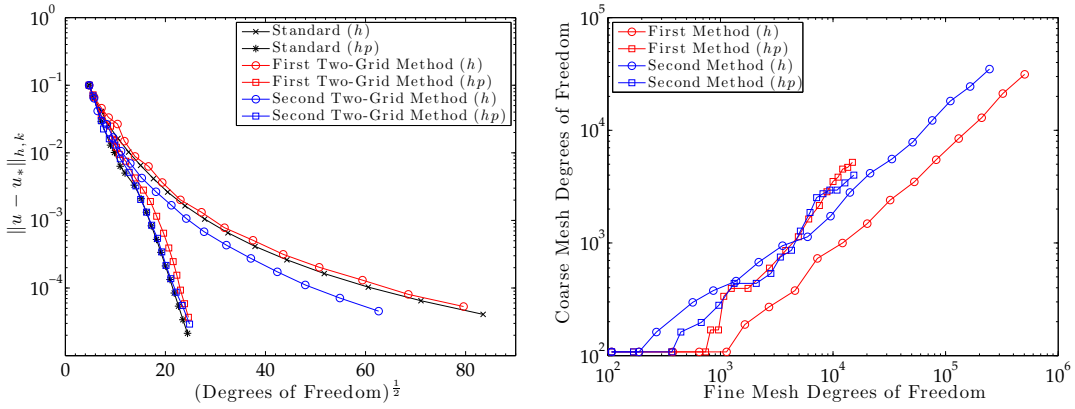

(a) *(b)*

Figure 5.6: Example 2. (a) Comparison of the error in the DG norm, for both the standard ($u_* = u_{h,k}$) and two-grid methods ($u_* = u_{2G}$), with respect to the number of degrees of freedom; (b) Comparison of number of degrees of freedom in the coarse and fine mesh at each iteration.

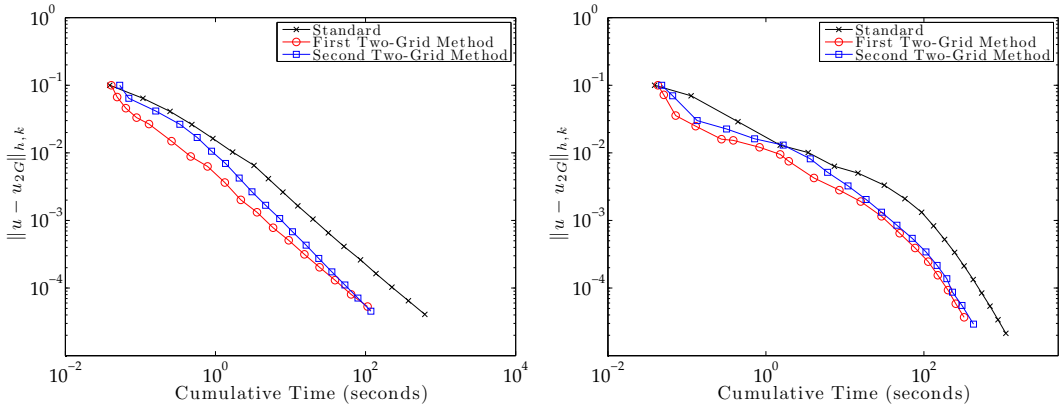

(a) h-refinement *(b) hp*-refinement

Figure 5.7: Example 2. Cumulative CPU timing of both the standard ($u_* = u_{h,k}$) and two-grid ($u_* = u_{2G}$) solvers compared to the error in the DG norm: (a) h-refinement; (b) hp-refinement.

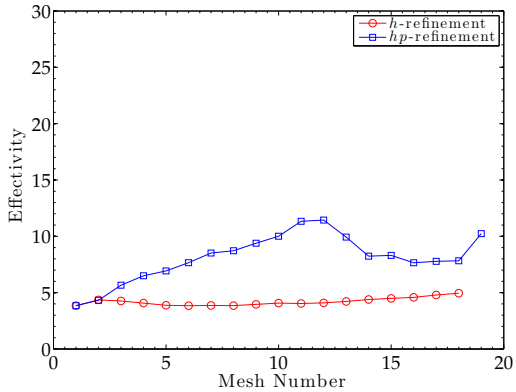

Figure 5.8: Example 2. Effectivity of the h- and hp-refinement using the two-grid method..

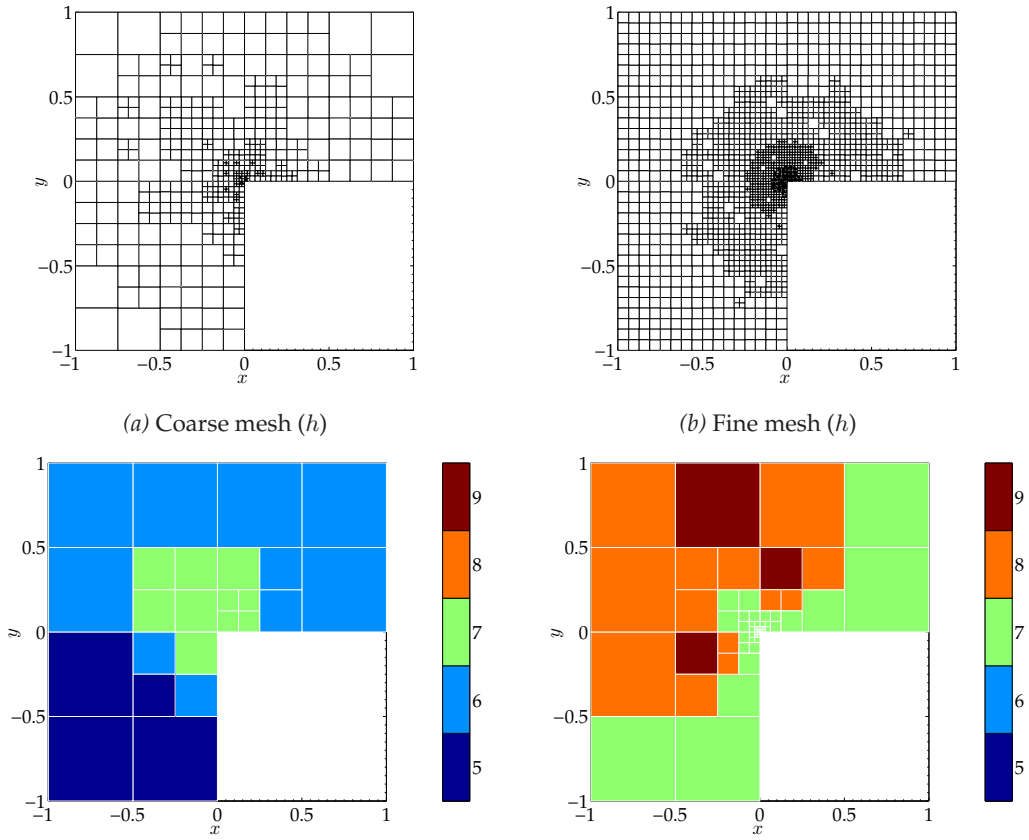

(a) Coarse mesh (h)

(b) Fine mesh (h)

(c) Coarse mesh (hp)

(d) Fine mesh (hp)

Figure 5.9: Example 2. Meshes after 11 h/hp-refinements.

mesh refinements, for the two-grid method based on a single Newton iteration. We note that the h-adaptive mesh refinement is concentrated around the singularity at the origin, as we would expect, for both the fine and coarse meshes. In the hp-refinement case, the h-refinement occurs mostly around the origin with high p-refinement in the rest of the domain in the fine mesh; whereas, the coarse appears to have done only minimal refinement around the origin. We note that the h-refinement strategy seems less refined compared to the first two-grid method from Chapter 3; cf. Figure 4.12. The hp-refinement strategy, however, seems less refined around the singularity but more p-refined in the rest of the mesh compared to the first two-grid method from Chapter 3; cf. Figure 4.13.

5.5 Summary

In this chapter, we have studied an alternative two-grid numerical approximation of a quasilinear elliptic problem of strongly monotone type by means of *hp*-interior penalty discontinuous Galerkin methods utilising a single step of a Newton iteration. We have derived both *a priori* and *a posteriori* bounds on the error with respect to the discontinuous Galerkin energy norm (3.9) and performed numerical experiments to validate them. We note that *a priori* this new method appears better than the original two-grid method proposed in Chapter 3 as it has a higher convergence rate. For *h*- and *hp*-adaptive mesh refinements, however, while the two-grid method based on a single Newton iteration gives lower errors compared to the number of degrees of freedom, when computation time is considered it does not appear to be much different and in some cases worse.

Having studied the two-grid methods for a simple scalar nonlinear problem we are now interested in extending the problem to more complicated nonlinear systems, such as a non-Newtonian fluid. However, in order to study the two-grid DGFEM method for this more complicated problem we first need to study the standard DGFEM method. Therefore, in the next chapter we study the *a priori* and *a posteriori* error bounds for a standard IP DGFEM for a non-Newtonian fluid.

CHAPTER 6

hp-Version Discontinuous Galerkin Finite Element Method for Non-Newtonian Fluid Flows

In this chapter we develop the *a priori* and *a posteriori* error analysis, with respect to a mesh-dependent energy norm, for the hp-version discontinuous Galerkin finite element discretisation of the quasi-Newtonian fluid flow problem:

$$-\nabla \cdot (\mu(\boldsymbol{x}, |\underline{e}(\boldsymbol{u})|)\,\underline{e}(\boldsymbol{u})) + \nabla p = \boldsymbol{f}(\boldsymbol{x}) \qquad \text{in } \Omega, \tag{6.1}$$

$$\nabla \cdot \boldsymbol{u} = 0 \qquad \text{in } \Omega, \tag{6.2}$$

$$\boldsymbol{u} = \boldsymbol{0} \qquad \text{on } \Gamma. \tag{6.3}$$

Here, $\Omega \subset \mathbb{R}^d$, $d = 2, 3$, is a bounded polygonal Lipschitz domain with boundary $\Gamma = \partial\Omega$, $\boldsymbol{f} \in \left[L^2(\Omega)\right]^d$ is a given source term, $\boldsymbol{u} = (u_1, \ldots, u_d)^\top$ is the velocity vector, $p \in L^2_0(\Omega)$ is the pressure and $\underline{e}(\boldsymbol{u})$ is the symmetric $d \times d$ strain tensor defined by

$$e_{ij}(\boldsymbol{u}) = \frac{1}{2}\left(\frac{\partial u_i}{\partial x_j} + \frac{\partial u_j}{\partial x_i}\right), \qquad i, j = 1 \ldots d.$$

We note that the work in this chapter forms parts of the published article [65].

Assumption D. We assume that for the nonlinearity $\mu \in C^0(\bar{\Omega} \times [0, \infty))$ there exists

positive constants m_μ and M_μ such that

$$m_\mu(t-s) \leq \mu(\boldsymbol{x},t)t - \mu(\boldsymbol{x},s)s \leq M_\mu(t-s), \qquad t \geq s \geq 0, \quad \boldsymbol{x} \in \bar{\Omega}. \tag{6.4}$$

From Barrett & Liu [16, Lemma 2.1], we note that as μ satisfies (6.4), there exists positive constants C_1 and C_2, such that for all $\underline{\tau}, \underline{\omega} \in \mathbb{R}^{d\times d}$ and all $\boldsymbol{x} \in \bar{\Omega}$,

$$|\mu(\boldsymbol{x}, |\underline{\tau}|)\underline{\tau} - \mu(\boldsymbol{x}, |\underline{\omega}|)\underline{\omega}| \leq C_1|\underline{\tau} - \underline{\omega}|, \tag{6.5}$$

$$C_2|\underline{\tau} - \underline{\omega}|^2 \leq (\mu(\boldsymbol{x}, |\underline{\tau}|)\underline{\tau} - \mu(\boldsymbol{x}, |\underline{\omega}|)\underline{\omega}) : (\underline{\tau} - \underline{\omega}). \tag{6.6}$$

For ease of notation we shall suppress the dependence of μ on $\boldsymbol{x}$ and write $\mu(t)$.

6.1 Weak Formulation

In this section, we present a weak formulation for (6.1)–(6.3) and prove it is well-posed.

6.1.1 Variational Form

By introducing the forms

$$A(\boldsymbol{u},\boldsymbol{v}) = \int_\Omega \mu(|\underline{e}(\boldsymbol{u})|)\underline{e}(\boldsymbol{u}) : \underline{e}(\boldsymbol{v})\,\mathrm{d}\boldsymbol{x}, \qquad B(\boldsymbol{v},q) = -\int_\Omega q\nabla\cdot\boldsymbol{v}\,\mathrm{d}\boldsymbol{x},$$

the standard weak formulation of the quasi-Newtonian problem (6.1)–(6.3) is given by: find $(\boldsymbol{u},p) \in \left[H_0^1(\Omega)\right]^d \times L_0^2(\Omega)$ such that

$$A(\boldsymbol{u},\boldsymbol{v}) + B(\boldsymbol{v},p) = \int_\Omega \boldsymbol{f}\cdot\boldsymbol{v}\,\mathrm{d}\boldsymbol{x}, \tag{6.7}$$

$$-B(\boldsymbol{u},q) = 0 \tag{6.8}$$

for all $(\boldsymbol{v},q) \in \left[H_0^1(\Omega)\right]^d \times L_0^2(\Omega)$. We note that the bilinear form $B(\cdot,\cdot)$ satisfies the following inf-sup condition: there exists a constant $\zeta > 0$ such that

$$\inf_{0\neq q\in L_0^2(\Omega)} \sup_{0\neq\boldsymbol{v}\in\left[H_0^1(\Omega)\right]^d} \frac{B(\boldsymbol{v},q)}{\|q\|_{L^2(\Omega)}\,\|\underline{e}(\boldsymbol{v})\|_{L^2(\Omega)}} \geq \zeta; \tag{6.9}$$

see, e.g., Brezzi & Fortin [46].

6.1.2 Well-Posedness

We will now show that the weak formulation (6.7)–(6.8) admits a unique solution in the given spaces. To this end, we first state the following general theorem.

Theorem 6.1. *Suppose that X and M are reflective Banach spaces. Furthermore, consider the forms $a(\cdot,\cdot) : X \times X \to \mathbb{R}$, $b(\cdot,\cdot) : X \times M \to \mathbb{R}$ and $l(\cdot) : X \to \mathbb{R}$ with*

(a) $a(\cdot,\cdot)$ is strongly monotone, hemicontinuous and coercive in the sense that,

- *$a(u, u-v) - a(v, u-v) \geq \|u-v\|_X \, \gamma(\|u-v\|_X)$ for all $u, v \in X$, where $\gamma : \mathbb{R}_{\geq 0} \to \mathbb{R}_{\geq 0}$ is a function with $\gamma(t) \to +\infty$ for $t \to +\infty$, and with $\gamma(t) = 0$ if and only if $t = 0$,*
- *$t \mapsto a(u + tv, w)$ is continuous on $[0, 1]$ for all $u, v, w \in X$ and*
- *$\sup\limits_{\|u\|_X \to +\infty} \dfrac{a(u,u)}{\|u\|_X} = +\infty$,*

respectively. Suppose further that the functional $v \mapsto a(w, v)$ is linear and continuous on X for any fixed $w \in X$.

(b) $b(\cdot,\cdot)$ is bilinear and continuous on $X \times M$; furthermore b is inf-sup stable in the sense that there exists a constant $\zeta > 0$ such that

$$\inf_{0 \neq q \in M} \sup_{0 \neq \boldsymbol{v} \in X} \frac{b(v,q)}{\|v\|_X \, \|q\|_M} \geq \zeta.$$

(c) $l(\cdot)$ is linear and continuous on X.

Then, there exists a unique solution $(u, p) \in X \times M$ to the variational equation

$$a(u,v) + b(v,p) - b(u,q) = l(v) \qquad \text{for all } (v,q) \in X \times M.$$

Proof. See Congreve *et al.* [65]. □

Theorem 6.2. *There exists exactly one solution $(\boldsymbol{u}, p) \in \left[H_0^1(\Omega)\right]^d \times L_0^2(\Omega)$ to the weak formulation (6.7)–(6.8).*

Proof. It can be shown that Theorem 6.1 holds for (6.7)–(6.8), cf. Congreve *et al.* [65]. □

6.2 hp-Version DGFEM

In this section we discuss the numerical approximation of the problem (6.1)–(6.3) based on employing the hp-version of the IP DGFEM. To this end, we use the notation from Section 2.1.2 to introduce the finite element spaces

$$\boldsymbol{V}(\mathcal{T}_h, \boldsymbol{k}) = \left\{ \boldsymbol{v} \in \left[L^2(\Omega)\right]^d : \boldsymbol{v}|_\kappa \circ T_\kappa \in \left[\mathcal{S}_{k_\kappa}(\widehat{\kappa})\right]^d, \kappa \in \mathcal{T}_h \right\}, \tag{6.10}$$

$$Q(\mathcal{T}_h, \boldsymbol{k}) = \left\{ q \in L^2_0(\Omega) : q|_\kappa \circ T_\kappa \in \mathcal{S}_{k_\kappa - 1}(\widehat{\kappa}), \kappa \in \mathcal{T}_h \right\}. \tag{6.11}$$

6.2.1 DGFEM Discretisation

For a partition $\mathcal{T}_h$ of Ω, with corresponding polynomial degree vector $\boldsymbol{k}$, the IP DGFEM formulation is defined as follows: find $(\boldsymbol{u}_{h,k}, p_{h,k}) \in \boldsymbol{V}(\mathcal{T}_h, \boldsymbol{k}) \times Q(\mathcal{T}_h, \boldsymbol{k})$ such that

$$A_{h,k}(\boldsymbol{u}_{h,k}, \boldsymbol{v}) + B_{h,k}(\boldsymbol{v}, p_{h,k}) = F_{h,k}(\boldsymbol{v}), \tag{6.12}$$

$$-B_{h,k}(\boldsymbol{u}_{h,k}, q) = 0 \tag{6.13}$$

for all $(\boldsymbol{v}, q) \in \boldsymbol{V}(\mathcal{T}_h, \boldsymbol{k}) \times Q(\mathcal{T}_h, \boldsymbol{k})$, where

$$\begin{aligned} A_{h,k}(\boldsymbol{u}, \boldsymbol{v}) = &\int_\Omega \mu\left(|\underline{e}_h(\boldsymbol{u})|\right) \underline{e}_h(\boldsymbol{u}) : \underline{e}_h(\boldsymbol{v}) \,\mathrm{d}\boldsymbol{x} - \sum_{F \in \mathcal{F}_h} \int_F \{\!\{\mu(|\underline{e}_h(\boldsymbol{u})|)\underline{e}_h(\boldsymbol{u})\}\!\} : \underline{[\![\boldsymbol{v}]\!]} \,\mathrm{d}s \\ &+ \theta \sum_{F \in \mathcal{F}_h} \int_F \{\!\{\mu(h_F^{-1}|\underline{[\![\boldsymbol{u}]\!]}|)\underline{e}_h(\boldsymbol{v})\}\!\} : \underline{[\![\boldsymbol{u}]\!]} \,\mathrm{d}s + \sum_{F \in \mathcal{F}_h} \int_F \sigma_{h,k} \underline{[\![\boldsymbol{u}]\!]} : \underline{[\![\boldsymbol{v}]\!]} \,\mathrm{d}s, \\ B_{h,k}(\boldsymbol{v}, q) = &-\int_\Omega q \nabla_h \cdot \boldsymbol{v} \,\mathrm{d}\boldsymbol{x} + \sum_{F \in \mathcal{F}_h} \int_F \{\!\{q\}\!\} [\![\boldsymbol{v}]\!] \,\mathrm{d}s \end{aligned}$$

and

$$F_{h,k}(\boldsymbol{v}) = \int_\Omega \boldsymbol{f} \cdot \boldsymbol{v} \,\mathrm{d}\boldsymbol{x}.$$

Here, $\underline{e}_h(\cdot)$ and ∇_h denote the elementwise strain tensor and gradient operator, respectively, and $\theta \in [-1, 1]$. The *interior penalty parameter* $\sigma_{h,k}$ is defined as

$$\sigma_{h,k} := \gamma \frac{k_F^2}{h_F}, \tag{6.14}$$

where $\gamma \geq 1$ is a constant, which must be chosen sufficiently large (independent of the local element sizes and the polynomial degree), see Theorem 6.4.

Remark 6.1. We note that the formulation (6.12)–(6.13) corresponds to the symmetric interior penalty (SIP) method when $\theta = -1$, the nonsymmetric interior penalty (NIP) method when $\theta = 1$ and the incomplete interior penalty method (IIP) when $\theta = 0$.

Moreover, we introduce the following *energy norms*

$$\|\boldsymbol{v}\|_{h,k}^2 = \|\underline{e}_h(\boldsymbol{v})\|_{L^2(\Omega)}^2 + \sum_{F \in \mathcal{F}_h} \int_F \sigma_{h,k} |\underline{[\![\boldsymbol{v}]\!]}|^2 \, \mathrm{d}s \tag{6.15}$$

and

$$\|(\boldsymbol{v}, q)\|_{\mathrm{DG}}^2 = \|\boldsymbol{v}\|_{h,k}^2 + \|q\|_{L^2(\Omega)}^2 . \tag{6.16}$$

Lemma 6.3. *There exists a constant $C_{\mathcal{K}} > 0$, independent of $\boldsymbol{h}$ and $\boldsymbol{k}$, such that*

$$\|\underline{e}_h(\boldsymbol{v})\|_{L^2(\Omega)}^2 \leq \|\nabla_h \boldsymbol{v}\|_{L^2(\Omega)}^2$$

and

$$\|\boldsymbol{v}\|_{L^2(\Omega)}^2 + \|\nabla_h \boldsymbol{v}\|_{L^2(\Omega)}^2 \leq C_{\mathcal{K}} \left(\|\underline{e}_h(\boldsymbol{v})\|_{L^2(\Omega)}^2 + \sum_{F \in \mathcal{F}_h} \int_F h_F^{-1} |\underline{[\![\boldsymbol{v}]\!]}|^2 \, \mathrm{d}s \right)$$

for all $\boldsymbol{v} \in H^1(\Omega, \mathcal{T}_h)$, where $H^1(\Omega, \mathcal{T}_h) = \left\{ \boldsymbol{v} \in \left[L^2(\Omega)\right]^d : \boldsymbol{v}|_\kappa \in \left[H^1(\kappa)\right]^d, \kappa \in \mathcal{T}_h \right\}$.

Proof. In order to proof the first bound we note that, as $\underline{e}(\boldsymbol{v}) = 1/2(\nabla \boldsymbol{v} + (\nabla \boldsymbol{v})^\top)$ and $\|\nabla_h \boldsymbol{v}\|_{L^2(\Omega)} = \left\| (\nabla_h \boldsymbol{v})^\top \right\|_{L^2(\Omega)}$,

$$\|\underline{e}_h(\boldsymbol{v})\|_{L^2(\Omega)} \leq \frac{1}{2} \|\nabla_h \boldsymbol{v}\|_{L^2(\Omega)} + \frac{1}{2} \left\| (\nabla_h \boldsymbol{v})^\top \right\|_{L^2(\Omega)} = \|\nabla_h \boldsymbol{v}\|_{L^2(\Omega)}$$

The proof of the second bound follows directly from the discrete Korn's inequality for

piecewise H^1 vector fields, see Brenner [43, 44]. □

6.2.2 Well-Posedness of the DGFEM Formulation

In this section we will prove that the DG formulation (6.12)–(6.13) admits a unique solution. To this end, we assume that the bilinear form $B_{h,k}(\cdot,\cdot)$ satisfies the following inf-sup condition:

$$\inf_{0\neq q\in Q(\mathcal{T}_h,\boldsymbol{k})}\sup_{\boldsymbol{v}\in\boldsymbol{V}(\mathcal{T}_h,\boldsymbol{k})}\frac{B_{h,k}(\boldsymbol{v},q)}{\|\boldsymbol{v}\|_{h,k}\,\|q\|_{L^2(\Omega)}}\geq\widehat{\zeta}k_{\max}^{-1}, \tag{6.17}$$

where $\widehat{\zeta}$ is a positive constant independent of $\boldsymbol{h}$ and $\boldsymbol{k}$. We note that this inf-sup condition holds

- for $k_\kappa\geq 2, \kappa\in\mathcal{T}_h$, or
- for $k\geq 1$ if $\mathcal{T}_h$ is conforming and $k_\kappa = k$ for all $\kappa\in\mathcal{T}_h$;

see Theorems 6.2 and 6.12, respectively, in Schötzau *et al.* [157].

Theorem 6.4. *Provided that the penalty parameter γ from (6.14) is chosen sufficiently large, there is exactly one solution $(\boldsymbol{u}_{h,k},p_{h,k})\in\boldsymbol{V}(\mathcal{T}_h,\boldsymbol{k})\times Q(\mathcal{T}_h,\boldsymbol{k})$ of the hp-DGFEM (6.12)–(6.13).*

Proof. We set

$$\mathcal{A}_{h,k}((\boldsymbol{u},p);(\boldsymbol{v},q)) = A_{h,k}(\boldsymbol{u},\boldsymbol{v}) + B_{h,k}(\boldsymbol{v},p) - B_{h,k}(\boldsymbol{u},q), \tag{6.18}$$

which allows the DGFEM defined in (6.12)–(6.13) to be written in the following compact form: find $(\boldsymbol{u}_{h,k},p_{h,k})\in\boldsymbol{V}(\mathcal{T}_h,\boldsymbol{k})\times Q(\mathcal{T}_h,\boldsymbol{k})$ such that

$$\mathcal{A}_{h,k}((\boldsymbol{u}_{h,k},p_{h,k});(\boldsymbol{v},q)) = F_{h,k}(\boldsymbol{v}) \tag{6.19}$$

for all $(\boldsymbol{v},q)\in\boldsymbol{V}(\mathcal{T}_h,\boldsymbol{k})\times Q(\mathcal{T}_h,\boldsymbol{k})$. We now check the conditions of Theorem 6.1 hold, with $l(\cdot)=F_{h,k}(\cdot)$, $X=\boldsymbol{V}(\mathcal{T}_h,\boldsymbol{k})$, with norm $\|\cdot\|_{h,k}$, and $M=Q(\mathcal{T}_h,\boldsymbol{k})$.

Proof of (a). Recalling (6.5) and Lemma 2.1 gives that

$$
\begin{aligned}
&|A_{h,k}(\boldsymbol{u},\boldsymbol{v}) - A_{h,k}(\boldsymbol{w},\boldsymbol{v})| \\
&\qquad \leq C_1 \left\|\underline{e}_h(\boldsymbol{u}-\boldsymbol{w})\right\|_{L^2(\Omega)} \left\|\underline{e}_h(\boldsymbol{v})\right\|_{L^2(\Omega)} \\
&\qquad\quad + C_1 \left(\sum_{F\in\mathcal{F}_h} \sigma_{h,k}^{-1} \left\|\{\!\{|\underline{e}_h(\boldsymbol{u}-\boldsymbol{w})|\}\!\}\right\|_{L^2(F)}^2\right)^{1/2} \left(\sum_{F\in\mathcal{F}_h} \sigma_{h,k} \left\|\underline{[\![\boldsymbol{v}]\!]}\right\|_{L^2(F)}^2\right)^{1/2} \\
&\qquad\quad + |\theta| C_1 \left(\sum_{F\in\mathcal{F}_h} \sigma_{h,k}^{-1} \left\|\{\!\{\underline{e}_h(\boldsymbol{v})\}\!\}\right\|_{L^2(F)}^2\right)^{1/2} \left(\sum_{F\in\mathcal{F}_h} \sigma_{h,k} \left\|\underline{[\![\boldsymbol{u}-\boldsymbol{w}]\!]}\right\|_{L^2(F)}^2\right)^{1/2} \\
&\qquad\quad + \left(\sum_{F\in\mathcal{F}_h} \sigma_{h,k} \left\|\underline{[\![\boldsymbol{u}-\boldsymbol{w}]\!]}\right\|_{L^2(F)}^2\right)^{1/2} \left(\sum_{F\in\mathcal{F}_h} \sigma_{h,k} \left\|\underline{[\![\boldsymbol{v}]\!]}\right\|_{L^2(F)}^2\right)^{1/2} \\
&\qquad \leq (C_1 C_T^{1/2} \gamma^{-1/2} + \max(1, C_1)) \left\|\boldsymbol{u}-\boldsymbol{w}\right\|_{h,k} \left\|\boldsymbol{v}\right\|_{h,k},
\end{aligned}
$$

which proves that the form $A_{h,k}(\cdot,\cdot)$ is Lipschitz-continuous in its first argument; hence, hemicontinuity follows. To prove the form $A_{h,k}(\cdot,\cdot)$ is strongly monotone we apply (6.5)–(6.6), Lemma 2.1 and the trivial inequality $2ab \leq a^2 + b^2$:

$$
\begin{aligned}
&A_{h,k}(\boldsymbol{u},\boldsymbol{u}-\boldsymbol{v}) - A_{h,k}(\boldsymbol{v},\boldsymbol{u}-\boldsymbol{v}) \\
&\qquad \geq C_2 \left\|\underline{e}_h(\boldsymbol{u}-\boldsymbol{v})\right\|_{L^2(\Omega)}^2 + \sum_{F\in\mathcal{F}_h} \int_F \sigma_{h,k} |\underline{[\![\boldsymbol{u}-\boldsymbol{v}]\!]}|^2 \,\mathrm{d}s \\
&\qquad\quad - C_1(1+|\theta|) C_T^{1/2} \gamma^{-1/2} \left\|\underline{e}_h(\boldsymbol{u}-\boldsymbol{v})\right\|_{L^2(\Omega)} \left(\sum_{F\in\mathcal{F}_h} \int_F \sigma_{h,k} |\underline{[\![\boldsymbol{u}-\boldsymbol{v}]\!]}|^2 \,\mathrm{d}s\right)^{1/2} \\
&\qquad \geq C_2 \left(1 - \frac{(1+|\theta|)^2 C_1^2 C_T}{2\gamma C_2}\right) \left\|\underline{e}_h(\boldsymbol{u}-\boldsymbol{v})\right\|_{L^2(\Omega)}^2 + \frac{1}{2} \sum_{F\in\mathcal{F}_h} \int_F \sigma_{h,k} |\underline{[\![\boldsymbol{u}-\boldsymbol{v}]\!]}|^2 \,\mathrm{d}s.
\end{aligned}
$$

Selecting $\gamma \geq (1+|\theta|)^2 C_1^2 C_T C_2^{-1}$ we deduce that

$$
A_{h,k}(\boldsymbol{u},\boldsymbol{u}-\boldsymbol{v}) - A_{h,k}(\boldsymbol{v},\boldsymbol{u}-\boldsymbol{v}) \geq \frac{1}{2} \min(C_2, 1) \left\|\boldsymbol{u}-\boldsymbol{v}\right\|_{h,k}^2, \tag{6.20}
$$

which proves that $A_{h,k}(\cdot,\cdot)$ is strongly monotone. Coercivity follows trivially by setting $\boldsymbol{v} = \boldsymbol{0}$. We note that $\boldsymbol{v} \mapsto A_{h,k}(\boldsymbol{w},\boldsymbol{v})$ is linear and continuous for a fixed $\boldsymbol{w} \in \boldsymbol{V}(\mathcal{T}_h, \boldsymbol{k})$.

Proof of (b). To prove the continuity of the bilinear form $B_{h,k}(\cdot,\cdot)$ we apply Lemma 2.1, noting that $\|\nabla_h \cdot \boldsymbol{v}\|^2_{L^2(\Omega)} \leq d\,\|\underline{e}_h(\boldsymbol{v})\|^2_{L^2(\Omega)}$ for all $\boldsymbol{v} \in \boldsymbol{V}(\mathcal{T}_h, \boldsymbol{k})$ and $\|[\![\boldsymbol{v}]\!]\|_{L^2(F)} \leq \left\|\underline{[\![\boldsymbol{v}]\!]}\right\|_{L^2(F)}$ for all $\boldsymbol{v} \in \boldsymbol{V}(\mathcal{T}_h, \boldsymbol{k})$ and $F \in \mathcal{F}_h$; hence,

$$
\begin{aligned}
B_{h.k}(\boldsymbol{v}, q) &\leq \|q\|_{L^2(\Omega)}\,\|\nabla_h \cdot \boldsymbol{v}\|_{L^2(\Omega)} \\
&\quad + \left(\sum_{F\in\mathcal{F}_h} \sigma^{-1}_{h,k}\,\|\{\!\{q\}\!\}\|^2_{L^2(F)}\right)^{1/2} \left(\sum_{F\in\mathcal{F}_h} \sigma_{h,k}\,\|[\![\boldsymbol{v}]\!]\|^2_{L^2(F)}\right)^{1/2} \\
&\leq d^{1/2}\,\|q\|_{L^2(\Omega)}\,\|\boldsymbol{v}\|_{h,k} + C_T^{1/2}\gamma^{-1/2}\,\|q\|_{L^2(\Omega)} \left(\sum_{F\in\mathcal{F}_h} \sigma_{h,k}\left\|\underline{[\![\boldsymbol{v}]\!]}\right\|^2_{L^2(F)}\right)^{1/2} \\
&\leq \sqrt{2}\max(d^{1/2}, C_T^{1/2}\gamma^{-1/2})\,\|q\|_{L^2(\Omega)}\,\|\boldsymbol{v}\|_{h,k}\,,
\end{aligned}
$$

as required. The inf-sup condition (6.17) completes the proof of the validity of hypothesis (b) in Theorem 6.1.

Proof of (c). Upon application of Lemma 6.3 we have

$$
\begin{aligned}
F_{h,k}(\boldsymbol{v}) = \int_\Omega \boldsymbol{f}\cdot\boldsymbol{v}\,\mathrm{d}\boldsymbol{x} &\leq \|\boldsymbol{f}\|_{L^2(\Omega)}\,\|\boldsymbol{v}\|_{L^2(\Omega)} \\
&\leq C_{\mathcal{K}}\,\|\boldsymbol{f}\|_{L^2(\Omega)} \left(\|\nabla_h\boldsymbol{v}\|^2_{L^2(\Omega)} + \sum_{F\in\mathcal{F}_h}\int_F h^{-1}|\underline{[\![\boldsymbol{v}]\!]}|^2\right)^{1/2} \\
&\leq C_F\,\|(\boldsymbol{v}, q)\|_{\mathrm{DG}}
\end{aligned}
$$

where C_F depends on the forcing function $\boldsymbol{f}$; hence, $F_{h,k}(\cdot)$ is continuous.

This completes the proof. □

6.3 *A Priori* Error Analysis

In this section, we derive an *a priori* error bound for the *hp*-DGFEM defined by (6.12)–(6.13). To this end, we state the following bound.

Theorem 6.5. *Let the penalty parameter γ be sufficiently large and the analytical solution $(\boldsymbol{u}, p)$ of (6.1)–(6.3) belong to $\left[C^1(\Omega)\cap H^2(\Omega)\right]^d \times [C^0(\Omega)\cap H^1(\Omega)]$, where $\boldsymbol{u}|_\kappa \in [H^{s_\kappa}(\kappa)]^d$,*

$p|_\kappa \in H^{s_\kappa-1}(\kappa)$, $s_\kappa \geq 2$, for all $\kappa \in \mathcal{T}_h$. Then, provided the discrete inf-sup condition (6.17) is valid, the DGFEM solution $(\boldsymbol{u}_{h,k}, p_{h,k})$ defined by (6.12)–(6.13) satisifies the error bound

$$\|(\boldsymbol{u}-\boldsymbol{u}_{h,k}, p-p_{h,k})\|_{\mathrm{DG}}^2 \leq C_8 k_{\max}^4 \sum_{\kappa\in\mathcal{T}_h} \left(\frac{h_\kappa^{2r_\kappa-2}}{k_\kappa^{2s_\kappa-3}} \|\boldsymbol{u}\|_{H^{s_\kappa}(\kappa)}^2 + \frac{h_\kappa^{2r_\kappa-2}}{k_\kappa^{2s_\kappa-2}} \|p\|_{H^{s_\kappa-1}(\kappa)}^2 \right),$$

with $1 \leq r_\kappa \leq \min(s_\kappa, k_\kappa+1), k_\kappa \geq 1$, for all $\kappa \in \mathcal{T}_h$, where the constant $C_8 > 0$ is independent of the mesh size and polynomial degree.

6.3.1 Proof of Theorem 6.5

In this section, we prove the *a priori* error bound stated in Theorem 6.5. To this end, it is first necessary to state the following *discrete inf-sup stability* result for the form $\mathcal{A}_{h,k}((\boldsymbol{u},p);(\boldsymbol{v},q))$ defined in (6.18).

Lemma 6.6. *Let the penalty parameter γ be sufficiently large then there exists a positive constant C_D, independent of $\boldsymbol{h}$ and $\boldsymbol{k}$, such that for any $(\boldsymbol{u},p),(\boldsymbol{w},r) \in \boldsymbol{V}(\mathcal{T}_h,\boldsymbol{k}) \times Q(\mathcal{T}_h,\boldsymbol{k})$, there exists $(\boldsymbol{v},q) \in \boldsymbol{V}(\mathcal{T}_h,\boldsymbol{k}) \times Q(\mathcal{T}_h,\boldsymbol{k})$ with*

$$\mathcal{A}_{h,k}((\boldsymbol{u},p);(\boldsymbol{v},q)) - \mathcal{A}_{h,k}((\boldsymbol{w},r);(\boldsymbol{v},q)) \geq C_D k_{\max}^{-2} \|(\boldsymbol{u}-\boldsymbol{w},p-r)\|_{DG},$$
$$\|(\boldsymbol{v},q)\|_{DG} \leq 1,$$

where C_D is a positive constant dependent on the constants ζ, C_1, C_2, C_T and γ from (6.17), (6.5), (6.6), Lemma 2.1 and (6.14), respectively.

Proof. Let $p-r \in Q(\mathcal{T}_h,\boldsymbol{k})$, then, from the discrete inf-sup condition (6.17) there exists $\boldsymbol{\xi} \in \boldsymbol{V}(\mathcal{T}_h,\boldsymbol{k})$ such that

$$-\int_\Omega (p-r)\nabla\cdot\boldsymbol{\xi}\,\mathrm{d}\boldsymbol{x} + \sum_{F\in\mathcal{F}_h}\int_F \{\!\{p-r\}\!\}[\![\boldsymbol{\xi}]\!]\,\mathrm{d}s \geq \widehat{\zeta} k_{\max}^{-1} \|p-r\|_{L^2(\Omega)}^2, \tag{6.21}$$

$$\|\boldsymbol{\xi}\|_{h,k} \leq \|p-r\|_{L^2(\Omega)}; \tag{6.22}$$

cf. Wihler & Wirz [174]. Now, we choose

$$\hat{\boldsymbol{v}} = \alpha(\boldsymbol{u}-\boldsymbol{w}) + \beta k_{\max}^{-1}\boldsymbol{\xi}, \qquad \hat{q} = \alpha(p-r),$$

with positive constants α and β, which will be selected later. Hence, we get that,

$$\mathcal{A}_{h,k}((\boldsymbol{u},p);(\hat{\boldsymbol{v}},\hat{q}))-\mathcal{A}_{h,k}((\boldsymbol{w},r);(\hat{\boldsymbol{v}},\hat{q}))=\alpha T_1+\beta k_{\max}^{-1}T_2, \tag{6.23}$$

where

$$\begin{aligned}T_1&=A_{h,k}(\boldsymbol{u},\boldsymbol{u}-\boldsymbol{w})-A_{h,k}(\boldsymbol{w},\boldsymbol{u}-\boldsymbol{w}),\\ T_2&=A_{h,k}(\boldsymbol{u},\boldsymbol{\xi})-A_{h,k}(\boldsymbol{w},\boldsymbol{\xi})+B_{h,k}(\boldsymbol{\xi},p-r).\end{aligned}$$

From (6.20) we have that

$$T_1\geq\frac{1}{2}\min(C_2,1)\left\|\boldsymbol{u}-\boldsymbol{w}\right\|_{h,k}^2,$$

providing that we select $\gamma\geq(1+|\theta|)^2C_1^2C_TC_2^{-1}$. We start bounding T_2 by applying (6.5) and (6.21) to get that

$$\begin{aligned}T_2\geq&-C_1\left\|\underline{e}_h(\boldsymbol{u}-\boldsymbol{w})\right\|_{L^2(\Omega)}\left\|\underline{e}_h(\boldsymbol{\xi})\right\|_{L^2(\Omega)}-C_1\sum_{F\in\mathcal{F}_h}\left\|\{\!\{|\underline{e}_h(\boldsymbol{u}-\boldsymbol{w})|\}\!\}\right\|_{L^2(F)}\left\|\underline{[\![\boldsymbol{\xi}]\!]}\right\|_{L^2(F)}\\&-C_1|\theta|\sum_{F\in\mathcal{F}_h}\left\|\{\!\{|\underline{e}_h(\boldsymbol{\xi})|\}\!\}\right\|_{L^2(F)}\left\|\underline{[\![\boldsymbol{u}-\boldsymbol{w}]\!]}\right\|_{L^2(F)}\\&-\sum_{F\in\mathcal{F}_h}\sigma_{h,k}\left\|\underline{[\![\boldsymbol{u}-\boldsymbol{w}]\!]}\right\|_{L^2(F)}\left\|\underline{[\![\boldsymbol{\xi}]\!]}\right\|_{L^2(F)}+\widehat{\zeta}k_{\max}^{-1}\left\|p-r\right\|_{L^2(\Omega)}^2.\end{aligned}$$

Applying the arithmetic-geometric mean inequality, introducing a positive constant λ, gives

$$\begin{aligned}T_2\geq&-\frac{C_1}{2}\left(\frac{2\lambda k_{\max}}{\hat{\zeta}}\left\|\underline{e}_h(\boldsymbol{u}-\boldsymbol{w})\right\|_{L^2(\Omega)}^2+\frac{\widehat{\zeta}}{2\lambda k_{\max}}\left\|\underline{e}_h(\boldsymbol{\xi})\right\|_{L^2(\Omega)}^2\right)\\&-\frac{C_1}{2}\sum_{F\in\mathcal{F}_h}\left(\frac{2\lambda k_{\max}}{\widehat{\zeta}}\sigma_{h,k}^{-1}\left\|\{\!\{|\underline{e}_h(\boldsymbol{u}-\boldsymbol{w})|\}\!\}\right\|_{L^2(F)}^2+\frac{\widehat{\zeta}}{2\lambda k_{\max}}\sigma_{h,k}\left\|\underline{[\![\boldsymbol{\xi}]\!]}\right\|_{L^2(F)}^2\right)\\&-\frac{C_1}{2}\sum_{F\in\mathcal{F}_h}\left(\frac{\widehat{\zeta}\gamma}{2\lambda k_{\max}C_T}\sigma_{h,k}^{-1}\left\|\{\!\{|\underline{e}_h(\boldsymbol{\xi})|\}\!\}\right\|_{L^2(F)}^2+\frac{2\lambda k_{\max}C_T}{\widehat{\zeta}\gamma}\sigma_{h,k}\left\|\underline{[\![\boldsymbol{u}-\boldsymbol{w}]\!]}\right\|_{L^2(F)}^2\right)\\&-\sum_{F\in\mathcal{F}_h}\left(\frac{\lambda k_{\max}}{\widehat{\zeta}}\sigma_{h,k}\left\|\underline{[\![\boldsymbol{u}-\boldsymbol{w}]\!]}\right\|_{L^2(F)}^2+\frac{\widehat{\zeta}}{4\lambda k_{\max}}\sigma_{h,k}\left\|\underline{[\![\boldsymbol{\xi}]\!]}\right\|_{L^2(F)}^2\right)+\frac{\widehat{\zeta}\left\|p-r\right\|_{L^2(\Omega)}^2}{k_{\max}}.\end{aligned}$$

Applying Lemma 2.1, (6.22) and setting $\lambda = \max(C_1, 1)$, completes the bound for T_2:

$$
\begin{aligned}
T_2 \geq & -\frac{C_1 \lambda k_{\max}}{\widehat{\zeta}} \left(\|\underline{e}_h(\boldsymbol{u}-\boldsymbol{v})\|^2_{L^2(\Omega)} + \sum_{F\in\mathcal{F}_h} \sigma_{h,k}^{-1} \|\{\!|\underline{e}_h(\boldsymbol{u}-\boldsymbol{v})|\!\}\|^2_{L^2(F)} \right) \\
& - \frac{\lambda k_{\max}}{\widehat{\zeta}} \left(1 + \frac{C_1 C_T}{\gamma}\right) \sum_{F\in\mathcal{F}_h} \sigma_{h,k} \left\| \underline{[\![\boldsymbol{u}-\boldsymbol{w}]\!]} \right\|^2_{L^2(F)} \\
& - \frac{C_1 \widehat{\zeta}}{4\lambda k_{\max}} \left(\|\underline{e}_h(\boldsymbol{\xi})\|^2_{L^2(\Omega)} + \frac{\gamma}{C_T} \sum_{F\in\mathcal{F}_h} \sigma_{h,k}^{-1} \|\{\!|\underline{e}_h(\boldsymbol{\xi})|\!\}\|^2_{L^2(F)} \right) \\
& - \frac{\widehat{\zeta}}{4\lambda k_{\max}} (C_1+1) \sum_{F\in\mathcal{F}_h} \sigma_{h,k} \left\| \underline{[\![\boldsymbol{\xi}]\!]} \right\|^2_{L^2(F)} + \widehat{\zeta} k_{\max}^{-1} \|p-r\|^2_{L^2(\Omega)} \\
T_2 \geq & -\frac{C_1 \lambda k_{\max}}{\widehat{\zeta}} \left(1 + \frac{C_T}{\gamma}\right) \|\underline{e}_h(\boldsymbol{u}-\boldsymbol{v})\|^2_{L^2(\Omega)} \\
& - \frac{\lambda k_{\max}}{\widehat{\zeta}} \left(1 + \frac{C_1 C_T}{\gamma}\right) \sum_{F\in\mathcal{F}_h} \sigma_{h,k} \left\| \underline{[\![\boldsymbol{u}-\boldsymbol{w}]\!]} \right\|^2_{L^2(F)} - \frac{C_1 \widehat{\zeta}}{2\lambda k_{\max}} \|\underline{e}_h(\boldsymbol{\xi})\|^2_{L^2(\Omega)} \\
& - \frac{\widehat{\zeta}}{4\lambda k_{\max}} (C_1+1) \sum_{F\in\mathcal{F}_h} \sigma_{h,k} \left\| \underline{[\![\boldsymbol{\xi}]\!]} \right\|^2_{L^2(\Omega)} + \widehat{\zeta} k_{\max}^{-1} \|p-r\|^2_{L^2(\Omega)} \\
\geq & -\frac{\max(C_1^2,1) k_{\max}}{\widehat{\zeta}} \left(1 + \frac{C_T}{\gamma}\right) \|\boldsymbol{u}-\boldsymbol{w}\|^2_{h,k} - \frac{\widehat{\zeta}}{2k_{\max}} \|\boldsymbol{\xi}\|^2_{h,k} + \frac{\widehat{\zeta}}{k_{\max}} \|p-r\|^2_{L^2(\Omega)} \\
\geq & -\frac{\max(C_1^2,1) k_{\max}}{\widehat{\zeta}} \left(1 + \frac{C_T}{\gamma}\right) \|\boldsymbol{u}-\boldsymbol{w}\|^2_{h,k} + \frac{\widehat{\zeta}}{2k_{\max}} \|p-r\|^2_{L^2(\Omega)} .
\end{aligned}
$$

Inserting the bounds for T_1 and T_2 into (6.23) gives that

$$
\begin{aligned}
& \mathcal{A}_{h,k}((\boldsymbol{u},p);(\hat{\boldsymbol{v}},\hat{q})) - \mathcal{A}_{h,k}((\boldsymbol{w},r);(\hat{\boldsymbol{v}},\hat{q})) \\
& \quad \geq \min\left(\frac{\alpha}{2} \min(C_2,1) - \frac{\beta \max(C_1^2,1)}{\zeta} \left(1 + \frac{C_T}{\gamma}\right), \frac{\beta\widehat{\zeta}}{2} \right) k_{\max}^{-2} \|(\boldsymbol{u}-\boldsymbol{w}, p-r)\|^2_{\mathrm{DG}}
\end{aligned}
$$

providing we select α and β such that $\alpha/2 \min(C_2,1) > \beta \max(C_1^2,1)\widehat{\zeta}^{-1}\left(1 + C_T\gamma^{-1}\right)$. Using the triangle inequality with (6.22), noting that $k_{\max}^{-2} \leq 1$, we deduce that

$$
\begin{aligned}
\|(\hat{\boldsymbol{v}},\hat{q})\|^2_{DG} &\leq 2\alpha^2 \|\boldsymbol{u}-\boldsymbol{w}\|^2_{h,k} + 2\beta^2 k_{\max}^{-2} \|\boldsymbol{\xi}\|^2_{h,k} + \alpha^2 \|p-r\|^2_{L^2(\Omega)} \\
&\leq \max(2\alpha^2, \alpha^2 + 2\beta^2) \|(\boldsymbol{u}-\boldsymbol{w}, p-r)\|^2_{DG} .
\end{aligned}
$$

Setting $(\boldsymbol{v}, q) = (\max(2\alpha^2, \alpha^2 + 2\beta^2))^{-1/2} \|(\boldsymbol{u} - \boldsymbol{w}, p - r)\|_{DG}^{-1} (\hat{\boldsymbol{v}}, \hat{q})$ completes the proof. □

We are now able to prove the *a priori* error bound in Theorem 6.5. We first consider two interpolants $\Pi_{\boldsymbol{u}}$ and Π_p onto the finite element space satisfying

$$\|\boldsymbol{u} - \Pi_{\boldsymbol{u}}\boldsymbol{u}\|_{h,k}^2 \leq C_u \sum_{\kappa \in \mathcal{T}_h} \frac{h_\kappa^{2r_\kappa - 2}}{k_\kappa^{2s_\kappa - 3}} \|\boldsymbol{u}\|_{H^{s_\kappa}(\kappa)}^2 , \tag{6.24}$$

$$\sum_{\kappa \in \mathcal{T}_h} \left(\|p - \Pi_p p\|_{L^2(\kappa)}^2 + h_\kappa k_\kappa^{-1} \|p - \Pi_p p\|_{L^2(\partial\kappa)}^2 \right) \leq C_p \sum_{\kappa \in \mathcal{T}_h} \frac{h_\kappa^{2r_\kappa - 2}}{k_\kappa^{2s_\kappa - 2}} \|p\|_{H^{s_\kappa - 1}(\kappa)}^2 \tag{6.25}$$

where $1 \leq r_\kappa \leq \min(s_\kappa, k_\kappa + 1)$; see Houston *et al.* [122, Equation 3.2] and [119], respectively. We define

$$\boldsymbol{\eta}_{\boldsymbol{u}} := \boldsymbol{u} - \Pi_{\boldsymbol{u}}\boldsymbol{u}, \qquad \boldsymbol{\xi}_{\boldsymbol{u}} := \Pi_{\boldsymbol{u}}\boldsymbol{u} - \boldsymbol{u}_{h,k} \in \boldsymbol{V}(\mathcal{T}_h, \boldsymbol{k})$$

$$\eta_p := p - \Pi_p p, \qquad \xi_p := \Pi_p p - p_{h,k} \in Q(\mathcal{T}_h, \boldsymbol{k}).$$

As $\boldsymbol{u} - \boldsymbol{u}_{h,k} = \boldsymbol{\eta}_{\boldsymbol{u}} + \boldsymbol{\xi}_{\boldsymbol{u}}$ and $p - p_{h,k} = \eta_p + \xi_p$ we note, via the triangle inequality, that

$$\|(\boldsymbol{u} - \boldsymbol{u}_{h,k}, p - p_{h,k})\|_{\mathrm{DG}}^2 \leq 2 \|(\boldsymbol{\eta}_{\boldsymbol{u}}, \eta_p)\|_{\mathrm{DG}}^2 + 2 \|(\boldsymbol{\xi}_{\boldsymbol{u}}, \xi_p)\|_{\mathrm{DG}}^2 . \tag{6.26}$$

From (6.24)–(6.25) we get that

$$\|(\boldsymbol{\eta}_{\boldsymbol{u}}, \eta_p)\|_{\mathrm{DG}}^2 \leq \max(C_u, C_p) \sum_{\kappa \in \mathcal{T}_h} \left(\frac{h_\kappa^{2r_\kappa - 2}}{k_\kappa^{2s_\kappa - 3}} \|\boldsymbol{u}\|_{H^{s_\kappa}(\kappa)}^2 + \frac{h_\kappa^{2r_\kappa - 2}}{k_\kappa^{2s_\kappa - 2}} \|p\|_{H^{s_\kappa - 1}(\kappa)}^2 \right) \tag{6.27}$$

and from the discrete inf-sup stability result, Lemma 6.6, we have that there exists a $(\hat{\boldsymbol{\xi}}_{\boldsymbol{u}}, \hat{\xi}_p)$ such that $\left\| (\hat{\boldsymbol{\xi}}_{\boldsymbol{u}}, \hat{\xi}_p) \right\|_{\mathrm{DG}} \leq 1$ and

$$C_D k_{\max}^{-2} \|(\boldsymbol{\xi}_{\boldsymbol{u}}, \xi_p)\|_{\mathrm{DG}} \leq \mathcal{A}_{h,k}((\Pi_{\boldsymbol{u}}\boldsymbol{u}, \Pi_p p), (\hat{\boldsymbol{\xi}}_{\boldsymbol{u}}, \hat{\xi}_p)) - \mathcal{A}_{h,k}((\boldsymbol{u}_{h,k}, p_{h,k}), (\hat{\boldsymbol{\xi}}_{\boldsymbol{u}}, \hat{\xi}_p)).$$

Due to the regularity assumptions the DGFEM (6.12)–(6.13) is consistent; thus, from

(6.18) and (6.7)–(6.8) we get that

$$
\begin{aligned}
&C_D k_{\max}^{-2} \left\| (\boldsymbol{\xi_u}, \xi_p) \right\|_{\mathrm{DG}} \\
&\qquad \leq \mathcal{A}_{h,k}((\Pi_{\boldsymbol{u}}\boldsymbol{u}, \Pi_p p), (\hat{\boldsymbol{\xi}}_{\boldsymbol{u}}, \hat{\xi}_p)) - \mathcal{A}_{h,k}((\boldsymbol{u}, p), (\hat{\boldsymbol{\xi}}_{\boldsymbol{u}}, \hat{\xi}_p)) \\
&\qquad \leq \int_\Omega |\mu(|\underline{e}_h(\Pi_{\boldsymbol{u}}\boldsymbol{u})|)\underline{e}_h(\Pi_{\boldsymbol{u}}\boldsymbol{u}) - \mu(|\underline{e}_h(\boldsymbol{u})|)\underline{e}_h(\boldsymbol{u})||\underline{e}(\hat{\boldsymbol{\xi}}_{\boldsymbol{u}})| \,\mathrm{d}\boldsymbol{x} \\
&\qquad\quad + \sum_{F\in\mathcal{F}_h} \int_F \{\!\{|\mu(|\underline{e}_h(\Pi_{\boldsymbol{u}}\boldsymbol{u})|)\underline{e}_h(\Pi_{\boldsymbol{u}}\boldsymbol{u}) - \mu(|\underline{e}_h(\boldsymbol{u})|)\underline{e}_h(\boldsymbol{u})|\}\!\}|\underline{[\![\hat{\boldsymbol{\xi}}_{\boldsymbol{u}}]\!]}| \,\mathrm{d}s \\
&\qquad\quad + |\theta| \sum_{F\in\mathcal{F}_h} \int_F |\mu(h_F^{-1}|\underline{[\![\Pi_{\boldsymbol{u}}\boldsymbol{u}]\!]}|)\underline{[\![\Pi_{\boldsymbol{u}}\boldsymbol{u}]\!]} - \mu(h_F^{-1}|\underline{[\![\boldsymbol{u}]\!]}|)\underline{[\![\boldsymbol{u}]\!]}||\{\!\{\underline{e}_h(\hat{\boldsymbol{\xi}}_{\boldsymbol{u}})\}\!\}| \,\mathrm{d}s \\
&\qquad\quad + \sum_{F\in\mathcal{F}_h} \int_F \sigma_{h,k}|\underline{[\![\Pi_{\boldsymbol{u}}\boldsymbol{u} - \boldsymbol{u}]\!]}||\underline{[\![\hat{\boldsymbol{\xi}}_{\boldsymbol{u}}]\!]}| \,\mathrm{d}s + \int_\Omega |\Pi_p p - p||\nabla_h \cdot \hat{\boldsymbol{\xi}}_{\boldsymbol{u}}| \,\mathrm{d}\boldsymbol{x} \\
&\qquad\quad + \sum_{F\in\mathcal{F}_h} \int_F |\{\!\{\Pi_p p - p\}\!\}||[\![\hat{\boldsymbol{\xi}}_{\boldsymbol{u}}]\!]| \,\mathrm{d}s + \int_\Omega |\hat{\xi}_p||\nabla_h \cdot (\Pi_{\boldsymbol{u}}\boldsymbol{u} - \boldsymbol{u})| \,\mathrm{d}\boldsymbol{x} \\
&\qquad\quad + \sum_{F\in\mathcal{F}_h} \int_F |\{\!\{\hat{\xi}_p\}\!\}||[\![\Pi_{\boldsymbol{u}}\boldsymbol{u} - \boldsymbol{u}]\!]| \,\mathrm{d}s \\
&\qquad \leq C_1 \left\| \underline{e}_h(\boldsymbol{\eta_u}) \right\|_{L^2(\Omega)} \left\| \underline{e}_h(\hat{\boldsymbol{\xi}}_{\boldsymbol{u}}) \right\|_{L^2(\Omega)} \\
&\qquad\quad + C_1 \left(\sum_{F\in\mathcal{F}_h} \sigma_{h,k}^{-1} \left\| \{\!\{|\underline{e}_h(\boldsymbol{\eta_u})|\}\!\} \right\|_{L^2(F)}^2 \right)^{1/2} \left(\sum_{F\in\mathcal{F}_h} \int_F \sigma_{h,k}|\underline{[\![\hat{\boldsymbol{\xi}}_{\boldsymbol{u}}]\!]}|^2 \,\mathrm{d}s \right)^{1/2} \\
&\qquad\quad + C_1|\theta| \left(\sum_{F\in\mathcal{F}_h} \int_F \sigma_{h,k}|\underline{[\![\boldsymbol{\eta_u}]\!]}|^2 \,\mathrm{d}s \right)^{1/2} \left(\sum_{F\in\mathcal{F}_h} \sigma_{h,k}^{-1} \left\| \{\!\{\underline{e}_h(\hat{\boldsymbol{\xi}}_{\boldsymbol{u}})\}\!\} \right\|_{L^2(F)}^2 \right)^{1/2} \\
&\qquad\quad + \left(\sum_{F\in\mathcal{F}_h} \int_F \sigma_{h,k}|\underline{[\![\boldsymbol{\eta_u}]\!]}|^2 \,\mathrm{d}s \right)^{1/2} \left(\sum_{F\in\mathcal{F}_h} \int_F \sigma_{h,k}|\underline{[\![\hat{\boldsymbol{\xi}}_{\boldsymbol{u}}]\!]}|^2 \,\mathrm{d}s \right)^{1/2} \\
&\qquad\quad + \|\eta_p\|_{L^2(\Omega)} \left\| \nabla_h \cdot \hat{\boldsymbol{\xi}}_{\boldsymbol{u}} \right\|_{L^2(\Omega)} + \left\| \hat{\xi}_p \right\|_{L^2(\Omega)} \|\nabla_h \cdot \boldsymbol{\eta_u}\|_{L^2(\Omega)} \\
&\qquad\quad + \left(\sum_{F\in\mathcal{F}_h} \sigma_{h,k}^{-1} \|\{\!\{\eta_p\}\!\}\|_{L^2(F)}^2 \right)^{1/2} \left(\sum_{F\in\mathcal{F}_h} \int_F \sigma_{h,k}|[\![\hat{\boldsymbol{\xi}}_{\boldsymbol{u}}]\!]|^2 \,\mathrm{d}s \right)^{1/2} \\
&\qquad\quad + \left(\sum_{F\in\mathcal{F}_h} \sigma_{h,k}^{-1} \left\| \{\!\{\hat{\xi}_p\}\!\} \right\|_{L^2(F)}^2 \right)^{1/2} \left(\sum_{F\in\mathcal{F}_h} \int_F \sigma_{h,k}|[\![\boldsymbol{\eta_u}]\!]|^2 \,\mathrm{d}s \right)^{1/2}.
\end{aligned}
$$

By applying Lemma 2.1, (2.1)–(2.2), the fact that $|\theta| \leq 1$, $\gamma \geq 1$, $k_\kappa \geq 1$, $|[\![\boldsymbol{v}]\!]| \leq |\underline{[\![\boldsymbol{v}]\!]}|$, for

all $\boldsymbol{v} \in \boldsymbol{V}(\mathcal{T}_h, \boldsymbol{k})$, and $|\nabla \cdot \boldsymbol{v}|^2 \leq d|\underline{e}(\boldsymbol{v})|^2$, for all $\boldsymbol{v} \in \boldsymbol{V}(\mathcal{T}_h, \boldsymbol{k})$, we get that

$$k_{\max}^{-2} \left\|(\boldsymbol{\xi_u}, \xi_p)\right\|_{\mathrm{DG}} \leq C \left(\|\boldsymbol{\eta_u}\|_{h,k}^2 + \sum_{\kappa \in \mathcal{T}_h} \left(\|\eta_p\|_{L^2(\kappa)}^2 + h_\kappa k_\kappa^{-1} \|\eta_p\|_{L^2(\partial\kappa)}^2 \right) \right)^{1/2} \left\| (\hat{\boldsymbol{\xi}}_{\boldsymbol{u}}, \hat{\xi}_p) \right\|_{\mathrm{DG}}.$$

Therefore, applying (6.24)–(6.25) and noting that $\left\| (\hat{\boldsymbol{\xi}}_{\boldsymbol{u}}, \hat{\xi}_p) \right\|_{DG} \leq 1$ we get that

$$\left\|(\boldsymbol{\xi_u}, \xi_p)\right\|_{\mathrm{DG}}^2 \leq C k_{\max}^4 \left(\sum_{\kappa \in \mathcal{T}_h} \frac{h_\kappa^{2r_\kappa - 2}}{k_\kappa^{2s_\kappa - 3}} \|\boldsymbol{u}\|_{H^{s_\kappa}(\kappa)}^2 + \sum_{\kappa \in \mathcal{T}_h} \frac{h_\kappa^{2r_\kappa - 2}}{k_\kappa^{2s_\kappa - 2}} \|p\|_{H^{s_\kappa - 1}(\kappa)}^2 \right). \tag{6.28}$$

Inserting (6.27) and (6.28) into (6.26) completes the proof. □

6.4 *A Posteriori* Error Analysis

In this section, we develop the *a posteriori* error analysis of the DGFEM defined by (6.12)–(6.13). We define, for an element $\kappa \in \mathcal{T}_h$ and face $F \in \mathcal{F}_h^{\mathcal{I}}$, the data-oscillation terms

$$\mathcal{O}_\kappa^{(1)} = h_\kappa^2 k_\kappa^{-2} \left\| (\mathbb{I} - \Pi_{\kappa,k_\kappa})|_\kappa (\boldsymbol{f} + \nabla \cdot (\mu(|\underline{e}(\boldsymbol{u}_{h,k})|)\underline{e}(\boldsymbol{u}_{h,k}))) \right\|_{L^2(\kappa)}^2$$

and

$$\mathcal{O}_F^{(2)} = h_F k_F^{-1} \left\| (\mathbb{I} - \Pi_{F,k_F})|_F [\![\mu(|\underline{e}_h(\boldsymbol{u}_{h,k})|)\underline{e}_h(\boldsymbol{u}_{h,k})]\!] \right\|_{L^2(F)}^2,$$

respectively, which depend on the right-hand side $\boldsymbol{f}$ in (6.1) and the numerical solution $\boldsymbol{u}_{h,k}$ from (6.12)–(6.13). Here, $\mathbb{I}$ represents a generic identity operator, Π_{κ,k_κ} is an elementwise L^2-projector onto the space $\mathcal{S}_{k_\kappa - 1}(\kappa)$. and Π_{F,k_F} is the L^2-projector onto $\mathcal{Q}_{k_F - 1}(F)$.

6.4.1 Upper Bounds

We now state the following *a posteriori* upper bound for the DGFEM defined by (6.12)–(6.13). The proof of this result will follow in Section 6.4.3.

Theorem 6.7. *Let* $(\boldsymbol{u}, p) \in \left[H_0^1(\Omega)\right]^d \times L_0^2(\Omega)$ *be the analytical solution to the problem* (6.1)–(6.3) *and* $(\boldsymbol{u}_{h,k}, p_{h,k}) \in \boldsymbol{V}(\mathcal{T}_h, \boldsymbol{k}) \times Q(\mathcal{T}_h, \boldsymbol{k})$ *be its DGFEM approximation obtained from*

(6.12)–(6.13); *then, the following* hp*-version* a posteriori *error bound holds:*

$$\|(\boldsymbol{u}-\boldsymbol{u}_{h,k},p-p_{h,k})\|_{\mathrm{DG}} \leq C_9 \left(\sum_{\kappa\in\mathcal{T}_h}\eta_\kappa^2+\mathcal{O}(\boldsymbol{f},\boldsymbol{u}_{h,k})\right)^{1/2},$$

where the local error indicators $\eta_\kappa, \kappa\in\mathcal{T}_h$, *are defined by*

$$\begin{aligned}\eta_\kappa^2 &= h_\kappa^2 k_\kappa^{-2}\,\|\Pi_{\kappa,k_\kappa}(\boldsymbol{f}+\nabla\cdot(\mu(|\underline{e}(\boldsymbol{u}_{h,k})|)\underline{e}(\boldsymbol{u}_{h,k})))-\nabla p_{h,k}\|_{L^2(\kappa)}^2+\|\nabla\cdot\boldsymbol{u}_{h,k}\|_{L^2(\kappa)}^2\\ &\quad+h_\kappa k_\kappa^{-1}\,\|[\![p_{h,k}]\!]-\Pi_{F,k_F}[\![\mu(|\underline{e}_h(\boldsymbol{u}_{h,k})|)\underline{e}_h(\boldsymbol{u}_{h,k})]\!]\|_{L^2(\partial\kappa\setminus\Gamma)}^2+\gamma^2 h_\kappa^{-1}k_\kappa^3\left\|\underline{[\![\boldsymbol{u}_{h,k}]\!]}\right\|_{L^2(\partial\kappa)}^2\end{aligned}$$

and

$$\mathcal{O}(\boldsymbol{f},\boldsymbol{u}_{h,k})=\sum_{\kappa\in\mathcal{T}_h}\mathcal{O}_\kappa^{(1)}+\sum_{F\in\mathcal{F}_h^{\mathcal{I}}}\mathcal{O}_F^{(2)}.$$

Here, the constant $C_9>0$ *is independent of* $\boldsymbol{h}$*, the polynomial degree vector* $\boldsymbol{k}$ *and the parameter* γ *and only depends on the shape-regularity of the mesh and the constants* ρ_1 *and* ρ_2 *from* (2.1) *and* (2.2)*, respectively.*

6.4.2 Local Lower Bounds

For simplicity we shall restrict ourselves to local lower bounds on conforming meshes $\mathcal{T}_h$; the extension to nonconforming 1-irregular meshes follows analogously, cf., for example, Houston *et al.* [125, Remark 3.9]. The following result is proven in Section 6.4.4.

Theorem 6.8. *Let* κ *and* κ' *be any two neighbouring elements,* $F=\partial\kappa\cap\partial\kappa'$ *and* $\omega_F=(\bar{\kappa}\cup\bar{\kappa}')^\circ$*. Then, for all* $\delta\in(0,1/2]$*, the following* hp*-version* a posteriori *local bounds on the error between the analytical solution* $(\boldsymbol{u},p)\in\left[H_0^1(\Omega)\right]^d\times L_0^2(\Omega)$ *satisfying* (6.1)–(6.3) *and the numerical solution* $(\boldsymbol{u}_{h,k},p_{h,k})\in\boldsymbol{V}(\mathcal{T}_h,\boldsymbol{k})\times Q(\mathcal{T}_h,\boldsymbol{k})$ *obtained by* (6.12)–(6.13) *holds:*

(a)
$$\begin{aligned}&\|\Pi_{\kappa,k_\kappa}|_\kappa(\boldsymbol{f}+\nabla\cdot(\mu(|\underline{e}(\boldsymbol{u}_{h,k})|)\underline{e}(\boldsymbol{u}_{h,k})))-\nabla p\|_{L^2(\kappa)}\\ &\qquad\leq Ch_\kappa^{-1}k_\kappa^2\left(\|\underline{e}(\boldsymbol{u}-\boldsymbol{u}_{h,k})\|_{L^2(\kappa)}+\|p-p_{h,k}\|_{L^2(\kappa)}+k_\kappa^{\delta-1/2}\sqrt{\mathcal{O}_\kappa^{(1)}}\right),\end{aligned}$$

(b)
$$\|\nabla\cdot\boldsymbol{u}_{h,k}\|_{L^2(\kappa)}\leq C\,\|\underline{e}(\boldsymbol{u}-\boldsymbol{u}_{h,k})\|_{L^2(\kappa)},$$

(c) $$\begin{aligned}\|[\![p_{h,k}]\!] - \Pi_{F,k_F}|_F[\![\mu(|\underline{e}_h(\boldsymbol{u}_{h,k})|)\underline{e}_h(\boldsymbol{u}_{h,k})]\!]\|_{L^2(F)} \\ \leq Ch_\kappa^{-1/2}k_\kappa^{\delta+3/2}\Bigg(\|\underline{e}(\boldsymbol{u}-\boldsymbol{u}_{h,k})\|_{L^2(\omega_F)} + \|p-p_{h,k}\|_{L^2(\omega_F)} \\ + k_\kappa^{\delta-1/2}\sum_{\tau\in\{\kappa,\kappa'\}}\sqrt{\mathcal{O}_\tau^{(1)}} + k_\kappa^{-1/2}\sqrt{\mathcal{O}_F^{(2)}}\Bigg),\end{aligned}$$

(d) $$\left\|\underline{[\![\boldsymbol{u}_{h,k}]\!]}\right\|_{L^2(F)} \leq C\gamma^{-1/2}h_\kappa^{1/2}k_\kappa^{-1}\left\|\sigma_{h,k}^{1/2}\underline{[\![\boldsymbol{u}-\boldsymbol{u}_{h,k}]\!]}\right\|_{L^2(F)}.$$

Here, the generic constant $C>0$ depends on δ, but is independent of $\boldsymbol{h}$ and $\boldsymbol{k}$.

6.4.3 Proof of Theorem 6.7

In this section, we prove Theorem 6.7, based on the techniques developed in Houston *et al.* [120, 125].

DGFEM Decomposition

Given that the mesh partition $\mathcal{T}_h$ contains hanging nodes we note that we can create an 1-irregular auxiliary mesh $\mathcal{T}_{\widetilde{h}}$ as outlined in Section 2.1.2, with corresponding DGFEM finite element spaces $\boldsymbol{V}(\mathcal{T}_{\widetilde{h}},\widetilde{\boldsymbol{k}})$ and $Q(\mathcal{T}_{\widetilde{h}},\widetilde{\boldsymbol{k}})$ and polynomial degree vector $\widetilde{\boldsymbol{k}}$ such that $\boldsymbol{V}(\mathcal{T}_h,\boldsymbol{k})\subseteq\boldsymbol{V}(\mathcal{T}_{\widetilde{h}},\widetilde{\boldsymbol{k}})$ and $Q(\mathcal{T}_h,\boldsymbol{k})\subseteq Q(\mathcal{T}_{\widetilde{h}},\widetilde{\boldsymbol{k}})$; cf. Section 3.4.1. We note that there exist constants $N_1,N_2>0$, independent of $\boldsymbol{h}$ and $\boldsymbol{k}$, such that

$$N_1\sum_{F\in\mathcal{F}_h}\int_F\sigma_{h,k}|\underline{[\![\boldsymbol{u}]\!]}|^2\,\mathrm{d}s \leq \sum_{\widetilde{F}\in\mathcal{F}_{\widetilde{h}}}\int_{\widetilde{F}}\sigma_{\widetilde{h,k}}|\underline{[\![\boldsymbol{u}]\!]}|^2\,\mathrm{d}s \leq N_2\sum_{F\in\mathcal{F}_h}\int_F\sigma_{h,k}|\underline{[\![\boldsymbol{u}]\!]}|^2\,\mathrm{d}s, \tag{6.29}$$

for all $v\in V(\mathcal{T}_h,\boldsymbol{k})$; cf. (3.22).

As in Section 3.4.1 we decompose the DGFEM space $\boldsymbol{V}(\mathcal{T}_{\widetilde{h}},\widetilde{\boldsymbol{k}})$ into two orthogonal subspaces, cf. Karakashian & Pascal [131]; a conforming part $\left[\boldsymbol{V}(\mathcal{T}_{\widetilde{h}},\widetilde{\boldsymbol{k}})\right]^c=\boldsymbol{V}(\mathcal{T}_{\widetilde{h}},\widetilde{\boldsymbol{k}})\cap\left[H_0^1(\Omega)\right]^d$ and a nonconforming part $\left[\boldsymbol{V}(\mathcal{T}_{\widetilde{h}},\widetilde{\boldsymbol{k}})\right]^\perp$, which is defined as the orthogonal complement of $\left[\boldsymbol{V}(\mathcal{T}_{\widetilde{h}},\widetilde{\boldsymbol{k}})\right]^c$. Based on this setting the DGFEM solution $\boldsymbol{u}_{h,k}$ may be split accordingly,

$$\boldsymbol{u}_{h,k}=\boldsymbol{u}_{h,k}^c+\boldsymbol{u}_{h,k}^\perp, \tag{6.30}$$

where $\boldsymbol{u}_{h,k}^c \in \left[\boldsymbol{V}(\mathcal{T}_{\widetilde{h}}, \widetilde{\boldsymbol{k}})\right]^c$ and $\boldsymbol{u}_{h,k}^{\perp} \in \left[\boldsymbol{V}(\mathcal{T}_{\widetilde{h}}, \widetilde{\boldsymbol{k}})\right]^{\perp}$. Furthermore, we define the error in the velocity vector as

$$\boldsymbol{e}_{\boldsymbol{u}} = \boldsymbol{u} - \boldsymbol{u}_{h,k}, \tag{6.31}$$

the error in the pressure as

$$e_p = p - p_{h,k}, \tag{6.32}$$

and let

$$\boldsymbol{e}_{\boldsymbol{u}}^c = \boldsymbol{u} - \boldsymbol{u}_{h,k}^c \in \left[H_0^1(\Omega)\right]^d.$$

Auxiliary Results

In order to prove Theorem 6.7, we require the following auxiliary results.

Lemma 6.9. *With $\boldsymbol{u}_{h,k}^{\perp}$ defined by (6.30), the following bound holds*

$$\left\|\boldsymbol{u}_{h,k}^{\perp}\right\|_{\widetilde{h,k}} \leq D \left(\sum_{F \in \mathcal{F}_h} \int_F \sigma_{h,k} |\underline{[\![\boldsymbol{u}_{h,k}^{\perp}]\!]}|^2 \, \mathrm{d}s\right)^{1/2},$$

where the constant $D > 0$ is independent of γ, $\boldsymbol{h}$ and $\boldsymbol{k}$, but depends only on the shape regularity of the mesh and the constants ρ_1 and ρ_2 from (2.1) and (2.2), respectively.

Proof. The proof follows by first applying Lemma 6.3 and then extending Lemma 3.5 to vector-valued functions; cf. Zhu & Schötzau [182, Lemma 4.6], Zhu *et al.* [183, Lemma 4.1] and Houston *et al.* [125, Corollary 3.6]. □

We now state the following approximation result:

Lemma 6.10. *For any $\boldsymbol{v} \in \left[H_0^1(\Omega)\right]^d$, there exists $\boldsymbol{v}_{h,k} \in \boldsymbol{V}(\mathcal{T}_h, \boldsymbol{k})$, such that*

$$\sum_{\kappa \in \mathcal{T}_h} \left(\frac{k_\kappa^2}{h_\kappa^2} \|\boldsymbol{v} - \boldsymbol{v}_{h,k}\|_{L^2(\kappa)}^2 + \|\underline{\boldsymbol{\varepsilon}}(\boldsymbol{v} - \boldsymbol{v}_{h,k})\|_{L^2(\kappa)}^2 + \frac{k_\kappa}{h_\kappa} \|\boldsymbol{v} - \boldsymbol{v}_{h,k}\|_{L^2(\partial\kappa)}^2\right) \leq C_I \, \|\underline{\boldsymbol{\varepsilon}}(\boldsymbol{v})\|_{L^2(\Omega)}^2,$$

with an interpolation constant $C_I > 0$ independent of $\boldsymbol{h}$ and $\boldsymbol{k}$ which depends only on the shape regularity of the mesh and the constants ρ_1 and ρ_2 from (2.1) and (2.2), respectively.

Proof. We begin by applying Lemma 6.3, then applying Lemma 3.6 componentwise to the vector field $\boldsymbol{v}$ and finally using the continuous Korn's inequality [114]; cf. Houston *et al.* [125, Lemma 3.7]. □

We also require the following *inf-sup stability* result for the form $\mathcal{A}_{h,k}((\boldsymbol{u},p),(\boldsymbol{v},q))$ restricted to $\left[H_0^1(\Omega)\right]^d \times L_0^2(\Omega)$, which is derived in a similar way to the discrete inf-sup stability result from Lemma 6.6.

Lemma 6.11. *There exists a positive constant C_S, independent of $\boldsymbol{h}$ and $\boldsymbol{k}$, such that for any $(\boldsymbol{u},p),(\boldsymbol{w},r) \in \left[H_0^1(\Omega)\right]^d \times L_0^2(\Omega)$, there exists $(\boldsymbol{v},q) \in \left[H_0^1(\Omega)\right]^d \times L_0^2(\Omega)$ with*

$$\mathcal{A}_{h,k}((\boldsymbol{u},p);(\boldsymbol{v},q)) - \mathcal{A}_{h,k}((\boldsymbol{w},r);(\boldsymbol{v},q)) \geq C_S \left\|(\boldsymbol{u}-\boldsymbol{w},p-r)\right\|_{DG},$$
$$\left\|(\boldsymbol{v},q)\right\|_{DG} \leq 1,$$

where $C_S = (\max(2\alpha^2, \alpha^2+2\beta^2))^{-1}, \alpha = C_2^{-1}(1+C_1^2\zeta^{-2}), \beta = 2\zeta^{-1}$ and ζ, C_1 and C_2 are the constants from (6.9), (6.5) and (6.6), respectively.

Proof. Let $p-r \in L_0^2(\Omega)$, then, from the inf-sup condition (6.9) there exists a function $\boldsymbol{\xi} \in \left[H_0^1(\Omega)\right]^d$ such that

$$-\int_\Omega (p-r)\nabla\cdot\boldsymbol{\xi}\,\mathrm{d}\boldsymbol{x} \geq \zeta \left\|p-r\right\|_{L^2(\Omega)}^2, \qquad \left\|\boldsymbol{\xi}\right\|_{h,k} = \left\|\underline{\varepsilon}(\boldsymbol{\xi})\right\|_{L^2(\Omega)} \leq \left\|p-r\right\|_{L^2(\Omega)}; \quad (6.33)$$

cf. Houston *et al.* [123, Lemma 4.3]. Now, we choose

$$\hat{\boldsymbol{v}} = \alpha(\boldsymbol{u}-\boldsymbol{w}) + \beta\boldsymbol{\xi}, \qquad \hat{q} = \alpha(p-r),$$

with

$$\alpha = C_2^{-1}(1+C_1^2\zeta^{-2}), \qquad \beta = 2\zeta^{-1}.$$

Since $\boldsymbol{u}$ and $\hat{\boldsymbol{v}}$ are in $\left[H_0^1(\Omega)\right]^d$, we note that $\underline{[\![\boldsymbol{u}]\!]} = \underline{[\![\hat{\boldsymbol{v}}]\!]} = \underline{0}$ and $[\![\boldsymbol{u}]\!] = [\![\hat{\boldsymbol{v}}]\!] = 0$ on all $F \in \mathcal{F}_h$. Hence, using (6.5), (6.6), (6.33) and the arithmetic-geometric mean inequality

we deduce that

$$\begin{aligned}
&\mathcal{A}_{h,k}((\boldsymbol{u},p);(\hat{\boldsymbol{v}},\hat{q})) - \mathcal{A}_{h,k}((\boldsymbol{w},r);(\hat{\boldsymbol{v}},\hat{q})) \\
&\qquad \geq \alpha C_2 \int_\Omega |\underline{e}(\boldsymbol{u}-\boldsymbol{w})|^2 \,\mathrm{d}\boldsymbol{x} - \frac{1}{2}\zeta\beta \int_\Omega |\underline{e}(\boldsymbol{\xi})|^2 \,\mathrm{d}\boldsymbol{x} + \beta\zeta \left\|p-r\right\|^2_{L^2(\Omega)} \\
&\qquad\quad - \frac{1}{2}\zeta^{-1}\beta \int_\Omega |\mu(|\underline{e}(\boldsymbol{u})|)\underline{e}(\boldsymbol{u}) - \mu(|\underline{e}(\boldsymbol{w})|)\underline{e}(\boldsymbol{w})|^2 \,\mathrm{d}\boldsymbol{x} \\
&\qquad \geq (\alpha C_2 - \frac{1}{2}\zeta^{-1}\beta C_1^2) \left\|\underline{e}(\boldsymbol{u}-\boldsymbol{w})\right\|^2_{L^2(\Omega)} + \frac{1}{2}\beta\zeta \left\|p-r\right\|^2_{L^2(\Omega)} \\
&\qquad = \left\|(\boldsymbol{u}-\boldsymbol{w},p-r)\right\|^2_{DG}.
\end{aligned}$$

Using the triangle inequality, we deduce that

$$\begin{aligned}
\left\|(\hat{\boldsymbol{v}},\hat{q})\right\|^2_{DG} &\leq 2\alpha^2 \left\|\boldsymbol{u}-\boldsymbol{w}\right\|^2_{h,k} + 2\beta^2 \left\|\boldsymbol{\xi}\right\|^2_{h,k} + \alpha^2 \left\|p-r\right\|^2_{L^2(\Omega)} \\
&\leq \max(2\alpha^2, \alpha^2+2\beta^2) \left\|(\boldsymbol{u}-\boldsymbol{w},p-r)\right\|^2_{DG}.
\end{aligned}$$

Setting $(\boldsymbol{v},q) = (\max(2\alpha^2,\alpha^2+2\beta^2))^{-1/2} \left\|(\boldsymbol{u}-\boldsymbol{w},p-r)\right\|^{-1}_{DG} (\hat{\boldsymbol{v}},\hat{q})$ completes the proof.

□

Proof of Theorem 6.7

We now complete the proof of Theorem 6.7. To this end, we recall the compact formulation (6.19) as well as the definition of the error, defined in (6.31) and (6.32), then by (6.29), Lemma 6.9 and the fact that $\gamma \geq 1$ and $k_\kappa \geq 1$, we have that

$$\begin{aligned}
\left\|(\boldsymbol{e_u},e_p)\right\|_{\mathrm{DG}} &\leq \left\|(\boldsymbol{e}^c_{\boldsymbol{u}},e_p)\right\|_{\mathrm{DG}} + \left\|\boldsymbol{u}^\perp_{h,k}\right\|_{h,k} \\
&\leq \left\|(\boldsymbol{e}^c_{\boldsymbol{u}},e_p)\right\|_{\mathrm{DG}} + \max(1,N_1^{-1/2}) \left\|\boldsymbol{u}^\perp_{h,k}\right\|_{\widetilde{h,k}} \\
&\leq \left\|(\boldsymbol{e}^c_{\boldsymbol{u}},e_p)\right\|_{\mathrm{DG}} + \max(1,N_1^{-1/2}) D \left(\sum_{F\in\mathcal{F}_h} \int_F \sigma_{h,k} |\underline{[\![\boldsymbol{u}_{h,k}]\!]}|^2 \,\mathrm{d}s\right)^{1/2} \\
&\leq \left\|(\boldsymbol{e}^c_{\boldsymbol{u}},e_p)\right\|_{\mathrm{DG}} + \max(1,N_1^{-1/2}) D \left(\sum_{\kappa\in\mathcal{T}_h} \eta_\kappa^2\right)^{1/2}. \qquad (6.34)
\end{aligned}$$

To bound the term $\|(\boldsymbol{e}_{\boldsymbol{u}}^c, e_p)\|_{\mathrm{DG}}$, we invoke the result from Lemma 6.11 which gives a function $(\boldsymbol{v}, q) \in \left[H_0^1(\Omega)\right]^d \times L_0^2(\Omega)$ such that

$$C_S \|(\boldsymbol{e}_{\boldsymbol{u}}^c, e_p)\|_{\mathrm{DG}} \leq \mathcal{A}_{h,k}((\boldsymbol{u}, p); (\boldsymbol{v}, q)) - \mathcal{A}_{h,k}((\boldsymbol{u}_{h,k}^c, p_{h,k}); (\boldsymbol{v}, q)), \quad \|(\boldsymbol{v}, q)\|_{\mathrm{DG}} \leq 1, \tag{6.35}$$

Notice that, since $\boldsymbol{v} \in \left[H_0^1(\Omega)\right]^d$, we have that $\underline{[\![\boldsymbol{v}]\!]} = \underline{0}$ on $\mathcal{F}_h$. Therefore, from (6.30),

$$\begin{aligned} C_S \|(\boldsymbol{e}_{\boldsymbol{u}}^c, e_p)\|_{\mathrm{DG}} \leq & \sum_{\widetilde{\kappa} \in \mathcal{T}_{\widetilde{h}}} \int_{\widetilde{\kappa}} (\mu(|\underline{e}(\boldsymbol{u})|)\underline{e}(\boldsymbol{u}) - \mu(|\underline{e}(\boldsymbol{u}_{h,k})|)\underline{e}(\boldsymbol{u}_{h,k})) : \underline{e}(\boldsymbol{v}) \, \mathrm{d}\boldsymbol{x} \\ & + \sum_{\widetilde{\kappa} \in \mathcal{T}_{\widetilde{h}}} \int_{\widetilde{\kappa}} \left(\mu(|\underline{e}(\boldsymbol{u}_{h,k})|)\underline{e}(\boldsymbol{u}_{h,k}) - \mu(|\underline{e}(\boldsymbol{u}_{h,k}^c)|)\underline{e}(\boldsymbol{u}_{h,k}^c)\right) : \underline{e}(\boldsymbol{v}) \, \mathrm{d}\boldsymbol{x} \\ & - \sum_{\widetilde{\kappa} \in \mathcal{T}_{\widetilde{h}}} \int_{\widetilde{\kappa}} (p - p_{h,k}) \nabla \cdot \boldsymbol{v} \, \mathrm{d}\boldsymbol{x} + \sum_{\widetilde{\kappa} \in \mathcal{T}_{\widetilde{h}}} \int_{\widetilde{\kappa}} q \nabla \cdot (\boldsymbol{u} - \boldsymbol{u}_{h,k}) \, \mathrm{d}\boldsymbol{x} \\ & + \sum_{\widetilde{\kappa} \in \mathcal{T}_{\widetilde{h}}} \int_{\widetilde{\kappa}} q \nabla \cdot \boldsymbol{u}_{h,k}^{\perp} \, \mathrm{d}\boldsymbol{x} \\ \equiv & \, T_1 + T_2, \end{aligned} \tag{6.36}$$

where

$$\begin{aligned} T_1 = & \sum_{\widetilde{\kappa} \in \mathcal{T}_{\widetilde{h}}} \int_{\widetilde{\kappa}} (\mu(|\underline{e}(\boldsymbol{u})|)\underline{e}(\boldsymbol{u}) - \mu(|\underline{e}(\boldsymbol{u}_{h,k})|)\underline{e}(\boldsymbol{u}_{h,k})) : \underline{e}(\boldsymbol{v}) \, \mathrm{d}\boldsymbol{x} \\ & - \sum_{\widetilde{\kappa} \in \mathcal{T}_{\widetilde{h}}} \int_{\widetilde{\kappa}} (p - p_{h,k}) \nabla \cdot \boldsymbol{v} \, \mathrm{d}\boldsymbol{x} + \sum_{\widetilde{\kappa} \in \mathcal{T}_{\widetilde{h}}} \int_{\widetilde{\kappa}} q \nabla \cdot (\boldsymbol{u} - \boldsymbol{u}_{h,k}) \, \mathrm{d}\boldsymbol{x}, \\ T_2 = & \sum_{\widetilde{\kappa} \in \mathcal{T}_{\widetilde{h}}} \int_{\widetilde{\kappa}} \left(\mu(|\underline{e}(\boldsymbol{u}_{h,k})|)\underline{e}(\boldsymbol{u}_{h,k}) - \mu(|\underline{e}(\boldsymbol{u}_{h,k}^c)|)\underline{e}(\boldsymbol{u}_{h,k}^c)\right) : \underline{e}(\boldsymbol{v}) \, \mathrm{d}\boldsymbol{x} + \sum_{\widetilde{\kappa} \in \mathcal{T}_{\widetilde{h}}} \int_{\widetilde{\kappa}} q \nabla \cdot \boldsymbol{u}_{h,k}^{\perp} \, \mathrm{d}\boldsymbol{x}. \end{aligned}$$

We start by bounding T_1. To this end, employing integration by parts and equations (6.1) and (6.2), we get

$$\begin{aligned} T_1 = & \sum_{\kappa \in \mathcal{T}_h} \int_{\kappa} \boldsymbol{f} \cdot \boldsymbol{v} \, \mathrm{d}\boldsymbol{x} - \sum_{\kappa \in \mathcal{T}_h} \int_{\kappa} \mu(|\underline{e}(\boldsymbol{u}_{h,k})|)\underline{e}(\boldsymbol{u}_{h,k}) : \underline{e}(\boldsymbol{v}) \, \mathrm{d}\boldsymbol{x} \\ & + \sum_{\kappa \in \mathcal{T}_h} \int_{\kappa} p_{h,k} \nabla \cdot \boldsymbol{v} \, \mathrm{d}\boldsymbol{x} - \sum_{\kappa \in \mathcal{T}_h} \int_{\kappa} q \nabla \cdot \boldsymbol{u}_{h,k} \, \mathrm{d}\boldsymbol{x}. \end{aligned}$$

We let $\boldsymbol{v}_{h,k} \in \boldsymbol{V}(\mathcal{T}_h, \boldsymbol{k})$ be the elementwise interpolant of $\boldsymbol{v}$ which satisfies Lemma 6.10. Then, applying (6.19) with $q = 0$, and performing integration by parts yields

$$
\begin{aligned}
T_1 = &\sum_{\kappa\in\mathcal{T}_h}\int_\kappa \boldsymbol{f}\cdot(\boldsymbol{v}-\boldsymbol{v}_{h,k})\,\mathrm{d}\boldsymbol{x} - \sum_{\kappa\in\mathcal{T}_h}\int_\kappa \mu(|\underline{e}(\boldsymbol{u}_{h,k})|)\underline{e}(\boldsymbol{u}_{h,k}) : \underline{e}(\boldsymbol{v}-\boldsymbol{v}_{h,k})\,\mathrm{d}\boldsymbol{x}\\
&- \sum_{F\in\mathcal{F}_h}\int_F \{\!\!\{\mu(|\underline{e}_h(\boldsymbol{u}_{h,k})|)\underline{e}_h(\boldsymbol{u}_{h,k})\}\!\!\} : \underline{[\![\boldsymbol{v}_{h,k}]\!]}\,\mathrm{d}s\\
&+\theta\sum_{F\in\mathcal{F}_h}\int_F \{\!\!\{\mu(h_F^{-1}|\underline{[\![\boldsymbol{u}_{h,k}]\!]}|)\underline{e}_h(\boldsymbol{v}_{h,k})\}\!\!\} : \underline{[\![\boldsymbol{u}_{h,k}]\!]}\,\mathrm{d}s\\
&+\sum_{F\in\mathcal{F}_h}\int_F \sigma_{h,k}\underline{[\![\boldsymbol{u}_{h,k}]\!]} : \underline{[\![\boldsymbol{v}_{h,k}]\!]}\,\mathrm{d}s + \sum_{\kappa\in\mathcal{T}_h}\int_\kappa p_{h,k}\nabla\cdot(\boldsymbol{v}-\boldsymbol{v}_{h,k})\,\mathrm{d}\boldsymbol{x}\\
&+\sum_{F\in\mathcal{F}_h}\int_F \{\!\!\{p_{h,k}\}\!\!\}[\![\boldsymbol{v}_{h,k}]\!]\,\mathrm{d}s - \sum_{\kappa\in\mathcal{T}_h}\int_\kappa q\nabla\cdot\boldsymbol{u}_{h,k}\,\mathrm{d}\boldsymbol{x}\\
= &\sum_{\kappa\in\mathcal{T}_h}\int_\kappa (\boldsymbol{f}+\nabla\cdot(\mu(|\underline{e}(\boldsymbol{u}_{h,k})|)\underline{e}(\boldsymbol{u}_{h,k})) - \nabla p_{h,k})\cdot(\boldsymbol{v}-\boldsymbol{v}_{h,k})\,\mathrm{d}\boldsymbol{x}\\
&+\sum_{\kappa\in\mathcal{T}_h}\int_{\partial\kappa}(p_{h,k}(\boldsymbol{v}-\boldsymbol{v}_{h,k})\cdot\boldsymbol{n}_\kappa - \mu(|\underline{e}(\boldsymbol{u}_{h,k})|)\underline{e}(\boldsymbol{u}_{h,k}) : (\boldsymbol{v}-\boldsymbol{v}_{h,k})\otimes\boldsymbol{n}_\kappa)\,\mathrm{d}s\\
&- \sum_{F\in\mathcal{F}_h}\int_F \{\!\!\{\mu(|\underline{e}_h(\boldsymbol{u}_{h,k})|)\underline{e}_h(\boldsymbol{u}_{h,k})\}\!\!\} : \underline{[\![\boldsymbol{v}_{h,k}]\!]}\,\mathrm{d}s\\
&+\theta\sum_{F\in\mathcal{F}_h}\int_F \{\!\!\{\mu(h_F^{-1}|\underline{[\![\boldsymbol{u}_{h,k}]\!]}|)\underline{e}_h(\boldsymbol{v}_{h,k})\}\!\!\} : \underline{[\![\boldsymbol{u}_{h,k}]\!]}\,\mathrm{d}s\\
&+\sum_{F\in\mathcal{F}_h}\int_F \sigma_{h,k}\underline{[\![\boldsymbol{u}_{h,k}]\!]} : \underline{[\![\boldsymbol{v}_{h,k}]\!]}\,\mathrm{d}s + \sum_{F\in\mathcal{F}_h}\int_F \{\!\!\{p_{h,k}\}\!\!\}[\![\boldsymbol{v}_{h,k}]\!]\,\mathrm{d}s - \sum_{\kappa\in\mathcal{T}_h}\int_\kappa q\nabla\cdot\boldsymbol{u}_{h,k}\,\mathrm{d}\boldsymbol{x}.
\end{aligned}
$$

Since $\boldsymbol{v} \in \left[H_0^1(\Omega)\right]^d$, we have that $\underline{[\![\boldsymbol{v}]\!]} = \underline{0}$. Thereby, application of (2.3) and (2.4), gives

$$
\begin{aligned}
T_1 = &\sum_{\kappa\in\mathcal{T}_h}\int_\kappa (\boldsymbol{f}+\nabla\cdot(\mu(|\underline{e}(\boldsymbol{u}_{h,k})|)\underline{e}(\boldsymbol{u}_{h,k})) - \nabla p_{h,k})\cdot(\boldsymbol{v}-\boldsymbol{v}_{h,k})\,\mathrm{d}\boldsymbol{x}\\
&+\sum_{F\in\mathcal{F}_h^{\mathcal{I}}}\int_F ([\![p_{h,k}]\!] - [\![\mu(|\underline{e}_h(\boldsymbol{u}_{h,k})|)\underline{e}_h(\boldsymbol{u}_{h,k})]\!])\cdot\{\!\!\{\boldsymbol{v}-\boldsymbol{v}_{h,k}\}\!\!\}\,\mathrm{d}s\\
&+\theta\sum_{F\in\mathcal{F}_h}\int_F \{\!\!\{\mu(h_F^{-1}|\underline{[\![\boldsymbol{u}_{h,k}]\!]}|)\underline{e}_h(\boldsymbol{v}_{h,k})\}\!\!\} : \underline{[\![\boldsymbol{u}_{h,k}]\!]}\,\mathrm{d}s\\
&+\sum_{F\in\mathcal{F}_h}\int_F \sigma_{h,k}\underline{[\![\boldsymbol{u}_{h,k}]\!]} : \underline{[\![\boldsymbol{v}-\boldsymbol{v}_{h,k}]\!]}\,\mathrm{d}s - \sum_{\kappa\in\mathcal{T}_h}\int_\kappa q\nabla\cdot\boldsymbol{u}_{h,k}\,\mathrm{d}\boldsymbol{x}
\end{aligned}
$$

From Lemma 2.1 and (2.1)–(2.2), noting that $k_F \geq 1$ and $\gamma \geq 1$, we get

$$
\begin{aligned}
T_1 \leq & \sum_{\kappa\in\mathcal{T}_h} \|\boldsymbol{f} + \nabla\cdot(\mu(|\underline{e}(\boldsymbol{u}_{h,k})|)\underline{e}(\boldsymbol{u}_{h,k})) - \nabla p_{h,k}\|_{L^2(\kappa)} \|\boldsymbol{v}-\boldsymbol{v}_{h,k}\|_{L^2(\kappa)} \\
& + \frac{1}{2}\sum_{\kappa\in\mathcal{T}_h} \|[\![p_{h,k}]\!] - [\![\mu(|\underline{e}_h(\boldsymbol{u}_{h,k})|)\underline{e}_h(\boldsymbol{u}_{h,k})]\!]\|_{L^2(\partial\kappa\setminus\Gamma)} \|\boldsymbol{v}-\boldsymbol{v}_{h,k}\|_{L^2(\partial\kappa\setminus\Gamma)} \\
& + M_\mu|\theta| \left(\sum_{F\in\mathcal{F}_h}\int_F \frac{k_F^2}{h_F}|\underline{[\![\boldsymbol{u}_{h,k}]\!]}|^2\,\mathrm{d}s\right)^{1/2} \left(\sum_{F\in\mathcal{F}_h}\int_F \frac{h_F}{k_F^2}|\{\!\{|\underline{e}_h(\boldsymbol{v}_{h,k})|\}\!\}|^2\,\mathrm{d}s\right)^{1/2} \\
& + \left(\sum_{F\in\mathcal{F}_h}\int_F \sigma_{h,k}k_F|\underline{[\![\boldsymbol{u}_{h,k}]\!]}|^2\,\mathrm{d}s\right)^{1/2} \left(\sum_{F\in\mathcal{F}_h}\int_F \sigma_{h,k}k_F^{-1}|\underline{[\![\boldsymbol{v}-\boldsymbol{v}_{h,k}]\!]}|^2\,\mathrm{d}s\right)^{1/2} \\
& + \sum_{\kappa\in\mathcal{T}_h} \|q\|_{L^2(\kappa)} \|\nabla\cdot\boldsymbol{u}_{h,k}\|_{L^2(\kappa)} \\
\leq & \sum_{\kappa\in\mathcal{T}_h} \frac{h_\kappa}{k_\kappa} \|\boldsymbol{f} + \nabla\cdot(\mu(|\underline{e}(\boldsymbol{u}_{h,k})|)\underline{e}(\boldsymbol{u}_{h,k})) - \nabla p_{h,k}\|_{L^2(\kappa)} \frac{k_\kappa}{h_\kappa} \|\boldsymbol{v}-\boldsymbol{v}_{h,k}\|_{L^2(\kappa)} \\
& + \frac{1}{2}\sum_{\kappa\in\mathcal{T}_h} \frac{h_\kappa^{1/2}}{k_\kappa^{1/2}} \|[\![p_{h,k}]\!] - [\![\mu(|\underline{e}_h(\boldsymbol{u}_{h,k})|)\underline{e}_h(\boldsymbol{u}_{h,k})]\!]\|_{L^2(\partial\kappa\setminus\Gamma)} \frac{k_\kappa^{1/2}}{h_\kappa^{1/2}} \|\boldsymbol{v}-\boldsymbol{v}_{h,k}\|_{L^2(\partial\kappa\setminus\Gamma)} \\
& + C_T^{1/2} M_\mu|\theta| \left(\sum_{F\in\mathcal{F}_h}\int_F \sigma_{h,k}|\underline{[\![\boldsymbol{u}_{h,k}]\!]}|^2\,\mathrm{d}s\right)^{1/2} \left(\sum_{\kappa\in\mathcal{T}_h} \|\underline{e}(\boldsymbol{v}_{h,k})\|_{L^2(\kappa)}^2\right)^{1/2} \\
& + C_T^{1/2}\gamma^{1/2} C \left(\sum_{F\in\mathcal{F}_h}\int_F \sigma_{h,k}k_F|\underline{[\![\boldsymbol{u}_{h,k}]\!]}|^2\,\mathrm{d}s\right)^{1/2} \left(\sum_{\kappa\in\mathcal{T}_h} \frac{k_\kappa}{h_\kappa}\|\boldsymbol{v}-\boldsymbol{v}_{h,k}\|_{L^2(\partial\kappa)}^2\right)^{1/2} \\
& + \sum_{\kappa\in\mathcal{T}_h} \|q\|_{L^2(\kappa)} \|\nabla\cdot\boldsymbol{u}_{h,k}\|_{L^2(\kappa)} \\
\leq & \left(\sum_{\kappa\in\mathcal{T}_h} \left(\frac{k_\kappa^2}{h_\kappa^2}\|\boldsymbol{v}-\boldsymbol{v}_{h,k}\|_{L^2(\kappa)}^2 + \frac{k_\kappa}{h_\kappa}\|\boldsymbol{v}-\boldsymbol{v}_{h,k}\|_{L^2(\partial\kappa)}^2 + \|\underline{e}(\boldsymbol{v}_{h,k})\|_{L^2(\kappa)}^2 + \|q\|_{L^2(\kappa)}^2\right)\right)^{1/2} \\
& \times C \left(\sum_{\kappa\in\mathcal{T}_h} \widetilde{\eta}_\kappa^2\right)^{1/2},
\end{aligned}
$$

where, for $\kappa \in \mathcal{T}_h$,

$$
\begin{aligned}
\widetilde{\eta}_\kappa^2 = & \, h_\kappa^2 k_\kappa^{-2} \|\boldsymbol{f} + \nabla\cdot(\mu(|\underline{e}(\boldsymbol{u}_{h,k})|)\underline{e}(\boldsymbol{u}_{h,k})) - \nabla p_{h,k}\|_{L^2(\kappa)}^2 + \|\nabla\cdot\boldsymbol{u}_{h,k}\|_{L^2(\kappa)}^2 \\
& + h_\kappa k_\kappa^{-1} \|[\![p_{h,k}]\!] - [\![\mu(|\underline{e}_h(\boldsymbol{u}_{h,k})|)\underline{e}_h(\boldsymbol{u}_{h,k})]\!]\|_{L^2(\partial\kappa\setminus\Gamma)}^2 + \gamma^2 h_\kappa^{-1} k_\kappa^3 \left\|\underline{[\![\boldsymbol{u}_{h,k}]\!]}\right\|_{L^2(\partial\kappa)}^2.
\end{aligned}
$$

Then, as $\|\underline{e}(\boldsymbol{v}_{h,k})\|^2_{L^2(\kappa)} \leq \|\underline{e}(\boldsymbol{v}-\boldsymbol{v}_{h,k})\|^2_{L^2(\kappa)} + \|\underline{e}(\boldsymbol{v})\|^2_{L^2(\kappa)}$, we apply Lemma 6.10 and (6.35) to give that

$$T_1 \leq C\left(\sum_{\kappa\in\mathcal{T}_h}\widetilde{\eta}_\kappa^2\right)^{1/2}\|(\boldsymbol{v},q)\|_{\mathrm{DG}} \leq C\left(\sum_{\kappa\in\mathcal{T}_h}\widetilde{\eta}_\kappa^2\right)^{1/2}.$$

By application of the triangle inequality we deduce the following bound for T_1:

$$T_1 \leq C\left(\sum_{\kappa\in\mathcal{T}_h}\eta_\kappa^2 + \mathcal{O}(\boldsymbol{f},\boldsymbol{u}_{h,k})\right)^{1/2}. \tag{6.37}$$

We now consider the T_2 term; to this end, using the bound (6.5), we get

$$\begin{aligned}
T_2 &\leq C_1\sum_{\widetilde{\kappa}\in\mathcal{T}_{\widetilde{h}}}\int_{\widetilde{\kappa}}|\underline{e}(\boldsymbol{u}_{h,k}^\perp)||\underline{e}(\boldsymbol{v})|\,\mathrm{d}\boldsymbol{x} + \sum_{\widetilde{\kappa}\in\mathcal{T}_{\widetilde{h}}}\int_{\widetilde{\kappa}}|q||\nabla\cdot\boldsymbol{u}_{h,k}^\perp|\,\mathrm{d}\boldsymbol{x}\\
&\leq \max(C_1,1)\sum_{\widetilde{\kappa}\in\mathcal{T}_{\widetilde{h}}}\left(\left\|\underline{e}(\boldsymbol{u}_{h,k}^\perp)\right\|_{L^2(\widetilde{\kappa})}\|\underline{e}(\boldsymbol{v})\|_{L^2(\widetilde{\kappa})} + \|q\|_{L^2(\widetilde{\kappa})}\left\|\nabla\cdot\boldsymbol{u}_{h,k}^\perp\right\|_{L^2(\widetilde{\kappa})}\right)\\
&\leq \max(C_1,1)\left(\sum_{\widetilde{\kappa}\in\mathcal{T}_{\widetilde{h}}}\left(\left\|\underline{e}(\boldsymbol{u}_{h,k}^\perp)\right\|^2_{L^2(\widetilde{\kappa})} + \left\|\nabla\cdot\boldsymbol{u}_{h,k}^\perp\right\|^2_{L^2(\widetilde{\kappa})}\right)\right)^{1/2}\|(\boldsymbol{v},q)\|_{\mathrm{DG}}.
\end{aligned}$$

We note that

$$\sum_{\widetilde{\kappa}\in\mathcal{T}_{\widetilde{h}}}\left\|\nabla\cdot\boldsymbol{u}_{h,k}^\perp\right\|^2_{L^2(\widetilde{\kappa})} \leq d\sum_{\widetilde{\kappa}\in\mathcal{T}_{\widetilde{h}}}\left\|\underline{e}(\boldsymbol{u}_{h,k}^\perp)\right\|^2_{L^2(\widetilde{\kappa})};$$

therefore, applying Lemma 6.9, gives

$$T_2 \leq C\left\|\boldsymbol{u}_{h,k}^\perp\right\|_{\widetilde{h},k}\|(\boldsymbol{v},q)\|_{\mathrm{DG}} \leq C\left(\sum_{F\in\mathcal{F}_h}\int_F\sigma_{h,k}|\underline{[\![\boldsymbol{u}_{h,k}]\!]}|^2\,\mathrm{d}s\right)^{1/2}\|(\boldsymbol{v},q)\|_{\mathrm{DG}}.$$

Recalling (6.35), we deduce that

$$T_2 \leq C\left(\sum_{\kappa\in\mathcal{T}_h}\eta_\kappa^2\right)^{1/2}. \tag{6.38}$$

Substituting (6.36), (6.37) and (6.38) into (6.34) completes the proof. □

6.4.4 Proof of Theorem 6.8

In this section, we prove Theorem 6.8, which follows as an extension of the analysis contained in Houston *et al.* [120, 125], see also Melenk & Wohlmuth [140]. To this end we introduce the following cut-off functions: on the reference triangle $\widehat{S} = \{(x, y) : -1 < x < 1, -1 < y < -x\}$, we define a weight function $\Phi_{\widehat{S}}(\boldsymbol{x}) = \min_{\boldsymbol{y}\in\partial\widehat{\kappa}}|\boldsymbol{x} - \boldsymbol{y}|$, and on the reference hypercube $\widehat{I}^d = (-1, 1)^d$, $d = 1, 2, 3$, we define the weight function $\Phi_d(\boldsymbol{x}) = \prod_{i=1}^d (1 - x_i^2)$. We can state the following auxilary result for these functions:

Lemma 6.12. *Let $\widehat{\kappa}$ be either the reference triangle $\widehat{S}$ or the reference hypercube $\widehat{I}^d$ and $\Phi_{\widehat{\kappa}}$ be the suitable weight function as defined above. Let $\alpha, \beta \in \mathbb{R}$ satisfying $-1 < \alpha < \beta$ and $\delta \in [0, 1]$, then there exists positive constants C_a, C_b and C_c such that for all polynomials $\phi \in \mathcal{S}_k(\widehat{\kappa})$*

$$\begin{aligned}
\int_{\widehat{\kappa}} \Phi_{\widehat{\kappa}} |\nabla\phi|^2 \,\mathrm{d}\boldsymbol{x} &\leq C_a k^2 \int_{\widehat{\kappa}} |\phi|^2 \,\mathrm{d}\boldsymbol{x}, \\
\int_{\widehat{\kappa}} (\Phi_{\widehat{\kappa}})^{\alpha} \phi^2 \,\mathrm{d}\boldsymbol{x} &\leq C_b k^{2(\beta-\alpha)} \int_{\widehat{\kappa}} (\Phi_{\widehat{\kappa}})^{\beta} \phi^2 \,\mathrm{d}\boldsymbol{x}, \\
\int_{\widehat{\kappa}} (\Phi_{\widehat{\kappa}})^{2\delta} |\nabla\phi|^2 \,\mathrm{d}\boldsymbol{x} &\leq C_c k^{2(2-\delta)} \int_{\widehat{\kappa}} (\Phi_{\widehat{\kappa}})^{\delta} \phi^2 \,\mathrm{d}\boldsymbol{x}.
\end{aligned}$$

Additionally, if $\phi = 0$ on $\partial\widehat{\kappa}$, then

$$\int_{\widehat{\kappa}} |\nabla\phi|^2 \,\mathrm{d}\boldsymbol{x} \leq C_a k^2 \int_{\widehat{\kappa}} (\Phi_{\widehat{\kappa}})^{-1} \phi^2 \,\mathrm{d}\boldsymbol{x}.$$

Proof. For $d = 1$ the results can be found in Bernardi & Maday [29] and Bernardi *et al.* [30]. Extension for the hypercube to $d = 2, 3$ follows by tensor-product arguments; cf. Zhu [181, Lemma 4.5.1]. The result for the reference triangle can be found in Melenk & Wohlmuth [140, Theorem 2.5]. □

For $\kappa \in \mathcal{T}_h$, we let

$$\Phi_\kappa = \begin{cases} c_\kappa \Phi_{\widehat{S}} \circ T_\kappa^{-1}, & \text{if } d = 2 \text{ and } \kappa \text{ is a triangle,} \\ c_\kappa \Phi_d \circ T_\kappa^{-1}, & \text{otherwise,} \end{cases}$$

where c_κ is chosen such that $\int_\kappa (\Phi_\kappa - 1)\,\mathrm{d}\boldsymbol{x} = 0$, and for an interior face $F \in \mathcal{F}_h^{\mathcal{I}}$, we let $\Phi_F = c_F \Phi_{d-1} \circ T_F^{-1}$ where T_F is the affine mapping from the $(d-1)$ dimensional reference hypercube to F and c_F is chosen such that $\int_F (\Phi_F - 1)\,\mathrm{d}s = 0$.

We are now able to prove the four results in Theorem 6.8 separately.

Proof of (a). We define $\boldsymbol{v}_\kappa = \Phi_\kappa^\alpha \Pi_{\kappa,k_\kappa}|_\kappa (\boldsymbol{f} + \nabla \cdot (\mu(|\underline{\boldsymbol{e}}(\boldsymbol{u}_{h,k})|)\underline{\boldsymbol{e}}(\boldsymbol{u}_{h,k}))) - \nabla p_{h,k}$ for $\kappa \in \mathcal{T}_h$ where $\alpha \in (1/2, 1]$. Using (6.1) and integrating by parts yields

$$
\begin{aligned}
\left\| \Phi_\kappa^{-\alpha/2} \boldsymbol{v}_\kappa \right\|_{L^2(\kappa)}^2 &= \int_\kappa \boldsymbol{v}_\kappa \cdot (\nabla \cdot (\mu(|\underline{\boldsymbol{e}}(\boldsymbol{u}_{h,k})|)\underline{\boldsymbol{e}}(\boldsymbol{u}_{h,k}) - \mu(|\underline{\boldsymbol{e}}(\boldsymbol{u})|)\underline{\boldsymbol{e}}(\boldsymbol{u})) + \nabla(p - p_{h,k}))\,\mathrm{d}\boldsymbol{x} \\
&\quad + \int_\kappa \boldsymbol{v}_\kappa \cdot (\Pi_{\kappa,k_\kappa} - \mathbb{I})\,(\boldsymbol{f} + \nabla \cdot (\mu(|\underline{\boldsymbol{e}}(\boldsymbol{u}_{h,k})|)\underline{\boldsymbol{e}}(\boldsymbol{u}_{h,k})))\,\mathrm{d}\boldsymbol{x} \\
&= -\int_\kappa \nabla \boldsymbol{v}_\kappa : (\mu(|\underline{\boldsymbol{e}}(\boldsymbol{u}_{h,k})|)\underline{\boldsymbol{e}}(\boldsymbol{u}_{h,k}) - \mu(|\underline{\boldsymbol{e}}(\boldsymbol{u})|)\underline{\boldsymbol{e}}(\boldsymbol{u})) + \nabla \cdot \boldsymbol{v}_\kappa\,(p - p_{h,k})\,\mathrm{d}\boldsymbol{x} \\
&\quad + \int_\kappa \boldsymbol{v}_\kappa \cdot (\Pi_{\kappa,k_\kappa} - \mathbb{I})\,(\boldsymbol{f} + \nabla \cdot (\mu(|\underline{\boldsymbol{e}}(\boldsymbol{u}_{h,k})|)\underline{\boldsymbol{e}}(\boldsymbol{u}_{h,k})))\,\mathrm{d}\boldsymbol{x} \\
&\leq \int_\kappa |\nabla \boldsymbol{v}_\kappa||\mu(|\underline{\boldsymbol{e}}(\boldsymbol{u}_{h,k})|)\underline{\boldsymbol{e}}(\boldsymbol{u}_{h,k}) - \mu(|\underline{\boldsymbol{e}}(\boldsymbol{u})|)\underline{\boldsymbol{e}}(\boldsymbol{u})|\,\mathrm{d}\boldsymbol{x} \\
&\quad + \int_\kappa |\nabla \cdot \boldsymbol{v}_\kappa||p - p_{h,k}|\,\mathrm{d}\boldsymbol{x} \\
&\quad + \int_\kappa |\boldsymbol{v}_\kappa||(\Pi_{\kappa,k_\kappa} - \mathbb{I})\,(\boldsymbol{f} + \nabla \cdot (\mu(|\underline{\boldsymbol{e}}(\boldsymbol{u}_{h,k})|)\underline{\boldsymbol{e}}(\boldsymbol{u}_{h,k})))|\,\mathrm{d}\boldsymbol{x}.
\end{aligned}
$$

Using (6.5) and the fact that $\|\nabla \cdot \boldsymbol{v}\|_{L^2(\kappa)} \leq d\,\|\nabla \boldsymbol{v}\|_{L^2(\kappa)}$ for all vector-valued functions $\boldsymbol{v}$, this becomes

$$
\begin{aligned}
\left\| \Phi_\kappa^{-\alpha/2} \boldsymbol{v}_\kappa \right\|_{L^2(\kappa)}^2 &\leq C_1\,\|\nabla \boldsymbol{v}_\kappa\|_{0,\kappa}\,\|\underline{\boldsymbol{e}}(\boldsymbol{u} - \boldsymbol{u}_{h,k})\|_{L^2(\kappa)} + d\,\|\nabla \boldsymbol{v}_\kappa\|_{L^2(\kappa)}\,\|p - p_{h,k}\|_{L^2(\kappa)} \\
&\quad + \left\| \Phi_\kappa^{-\alpha/2} \boldsymbol{v}_\kappa \right\|_{L^2(\kappa)} \left\| \Phi_\kappa^{\alpha/2}\,(\Pi_{\kappa,k_\kappa} - \mathbb{I})\,(\boldsymbol{f} + \nabla \cdot (\mu(|\underline{\boldsymbol{e}}(\boldsymbol{u}_{h,k})|)\underline{\boldsymbol{e}}(\boldsymbol{u}_{h,k}))) \right\|_{L^2(\kappa)} \\
&\leq \|\nabla \boldsymbol{v}_\kappa\|_{L^2(\kappa)} \left(C_1\,\|\underline{\boldsymbol{e}}(\boldsymbol{u} - \boldsymbol{u}_{h,k})\|_{L^2(\kappa)} + d\,\|p - p_{h,k}\|_{L^2(\kappa)} \right) \\
&\quad + h_\kappa^{-1} k_\kappa \left\| \Phi_\kappa^{-\alpha/2} \boldsymbol{v}_\kappa \right\|_{L^2(\kappa)} \sqrt{\mathcal{O}_\kappa^{(1)}}.
\end{aligned}
$$

As Lemma 6.12 holds then from the proof of Melenk & Wohlmuth [140, Lemma 3.4] we have that

$$
\|\nabla \boldsymbol{v}_\kappa\|_{L^2(\kappa)} \leq C h_\kappa^{-1} k_\kappa^{2-\alpha} \left\| \Phi_\kappa^{-\alpha/2} \boldsymbol{v}_\kappa \right\|_{L^2(\kappa)}.
$$

Thereby,

$$\left\|\Phi_\kappa^{-\alpha/2}\boldsymbol{v}_\kappa\right\|_{L^2(\kappa)}^2 \leq Ch_\kappa^{-1}k_\kappa \left\|\Phi_\kappa^{-\alpha/2}\boldsymbol{v}_\kappa\right\|_{L^2(\kappa)} \times \left(k_\kappa^{1-\alpha}\left(\|\underline{e}(\boldsymbol{u}-\boldsymbol{u}_{h,k})\|_{L^2(\kappa)} + \|p-p_{h,k}\|_{L^2(\kappa)}\right) + \sqrt{\mathcal{O}_\kappa^{(1)}}\right).$$

Dividing both sides by $\left\|\Phi_\kappa^{-\alpha/2}\boldsymbol{v}_\kappa\right\|_{L^2(\kappa)}$ gives that

$$\left\|\Phi_\kappa^{-\alpha/2}\boldsymbol{v}_\kappa\right\|_{L^2(\kappa)}^2 \leq Ch_\kappa^{-1}k_\kappa \left(k_\kappa^{1-\alpha}\left(\|\underline{e}(\boldsymbol{u}-\boldsymbol{u}_{h,k})\|_{L^2(\kappa)} + \|p-p_{h,k}\|_{L^2(\kappa)}\right) + \sqrt{\mathcal{O}_\kappa^{(1)}}\right).$$

From Lemma 6.12

$$\begin{aligned}
&\|\Pi_{\kappa,k_\kappa}|_\kappa(\boldsymbol{f}+\nabla\cdot(\mu(|\underline{e}(\boldsymbol{u}_{h,k})|)\underline{e}(\boldsymbol{u}_{h,k}))) - \nabla p\|_{L^2(\kappa)} \\
&\quad\leq Ck_\kappa^\alpha \left\|\Phi_\kappa^{\alpha/2}\left(\Pi_{\kappa,k_\kappa}|_\kappa(\boldsymbol{f}+\nabla\cdot(\mu(|\underline{e}(\boldsymbol{u}_{h,k})|)\underline{e}(\boldsymbol{u}_{h,k}))) - \nabla p\right)\right\|_{L^2(\kappa)} \\
&\quad\leq Ch_\kappa^{-1}k_\kappa^{1+\alpha}\left(k_\kappa^{1-\alpha}\left(\|\underline{e}(\boldsymbol{u}-\boldsymbol{u}_{h,k})\|_{L^2(\kappa)} + \|p-p_{h,k}\|_{L^2(\kappa)}\right) + \sqrt{\mathcal{O}_\kappa^{(1)}}\right). \quad (6.39)
\end{aligned}$$

Selecting $\delta = \alpha - 1/2$ completes the proof of Theorem 6.8(a).

Proof of (b). Noting for all vector-valued functions $\boldsymbol{v}$ that $\|\nabla\cdot\boldsymbol{v}\|_{L^2(\kappa)} \leq d\,\|\underline{e}(\boldsymbol{v})\|_{L^2(\kappa)}$ for all $\kappa\in\mathcal{T}_h$ and applying (6.2) we have that

$$\|\nabla\cdot\boldsymbol{u}_{h,k}\|_{0,\kappa} = \|\nabla\cdot(\boldsymbol{u}-\boldsymbol{u}_{h,k})\|_{L^2(\kappa)} \leq d\,\|\underline{e}(\boldsymbol{u}-\boldsymbol{u}_{h,k})\|_{L^2(\kappa)}$$

which completes the proof of Theorem 6.8(b).

Proof of (c). Define $\boldsymbol{q}_F = \Phi_F^\alpha([\![p_{h,k}]\!] - \Pi_{F,k_F}|_F[\![\mu(|\underline{e}_h(\boldsymbol{u}_{h,k})|)\underline{e}_h(\boldsymbol{u}_{h,k})]\!]|_F)$ for $F\in\mathcal{F}_h^{\mathcal{I}}$, where $\alpha\in(1/2,1]$, then, from Melenk & Wohlmuth [140, Lemma 2.6] with $\varepsilon = k_\kappa^{-2}$, there exists a function $\boldsymbol{\chi}_F\in\left[H_0^1(\omega_F)\right]^d$ such that $\boldsymbol{\chi}_F|_F = \boldsymbol{q}_F$ and

$$\|\boldsymbol{\chi}_F\|_{L^2(\omega_F)} \leq Ch_\kappa^{1/2}k_\kappa^{-1}\left\|\Phi_F^{-\alpha/2}\boldsymbol{q}_F\right\|_{L^2(F)}, \quad (6.40)$$

$$\|\nabla\boldsymbol{\chi}_F\|_{L^2(\omega_F)} \leq Ch_\kappa^{-1/2}k_\kappa\left\|\Phi_F^{-\alpha/2}\boldsymbol{q}_F\right\|_{L^2(F)}; \quad (6.41)$$

cf. Houston *et al.* [125] and Zhu [181]. Noting that $-\nabla\cdot(\mu(|\underline{e}(\boldsymbol{u})|)\underline{e}(\boldsymbol{u}))+\nabla p=\boldsymbol{f}\in\left[L^2(\Omega)\right]^d$, we conclude $[\![\mu(|\underline{e}(\boldsymbol{u})|)\underline{e}(\boldsymbol{u})]\!]-[\![p]\!]=0$ on $F\in\mathcal{F}_h^{\mathcal{I}}$. Hence,

$$\begin{aligned}
\left\|\Phi_F^{-\alpha/2}\boldsymbol{q}_F\right\|_{L^2(F)}^2 &= \int_F([\![p_{h,k}-p]\!]-[\![\mu(|\underline{e}(\boldsymbol{u}_{h,k})|)\underline{e}_h(\boldsymbol{u}_{h,k})-\mu(|\underline{e}_h(\boldsymbol{u})|)\underline{e}(\boldsymbol{u})]\!])\cdot\boldsymbol{\chi}_F\,\mathrm{d}s\\
&\quad-\int_F(\Pi_{F,k_F}-\mathbb{I})\,[\![\mu(|\underline{e}_h(\boldsymbol{u}_{h,k})|)\underline{e}_h(\boldsymbol{u}_{h,k})]\!]\cdot\boldsymbol{\chi}_F\,\mathrm{d}s\\
&=\int_{\partial\kappa}(p_{h,k}-p)\boldsymbol{n}_\kappa\cdot\boldsymbol{\chi}_F\,\mathrm{d}s+\int_{\partial\kappa'}(p_{h,k}-p)\boldsymbol{n}_{\kappa'}\cdot\boldsymbol{\chi}_F\,\mathrm{d}s\\
&\quad-\int_{\partial\kappa}(\mu(|\underline{e}_h(\boldsymbol{u}_{h,k})|)\underline{e}_h(\boldsymbol{u}_{h,k})-\mu(|\underline{e}(\boldsymbol{u})|)\underline{e}(\boldsymbol{u}))\boldsymbol{n}_\kappa\cdot\boldsymbol{\chi}_F\,\mathrm{d}s\\
&\quad-\int_{\partial\kappa'}(\mu(|\underline{e}_h(\boldsymbol{u}_{h,k})|)\underline{e}_h(\boldsymbol{u}_{h,k})-\mu(|\underline{e}(\boldsymbol{u})|)\underline{e}(\boldsymbol{u}))\boldsymbol{n}_{\kappa'}\cdot\boldsymbol{\chi}_F\,\mathrm{d}s\\
&\quad-\int_F(\Pi_{F,k_F}-\mathbb{I})\,[\![\mu(|\underline{e}_h(\boldsymbol{u}_{h,k})|)\underline{e}_h(\boldsymbol{u}_{h,k})]\!]\cdot\boldsymbol{\chi}_F\,\mathrm{d}s\\
&=\int_{\omega_F}(p_{h,k}-p)\nabla_h\cdot\boldsymbol{\chi}_F\,\mathrm{d}\boldsymbol{x}\\
&\quad-\int_{\omega_F}(\mu(|\underline{e}_h(\boldsymbol{u}_{h,k})|)\underline{e}_h(\boldsymbol{u}_{h,k})-\mu(|\underline{e}(\boldsymbol{u})|)\underline{e}(\boldsymbol{u})):\nabla_h\boldsymbol{\chi}_F\,\mathrm{d}\boldsymbol{x}\\
&\quad-\int_{\omega_F}(\boldsymbol{f}+\nabla_h\cdot(\mu(|\underline{e}_h(\boldsymbol{u}_{h,k})|)\underline{e}_h(\boldsymbol{u}_{h,k}))-\nabla_h p_{h,k})\cdot\boldsymbol{\chi}_F\,\mathrm{d}\boldsymbol{x}\\
&\quad-\int_F(\Pi_{F,k_F}-\mathbb{I})\,[\![\mu(|\underline{e}_h(\boldsymbol{u}_{h,k})|)\underline{e}_h(\boldsymbol{u}_{h,k})]\!]\cdot\boldsymbol{\chi}_F\,\mathrm{d}s\\
&\equiv R_1+R_2+R_3,
\end{aligned}\tag{6.42}$$

where

$$\begin{aligned}
R_1&=\int_{\omega_F}(p_{h,k}-p)\nabla_h\cdot\boldsymbol{\chi}_F\,\mathrm{d}\boldsymbol{x}-\int_{\omega_F}(\mu(|\underline{e}_h(\boldsymbol{u}_{h,k})|)\underline{e}_h(\boldsymbol{u}_{h,k})-\mu(|\underline{e}(\boldsymbol{u})|)\underline{e}(\boldsymbol{u})):\nabla_h\boldsymbol{\chi}_F\,\mathrm{d}\boldsymbol{x},\\
R_2&=-\int_{\omega_F}(\boldsymbol{f}+\nabla_h\cdot(\mu(|\underline{e}_h(\boldsymbol{u}_{h,k})|)\underline{e}_h(\boldsymbol{u}_{h,k}))-\nabla_h p_{h,k})\cdot\boldsymbol{\chi}_F\,\mathrm{d}\boldsymbol{x},\\
R_3&=-\int_F(\Pi_{F,k_F}-\mathbb{I})\,[\![\mu(|\underline{e}_h(\boldsymbol{u}_{h,k})|)\underline{e}_h(\boldsymbol{u}_{h,k})]\!]\cdot\boldsymbol{\chi}_F\,\mathrm{d}s.
\end{aligned}$$

Employing (6.5) and (6.41), R_1 can be bounded as follows

$$\begin{aligned}
R_1&\le\|p-p_{h,k}\|_{L^2(\omega_F)}\|\nabla_h\cdot\boldsymbol{\chi}_F\|_{L^2(\omega_F)}+C_1\|\underline{e}_h(\boldsymbol{u}-\boldsymbol{u}_{h,k})\|_{L^2(\omega_F)}\|\nabla_h\boldsymbol{\chi}_F\|_{L^2(\omega_F)}\\
&\le Ch_\kappa^{-1/2}k_\kappa\left(d\|p-p_{h,k}\|_{L^2(\omega_F)}+C_1\|\underline{e}_h(\boldsymbol{u}-\boldsymbol{u}_{h,k})\|_{L^2(\omega_F)}\right)\left\|\Phi_F^{-\alpha/2}\boldsymbol{q}_F\right\|_{L^2(F)}.
\end{aligned}\tag{6.43}$$

To obtain a bound for R_2 we employ (6.39), the definition of $\mathcal{O}_\kappa^{(1)}$ and (6.40); therefore,

$$\begin{aligned}
R_2 &= -\int_{\omega_F} \left(\Pi_{\kappa,k_\kappa}\left(\boldsymbol{f} + \nabla_h \cdot (\mu(|\underline{e}_h(\boldsymbol{u}_{h,k})|)\underline{e}_h(\boldsymbol{u}_{h,k}))\right) - \nabla_h p_{h,k}\right) \cdot \boldsymbol{\chi}_F \,\mathrm{d}\boldsymbol{x} \\
&\quad + \int_{\omega_F} \left(\Pi_{\kappa,k_\kappa} - \mathbb{I}\right)\left(\boldsymbol{f} + \nabla_h \cdot (\mu(|\underline{e}_h(\boldsymbol{u}_{h,k})|)\underline{e}_h(\boldsymbol{u}_{h,k}))\right) \cdot \boldsymbol{\chi}_F \,\mathrm{d}\boldsymbol{x} \\
&\leq \left\|\Pi_{\kappa,k_\kappa}\left(\boldsymbol{f} + \nabla_h \cdot (\mu(|\underline{e}_h(\boldsymbol{u}_{h,k})|)\underline{e}_h(\boldsymbol{u}_{h,k}))\right) - \nabla_h p_{h,k}\right\|_{L^2(\omega_F)} \|\boldsymbol{\chi}_F\|_{L^2(\omega_F)} \\
&\quad + \left\|\left(\Pi_{\kappa,k_\kappa} - \mathbb{I}\right)\left(\boldsymbol{f} + \nabla_h \cdot (\mu(|\underline{e}_h(\boldsymbol{u}_{h,k})|)\underline{e}_h(\boldsymbol{u}_{h,k}))\right)\right\|_{L^2(\omega_F)} \|\boldsymbol{\chi}_F\|_{L^2(\omega_F)} \\
&\leq C h_\kappa^{-1/2} k_\kappa^\alpha \left\|\Phi_F^{-\alpha/2}\boldsymbol{q}_F\right\|_{L^2(F)} \\
&\quad \times \left(k_\kappa^{1-\alpha}\left(\|\underline{e}_h(\boldsymbol{u} - \boldsymbol{u}_{h,k})\|_{L^2(\omega_F)} - \|p - p_{h,k}\|_{L^2(\omega_F)}\right) + \sum_{\tau\in\{\kappa,\kappa'\}} \sqrt{\mathcal{O}_\tau^{(1)}}\right). \qquad (6.44)
\end{aligned}$$

The bound for R_3 follows from the definition of $\mathcal{O}_F^{(2)}$ and the fact that $\boldsymbol{\chi}_F = \boldsymbol{q}_F$ on $F \in \mathcal{F}_h^{\mathcal{I}}$:

$$\begin{aligned}
R_3 &\leq \left\|\Phi_F^{\alpha/2}\left(\Pi_{F,k_F} - \mathbb{I}\right)[\![\mu(|\underline{e}_h(\boldsymbol{u}_{h,k})|)\underline{e}_h(\boldsymbol{u}_{h,k})]\!]\right\|_{L^2(F)} \left\|\Phi_F^{-\alpha/2}\boldsymbol{\chi}_F\right\|_{L^2(F)} \\
&\leq C h_\kappa^{-1/2} k_\kappa^{1/2} \sqrt{\mathcal{O}_F^{(2)}} \left\|\Phi_F^{-\alpha/2}\boldsymbol{q}_F\right\|_{L^2(F)}. \qquad (6.45)
\end{aligned}$$

Combining (6.42)–(6.45) and dividing through by $\left\|\Phi_F^{-\alpha/2}\boldsymbol{q}_F\right\|_{L^2(F)}$ gives

$$\begin{aligned}
\left\|\Phi_F^{-\alpha/2}\boldsymbol{q}_F\right\|_{L^2(F)} \leq C h_\kappa^{-1/2} k_\kappa \Bigg(&\|\underline{e}_h(\boldsymbol{u} - \boldsymbol{u}_{h,k})\|_{L^2(\omega_F)} - \|p - p_{h,k}\|_{L^2(\omega_F)} \\
&+ k_\kappa^{\alpha-1} \sum_{\tau\in\{\kappa,\kappa'\}} \sqrt{\mathcal{O}_\tau^{(1)}} + k_\kappa^{1/2}\sqrt{\mathcal{O}_F^{(2)}}\Bigg).
\end{aligned}$$

From Lemma 6.12 we have that

$$\begin{aligned}
&\|[\![p_{h,k}]\!] - \Pi_{F,k_F}[\![\mu(|\underline{e}_h(\boldsymbol{u}_{h,k})|)\underline{e}_h(\boldsymbol{u}_{h,k})]\!]\|_{L^2(F)} \\
&\qquad \leq C k_\kappa^\alpha \left\|\Phi_F^{\alpha/2}([\![p_{h,k}]\!] - \Pi_{F,k_F}[\![\mu(|\underline{e}_h(\boldsymbol{u}_{h,k})|)\underline{e}_h(\boldsymbol{u}_{h,k})]\!])\right\|_{L^2(F)} \\
&\qquad = C k_\kappa^\alpha \left\|\Phi_F^{-\alpha/2}\boldsymbol{q}_F\right\|_{L^2(F)}.
\end{aligned}$$

Therefore,

$$\begin{aligned}\|[\![p_{h,k}]\!] - \Pi_{F,k_F}[\![\mu(|\underline{e}_h(\boldsymbol{u}_{h,k})|)\underline{e}_h(\boldsymbol{u}_{h,k})]\!]\|_{L^2(F)} \\ \leq Ch_\kappa^{-1/2}k_\kappa^{1+\alpha}\Bigg(\|\underline{e}_h(\boldsymbol{u}-\boldsymbol{u}_{h,k})\|_{L^2(\omega_F)} - \|p-p_{h,k}\|_{L^2(\omega_F)} \\ + k_\kappa^{\alpha-1}\sum_{\tau\in\{\kappa,\kappa'\}}\sqrt{\mathcal{O}_\tau^{(1)}} + k_\kappa^{1/2}\sqrt{\mathcal{O}_F^{(2)}}\Bigg).\end{aligned}$$

Selecting $\delta = \alpha - 1/2$ again completes the proof of Theorem 6.8(c).

Proof of (d). Since $\boldsymbol{u} \in \left[H_0^1(\Omega)\right]^d$, then $|[\![\underline{\boldsymbol{u}}]\!]| = 0$ on $F \in \mathcal{F}_h$; thereby, from (2.1)–(2.2), we have that

$$\left\||[\![\underline{\boldsymbol{u}_{h,k}}]\!]|\right\|_{L^2(F)} = \left\||[\![\underline{\boldsymbol{u}-\boldsymbol{u}_{h,k}}]\!]|\right\|_{L^2(F)} \leq C\gamma^{-1/2}h_\kappa^{1/2}k_\kappa^{-1}\left\|\sigma_{h,k}^{1/2}[\![\underline{\boldsymbol{u}-\boldsymbol{u}_{h,k}}]\!]\right\|_{L^2(F)}$$

This completes the proof of Theorem 6.8. □

6.5 Numerical Experiments

In this section, we present a series of numerical experiments to computationally verify the *a priori* error estimate derived in Theorem 6.5, as well as to demonstrate the performance of the *a posteriori* error bound derived in Theorem 6.7 within an automatic hp-adaptive refinement procedure based on 1-irregular quadrilateral elements for $\Omega \subset \mathbb{R}^2$. Throughout this section the DGFEM solution $(\boldsymbol{u}_{h,k}, p_{h,k})$ defined by (6.12)–(6.13) is computed with $\theta = 0$, i.e., we employ the IIP DGFEM. Additionally, we set the constant γ appearing in the interior penalty parameter $\sigma_{h,k}$ defined by (6.14) equal to 10. The resulting system of nonlinear equations is solved based on employing a damped Newton method; for each inner (linear) iteration, we employ the Multifrontal Massively Parallel Solver (MUMPS), see Amestoy *et al.* [2, 3, 4].

The hp-adaptive meshes are constructed by first marking the elements for refinement/derefinement according to the size of the local error indicators η_κ; this is achieved via a fixed fraction strategy where the refinement and derefinement fractions are set to

25% and 5%, respectively. We employ the hp-adaptive strategy developed by Houston & Süli [116] to decide whether h- or p-refinement/derefinement should be performed on an element $\kappa \in \mathcal{T}_h$ marked for refinement/derefinement. We note here that we start with a polynomial degree of $k_\kappa = 3$ for all $\kappa \in \mathcal{T}_h$.

The purpose of these experiments is to demonstrate that the *a posteriori* error indicator in Theorem 6.7 converges to zero at the same asymptotic rate as the actual error in the DGFEM energy norm $\|(\cdot,\cdot)\|_{\mathrm{DG}}$, on a sequence of non-uniform hp-adaptively refined meshes. We also demonstrate that the hp-adaptive strategy converges at a higher rate than an h-adaptive refinement strategy, which uses the same 25% and 5% refinement/derefinement fixed fraction strategy, but only undertakes mesh subdivision for a fixed (uniform) polynomial degree distribution.

6.5.1 Example 1: Smooth Solution

In this first example, we let Ω be the L-shaped domain $(-1,1)^2 \setminus [0,1) \times (-1,0]$, and consider the nonlinearity

$$\mu(|\underline{e}(\boldsymbol{u})|) = 2 + \frac{1}{1+|\underline{e}(\boldsymbol{u})|^2}.$$

In addition, we select $\boldsymbol{f}$ so that the analytical solution to (6.1)–(6.3) is given by

$$\boldsymbol{u}(x,y) = \begin{pmatrix} -\mathrm{e}^x(y\cos(y)+\sin(y)) \\ \mathrm{e}^x y \sin(y) \end{pmatrix},$$
$$p(x,y) = 2\mathrm{e}^x \sin(y) - 2/3(1-\mathrm{e})(\cos(1)-1).$$

Here, we investigate the convergence of the DGFEM (6.12)–(6.13) on a sequence of uniformly refined square meshes for different (fixed) values of the polynomial degree k. To this end, in Figure 6.1(a) we present a comparison of the DGFEM energy norm $\|(\cdot,\cdot)\|_{\mathrm{DG}}$ with the mesh function h for k ranging between 1 and 5. Here, we clearly see that $\|(\boldsymbol{u}-\boldsymbol{u}_{h,k}, p-p_{h,k})\|_{\mathrm{DG}}$ converges like $\mathcal{O}(h^k)$ as h tends to zero for each (fixed) k, which is in complete agreement with Theorem 6.7. Secondly, we investigate the

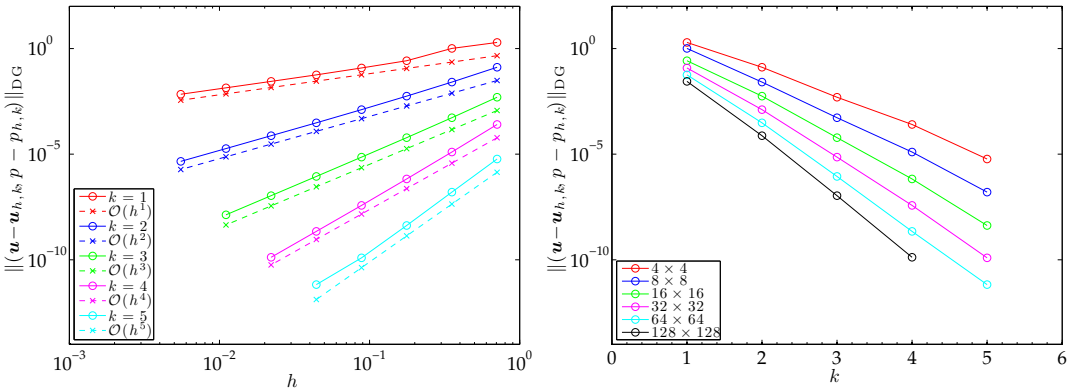

Figure 6.1: Example 1. Convergence of the DGFEM with (a) h-refinement; (b) p-refinement.

convergence of the DGFEM with k-enrichment for fixed h. Since the analytical solution to this problem is a real analytic function, we expect to observe exponential rates of convergence. Indeed, Figure 6.1(b) clearly illustrates this behaviour: on the linear-log scale, the convergence plots for each mesh become straight lines as the degree of the approximating polynomial is increased.

6.5.2 Example 2: Cavity Problem

In this example, we consider the cavity-like problem from Berrone & Süli [31, Section 6.1] using the Carreau law nonlinearity

$$\mu(|\underline{e}(\boldsymbol{u})|) = k_\infty + (k_0 - k_\infty)(1+\lambda|\underline{e}(\boldsymbol{u})|^2)^{(\vartheta-2)/2},$$

with $k_\infty = 1, k_0 = 2, \lambda = 1$ and $\vartheta = 1.2$. We let Ω be the unit square $(0,1)^2 \subset \mathbb{R}^2$ and select the forcing function $\boldsymbol{f}$ so that the analytical solution to (6.1)–(6.3) is given by

$$\boldsymbol{u}(x,y) = \begin{pmatrix} \left(1-\cos\left(2\frac{\pi\left(\mathrm{e}^{\vartheta x}-1\right)}{\mathrm{e}^{\vartheta}-1}\right)\right)\sin(2\pi y) \\ -\vartheta \mathrm{e}^{\vartheta x}\sin\left(2\frac{\pi\left(\mathrm{e}^{\vartheta x}-1\right)}{\mathrm{e}^{\vartheta}-1}\right)\frac{1-\cos(2\pi y)}{\mathrm{e}^{\vartheta}-1} \end{pmatrix},$$

$$p(x,y) = 2\pi\vartheta \mathrm{e}^{\vartheta x}\sin\left(2\frac{\pi\left(\mathrm{e}^{\vartheta x}-1\right)}{\mathrm{e}^{\vartheta}-1}\right)\frac{\sin(2\pi y)}{\mathrm{e}^{\vartheta}-1}.$$

In this example, we now turn our attention to the performance of the proposed

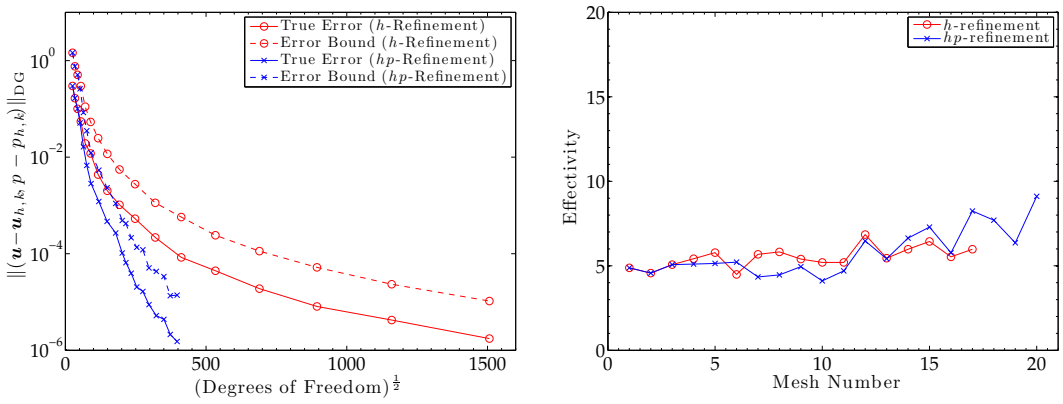

Figure 6.2: Example 2. (a) Comparison of the error in the DGFEM norm employing both h- and hp-refinement, with respect to the number of degrees of freedom; (b) Effectivity index using both h- and hp-refinement.

hp-adaptive refinement algorithm. To this end, in Figure 6.2(a) we present a comparison of the actual error measured in the DGFEM norm and the *a posteriori* error bound versus the square root of the number of degrees of freedom on a linear-log scale for the sequence of meshes generated by both the h- and hp-adaptive algorithms; in each case the initial value of the polynomial degree k is set equal to 3. We observe that the error bound over-estimates the true error by roughly a consistent factor; this is confirmed in Figure 6.2(b), where the effectivity indices for the sequence of meshes which, although slightly oscillatory, all lie in roughly the range 4–8. From Figure 6.2(a) we can also see that the DGFEM norm of the error converges to zero at an exponential rate when hp-adaptivity is employed. Consequently, we observe the superiority of the grid adaptation algorithm based on employing hp-refinement in comparison to a standard h-version method; on the final mesh the DGFEM norm of the discretization error is over an order of magnitude smaller when the former algorithm is employed, in comparison to the latter, for a fixed number of degrees of freedom.

In Figures 6.3(a) and (b) we show the meshes generated after 10 mesh refinements using the h- and hp-adaptive mesh refinement strategies, respectively. Figure 6.3(c) displays the analytical solution to this example for comparison to the meshes; as noted in Berrone & Süli [31] the flow exhibits a counter-clockwise vortex around the point

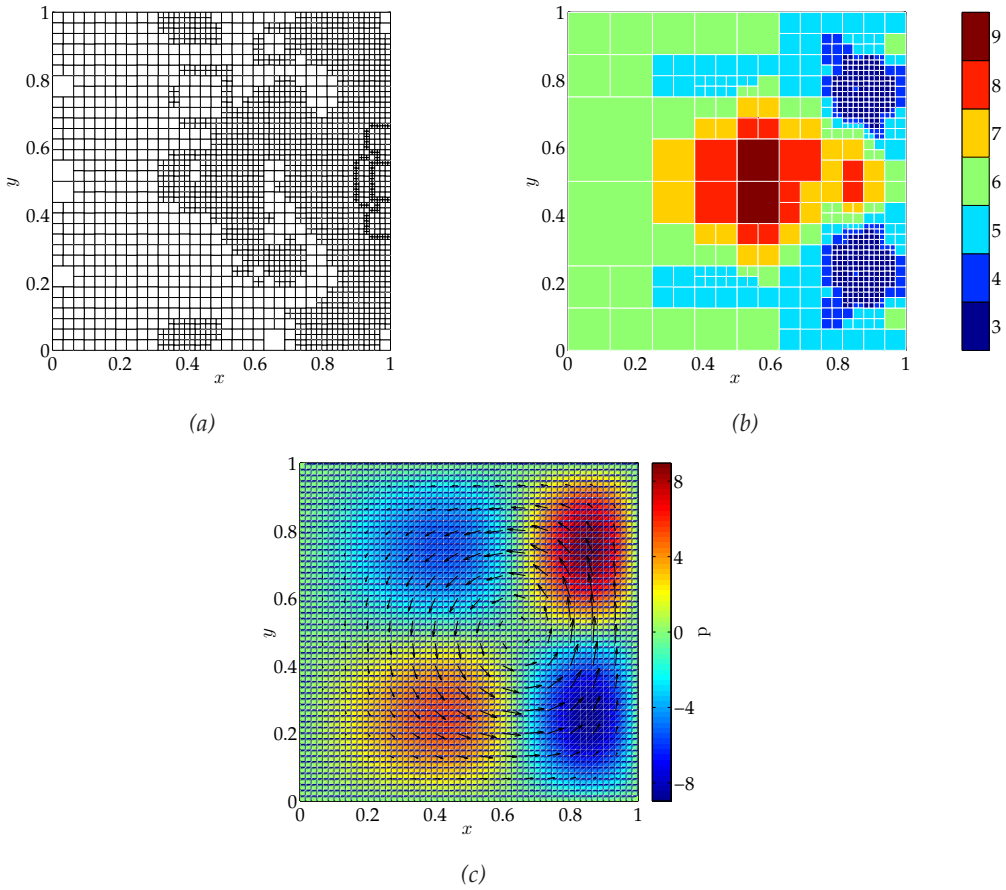

Figure 6.3: Example 2. Finite element mesh after 10 adaptive refinement steps: (a) h-adaptivity; (b) hp-adaptivity; (c) Analytical solution.

$(1/\vartheta \log((e^{\vartheta}+1)/2), 1/2)$, though the analytical solution is relatively smooth. We can see that the h-adaptive refinement strategy performs nearly uniform h-refinement as we would expect for such a smooth analytical solution, with more refinement around the vortex centre and the hill and valley on the right side of the vortex. With the hp-refinement strategy, we note that mostly p-refinement has occurred, which is as expected for a smooth analytical solution, with the main p-refinement occurring around the vortex centre and more h-refinement occurring around the centre of the hills and valleys in the pressure function; further h-refinement has also occurred in the 'tighter' hill and valley on the right caused by the off-centre vortex.

6.5.3 Example 3: Singular Solution

For this example we consider a nonlinear version of the singular solution from Verfürth [170, p. 113], see also Houston *et al.* [120], using the nonlinearity

$$\mu(|\underline{e}(\boldsymbol{u})|) = 1 + \mathrm{e}^{-|\underline{e}(\boldsymbol{u})|^2}.$$

We let Ω be the L-shaped domain $(-1,1)^2 \setminus [0,1) \times (-1,0]$ and select $\boldsymbol{f}$ so that the analytical solution to (6.1)–(6.3), where (r,φ) denotes the system of polar coordinates, is given by

$$\begin{aligned}\boldsymbol{u}(r,\varphi) &= r^{\lambda} \begin{pmatrix} (1+\lambda)\sin(\varphi)\Psi(\varphi) + \cos(\varphi)\Psi'(\varphi) \\ \sin(\varphi)\Psi'(\varphi) - (1+\lambda)\cos(\varphi)\Psi(\varphi) \end{pmatrix}, \\ p(r,\varphi) &= -r^{\lambda-1}\frac{(1+\lambda)^2\Psi'(\varphi) + \Psi'''(\varphi)}{(1-\lambda)},\end{aligned}$$

where

$$\Psi(\varphi) = \frac{\sin((1+\lambda)\varphi)\cos(\lambda\omega)}{1+\lambda} - \cos((1+\lambda)\varphi) - \frac{\sin((1-\lambda)\varphi)\cos(\lambda\omega)}{1-\lambda} + \cos((1-\lambda)\varphi),$$

and $\omega = {}^{3\pi}/_{2}$. Here, the exponent λ is the smallest positive solution of $\sin(\lambda\omega) + \lambda\sin(\omega) = 0$; thereby, $\lambda \approx 0.54448373678246$. We note that $(\boldsymbol{u}, p)$ is analytic in $\overline{\Omega} \setminus \{\boldsymbol{0}\}$, but both $\nabla\boldsymbol{u}$ and p are singular at the origin; indeed, $\boldsymbol{u} \notin \left[H^2(\Omega)\right]^2$ and $p \notin H^1(\Omega)$.

Figure 6.4(a) presents the comparison of the actual error in the DGFEM norm and the *a posteriori* error bound versus the third root of the number of degrees of freedom on a linear-log scale for the sequence of meshes generated by the h- and hp-adaptive algorithms. We remark that the choice of the third root of the number of degrees of freedom is based on the *a priori* analysis performed in Schötzau & Wihler [156] for the linear Stokes problem, cf. Houston *et al.* [121]. We again observe that the error bound overestimates the true error by a roughly consistent factor, although the hp-refinement has some initial increase before stabilizing at a higher value than for h-refinement; this is

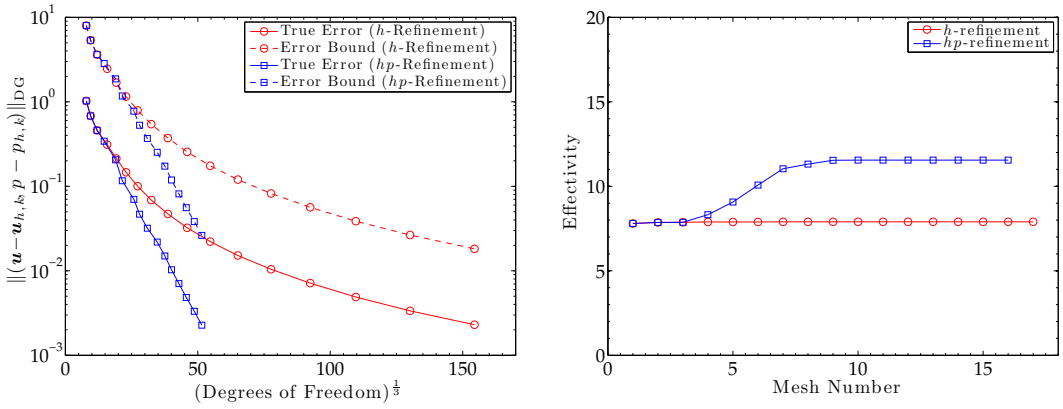

(a) *(b)*

Figure 6.4: Example 3. (a) Comparison of the error in the DGFEM norm employing both h- and hp-refinement, with respect to the number of degrees of freedom; (b) Effectivity index using both h- and hp-refinement.

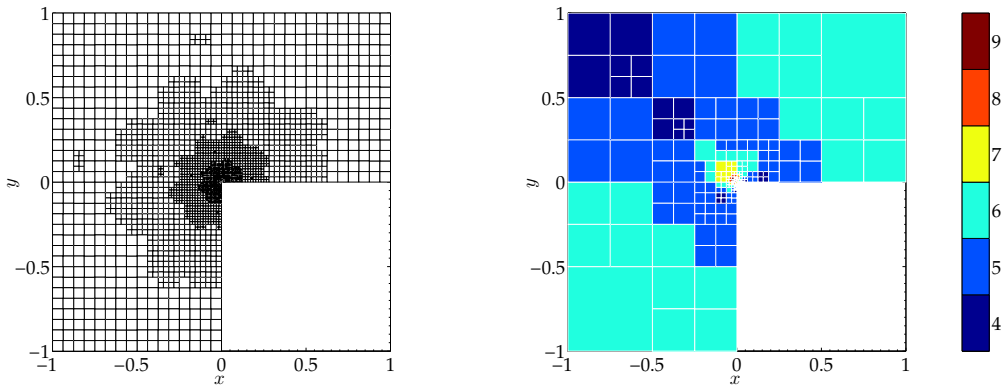

(a) *(b)*

Figure 6.5: Example 3. Finite element mesh after 10 adaptive refinement steps: (a) h-adaptivity; (b) hp-adaptivity.

confirmed again by the effectivity indices for the sequence of meshes, cf. Figure 6.4(b). From Figure 6.4(a) we can also see that yet again the error in the DGFEM norm converges to zero at an exponential rate when the hp-adaptive algorithm is employed, leading to a greater reduction in the error for a given number of degrees of freedom when compared with the corresponding quantity computed using h-refinement.

Figures 6.5(a) and (b) show the meshes generated after 10 mesh refinements using the h- and hp-adaptive mesh refinement strategies, respectively. We can see that both refinement strategies perform mostly h-refinement in the region of the singularity at the origin. However, the hp-adaptive strategy is able to perform less h-refinement around

the origin as it only performs enough to isolate the singularity; then it performs mostly uniform p-refinement, with a larger p-refinement to the immediate top-left of the singularity.

6.6 Summary

In this chapter, we have studied the numerical approximation of a quasi-Newtonian flow problem of strongly monotone type by means of hp-interior penalty discontinuous Galerkin methods. We have derived *a priori* and *a posteriori* error bounds in the discontinuous Galerkin energy norm (6.16). In the latter case, both global upper and local lower residual-based *a posteriori* error bounds have been given. The proof of the upper bound is based on employing a suitable DGFEM space decomposition, together with a hp-version projection operator. The numerical experiments undertaken in this chapter demonstrates the theoretical results. In particular, we have shown that the *a posteriori* upper bound converges to zero at the same asymptotic rate as the true error measured in the DGFEM energy norm on sequences of hp-adaptively refined meshes.

In the next chapter, we shall study the application of the so-called two-grid method to a quasi-Newtonian flow problem of strongly monotone type using hp-interior penalty discontinuous Galerkin methods. We shall also extend the *a priori* and *a posteriori* error bounds from this chapter to the two-grid case.

CHAPTER 7

Two-Grid hp-Version Discontinuous Galerkin Finite Element Method for Non-Newtonian Fluid Flows

In this chapter we develop the *a priori* and *a posteriori* error analysis, with respect to a mesh-dependent energy norm, of both two-grid variants of the hp-version DGFEM applied to the quasi-Newtonian fluid flow problem:

$$-\nabla \cdot (\mu(\boldsymbol{x}, |\underline{e}(\boldsymbol{u})|)\,\underline{e}(\boldsymbol{u})) + \nabla p = \boldsymbol{f}(\boldsymbol{x}) \qquad \text{in } \Omega, \tag{7.1}$$

$$\nabla \cdot \boldsymbol{u} = 0 \qquad \text{in } \Omega, \tag{7.2}$$

$$\boldsymbol{u} = \boldsymbol{0} \qquad \text{on } \Gamma. \tag{7.3}$$

Here, $\Omega \subset \mathbb{R}^d$, $d = 2, 3$, is a bounded polygonal, or polyhedral, Lipschitz domain with boundary $\Gamma = \partial\Omega$, $\boldsymbol{f} \in \left[L^2(\Omega)\right]^d$ is a given source term, $\boldsymbol{u} = (u_1, \ldots, u_d)^\top$ is the velocity vector, $p \in L^2_0(\Omega)$ is the pressure, and $\underline{e}(\boldsymbol{u})$ is the symmetric $d \times d$ strain tensor defined by

$$e_{ij}(\boldsymbol{u}) = \frac{1}{2}\left(\frac{\partial u_i}{\partial x_j} + \frac{\partial u_j}{\partial x_i}\right), \qquad i, j = 1 \ldots d.$$

We note we assume that the nonlinearity μ meets Assumption D and for ease of notation we shall suppress the dependence of μ on $\boldsymbol{x}$ and write $\mu(t)$ instead of $\mu(\boldsymbol{x}, t)$. As in Chapter 3 we use the notation from Section 2.1.2 to consider the fine $\mathcal{T}_h$ and coarse

$\mathcal{T}_H$ partitions of the computational domain Ω, of granularity h and H, respectively. We again associate the corresponding polynomial degree distributions $\boldsymbol{k} = \{k_\kappa : \kappa \in \mathcal{T}_h\}$ and $\boldsymbol{K} = \{K_\kappa : \kappa \in \mathcal{T}_H\}$ and assume that Assumption B holds. Given $\mathcal{T}_h$, $\boldsymbol{k}$, $\mathcal{T}_H$, $\boldsymbol{K}$ we construct the fine and coarse hp-finite element spaces $\boldsymbol{V}(\mathcal{T}_h, \boldsymbol{k}) \times Q(\mathcal{T}_h, \boldsymbol{k})$ and $\boldsymbol{V}(\mathcal{T}_H, \boldsymbol{K}) \times Q(\mathcal{T}_H, \boldsymbol{K})$, respectively, which satisfy $\boldsymbol{V}(\mathcal{T}_H, \boldsymbol{K}) \subseteq \boldsymbol{V}(\mathcal{T}_h, \boldsymbol{k})$ and $Q(\mathcal{T}_H, \boldsymbol{K}) \subseteq Q(\mathcal{T}_h, \boldsymbol{k})$, cf. Section 6.2.

7.1 Two-Grid hp-Version DGFEM

In this section we now propose the so-called two-grid version of the family of interior penalty DGFEMs for the numerical approximation of (7.1)–(7.3) based on the formulation proposed in Bi & Ginting [36] and Chapter 3:

1. (Nonlinear solve) Compute $(\boldsymbol{u}_{H,K}, p_{H,K}) \in \boldsymbol{V}(\mathcal{T}_H, \boldsymbol{K}) \times Q(\mathcal{T}_H, \boldsymbol{K})$ such that

$$A_{H,K}(\boldsymbol{u}_{H,K}; \boldsymbol{u}_{H,K}, \boldsymbol{v}_{H,K}) + B_{H,K}(\boldsymbol{v}_{H,K}, p_{H,K}) = F_{H,K}(\boldsymbol{v}_{H,K}), \tag{7.4}$$

$$-B_{H,K}(\boldsymbol{u}_{H,K}, q_{H,K}) = 0 \tag{7.5}$$

   for all $(\boldsymbol{v}_{H,K}, q_{H,K}) \in \boldsymbol{V}(\mathcal{T}_H, \boldsymbol{K}) \times Q(\mathcal{T}_H, \boldsymbol{K})$.

2. (Linear solve) Determine the fine grid solution $(\boldsymbol{u}_{2G}, p_{2G}) \in \boldsymbol{V}(\mathcal{T}_h, \boldsymbol{k}) \times Q(\mathcal{T}_h, \boldsymbol{k})$ such that

$$A_{h,k}(\boldsymbol{u}_{H,K}; \boldsymbol{u}_{2G}, \boldsymbol{v}_{h,k}) + B_{h,k}(\boldsymbol{v}_{h,k}, p_{2G}) = F_{h,k}(\boldsymbol{v}_{h,k}), \tag{7.6}$$

$$-B_{h,k}(\boldsymbol{u}_{2G}, q_{h,k}) = 0 \tag{7.7}$$

   for all $(\boldsymbol{v}_{h,k}, q_{h,k}) \in \boldsymbol{V}(\mathcal{T}_h, \boldsymbol{k}) \times Q(\mathcal{T}_h, \boldsymbol{k})$.

Here,

$$A_{h,k}(\boldsymbol{\psi}; \boldsymbol{u}, \boldsymbol{v}) = \int_\Omega \mu(|\underline{e}_h(\boldsymbol{\psi})|)\underline{e}_h(\boldsymbol{u}) : \underline{e}_h(\boldsymbol{v})\,\mathrm{d}\boldsymbol{x} + \sum_{F\in\mathcal{F}_h}\int_F \{\!\{\mu(|\underline{e}_h(\boldsymbol{\psi})|)\underline{e}_h(\boldsymbol{u})\}\!\} : \underline{[\![\boldsymbol{v}]\!]}\,\mathrm{d}s$$
$$+ \theta \sum_{F\in\mathcal{F}_h}\int_F \{\!\{\mu(h_F^{-1}|\underline{[\![\boldsymbol{\psi}]\!]}|)\underline{e}_h(\boldsymbol{v})\}\!\} : \underline{[\![\boldsymbol{u}]\!]}\,\mathrm{d}s + \sum_{F\in\mathcal{F}_h}\int_F \sigma_{h,k}\underline{[\![\boldsymbol{u}]\!]} : \underline{[\![\boldsymbol{v}]\!]}\,\mathrm{d}s,$$

$$B_{h,k}(\boldsymbol{v},q) = -\int_\Omega q\nabla_h\cdot\boldsymbol{v}\,\mathrm{d}s + \sum_{F\in\mathcal{F}_h}\int_F \{\!\{q\}\!\}[\![\boldsymbol{v}]\!]\,\mathrm{d}s,$$
$$F_{h,k}(\boldsymbol{v}) = \int_\Omega \boldsymbol{f}\cdot\boldsymbol{v}\,\mathrm{d}\boldsymbol{x},$$

$\underline{e}_h(\cdot)$ and ∇_h denote the elementwise strain tensor and gradient operator, respectively, and $\theta\in[-1,1]$. The *interior penalty parameter* $\sigma_{h,k}$ is defined as

$$\sigma_{h,k} := \gamma\frac{k_F^2}{h_F},$$

where $\gamma\geq 1$ is a constant, which must be chosen sufficiently large (independent of the local element sizes and the polynomial degree); see Theorem 6.4. By re-introducing the *energy norms*,

$$\|\boldsymbol{v}\|_{h,k}^2 = \|\underline{e}_h(\boldsymbol{v})\|_{L^2(\Omega)}^2 + \sum_{F\in\mathcal{F}_h}\int_F \sigma_{h,k}|[\![\underline{\boldsymbol{v}}]\!]|^2\,\mathrm{d}s,$$
$$\|(\boldsymbol{v},q)\|_{\mathrm{DG}(h,k)}^2 = \|\boldsymbol{v}\|_{h,k}^2 + \|q\|_{L^2(\Omega)}^2,$$

cf. (6.15)–(6.16), we assume that the bilinear form $B_{h,k}(\cdot,\cdot)$ satisfies the inf-sup condition (6.17) and we can show that the form $A_{h,k}(\boldsymbol{u}_{H,K};\cdot,\cdot)$ is coercive in the following sense.

Lemma 7.1. *There exists a constant $\gamma_{\min}$ such that the semilinear form $A_{h,k}(\cdot;\cdot;\cdot)$ is coercive in the sense that there exists a positive constant C_C such that*

$$A_{h,k}(\boldsymbol{\phi};\boldsymbol{v},\boldsymbol{v}) \geq C_C\,\|\boldsymbol{v}\|_{h,k}^2$$

for all $\boldsymbol{v},\boldsymbol{\phi}\in\boldsymbol{V}(\mathcal{T}_h,\boldsymbol{k})$, providing that the interior penalty parameter $\gamma\geq\gamma_{\min}$.

Proof. We note this proof follows in a similar manner to the proof of coercivity and strong monotonicity from Theorem 6.4. □

Existence and uniqueness of the solution $(\boldsymbol{u}_{H,K},p_{H,K})$ follows immediately from Theorem 6.4. Since $A_{h,k}(\boldsymbol{u}_{H,K};\cdot,\cdot)$ is coercive on $\boldsymbol{V}(\mathcal{T}_h,\boldsymbol{k})\times\boldsymbol{V}(\mathcal{T}_h,\boldsymbol{k})$, the continuity of

$A_{h,k}(\boldsymbol{u}_{H,K};\cdot,\cdot)$ on $\boldsymbol{V}(\mathcal{T}_h,\boldsymbol{k})\times Q(\mathcal{T}_h,\boldsymbol{k})$, $B_{h,k}(\cdot,\cdot)$ on $\boldsymbol{V}(\mathcal{T}_h,\boldsymbol{k})\times Q(\mathcal{T}_h,\boldsymbol{k})$ and $F_{h,k}(\cdot)$ on $\boldsymbol{V}(\mathcal{T}_h,\boldsymbol{k})$, together with the discrete inf-sup condition (6.17) implies the existence and uniqueness of $(\boldsymbol{u}_{2G},p_{2G})$, cf. Brezzi & Fortin [46], Hansbo & Larson [107], Schötzau *et al.* [157], Toselli [166]. Hence, the formulation (7.4)–(7.7) is well-posed.

7.1.1 *A Priori* Error Bound

In this section we deduce the following error bound for the two-grid approximation defined in (7.4)–(7.7) of the quasi-Newtonian fluid flow problem (7.1)–(7.3) based on exploiting Theorem 6.5.

Theorem 7.2. *Assuming that* $(\boldsymbol{u},p)\in\left[C^1(\Omega)\cap H^2(\Omega)\right]^d\times(C^0(\Omega)\cap H^1(\Omega))$, $\boldsymbol{u}|_{\kappa_h}\in[H^{s_{\kappa_h}}(\kappa_h)]^d$, $p|_{\kappa_h}\in H^{s_{\kappa_h}-1}(\kappa_h)$, $s_{\kappa_h}\geq 2$, *for* $\kappa_h\in\mathcal{T}_h$, *and* $\boldsymbol{u}|_{\kappa_H}\in\left[H^{S_{\kappa_H}}(\kappa_H)\right]^d$, $p|_{\kappa_H}\in H^{S_{\kappa_H}-1}(\kappa_H)$, $S_{\kappa_H}\geq 2$, *for* $\kappa_H\in\mathcal{T}_H$, *then the solution* $(\boldsymbol{u}_{2G},p_{2G})\in\boldsymbol{V}(\mathcal{T}_h,\boldsymbol{k})\times Q(\mathcal{T}_h,\boldsymbol{k})$ *of* (7.4)–(7.7) *satisfies the bounds*

$$\|\boldsymbol{u}_{h,k}-\boldsymbol{u}_{2G}\|_{h,k}^2\leq C_{10}k_{\max}^4\sum_{\kappa\in\mathcal{T}_H}\left(\frac{H_\kappa^{2R_\kappa-2}}{K_\kappa^{2S_\kappa-3}}\|\boldsymbol{u}\|_{H^{S_\kappa}(\kappa)}^2+\frac{H_\kappa^{2R_\kappa-2}}{K_\kappa^{2S_\kappa-2}}\|p\|_{H^{S_\kappa-1}(\kappa)}^2\right),$$

$$\|p_{h,k}-p_{2G}\|_{h,k}^2\leq C_{11}k_{\max}^6\sum_{\kappa\in\mathcal{T}_H}\left(\frac{H_\kappa^{2R_\kappa-2}}{K_\kappa^{2S_\kappa-3}}\|\boldsymbol{u}\|_{H^{S_\kappa}(\kappa)}^2+\frac{H_\kappa^{2R_\kappa-2}}{K_\kappa^{2S_\kappa-2}}\|p\|_{H^{S_\kappa-1}(\kappa)}^2\right),$$

$$\begin{aligned}\|(\boldsymbol{u}-\boldsymbol{u}_{2G},p-p_{2G})\|_{\mathrm{DG}(h,k)}^2&\leq 2C_8k_{\max}^4\sum_{\kappa_h\in\mathcal{T}_h}\left(\frac{h_{\kappa_h}^{2r_{\kappa_h}-2}}{k_{\kappa_h}^{2s_{\kappa_h}-3}}\|\boldsymbol{u}\|_{H^{s_{\kappa_h}}(\kappa_h)}^2+\frac{h_{\kappa_h}^{2r_{\kappa_h}-2}}{k_{\kappa_h}^{2s_{\kappa_h}-2}}\|p\|_{H^{s_{\kappa_h}-1}(\kappa_h)}^2\right)\\&\quad+2C_{1*}k_{\max}^6\sum_{\kappa_H\in\mathcal{T}_H}\left(\frac{H_{\kappa_H}^{2R_{\kappa_H}-2}}{K_{\kappa_H}^{2S_{\kappa_H}-3}}\|\boldsymbol{u}\|_{H^{S_{\kappa_H}}(\kappa_H)}^2+\frac{H_{\kappa_H}^{2R_{\kappa_H}-2}}{K_{\kappa_H}^{2S_{\kappa_H}-2}}\|p\|_{H^{S_{\kappa_H}-1}(\kappa_H)}^2\right),\end{aligned}$$

with $C_{1*}=\max(C_{10},C_{11})$, $1\leq r_{\kappa_h}\leq\min(s_{\kappa_h},k_{\kappa_h}+1),k_{\kappa_h}\geq 1$, *for all* $\kappa_h\in\mathcal{T}_h$, $1\leq R_{\kappa_H}\leq\min(S_{\kappa_H},K_{\kappa_H}+1),K_{\kappa_H}\geq 1$, *for all* $\kappa_H\in\mathcal{T}_H$, *and* C_8,C_{10},C_{11} *are positive constants independent of* $\boldsymbol{u},p,\boldsymbol{h},\boldsymbol{H},\boldsymbol{k}$ *and* $\boldsymbol{K}$.

Proof of Theorem 7.2

In order to prove Theorem 7.2, we first state the following auxiliary result.

Lemma 7.3. *Let* $\boldsymbol{u}_{h,k}\in\boldsymbol{V}(\mathcal{T}_h,\boldsymbol{k})$ *and* $\boldsymbol{u}_{2G}\in\boldsymbol{V}(\mathcal{T}_h,\boldsymbol{k})$ *be the velocity vector components*

of the solutions to (6.12)–(6.13) *and* (7.4)–(7.7)*, respectively; then, assuming that* $(\boldsymbol{u}, p) \in \left[C^1(\Omega) \cap H^2(\Omega)\right]^d \times (C^0(\Omega) \cap H^1(\Omega))$*,* $\boldsymbol{u}|_\kappa \in \left[H^{S_\kappa}(\kappa)\right]^d$*,* $p|_\kappa \in H^{S_\kappa - 1}(\kappa), S_\kappa \geq 2$*, for* $\kappa \in \mathcal{T}_H$*,*

$$
\begin{aligned}
&A_{h,k}(\boldsymbol{u}_{H,K}; \boldsymbol{u}_{h,k}, \boldsymbol{\phi}) - A_{h,k}(\boldsymbol{u}_{h,k}; \boldsymbol{u}_{h,k}, \boldsymbol{\phi}) \\
&\qquad \leq C_A \left\|\boldsymbol{\phi}\right\|_{h,k} k_{\max}^2 \left(\sum_{\kappa \in \mathcal{T}_H} \left(\frac{H_\kappa^{2R_\kappa - 2}}{K_\kappa^{2S_\kappa - 3}} \left\|\boldsymbol{u}\right\|_{H^{S_\kappa}(\kappa)}^2 + \frac{H_\kappa^{2R_\kappa - 2}}{K_\kappa^{2S_\kappa - 2}} \left\|p\right\|_{H^{S_\kappa - 1}(\kappa)}^2 \right) \right)^{1/2},
\end{aligned}
$$

for all $\boldsymbol{\phi} \in \boldsymbol{V}(\mathcal{T}_h, \boldsymbol{k})$*, with* $1 \leq R_\kappa \leq \min(S_\kappa, K_\kappa + 1)$*,* $K_\kappa \geq 1$*, for all* $\kappa \in \mathcal{T}_H$*, where* C_A *is a positive constant independent of* $\boldsymbol{u}$*,* p*,* $\boldsymbol{h}$*,* $\boldsymbol{H}$*,* $\boldsymbol{k}$ *and* $\boldsymbol{K}$*.*

Proof. We write $A_{h,k}(\boldsymbol{u}_{H,K}; \boldsymbol{u}_{h,k}, \boldsymbol{\phi}) - A_{h,k}(\boldsymbol{u}_{h,k}; \boldsymbol{u}_{h,k}, \boldsymbol{\phi}) \equiv T_1 + T_2 + T_3$, where

$$
\begin{aligned}
T_1 &= \int_\Omega (\mu(|\underline{e}_h(\boldsymbol{u}_{H,K})|) - \mu(|\underline{e}_h(\boldsymbol{u}_{h,k})|)) \underline{e}_h(\boldsymbol{u}_{h,k}) : \underline{e}_h(\boldsymbol{\phi}) \, \mathrm{d}\boldsymbol{x}, \\
T_2 &= -\sum_{F \in \mathcal{F}_h} \int_F \{\!\{(\mu(|\underline{e}_h(\boldsymbol{u}_{H,K})|) - \mu(|\underline{e}_h(\boldsymbol{u}_{h,k})|)) \underline{e}_h(\boldsymbol{u}_{h,k})\}\!\} : \underline{[\![\boldsymbol{\phi}]\!]} \, \mathrm{d}s, \\
T_3 &= \theta \sum_{F \in \mathcal{F}_h} \int_F \{\!\{(\mu(|h_F^{-1} \underline{[\![\boldsymbol{u}_{H,K}]\!]}|) - \mu(h_F^{-1} |\underline{[\![\boldsymbol{u}_{h,k}]\!]}|)) \underline{e}_h(\boldsymbol{\phi})\}\!\} : \underline{[\![\boldsymbol{u}_{h,k}]\!]} \, \mathrm{d}s.
\end{aligned}
$$

We first consider the term T_1; upon application of (6.4), (6.5) and the triangle inequality, we deduce that

$$
\begin{aligned}
|T_1| &\leq \int_\Omega |\mu(|\underline{e}_h(\boldsymbol{u}_{H,K})|) \underline{e}_h(\boldsymbol{u}_{H,K}) - \mu(|\underline{e}_h(\boldsymbol{u}_{h,k})|) \underline{e}_h(\boldsymbol{u}_{h,k})| |\underline{e}_h(\boldsymbol{\phi})| \, \mathrm{d}\boldsymbol{x} \\
&\quad + \int_\Omega |\mu(|\underline{e}_h(\boldsymbol{u}_{H,K})|) \underline{e}_h(\boldsymbol{u}_{h,k} - \boldsymbol{u}_{H,K})| |\underline{e}_h(\boldsymbol{\phi})| \, \mathrm{d}\boldsymbol{x} \\
&\leq (C_1 + M_\mu) \left(\left\|\underline{e}_h(\boldsymbol{u} - \boldsymbol{u}_{h,k})\right\|_{L^2(\Omega)} + \left\|\underline{e}_H(\boldsymbol{u} - \boldsymbol{u}_{H,K})\right\|_{L^2(\Omega)} \right) \left\|\underline{e}_h(\boldsymbol{\phi})\right\|_{L^2(\Omega)}.
\end{aligned}
$$

Similarly, for term T_2,

$$
\begin{aligned}
|T_2| &\leq \sum_{F \in \mathcal{F}_h} \int_F \{\!\{|\mu(|\underline{e}_h(\boldsymbol{u}_{H,K})|) \underline{e}_h(\boldsymbol{u}_{H,K}) - \mu(|\underline{e}_h(\boldsymbol{u}_{h,k})|) \underline{e}_h(\boldsymbol{u}_{h,k})|\}\!\} |\underline{[\![\boldsymbol{\phi}]\!]}| \, \mathrm{d}s \\
&\quad + \sum_{F \in \mathcal{F}_h} \int_F \{\!\{|\mu(|\underline{e}_h(\boldsymbol{u}_{H,K})|) \underline{e}_h(\boldsymbol{u}_{h,k} - \boldsymbol{u}_{H,K})|\}\!\} |\underline{[\![\boldsymbol{\phi}]\!]}| \, \mathrm{d}s,
\end{aligned}
$$

which, upon application of Lemma 2.1, gives

$$
\begin{aligned}
|T_2| &\leq (C_1 + M_\mu) \left(\sum_{F \in \mathcal{F}_h} \int_F \sigma_{h,k} |\underline{[\![\boldsymbol{\phi}]\!]}|^2 \, \mathrm{d}s \right)^{1/2} \\
&\quad \times \left\{ \left(\sum_{F \in \mathcal{F}_h} \sigma_{h,k}^{-1} \| \{\!\{ |\underline{e}_h(\boldsymbol{u} - \boldsymbol{u}_{h,k})| \}\!\} \|_{L^2(F)}^2 \right)^{1/2} \right. \\
&\qquad \left. + \left(\sum_{F \in \mathcal{F}_h} \sigma_{h,k}^{-1} \| \{\!\{ |\underline{e}_h(\boldsymbol{u} - \boldsymbol{u}_{H,K})| \}\!\} \|_{L^2(F)}^2 \right)^{1/2} \right\} \\
&\leq (C_1 + M_\mu) C_T^{1/2} \gamma^{-1/2} \left(\|\underline{e}_h(\boldsymbol{u} - \boldsymbol{u}_{h,k})\|_{L^2(\Omega)} - \|\underline{e}_H(\boldsymbol{u} - \boldsymbol{u}_{H,K})\|_{L^2(\Omega)} \right) \|\boldsymbol{\phi}\|_{h,k} \, .
\end{aligned}
$$

If $\theta = 0$ then $T_3 \equiv 0$; for $\theta \neq 0$, we note that

$$
\begin{aligned}
|T_3| &\leq |\theta| \sum_{F \in \mathcal{F}_h} \int_F \{\!\{ |(\mu(h_F^{-1} |\underline{[\![\boldsymbol{u}_{H,K}]\!]}|) - \mu(h_F^{-1} |\underline{[\![\boldsymbol{u}_{h,k}]\!]}|)) \underline{e}_h(\boldsymbol{\phi})| \}\!\} |\underline{[\![\boldsymbol{u}_{h,k}]\!]}| \, \mathrm{d}s \\
&\leq |\theta| \sum_{F \in \mathcal{F}_h} \left\| \mu(h_F^{-1} |\underline{[\![\boldsymbol{u}_{H,K}]\!]}|) - \mu(h_F^{-1} |\underline{[\![\boldsymbol{u}_{h,k}]\!]}|) \right\|_{L^\infty(F)} \| \{\!\{ |\underline{e}_h(\boldsymbol{\phi})| \}\!\} \|_{L^2(F)} \left\| \underline{[\![\boldsymbol{u}_{h,k}]\!]} \right\|_{L^2(F)} .
\end{aligned}
$$

Since $\boldsymbol{u} \in \left[H_0^1(\Omega) \right]^d$, $|\underline{[\![\boldsymbol{u}_{h,k}]\!]}| = |\underline{[\![\boldsymbol{u} - \boldsymbol{u}_{h,k}]\!]}|$; moreover, exploiting (6.4) gives

$$
\begin{aligned}
&\left\| \mu(h_F^{-1} |\underline{[\![\boldsymbol{u}_{H,K}]\!]}|) - \mu(h_F^{-1} |\underline{[\![\boldsymbol{u}_{h,k}]\!]}|) \right\|_{L^\infty(F)} \\
&\qquad \leq \left\| \mu(h_F^{-1} |\underline{[\![\boldsymbol{u}_{h,k}]\!]}|) \right\|_{L^\infty(F)}^2 + \left\| \mu(h_F^{-1} |\underline{[\![\boldsymbol{u}_{H,K}]\!]}|^2) \right\|_{L^\infty(F)} \leq 2M_\mu .
\end{aligned}
$$

Thereby, employing Lemma 2.1, we deduce that

$$
\begin{aligned}
|T_3| &\leq 2M_\mu \left(\sum_{F \in \mathcal{F}_h} \sigma_{h,k}^{-1} \| \{\!\{ |\underline{e}_h(\boldsymbol{\phi})| \}\!\} \|_{L^2(F)}^2 \right)^{1/2} \left(\sum_{F \in \mathcal{F}_h} \sigma_{h,k} \left\| \underline{[\![\boldsymbol{u} - \boldsymbol{u}_{h,k}]\!]} \right\|_{L^2(F)}^2 \right)^{1/2} \\
&\leq 2M_\mu C_T^{1/2} \gamma^{-1/2} \|\boldsymbol{u} - \boldsymbol{u}_{h,k}\|_{h,k} \|\underline{e}_h(\boldsymbol{\phi})\|_{L^2(\Omega)} \, .
\end{aligned}
$$

Since $\boldsymbol{V}(\mathcal{T}_H, \boldsymbol{K}) \subseteq \boldsymbol{V}(\mathcal{T}_h, \boldsymbol{k})$ and $Q(\mathcal{T}_H, \boldsymbol{K}) \subseteq Q(\mathcal{T}_h, \boldsymbol{k})$, applying Theorem 6.5 to each of the bounds for T_1, T_2 and T_3, completes the proof. □

We now proceed to prove Theorem 7.2. Writing $\boldsymbol{\phi} = \boldsymbol{u}_{h,k} - \boldsymbol{u}_{2G} \in \boldsymbol{V}(\mathcal{T}_h, \boldsymbol{k})$, by Lemma 7.1 we note that there exists a positive constant C_C such that

$$\begin{aligned} C_C \left\| \boldsymbol{u}_{h,k} - \boldsymbol{u}_{2G} \right\|_{h,k}^2 &\leq A_{h,k}(\boldsymbol{u}_{H,K}; \boldsymbol{u}_{h,k} - \boldsymbol{u}_{2G}, \boldsymbol{\phi}) \\ &= A_{h,k}(\boldsymbol{u}_{H,K}; \boldsymbol{u}_{h,k}, \phi) - A_{h,k}(\boldsymbol{u}_{H,K}; \boldsymbol{u}_{2G}, \boldsymbol{\phi}). \end{aligned}$$

By subtracting (6.13) from (7.7) we note that

$$B_{h,k}(\boldsymbol{\phi}, q_{h,k}) = 0$$

for all $q_{h,k} \in Q(\mathcal{T}_h, \boldsymbol{k})$. Hence, since $\boldsymbol{\phi} \in \boldsymbol{V}(\mathcal{T}_h, \boldsymbol{k})$ and $p_{2G}, p_{h,k} \in Q(\mathcal{T}_h, \boldsymbol{k})$, applying (7.6) and (6.12) gives

$$\begin{aligned} C_C \left\| \boldsymbol{u}_{h,k} - \boldsymbol{u}_{2G} \right\|_{h,k}^2 &\leq A_{h,k}(\boldsymbol{u}_{H,K}; \boldsymbol{u}_{h,k}, \boldsymbol{\phi}) - A_{h,k}(\boldsymbol{u}_{H,K}; \boldsymbol{u}_{2G}, \boldsymbol{\phi}) - B_{h,k}(\boldsymbol{\phi}, p_{2G}) \\ &= A_{h,k}(\boldsymbol{u}_{H,K}; \boldsymbol{u}_{h,k}, \boldsymbol{\phi}) - F_{h,k}(\boldsymbol{\phi}) \\ &= A_{h,k}(\boldsymbol{u}_{H,K}; \boldsymbol{u}_{h,k}, \boldsymbol{\phi}) - A_{h,k}(\boldsymbol{u}_{h,k}; \boldsymbol{u}_{h,k}, \boldsymbol{\phi}) - B_{h,k}(\boldsymbol{\phi}, p_{h,k}) \\ &= A_{h,k}(\boldsymbol{u}_{H,K}; \boldsymbol{u}_{h,k}, \boldsymbol{\phi}) - A_{h,k}(\boldsymbol{u}_{h,k}; \boldsymbol{u}_{h,k}, \boldsymbol{\phi}). \end{aligned}$$

Application of Lemma 7.3 and dividing both sides by $\left\| \boldsymbol{u}_{h,k} - \boldsymbol{u}_{2G} \right\|_{h,k}$ completes the proof of the first bound in Theorem 7.2.

We now consider the proof of the second bound in Theorem 7.2. From the inf-sup condition (6.17), there exists $\boldsymbol{\xi} \in \boldsymbol{V}(\mathcal{T}_h, \boldsymbol{k})$ such that

$$\nu k_{\max}^{-1} \left\| p_{h,k} - p_{2G} \right\|_{L^2(\Omega)} \leq \frac{B_{h,k}(\boldsymbol{\xi}, p_{h,k} - p_{2G})}{\left\| \boldsymbol{\xi} \right\|_{h,k}}. \tag{7.8}$$

Subtracting (7.6) from (6.12) gives

$$\begin{aligned} B_{h,k}(\boldsymbol{\xi}, p_{h,k} - p_{2G}) &= A_{h,k}(\boldsymbol{u}_{H,K}; \boldsymbol{u}_{2G}, \boldsymbol{\xi}) - A_{h,k}(\boldsymbol{u}_{h,k}; \boldsymbol{u}_{h,k}, \boldsymbol{\xi}) \\ &= A_{h,k}(\boldsymbol{u}_{H,K}; \boldsymbol{u}_{2G} - \boldsymbol{u}_{h,k}, \boldsymbol{\xi}) + A_{h,k}(\boldsymbol{u}_{H,K}; \boldsymbol{u}_{h,k}, \boldsymbol{\xi}) \\ &\quad - A_{h,k}(\boldsymbol{u}_{h,k}; \boldsymbol{u}_{h,k}, \boldsymbol{\xi}). \end{aligned} \tag{7.9}$$

We note that the last two terms in (7.9) can be bounded based on employing Lemma 7.3. To bound the first term, we proceed as follows.

$$
\begin{aligned}
&A_{h,k}(\boldsymbol{u}_{H,K};\boldsymbol{u}_{2G}-\boldsymbol{u}_{h,k},\boldsymbol{\xi})\\
&\leq \int_\Omega |\mu(|\underline{e}_h(\boldsymbol{u}_{H,K})|)||\underline{e}_h(\boldsymbol{u}_{2G}-\boldsymbol{u}_{h,k})||\underline{e}_h(\boldsymbol{\xi})|\,\mathrm{d}\boldsymbol{x} + \sum_{F\in\mathcal{F}_h}\int_F \sigma_{h,k}|\underline{[\![\boldsymbol{u}_{2G}-\boldsymbol{u}_{h,k}]\!]}||\underline{[\![\boldsymbol{\xi}]\!]}|\,\mathrm{d}s\\
&\quad + \sum_{F\in\mathcal{F}_h}\int_F \{\!\{|\mu(|\underline{e}_h(\boldsymbol{u}_{H,K})|)||\underline{e}_h(\boldsymbol{u}_{2G}-\boldsymbol{u}_{h,k})|\}\!\}|\underline{[\![\boldsymbol{\xi}]\!]}|\,\mathrm{d}\boldsymbol{x}\\
&\quad + |\theta|\sum_{F\in\mathcal{F}_h}\int_F \{\!\{|\mu(h_F^{-1}|\underline{[\![\boldsymbol{u}_{H,K}]\!]}|)||\underline{e}_h(\boldsymbol{\xi})|\}\!\}|\underline{[\![\boldsymbol{u}_{2G}-\boldsymbol{u}_{h,k}]\!]}|\,\mathrm{d}\boldsymbol{x}\\
&\leq M_\mu \left\|\underline{e}_h(\boldsymbol{u}_{2G}-\boldsymbol{u}_{h,k})\right\|_{L^2(\Omega)}\left\|\underline{e}_h(\boldsymbol{\xi})\right\|_{L^2(\Omega)}\\
&\quad + M_\mu C_T^{1/2}\gamma^{-1/2}\left\|\underline{e}_h(\boldsymbol{u}_{2G}-\boldsymbol{u}_{h,k})\right\|_{L^2(\Omega)}\left(\sum_{F\in\mathcal{F}_h}\sigma_{h,k}\left\|\underline{[\![\boldsymbol{\xi}]\!]}\right\|_{L^2(F)}^2\right)^{1/2}\\
&\quad + M_\mu C_T^{1/2}\gamma^{-1/2}\left\|\underline{e}_h(\boldsymbol{\xi})\right\|_{L^2(\Omega)}\left(\sum_{F\in\mathcal{F}_h}\sigma_{h,k}\left\|\underline{[\![\boldsymbol{u}_{2G}-\boldsymbol{u}_{h,k}]\!]}\right\|_{L^2(F)}^2\right)^{1/2}\\
&\quad + \left(\sum_{F\in\mathcal{F}_h}\sigma_{h,k}\left\|\underline{[\![\boldsymbol{u}_{2G}-\boldsymbol{u}_{h,k}]\!]}\right\|_{L^2(F)}^2\right)^{1/2}\left(\sum_{F\in\mathcal{F}_h}\sigma_{h,k}\left\|\underline{[\![\boldsymbol{\xi}]\!]}\right\|_{L^2(F)}^2\right)^{1/2}\\
&\leq \left(\max(M_\mu,1)+M_\mu C_T^{1/2}\gamma^{-1/2}\right)\left\|\boldsymbol{u}_{h,k}-\boldsymbol{u}_{2G}\right\|_{h,k}\left\|\boldsymbol{\xi}\right\|_{h,k}.
\end{aligned}
$$

Employing the first bound in Theorem 7.2 gives

$$
\begin{aligned}
&A_{h,k}(\boldsymbol{u}_{H,K};\boldsymbol{u}_{2G}-\boldsymbol{u}_{h,k},\boldsymbol{\xi})\\
&\qquad\leq Ck_{\max}^2\left\|\boldsymbol{\xi}\right\|_{h,k}\left(\sum_{\kappa\in\mathcal{T}_H}\left(\frac{H_\kappa^{2R_\kappa-2}}{K_\kappa^{2S_\kappa-3}}\left\|\boldsymbol{u}\right\|_{H^{S_\kappa}(\kappa)}^2+\frac{H_\kappa^{2R_\kappa-2}}{K_\kappa^{2S_\kappa-2}}\left\|p\right\|_{H^{S_\kappa-1}(\kappa)}^2\right)\right)^{1/2}.
\end{aligned}
$$

Exploiting this result together with Lemma 7.3, equation (7.9) may be bounded by

$$
\begin{aligned}
&B_{h,k}(\xi,p_{h,k}-p_{2G})\\
&\qquad\leq Ck_{\max}^2\left\|\xi\right\|_{h,k}\left(\sum_{\kappa\in\mathcal{T}_H}\left(\frac{H_\kappa^{2R_\kappa-2}}{K_\kappa^{2S_\kappa-3}}\left\|\boldsymbol{u}\right\|_{H^{S_\kappa}(\kappa)}^2+\frac{H_\kappa^{2R_\kappa-2}}{K_\kappa^{2S_\kappa-2}}\left\|p\right\|_{H^{S_\kappa-1}(\kappa)}^2\right)\right)^{1/2}.
\end{aligned}
$$

Inserting this result into (7.8) and dividing through by $\nu k_{\max}^{-1}$ completes the proof of the second bound in Theorem 7.2. We note that an application of the triangle inequality and Theorem 6.5 gives the last bound and completes the proof. □

7.1.2 *A Posteriori* Error Bound

In this section we develop the *a posteriori* error analysis of the two-grid IP DGFEM defined by (7.4)–(7.7). Writing Π_{κ,k_κ} to denote the elementwise L^2-projection onto $\boldsymbol{V}(\mathcal{T}_h,\boldsymbol{k})$ we state the following upper bound.

Theorem 7.4. *Let* $(\boldsymbol{u},p) \in \left[H_0^1(\Omega)\right]^d \times L_0^2(\Omega)$ *be the analytical solution of* (7.1)–(7.3), $(\boldsymbol{u}_{H,K},p_{H,K}) \in \boldsymbol{V}(\mathcal{T}_H,\boldsymbol{K}) \times Q(\mathcal{T}_H,\boldsymbol{K})$ *the numerical approximation obtained from* (7.4)–(7.5) *and* $(\boldsymbol{u}_{2G},p_{2G}) \in \boldsymbol{V}(\mathcal{T}_h,\boldsymbol{k}) \times Q(\mathcal{T}_h,\boldsymbol{k})$ *the two-grid solution defined by* (7.6)– (7.7)*; then, the following* hp-a posteriori *error bound holds*

$$\|(\boldsymbol{u}-\boldsymbol{u}_{2G},p-p_{2G})\|_{\mathrm{DG}(h,k)} \leq C_{12}\left(\sum_{\kappa\in\mathcal{T}_h}\left(\eta_\kappa^2+\xi_\kappa^2\right)+\sum_{\kappa\in\mathcal{T}_h}h_\kappa^2k_\kappa^{-2}\left\|\boldsymbol{f}-\Pi_{\kappa,k_\kappa}\boldsymbol{f}\right\|_{L^2(\kappa)}^2\right)^{1/2},$$

with a constant $C_{12}>0$*, which is independent of* $\boldsymbol{h}$, $\boldsymbol{H}$, $\boldsymbol{k}$, $\boldsymbol{K}$*. Here, for all* $\kappa\in\mathcal{T}_h$*, the* local fine grid error indicators η_κ *are defined by*

$$\begin{aligned}\eta_\kappa^2 &= h_\kappa^2k_\kappa^{-2}\left\|\Pi_{\kappa,k_\kappa}\boldsymbol{f}+\nabla\cdot\left(\mu(|\underline{e}(\boldsymbol{u}_{H,K})|)\underline{e}(\boldsymbol{u}_{2G})\right)-\nabla p_{2G}\right\|_{L^2(\kappa)}^2+\|\nabla\cdot\boldsymbol{u}_{2G}\|_{L^2(\kappa)}^2\\&\quad+h_\kappa k_\kappa^{-1}\left\|[\![p_{2G}]\!]-\underline{[\![\mu(|\underline{e}(\boldsymbol{u}_{H,K})|)\underline{e}(\boldsymbol{u}_{2G})]\!]}\right\|_{L^2(\partial\kappa\setminus\Gamma)}^2+\gamma^2h_\kappa^{-1}k_\kappa^3\left\|\underline{[\![\boldsymbol{u}_{2G}]\!]}\right\|_{L^2(\partial\kappa)}^2\end{aligned}$$

and the local two-grid error indicators ξ_κ *are given, for all* $\kappa\in\mathcal{T}_h$*, by*

$$\xi_\kappa^2=\left\|\left(\mu(|\underline{e}(\boldsymbol{u}_{H,K})|)-\mu(|\underline{e}(\boldsymbol{u}_{2G})|)\right)\underline{e}(\boldsymbol{u}_{2G})\right\|_{L^2(\kappa)}^2.$$

Remark 7.1. We note here we omit lower error bounds for the numerical approximation (u_{2G},p_{2G}) obtained from (7.4)–(7.7) as the prove follows in an analogous manner to the two-grid method for quasilinear elliptic problems and the standard method for the non-Newtonian fluid flow; cf. Remark 3.5 and Section 6.4.4.

Proof of Theorem 7.4

The proof of Theorem 7.4 follows as a two-grid extension of the corresponding *a posteriori* error bound for the standard hp-version IP DGFEM for strongly monotone quasi-Newtonian fluid flows, cf. Chapter 6. As in Chapter 3 we consider an auxiliary one-irregular fine mesh partition $\mathcal{T}_{\widetilde{h}}$ obtained from $\mathcal{T}_h$ as outlined in Section 2.1.2, with corresponding DGFEM finite element spaces $\boldsymbol{V}(\mathcal{T}_{\widetilde{h}}, \widetilde{\boldsymbol{k}})$ and $Q(\mathcal{T}_{\widetilde{h}}, \widetilde{\boldsymbol{k}})$ and polynomial degree vector $\widetilde{\boldsymbol{k}}$ such that $\boldsymbol{V}(\mathcal{T}_{\widetilde{h}}, \widetilde{\boldsymbol{k}}) \subseteq \boldsymbol{V}(\mathcal{T}_h, \boldsymbol{k})$ and $Q(\mathcal{T}_{\widetilde{h}}, \widetilde{\boldsymbol{k}}) \subseteq Q(\mathcal{T}_h, \boldsymbol{k})$; cf. Section 3.4.1.

As in Section 6.4.3 we decompose the DGFEM space $\boldsymbol{V}(\mathcal{T}_{\widetilde{h}}, \widetilde{\boldsymbol{k}})$ into two orthogonal subspaces, cf. Karakashian & Pascal [131]; a conforming part $\left[\boldsymbol{V}(\mathcal{T}_{\widetilde{h}}, \widetilde{\boldsymbol{k}})\right]^c = \boldsymbol{V}(\mathcal{T}_{\widetilde{h}}, \widetilde{\boldsymbol{k}}) \cap \left[H_0^1(\Omega)\right]^d$ and a nonconforming part $\left[\boldsymbol{V}(\mathcal{T}_{\widetilde{h}}, \widetilde{\boldsymbol{k}})\right]^\perp$, defined as the orthogonal complement of $\left[\boldsymbol{V}(\mathcal{T}_{\widetilde{h}}, \widetilde{\boldsymbol{k}})\right]^c$. We split the DGFEM solution $\boldsymbol{u}_{2G}$ accordingly;

$$\boldsymbol{u}_{2G} = \boldsymbol{u}_{2G}^c + \boldsymbol{u}_{2G}^\perp, \tag{7.10}$$

where $\boldsymbol{u}_{2G}^c \in \left[\boldsymbol{V}(\mathcal{T}_{\widetilde{h}}, \widetilde{\boldsymbol{k}})\right]^c$ and $\boldsymbol{u}_{2G}^\perp \in \left[\boldsymbol{V}(\mathcal{T}_{\widetilde{h}}, \widetilde{\boldsymbol{k}})\right]^\perp$. Furthermore, we define the error as

$$\boldsymbol{e}_{\boldsymbol{u}} = \boldsymbol{u} - \boldsymbol{u}_{2G}, \tag{7.11}$$

$$e_p = p - p_{2G}, \tag{7.12}$$

and let

$$\boldsymbol{e}_{\boldsymbol{u}}^c = \boldsymbol{u} - \boldsymbol{u}_{2G}^c \in \left[H_0^1(\Omega)\right]^d.$$

The proof of Theorem 7.4 follows in a similar fashion as for the standard IP DGFEM for the numerical approximation of the non-Newtonian fluid flow problem (6.12)-(6.13), cf. Chapter 6. Recalling the definition of the error, defined in (7.11)–(7.12), by (7.10), Lemma 6.9 and the fact that $\gamma \geq 1$ and $k_\kappa \geq 1$, we have that

$$\|(\boldsymbol{e}_{\boldsymbol{u}}, e_p)\|_{\mathrm{DG}(h,k)} \leq \|(\boldsymbol{e}_{\boldsymbol{u}}^c, e_p)\|_{\mathrm{DG}(h,k)} + \max(1, N_1^{-1/2}) D \left(\sum_{\kappa \in \mathcal{T}_h} \eta_\kappa^2 \right)^{1/2}; \tag{7.13}$$

cf. (6.34). To bound the term $\|(\boldsymbol{e}_{\boldsymbol{u}}^c, e_p)\|_{\mathrm{DG}(h,k)}$ we set

$$\mathcal{A}_{h,k}(\boldsymbol{\psi};(\boldsymbol{u},p),(\boldsymbol{v},q)) = A_{h,k}(\boldsymbol{\psi};\boldsymbol{u},\boldsymbol{v}) + B_{h,k}(\boldsymbol{v},p) - B_{h,k}(\boldsymbol{u},q)$$

and invoke the result from Lemma 6.11 to note that there exists a $(\boldsymbol{v},q) \in \left[H_0^1(\Omega)\right]^d \times L_0^2(\Omega)$ such that

$$\begin{aligned} C_S\,\|(\boldsymbol{e}_{\boldsymbol{u}}^c, e_p)\|_{\mathrm{DG}(h,k)} &\leq \mathcal{A}_{h,k}(\boldsymbol{u};(\boldsymbol{u},p),(\boldsymbol{v},q)) - \mathcal{A}_{h,k}(\boldsymbol{u}_{2G}^c;(\boldsymbol{u}_{2G}^c,p_{2G}),(\boldsymbol{v},q)),\\ \|(\boldsymbol{v},q)\|_{\mathrm{DG}(h,k)} &\leq 1. \end{aligned}$$

Therefore, from (7.10), we deduce that

$$\begin{aligned} C_S\,\|(\boldsymbol{e}_{\boldsymbol{u}}^c, e_p)\|_{\mathrm{DG}(h,k)} &\leq \sum_{\widetilde{\kappa}\in\mathcal{T}_{\widetilde{h}}}\int_{\widetilde{\kappa}} (\mu(|\underline{\boldsymbol{e}}(\boldsymbol{u})|)\underline{\boldsymbol{e}}(\boldsymbol{u}) - \mu(|\underline{\boldsymbol{e}}(\boldsymbol{u}_{2G}^c)|)\underline{\boldsymbol{e}}(\boldsymbol{u}_{2G}^c)) : \underline{\boldsymbol{e}}(\boldsymbol{v})\,\mathrm{d}\boldsymbol{x}\\ &\quad - \sum_{\widetilde{\kappa}\in\mathcal{T}_{\widetilde{h}}}\int_{\widetilde{\kappa}} (p-p_{2G})\nabla\cdot\boldsymbol{v}\,\mathrm{d}\boldsymbol{x} + \sum_{\widetilde{\kappa}\in\mathcal{T}_{\widetilde{h}}}\int_{\widetilde{\kappa}} q\nabla\cdot(\boldsymbol{u}-\boldsymbol{u}_{2G}^c)\,\mathrm{d}\boldsymbol{x}\\ &= \sum_{\widetilde{\kappa}\in\mathcal{T}_{\widetilde{h}}}\int_{\widetilde{\kappa}} (\mu(|\underline{\boldsymbol{e}}(\boldsymbol{u})|)\underline{\boldsymbol{e}}(\boldsymbol{u}) - \mu(|\underline{\boldsymbol{e}}(\boldsymbol{u}_{H,K})|)\underline{\boldsymbol{e}}(\boldsymbol{u}_{2G})) : \underline{\boldsymbol{e}}(\boldsymbol{v})\,\mathrm{d}\boldsymbol{x}\\ &\quad + \sum_{\widetilde{\kappa}\in\mathcal{T}_{\widetilde{h}}}\int_{\widetilde{\kappa}} (\mu(|\underline{\boldsymbol{e}}(\boldsymbol{u}_{H,K})|)\underline{\boldsymbol{e}}(\boldsymbol{u}_{2G}) - \mu(|\underline{\boldsymbol{e}}(\boldsymbol{u}_{2G})|)\underline{\boldsymbol{e}}(\boldsymbol{u}_{2G})) : \underline{\boldsymbol{e}}(\boldsymbol{v})\,\mathrm{d}\boldsymbol{x}\\ &\quad + \sum_{\widetilde{\kappa}\in\mathcal{T}_{\widetilde{h}}}\int_{\widetilde{\kappa}} (\mu(|\underline{\boldsymbol{e}}(\boldsymbol{u}_{2G})|)\underline{\boldsymbol{e}}(\boldsymbol{u}_{2G}) - \mu(|\underline{\boldsymbol{e}}(\boldsymbol{u}_{2G}^c)|)\underline{\boldsymbol{e}}(\boldsymbol{u}_{2G}^c)) : \underline{\boldsymbol{e}}(\boldsymbol{v})\,\mathrm{d}\boldsymbol{x}\\ &\quad - \sum_{\widetilde{\kappa}\in\mathcal{T}_{\widetilde{h}}}\int_{\widetilde{\kappa}} (p-p_{2G})\nabla\cdot\boldsymbol{v}\,\mathrm{d}\boldsymbol{x} + \sum_{\widetilde{\kappa}\in\mathcal{T}_{\widetilde{h}}}\int_{\widetilde{\kappa}} q\nabla\cdot(\boldsymbol{u}-\boldsymbol{u}_{2G}+\boldsymbol{u}_{2G}^{\perp})\,\mathrm{d}\boldsymbol{x}\\ &\equiv T_1 + T_2 + T_3, \end{aligned} \tag{7.14}$$

where

$$\begin{aligned} T_1 &= \sum_{\widetilde{\kappa}\in\mathcal{T}_{\widetilde{h}}}\int_{\widetilde{\kappa}} (\mu(|\underline{\boldsymbol{e}}(\boldsymbol{u})|)\underline{\boldsymbol{e}}(\boldsymbol{u}) - \mu(|\underline{\boldsymbol{e}}(\boldsymbol{u}_{H,K})|)\underline{\boldsymbol{e}}(\boldsymbol{u}_{2G})) : \underline{\boldsymbol{e}}(\boldsymbol{v})\,\mathrm{d}\boldsymbol{x}\\ &\quad - \sum_{\widetilde{\kappa}\in\mathcal{T}_{\widetilde{h}}}\int_{\widetilde{\kappa}} (p-p_{2G})\nabla\cdot\boldsymbol{v}\,\mathrm{d}\boldsymbol{x} + \sum_{\widetilde{\kappa}\in\mathcal{T}_{\widetilde{h}}}\int_{\widetilde{\kappa}} q\nabla\cdot(\boldsymbol{u}-\boldsymbol{u}_{2G})\,\mathrm{d}\boldsymbol{x}, \end{aligned}$$

$$T_2 = \sum_{\widetilde{\kappa}\in\mathcal{T}_{\widetilde{h}}} \int_{\widetilde{\kappa}} (\mu(|\underline{e}(\boldsymbol{u}_{2G})|)\underline{e}(\boldsymbol{u}_{2G}) - \mu(|\underline{e}(\boldsymbol{u}^c_{2G})|)\underline{e}(\boldsymbol{u}^c_{2G})) : \underline{e}(\boldsymbol{v})\,\mathrm{d}\boldsymbol{x} + \sum_{\widetilde{\kappa}\in\mathcal{T}_{\widetilde{h}}} \int_{\widetilde{\kappa}} q\nabla\cdot\boldsymbol{u}^{\perp}_{2G}\,\mathrm{d}\boldsymbol{x},$$

$$T_3 = \sum_{\widetilde{\kappa}\in\mathcal{T}_{\widetilde{h}}} \int_{\widetilde{\kappa}} (\mu(|\underline{e}(\boldsymbol{u}_{H,K})|)\underline{e}(\boldsymbol{u}_{2G}) - \mu(|\underline{e}(\boldsymbol{u}_{2G})|)\underline{e}(\boldsymbol{u}_{2G})) : \underline{e}(\boldsymbol{v})\,\mathrm{d}\boldsymbol{x}.$$

We note that T_1 and T_2 are analogous to the corresponding terms that arise in the *a posteriori* error analysis of the standard IP DGFEM discretisation of (6.12)-(6.13), cf. Chapter 6. Indeed, by following the analysis in Section 6.4.3, we deduce that

$$|T_1| + |T_2| \leq C \left(\sum_{\kappa\in\mathcal{T}_h} \eta_\kappa^2 + \sum_{\kappa\in\mathcal{T}_h} h_\kappa^2 k_\kappa^{-2} \left\| \boldsymbol{f} - \Pi_{\kappa,k_\kappa}\boldsymbol{f} \right\|^2_{L^2(\kappa)} \right)^{1/2}. \tag{7.15}$$

We note that term T_3 may be bounded in a similar manner to the corresponding term which arises in the two-grid IP DGFEM of the second-order quasilinear elliptic problem, cf. Chapter 3; indeed, we have

$$\begin{aligned} |T_3| &\leq \sum_{\kappa\in\mathcal{T}_h} \int_{\widetilde{\kappa}} |\mu(|\underline{e}(\boldsymbol{u}_{H,K})|)\underline{e}(\boldsymbol{u}_{2G}) - \mu(|\underline{e}(\boldsymbol{u}_{2G})|)\underline{e}(\boldsymbol{u}_{2G})||\underline{e}(\boldsymbol{v})|\,\mathrm{d}\boldsymbol{x} \\ &\leq \left(\sum_{\kappa\in\mathcal{T}_h} \|\{\mu(|\underline{e}(\boldsymbol{u}_{H,K})|) - \mu(|\underline{e}(\boldsymbol{u}_{2G})|)\}\underline{e}(\boldsymbol{u}_{2G})\|^2_{L^2(\kappa)} \right)^{1/2} \left(\sum_{\kappa\in\mathcal{T}_h} \|\underline{e}(\boldsymbol{v})\|^2_{L^2(\kappa)} \right)^{1/2} \\ &\leq \left(\sum_{\kappa\in\mathcal{T}_h} \xi_\kappa^2 \right)^{1/2}. \end{aligned} \tag{7.16}$$

Inserting (7.15) and (7.16) into (7.14) gives

$$\|(\boldsymbol{e}^c_{\boldsymbol{u}}, e_p)\|_{\mathrm{DG}(h,k)} \leq C_S^{-1} C \left(\sum_{\kappa\in\mathcal{T}_h} \eta_\kappa^2 + \sum_{\kappa\in\mathcal{T}_h} h_\kappa^2 k_\kappa^{-2} \left\| \boldsymbol{f} - \Pi_{\kappa,k_\kappa}\boldsymbol{f} \right\|^2_{L^2(\kappa)} \right)^{1/2} + C_S^{-1} \left(\sum_{\kappa\in\mathcal{T}_h} \xi_\kappa^2 \right)^{1/2}.$$

Combining this result with (7.13) and applying the Cauchy inequality completes the proof of Theorem 7.4. □

7.2 Two-Grid hp-Version DGFEM Based on an Incomplete Newton Iteration

In this section we consider an alternative two-grid version of the family of IP DGFEMs for the numerical approximation of (7.1)–(7.2) based on employing a single step of a Newton iteration, cf. Axelsson & Layton [10], Xu [180] and Chapter 5. Using the same notation defined in the previous section, the alternative two-grid version of the IP DGFEM discretisation of (7.1)–(7.3) based on a single Newton iteration, cf. Xu [180, Section 5.2], can be defined as:

1. (Nonlinear solve) Compute $(\boldsymbol{u}_{H,K}, p_{H,K}) \in \boldsymbol{V}(\mathcal{T}_H, \boldsymbol{K}) \times Q(\mathcal{T}_H, \boldsymbol{K})$ such that

$$A_{H,K}(\boldsymbol{u}_{H,K}; \boldsymbol{u}_{H,K}, \boldsymbol{v}_{H,K}) + B_{H,K}(\boldsymbol{v}_{H,K}, p_{H,K}) = F_{H,K}(\boldsymbol{v}_{H,K}), \tag{7.17}$$

$$-B_{H,K}(\boldsymbol{u}_{H,K}, q_{H,K}) = 0 \tag{7.18}$$

   for all $(\boldsymbol{v}_{H,K}, q_{H,K}) \in \boldsymbol{V}(\mathcal{T}_H, \boldsymbol{K}) \times Q(\mathcal{T}_H, \boldsymbol{K})$.

2. (Linear solve) Determine the fine grid solution $(\boldsymbol{u}_{2G}, p_{2G}) \in \boldsymbol{V}(\mathcal{T}_h, \boldsymbol{k}) \times Q(\mathcal{T}_h, \boldsymbol{k})$ such that

$$A'_{h,k}[\boldsymbol{u}_{H,K}](\boldsymbol{u}_{2G}, \boldsymbol{v}_{h,k}) + B_{h,k}(\boldsymbol{v}_{h,k}, p_{2G}) = A'_{h,k}[\boldsymbol{u}_{H,K}](\boldsymbol{u}_{H,K}, \boldsymbol{v}_{h,k}) \tag{7.19}$$

$$- A_{h,k}(\boldsymbol{u}_{H,K}; \boldsymbol{u}_{H,K}, \boldsymbol{v}_{h,k}) + F_{h,k}(\boldsymbol{v}_{h,k}),$$

$$-B_{h,k}(\boldsymbol{u}_{2G}, q_{h,k}) = 0 \tag{7.20}$$

   for all $(\boldsymbol{v}_{h,k}, q_{h,k}) \in \boldsymbol{V}(\mathcal{T}_h, \boldsymbol{k}) \times Q(\mathcal{T}_h, \boldsymbol{k})$.

Here $A'_{h,k}[\boldsymbol{u}](\cdot, \boldsymbol{v})$ denotes the Fréchet derivative of $\boldsymbol{u} \to A_{h,k}(\boldsymbol{u}; \boldsymbol{u}, \boldsymbol{v})$, for fixed $\boldsymbol{v}$, evaluated at $\boldsymbol{u}$; thereby, given $\boldsymbol{\phi}$ we have

$$A'_{h,k}[\boldsymbol{u}](\boldsymbol{\phi}, \boldsymbol{v}) = \lim_{t \to 0} \frac{A_{h,k}(\boldsymbol{u} + t\boldsymbol{\phi}; \boldsymbol{u} + t\boldsymbol{\phi}, \boldsymbol{v}) - A_{h,k}(\boldsymbol{u}; \boldsymbol{u}, \boldsymbol{v})}{t}.$$

Remark 7.2. For simplicity of presentation, in this section we will only consider the IIP

DGFEM formulation corresponding to the case when $\theta = 0$.

Assumption E. In this section we assume that $\mu \in \mathrm{C}^2(\bar{\Omega} \times [0, \infty))$.

Lemma 7.5. *For any* $(\boldsymbol{w}_1, r_1) \in \boldsymbol{V}(\mathcal{T}_h, \boldsymbol{k}) \times Q(\mathcal{T}_h, \boldsymbol{k})$ *and* $\boldsymbol{w}_2 \in \boldsymbol{V}(\mathcal{T}_h, \boldsymbol{k})$*, there exists a* $(\boldsymbol{v}, q) \in \boldsymbol{V}(\mathcal{T}_h, \boldsymbol{k}) \times Q(\mathcal{T}_h, \boldsymbol{k})$ *such that*

$$
\begin{aligned}
C_S k_{max}^{-2} \, \|(\boldsymbol{w}_1, r_1)\|_{\mathrm{DG}(h,k)} &\leq A'_{h,k}[\boldsymbol{w}_2](\boldsymbol{w}_1, \boldsymbol{v}) + B_{h,k}(\boldsymbol{v}, r_1) - B_{h,k}(\boldsymbol{w}_1, q), \\
\|(\boldsymbol{v}, q)\|_{\mathrm{DG}(h,k)} &\leq 1,
\end{aligned}
$$

where C_S *is a positive constant.*

Proof. By setting $\boldsymbol{u} = \boldsymbol{w}_2 + t\boldsymbol{w}_1$, $\boldsymbol{w} = \boldsymbol{w}_2$, $p = tr_1$ and $q = 0$, where $t > 0$ in Lemma 6.11 there exists a $(\boldsymbol{v}, q) \in \boldsymbol{V}(\mathcal{T}_h, \boldsymbol{k}) \times Q(\mathcal{T}_h, \boldsymbol{k})$ such that

$$
\begin{aligned}
C_S k_{max}^{-2} \, \|(t\boldsymbol{w}_1, tr_1)\|_{\mathrm{DG}(h,k)} &\leq A_{h,k}(\boldsymbol{w}_2 + t\boldsymbol{w}_1; \boldsymbol{w}_2 + t\boldsymbol{w}_1, \boldsymbol{v}) - A_{h,k}(\boldsymbol{w}_2; \boldsymbol{w}_2, \boldsymbol{v}) \\
&\quad + B_{h,k}(\boldsymbol{v}, tr_1) - B_{h,k}(t\boldsymbol{w}_1, q), \\
\|(\boldsymbol{v}, q)\|_{\mathrm{DG}(h,k)} &\leq 1.
\end{aligned}
$$

Thereby,

$$
\begin{aligned}
C_S k_{max}^{-2} \, \|(\boldsymbol{w}_1, r_1)\|_{\mathrm{DG}(h,k)} &\leq \frac{A_{h,k}(\boldsymbol{w}_2 + t\boldsymbol{w}_1; \boldsymbol{w}_2 + t\boldsymbol{w}_1, \boldsymbol{v}) - A_{h,k}(\boldsymbol{w}_2; \boldsymbol{w}_2, \boldsymbol{v})}{t} \\
&\quad + B_{h,k}(\boldsymbol{v}, r_1) - B_{h,k}(\boldsymbol{w}_1, q).
\end{aligned}
$$

Taking the limit as $t \to 0$ completes the proof. □

7.2.1 *A Priori* Error Bound

In this section we state and prove an *a priori* error bound for the two-grid approximation defined in (7.17)–(7.20) for the numerical approximation of the non-Newtonian fluid flow problem (7.1)–(7.3). For simplicity of presentation, in this section we assume that the mesh is quasiuniform with (global) mesh size h; moreover, we assume that the polynomial degree is uniform over the mesh, and write k in lieu of $\boldsymbol{k}$.

Theorem 7.6. *Assuming that* $(\boldsymbol{u}, p) \in \left[C^1(\Omega) \cap H^s(\Omega)\right]^d \times (C^1(\Omega) \cap H^{s-1}(\Omega))$, $s \geq 2$; *then the solution* $(\boldsymbol{u}_{2G}, p_{h,k}) \in \boldsymbol{V}(\mathcal{T}_h, \boldsymbol{k}) \times Q(\mathcal{T}_h, \boldsymbol{k})$ *of the incomplete Newton two-grid method* (7.17)–(7.20) *satisfies the error bounds*

$$\|(\boldsymbol{u}_{h,k} - \boldsymbol{u}_{2G}, p_{h,k} - p_{2G})\|_{\mathrm{DG}(h,k)} \leq C_{13} \frac{k^{23/2}}{h} \left(\frac{H^{2R-2}}{K^{2s-3}} \|\boldsymbol{u}\|^2_{H^s(\Omega)} + \frac{H^{2R-2}}{K^{2s-2}} \|p\|^2_{H^{s-1}(\Omega)} \right),$$

$$\begin{aligned} \|(\boldsymbol{u} - \boldsymbol{u}_{2G}, p - p_{h,k})\|_{\mathrm{DG}(h,k)} \leq{}& C_8^{1/2} k^2 \left(\frac{h^{2r-2}}{k^{2s-3}} \|\boldsymbol{u}\|^2_{H^s(\Omega)} + \frac{h^{2r-2}}{k^{2s-2}} \|p\|^2_{H^{s-1}(\Omega)} \right)^{1/2} \\ &+ C_{13} \frac{k^{23/2}}{h} \left(\frac{H^{2R-2}}{K^{2s-3}} \|\boldsymbol{u}\|^2_{H^s(\Omega)} + \frac{H^{2R-2}}{K^{2s-2}} \|p\|^2_{H^{s-1}(\Omega)} \right), \end{aligned}$$

with $1 \leq r \leq \min(s, k+1)$, $k \geq 1$ *and* $1 \leq R \leq \min(s, K+1)$, $K \geq 1$, *and* C_8, C_{13} *are positive constants independent of* $\boldsymbol{u}, p, h, H, k$ *and* K.

Remark 7.3. We note that the first error bound in Theorem 7.6 results in a large dependency on the fine mesh polynomial degree k compared to the scalar quasilinear PDE, cf. Chapter 5. We note this is due to the dependency of the discrete inf-sup condition (6.17) on the maximum polynomial degree $k_{\max}$. It is worth remarking that Schötzau *et al.* [157, Remark 6.5] notes that numerical experiments for the Stokes equations in two dimensions, cf. Toselli [166], indicates that the discrete inf-sup condition is likely to be independent of k and hence (6.17) may not be a sharp estimate with respect to k.

Auxiliary Results

In order to prove Theorem 7.6 we first state and prove the following auxiliary results.

Lemma 7.7. *For any* $\boldsymbol{v}, \boldsymbol{w}, \boldsymbol{\phi} \in \boldsymbol{V}(\mathcal{T}_h, \boldsymbol{k})$,

$$A_{h,k}(\boldsymbol{w}; \boldsymbol{w}, \boldsymbol{\phi}) = A_{h,k}(\boldsymbol{v}; \boldsymbol{v}, \boldsymbol{\phi}) + A'_{h,k}[\boldsymbol{v}](\boldsymbol{w} - \boldsymbol{v}, \boldsymbol{\phi}) + \mathcal{Q}(\boldsymbol{v}, \boldsymbol{w}, \boldsymbol{\phi}),$$

where the remainder $\mathcal{Q}$ *satisfies*

$$|\mathcal{Q}(\boldsymbol{v}, \boldsymbol{w}, \boldsymbol{\phi})| \leq C_{\mathcal{Q}} k^2 h^{-1} \left(1 + \|\underline{e}(\boldsymbol{v})\|_{L^\infty(\Omega)} + \|\underline{e}(\boldsymbol{w})\|_{L^\infty(\Omega)}\right) \|\boldsymbol{w} - \boldsymbol{v}\|^2_{h,k} \|\boldsymbol{\phi}\|_{h,k},$$

where $C_{\mathcal{Q}}$ *is a positive constant, independent of the discretisation parameters.*

Proof. We note that this proof follows in an identical fashion to Lemma 5.5. □

Lemma 7.8. *Let $\boldsymbol{u} \in \left[H^2(\Omega)\right]^d$ be the velocity component of the analytical solution of (6.1)–(6.3) and $\boldsymbol{u}_{h,k} \in \boldsymbol{V}(\mathcal{T}_h, \boldsymbol{k})$ be the velocity component of the numerical solution defined by (6.12)–(6.13). Then, assuming that $\underline{\varepsilon}(\boldsymbol{u}) \in [L^\infty(\Omega)]^{d\times d}$, we have that*

$$\|\underline{\varepsilon}(\boldsymbol{u}_{h,k})\|_{L^\infty(\Omega)} \leq C_\infty k^{7/2},$$

where C_∞ is a positive constant, independent of the discretisation parameters.

Proof. Due to the fact that

$$\|\underline{\varepsilon}(\boldsymbol{v})\|_{L^\infty(\Omega)} \leq \frac{1}{2}\|\nabla \boldsymbol{v}\|_{L^\infty(\Omega)} + \frac{1}{2}\left\|(\nabla \boldsymbol{v})^\top\right\|_{L^\infty(\Omega)} = \|\nabla \boldsymbol{v}\|_{L^\infty(\Omega)}$$

for all $\boldsymbol{v} \in \boldsymbol{V}(\mathcal{T}_h, \boldsymbol{k})$ we can simply extend the proof of Lemma 5.6, noting that application of Theorem 6.5 results in an extra k^2 in the result. □

Proof of Theorem 7.6

We can now prove Theorem 7.6. To this end, we define $\delta_{\boldsymbol{u}} = \boldsymbol{u}_{h,k} - \boldsymbol{u}_{2G}$ and $\delta_p = p_{h,k} - p_{2G}$. Then, from Lemma 7.5, there exists a $(\boldsymbol{v}, p) \in \boldsymbol{V}(\mathcal{T}_h, \boldsymbol{k}) \times Q(\mathcal{T}_h, \boldsymbol{k})$ such that

$$\begin{aligned} C_S k^{-2}\,\|(\delta_{\boldsymbol{u}}, \delta_p)\|_{\mathrm{DG}(h,k)} &\leq A'_{h,k}[u_{H,K}](\delta_{\boldsymbol{u}}, \boldsymbol{v}) + B_{h,k}(\boldsymbol{v}, \delta_p) - B_{h,k}(\delta_{\boldsymbol{u}}, q), \\ \|(\boldsymbol{v}, q)\|_{\mathrm{DG}(h,k)} &\leq 1. \end{aligned} \tag{7.21}$$

Thereby, from (6.12), (6.13), (7.19), and (7.20), we deduce that

$$\begin{aligned} &C_S k_{max}^{-2}\,\|(\delta_{\boldsymbol{u}}, \delta_p)\|_{\mathrm{DG}(h,k)} \\ &\quad\leq A'_{h,k}[\boldsymbol{u}_{H,K}](\delta_{\boldsymbol{u}}, \boldsymbol{v}) + B_{h,k}(\boldsymbol{v}, \delta_p) - B_{h,k}(\delta_{\boldsymbol{u}}, q) \\ &\quad= A'_{h,k}[\boldsymbol{u}_{H,K}](\boldsymbol{u}_{h,k} - \boldsymbol{u}_{H,K}, \boldsymbol{v}) + A_{h,k}(\boldsymbol{u}_{H,K}; \boldsymbol{u}_{H,K}, \boldsymbol{v}) - F_{h,k}(\boldsymbol{v}) + B_{h,k}(\boldsymbol{v}, p_{h,k}) \\ &\quad= A'_{h,k}[\boldsymbol{u}_{H,K}](\boldsymbol{u}_{h,k} - \boldsymbol{u}_{H,K}, \boldsymbol{v}) + A_{h,k}(\boldsymbol{u}_{H,K}; \boldsymbol{u}_{H,K}, \boldsymbol{v}) - A_{h,k}(\boldsymbol{u}_{h,k}; \boldsymbol{u}_{h,k}, \boldsymbol{v}) \\ &\quad= -\mathcal{Q}(\boldsymbol{u}_{H,K}, \boldsymbol{u}_{h,k}, \boldsymbol{v}). \end{aligned}$$

Hence, from Lemma 7.7 we get

$$\begin{aligned}\|(\boldsymbol{u}_{h,k}-\boldsymbol{u}_{2G},p_{h,k}-p_{2G})\|_{\mathrm{DG}(h,k)}&\\ \leq Ck^4h^{-1}\left(1+\|\underline{e}(\boldsymbol{u}_{h,k})\|_{L^\infty(\Omega)}+\|\underline{e}(\boldsymbol{u}_{H,K})\|_{L^\infty(\Omega)}\right)\|\boldsymbol{u}_{h,k}-\boldsymbol{u}_{H,K}\|_{h,k}^2\,\|\boldsymbol{v}\|_{h,k}\,.&\end{aligned}$$

Applying Lemma 7.8, noting that $k \geq K \geq 1$, inequality (7.21) and the *a priori* error bound stated in Theorem 6.5, gives

$$\begin{aligned}\|(\boldsymbol{u}_{h,k}-\boldsymbol{u}_{2G},p_{h,k}-p_{2G})\|_{\mathrm{DG}(h,k)}&\leq C\frac{k^{15/2}}{h}\left(\|\boldsymbol{u}-\boldsymbol{u}_{h,k}\|_{h,k}^2+\|\boldsymbol{u}-\boldsymbol{u}_{H,K}\|_{h,k}^2\right)\\ &\leq C\frac{k^{23/2}}{h}\left(\frac{h^{2r-2}}{k^{2s-3}}\|\boldsymbol{u}\|_{H^s(\Omega)}^2+\frac{h^{2r-2}}{k^{2s-2}}\|p\|_{H^{s-1}(\Omega)}^2\right.\\ &\qquad\left.+\frac{H^{2R-2}}{K^{2s-3}}\|\boldsymbol{u}\|_{H^s(\Omega)}^2+\frac{H^{2R-2}}{K^{2s-2}}\|p\|_{H^{s-1}(\Omega)}^2\right).\end{aligned}$$

Noting that $h \leq H$ and that $k \geq K$ completes the proof of the first bound of Theorem 7.6. To prove the second bound of Theorem 7.6 we first employ the triangle inequality

$$\begin{aligned}\|(\boldsymbol{u}-\boldsymbol{u}_{2G},p-p_{2G})\|_{\mathrm{DG}(h,k)}&\leq\|(\boldsymbol{u}-\boldsymbol{u}_{h,k},p-p_{h,k})\|_{\mathrm{DG}(h,k)}\\ &\quad+\|(\boldsymbol{u}_{h,k}-\boldsymbol{u}_{2G},p_{h,k}-p_{2G})\|_{\mathrm{DG}(h,k)}\,.\end{aligned}$$

Thereby, applying the *a priori* error bound in Theorem 6.5, along with the first bound completes the proof of Theorem 7.6. □

7.2.2 *A Posteriori* Error Bound

In this section, writing Π_{κ,k_κ} to denote the elementwise L^2-projection into $\boldsymbol{V}(\mathcal{T}_h,\boldsymbol{k})$, we state the following *a posteriori* upper bound for the numerical approximation defined by (7.17)–(7.20).

Theorem 7.9. *Let* $(\boldsymbol{u},p) \in \left[H_0^1(\Omega)\right]^d \times L_0^2(\Omega)$ *be the analytical solution of* (7.1)–(7.3), $(\boldsymbol{u}_{H,K},p_{H,K}) \in \boldsymbol{V}(\mathcal{T}_H,\boldsymbol{K}) \times Q(\mathcal{T}_H,\boldsymbol{K})$ *the numerical approximation obtained from* (7.17)–(7.18) *and* $(\boldsymbol{u}_{2G},p_{2G}) \in \boldsymbol{V}(\mathcal{T}_h,\boldsymbol{k}) \times Q(\mathcal{T}_h,\boldsymbol{k})$ *the numerical approximation obtained from*

(7.19)–(7.20); *then, the following* hp-a posteriori *error bound holds*

$$\|(\boldsymbol{u}-\boldsymbol{u}_{2G},p-p_{2G})\|_{\mathrm{DG}(h,k)} \leq C_{14}\left(\sum_{\kappa\in\mathcal{T}_h}\left(\eta_\kappa^2+\xi_\kappa^2\right)+\sum_{\kappa\in\mathcal{T}_h}h_\kappa^2k_\kappa^{-2}\,\|\boldsymbol{f}-\Pi_{\kappa,k_\kappa}\boldsymbol{f}\|_{L^2(\kappa)}^2\right)^{1/2},$$

with a constant $C_{14}>0$, *which is independent of* $\boldsymbol{h}$, $\boldsymbol{H}$, $\boldsymbol{k}$, $\boldsymbol{K}$. *Here, for all* $\kappa\in\mathcal{T}_h$, *the* local fine grid error indicators η_κ *are defined by*

$$\begin{aligned}\eta_\kappa^2 &= h_\kappa^2k_\kappa^{-2}\,\|\Pi_{\kappa,k_\kappa}\boldsymbol{f}+\nabla\cdot(\mu(|\underline{e}(\boldsymbol{u}_{H,K})|)\underline{e}(\boldsymbol{u}_{2G}))-\nabla p_{2G}\|_{L^2(\kappa)}^2+\|\nabla\cdot\boldsymbol{u}_{2G}\|_{L^2(\kappa)}^2\\&\quad+h_\kappa k_\kappa^{-1}\left\|[\![p_{2G}]\!]-\underline{[\![\mu(|\underline{e}(\boldsymbol{u}_{H,K})|)\underline{e}(\boldsymbol{u}_{2G})]\!]}\right\|_{L^2(\partial\kappa\setminus\Gamma)}^2+\gamma^2h_\kappa^{-1}k_\kappa^3\left\|\underline{[\![\boldsymbol{u}_{2G}]\!]}\right\|_{L^2(\partial\kappa)}^2\end{aligned}$$

and the local two-grid error indicators ξ_κ *are defined, for all* $\kappa\in\mathcal{T}_h$, *as*

$$\begin{aligned}\xi_\kappa^2 &= \|(\mu(|\underline{e}(\boldsymbol{u}_{H,K})|)-\mu(|\underline{e}(\boldsymbol{u}_{2G})|))\underline{e}(\boldsymbol{u}_{2G})\|_{L^2(\kappa)}^2\\&\quad+\left\|\left(\mu'_{\underline{e}(u)}(|\underline{e}(\boldsymbol{u}_{H,K})|):(\underline{e}(\boldsymbol{u}_{2G})-\underline{e}(\boldsymbol{u}_{H,K}))\right)\underline{e}(\boldsymbol{u}_{H,K})\right\|_{L^2(\kappa)}^2\\&\quad+h_\kappa k_\kappa^{-1}\left\|\left(\mu'_{\underline{e}(u)}(|\underline{e}(\boldsymbol{u}_{H,K})|):(\underline{e}(\boldsymbol{u}_{2G})-\underline{e}(\boldsymbol{u}_{H,K}))\right)\underline{e}(\boldsymbol{u}_{H,K})\right\|_{L^2(\partial\kappa)}^2.\end{aligned}$$

Proof. The proof of this theorem follows in an analogous manner to the proof of Theorem 7.4. We note that the *a posteriori* error bound for the alternative two-grid method based on a single Newton iteration contains two extra terms in the local two-grid error indicators compared to the result derived in Theorem 7.4 for the two-grid approximation defined in (7.4)–(7.7). These two extra terms appear, trivially, from the bound of T_1 from (7.14) where, instead of adding (6.12), with a specific $\boldsymbol{v}_{h,k}$, (7.19) has to be added instead; cf. Section 5.3.1. □

7.3 Numerical Experiments

In this section we perform a series of numerical experiments to validate the *a priori* error bounds derived in Theorem 7.2, as well as to demonstrate the performance of the *a posteriori* error bounds from Theorem 7.4 and Theorem 7.9 within the automatic hp-adaptive mesh refinement procedure based on 1-irregular quadrilateral elements

for $\Omega \subset \mathbb{R}^2$ defined in Section 4.2. Throughout this section the DGFEM solutions obtained by (7.4)–(7.7) and (7.17)–(7.20) are calculated with $\theta = 0$. We additionally set the constant γ arising in the interior penalty parameter $\sigma_{h,k}$ to 10. The resulting system of nonlinear equations, on the coarse mesh, are solved based on employing a damped Newton method; for each inner (linear) iteration, as well as the linear fine mesh system, we employ the Multifrontal Massively Parallel Solver, see Amestoy *et al.* [2, 3, 4].

7.3.1 Validation of *A Priori* Error Bound

We shall first perform a series of experiments on fixed sized meshes to validate the sharpness of the bounds in Theorem 7.2. To this end we consider the cavity-like problem from Berrone & Süli [31, Section 6.1] using the Carreau law nonlinearity

$$\mu(|\underline{e}(\boldsymbol{u})|) = k_\infty + (k_0 - k_\infty)(1 + \lambda_c|\underline{e}(\boldsymbol{u})|^2)^{(\vartheta-2)/2}, \tag{7.22}$$

with $k_\infty = 0$, $k_0 = 2$, $\lambda_c = 1$ and $\vartheta = 1.2$. We let $\Omega = (0,1)^2$ be the unit square and select the forcing function $\boldsymbol{f}$ such that the analytical solution to (7.1)–(7.3) is given by

$$\boldsymbol{u}(x,y) = \begin{pmatrix} \left(1 - \cos\left(2\frac{\pi\left(\mathrm{e}^{\vartheta x}-1\right)}{\mathrm{e}^{\vartheta}-1}\right)\right)\sin(2\pi y) \\ -\vartheta \mathrm{e}^{\vartheta x}\sin\left(2\frac{\pi\left(\mathrm{e}^{\vartheta x}-1\right)}{\mathrm{e}^{\vartheta}-1}\right)\frac{1-\cos(2\pi y)}{\mathrm{e}^{\vartheta}-1} \end{pmatrix}, \tag{7.23}$$

$$p(x,y) = 2\pi\vartheta \mathrm{e}^{\vartheta x}\sin\left(2\frac{\pi\left(\mathrm{e}^{\vartheta x}-1\right)}{\mathrm{e}^{\vartheta}-1}\right)\frac{\sin(2\pi y)}{\mathrm{e}^{\vartheta}-1}. \tag{7.24}$$

We start by validating the first two error bounds from Theorem 7.2 by considering the case when the fine mesh $\mathcal{T}_h$ is fixed (256×256 uniform square mesh) and the coarse grid is uniformly refined. For this experiment we fix the coarse and fine polynomial degree vector $\boldsymbol{k}$ and $\boldsymbol{K}$, respectively, to be both uniform and equal, i.e., $K_\kappa = k$ for all $\kappa \in \mathcal{T}_H$ and $k_\kappa = k$ for all $\kappa \in \mathcal{T}_h$. We also compute the standard DGFEM solution $(\boldsymbol{u}_{h,k}, p_{h,k})$ defined by (6.12)–(6.13) on the fine mesh $\mathcal{T}_h$. In Figure 7.1(a) we plot the error between the two-grid solution and the standard DGFEM solution in the DG norm, $\|(\boldsymbol{u}_{h,k} - \boldsymbol{u}_{2G}, p_{h,k} - p_{2G})\|_{\mathrm{DG}(h,k)}$, against the coarse mesh size H in the case when $k =$

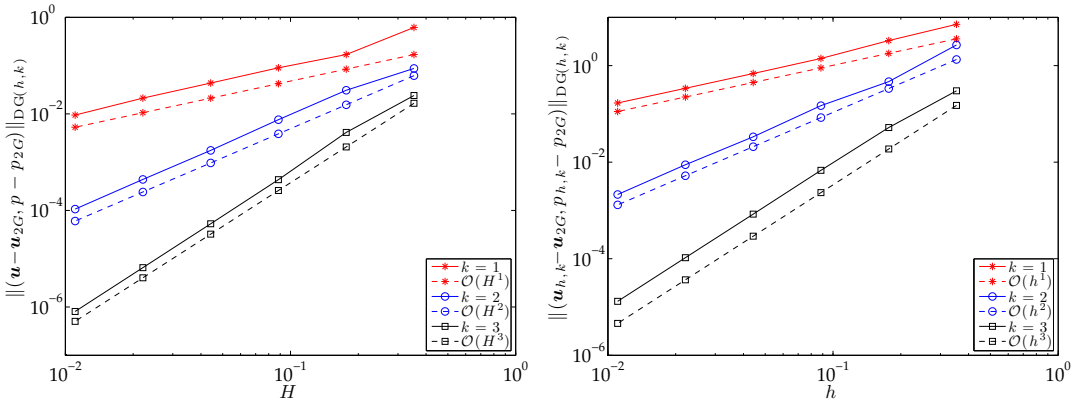

Figure 7.1: First two-grid method (Section 7.1): (a) Plot of $\|(\boldsymbol{u}_{h,k}-\boldsymbol{u}_{2G}, p_{h,k}-p_{2G})\|_{\mathrm{DG}(h,k)}$ against the coarse mesh size H for a fixed fine mesh (256×256); (b) Plot of $\|(\boldsymbol{u}-\boldsymbol{u}_{2G}, p-p_{2G})\|_{\mathrm{DG}(h,k)}$ against the fine mesh size h as both coarse and fine meshes are uniformly refined, with $h = H/2$

$1, 2, 3$. Here, we clearly observe that the energy norm of the error between the standard DGFEM and its two-grid variant converges to zero at the rate $\mathcal{O}(H^k)$, as H tends to zero, for each fixed polynomial degree. This result matches the expected results from the first two bounds in Theorem 7.2.

We now perform an experiment to validate the last error bound from Theorem 7.2. We note to obtain an optimal rate of convergence the coarse mesh and fine mesh $\mathcal{T}_h$ and $\mathcal{T}_H$, respectively, need to be refined at roughly the same rate. Indeed for a coarse and fine polynomial degree vector $\boldsymbol{k}$ and $\boldsymbol{K}$, respectively, which are both uniform and equal, i.e., $K_\kappa = k$ for all $\kappa \in \mathcal{T}_H$ and $k_\kappa = k$ for all $\kappa \in \mathcal{T}_h$, then $H = \mathcal{O}(h)$ gives optimal convergence of $\mathcal{O}(h^k)$, as h tends to zero. With this in mind, we initially set $h = H/2$ and perform uniform refinement on both fine and coarse meshes at the same rate, which ensures $h = H/2$ at all refinement steps, for a fixed polynomial degree k. Figure 7.1(b) plots the error between the two-grid solution and the analytical solution (7.23)–(7.24) compared to the fine mesh element size h for the case when $k = 1, 2, 3$. We note that the error in this graph converges to zero at the rate $\mathcal{O}(h^k)$, as h tends to zero, for each fixed polynomial degree, which confirms the analytical result. This completes the validation of the *a priori* error bound for the first two-grid method (7.4)–(7.7).

Remark 7.4. We note that for the *a priori* error bounds (7.17)–(7.20) from Theorem 7.6

we could not validate the second error bound as we are unable to select $\mathcal{T}_h$ and $\mathcal{T}_H$ so that the two terms of the last bound in Theorem 7.6 converge at the same rate such that $\boldsymbol{V}(\mathcal{T}_H, \boldsymbol{K}) \subseteq \boldsymbol{V}(\mathcal{T}_h, \boldsymbol{k})$ and $Q(\mathcal{T}_H, \boldsymbol{K}) \subseteq Q(\mathcal{T}_h, \boldsymbol{k})$. Validation of the first bound also was not possible because for the case when $k \geq 2$ the error quickly converges to machine precision and, hence, not enough results are obtained for validation.

7.3.2 Validation of *A Posteriori* Error Bound

In this section we perform numerical experiments to validate the *a posteriori* error bounds from Theorem 7.4 and Theorem 7.9. The mesh adaptation is undertaken based on using Algorithm 4.1 with the decision on whether to refine coarse or fine meshes, Step 2, based on utilising Algorithm 4.3 with steering parameters $\lambda_C = 1/2$ and $\lambda_F = 1$. The selection of regions to refine is achieved via a fixed fraction strategy, where the refinement and derefinement fractions are set to 25% and 5%, respectively. We employ the hp-adaptive strategy developed by Houston & Süli [116] to decide whether to perform h- or p-refinement/derefinement. We note here that we start with a polynomial degree of $k_{\kappa_h} = 3$ for all $\kappa_h \in \mathcal{T}_h$ and $K_{\kappa_H} = 3$ for all $\kappa_H \in \mathcal{T}_H$.

The aim of these experiments is to demonstrate that the two-grid DGFEM gives a similar error, in the DG norm $\|(\cdot,\cdot)\|_{\mathrm{DG}(h,k)}$ to the standard DGFEM, for a lower computational time. To this end, we perform a standard DGFEM hp-adaptive mesh refinement algorithm measuring the CPU computation time of both DGFEM methods. We also perform the two-grid and standard DGFEM methods using an h-adaptive refinement strategy, using the same 25% and 5% refinement/derefinement fixed fraction strategy, but only performing mesh subdivision for a fixed (uniform) polynomial degree, to demonstrate the superior convergence of the hp-adaptive algorithm. Here, we note that we use $\lambda_C = 1$ for h-refinement. We also calculate the *a posteriori* error bounds for the two-grid DGFEMs, setting the constants C_{12} and C_{14} arising from Theorem 7.4 and Theorem 7.9, respectively, equal to 1 for simplicity. We can then validate that the effectivity indices, defined as the ratio of the *a posteriori* error bound to the true error in the DG norm, are roughly constant. We also ignore in all our experiments the data

oscillation terms arising in Theorem 7.4 and Theorem 7.9.

Example 1: Smooth Solution

In this example we consider the cavity-like problem studied in Section 7.3.1 with non-linearity (7.22) and analytical solution (7.23)–(7.24). In Figure 7.2(a) we present a comparison of the true error, measured in the DGFEM norm, of the standard and two-grid DGFEMs with the square root of the number of degrees of freedom (of the fine mesh) on a linear-log scale for both h- and hp-adaptive mesh algorithms. Here, we can see that the true error stemming from the two-grid DGFEM based on a single Newton iteration (the second two-grid method) is similar to the corresponding quantity computed for the standard DGFEM, for a given number of degrees of freedom in the two-grid fine mesh as in the standard DGFEM mesh; in contrast the first two-grid method is notably inferior for h-refinement. In Figure 7.2(b) we plot the number of degrees of freedom in the coarse mesh compared to the number in the fine mesh for both two-grid methods; here we observe that there appears to be less coarse mesh degrees of freedom for the first method compared to the second method. The comparison of the true error, measured in the DGFEM norm, of the standard and two-grid DGFEMs with respect to the cumulative computation time, in seconds, on a log-log scale for both h- and hp-adaptive mesh algorithms is shown in Figure 7.3. As can be seen for both strategies the two-grid methods result in the same true error for a lower computation time, when compared to the standard (single-grid) DGFEM, cf. Chapter 4. The second two-grid method based on a single Newton iteration appears to perform slightly better than the first two-grid method in terms of computation time reduction. From Figure 7.4 we see that for both h- and hp-refinement strategies that the *a posteriori* error bound for the two-grid DGFEMs overestimate the true error by a roughly constant amount in the sense that the effectivity indices are roughly constant for all meshes; we point out that the second two-grid method based on a single Newton iteration gives rise to a slightly higher effectivity index for hp-refinement.

In Figure 7.5 we show the coarse and fine meshes for both two-grid DGFEMs after

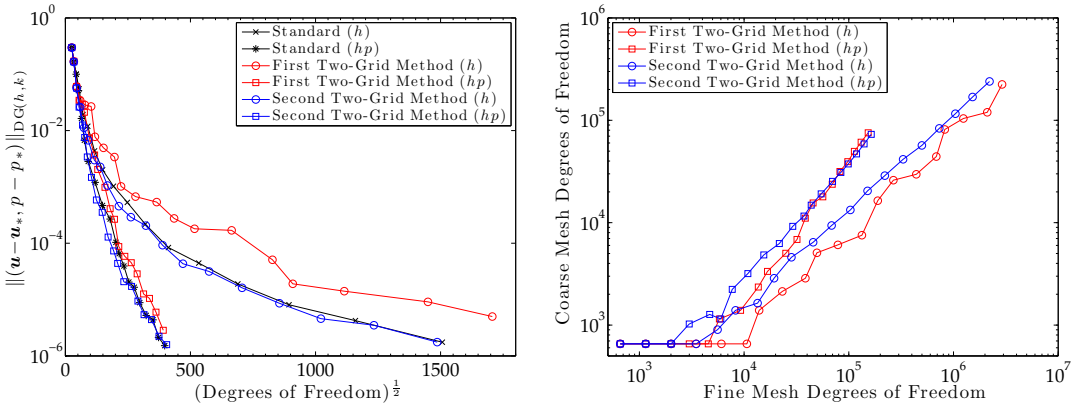

(a) *(b)*

Figure 7.2: Example 1. (a) Comparison of error in the DG norm, using the standard ($\boldsymbol{u}_* = \boldsymbol{u}_{h,k}$, $p_* = p_{h,k}$) and both two-grid methods ($\boldsymbol{u}_* = \boldsymbol{u}_{2G}$,$p_* = p_{2G}$), with respect to the number of degrees of freedom; (b) Comparison of number of degrees of freedom in coarse and fine mesh.

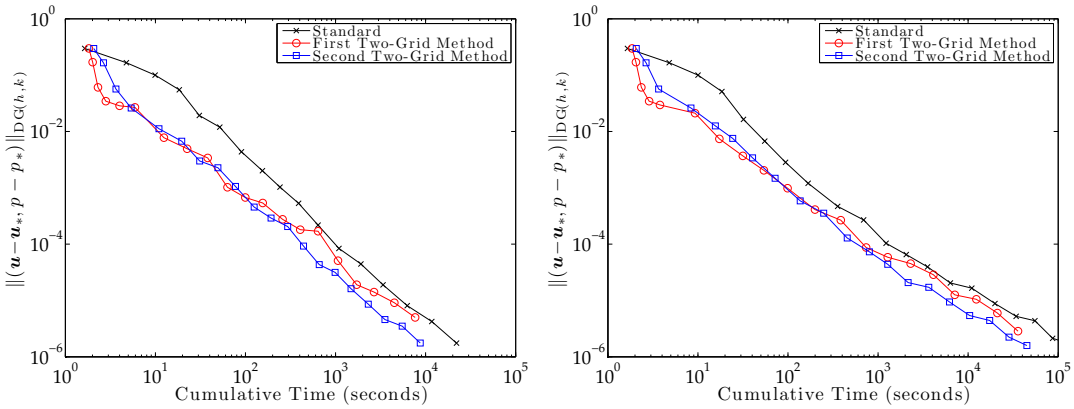

(a) h-refinement *(b)* hp-refinement

Figure 7.3: Example 1. Cumulative CPU timing of the standard ($\boldsymbol{u}_* = \boldsymbol{u}_{h,k}$,$p_* = p_{h,k}$) and both two-grid ($\boldsymbol{u}_* = \boldsymbol{u}_{2G}$,$p_* = p_{2G}$) solvers compared to the error in the DG norm.

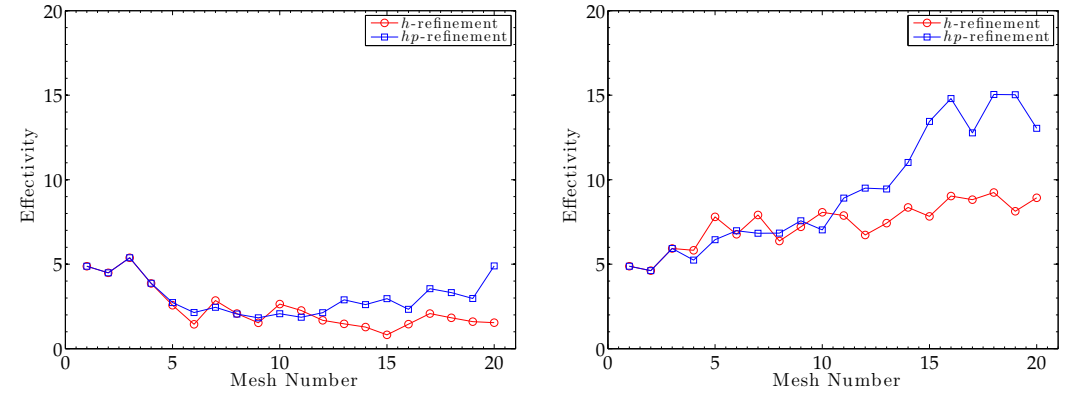

(a) First method (Section 7.1) *(b)* Second method (Section 7.2)

Figure 7.4: Example 1. Effectivity of the h- and hp-refinement using both two-grid methods.

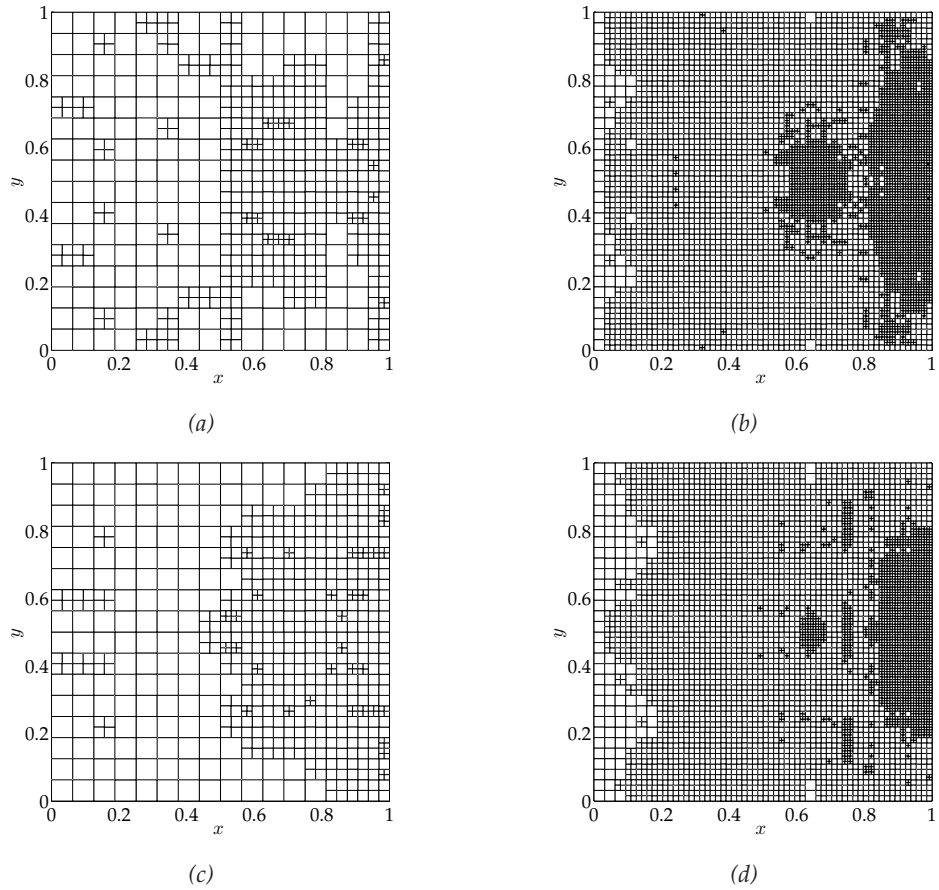

Figure 7.5: Example 1. Coarse and fine mesh after 13 h-adaptive mesh refinements: (a) & (b) Coarse and fine mesh, respectively, for first two-grid method (Section 7.1); (c) & (d) Coarse and fine mesh, respectively, for second two-grid method (Section 7.2)

13 h- mesh refinements. We note that the coarse and fine mesh appear to be refined in roughly the same manner, but with less refinement in the coarse mesh. We can also see that the second two-grid DGFEM based on a single Newton iteration has resulted in slightly more coarse refinement and less fine refinement. Figure 7.6 shows the coarse and fine meshes after 13 hp- mesh refinements. Here, the h-refinements have occured mostly around the interior of the hills and valleys of the analytical pressure with p-refinement in the rest of the domain which is largely smooth, as would be expected from a smooth analytical solution, with the highest p-refinement being around the vortex centre at the point $(1/\vartheta \log((e^{\vartheta}+1)/2), 1/2)$. We note here that the two different two-grid methods have broadly refined in a similar manner, the most noticable difference being on the coarse mesh.

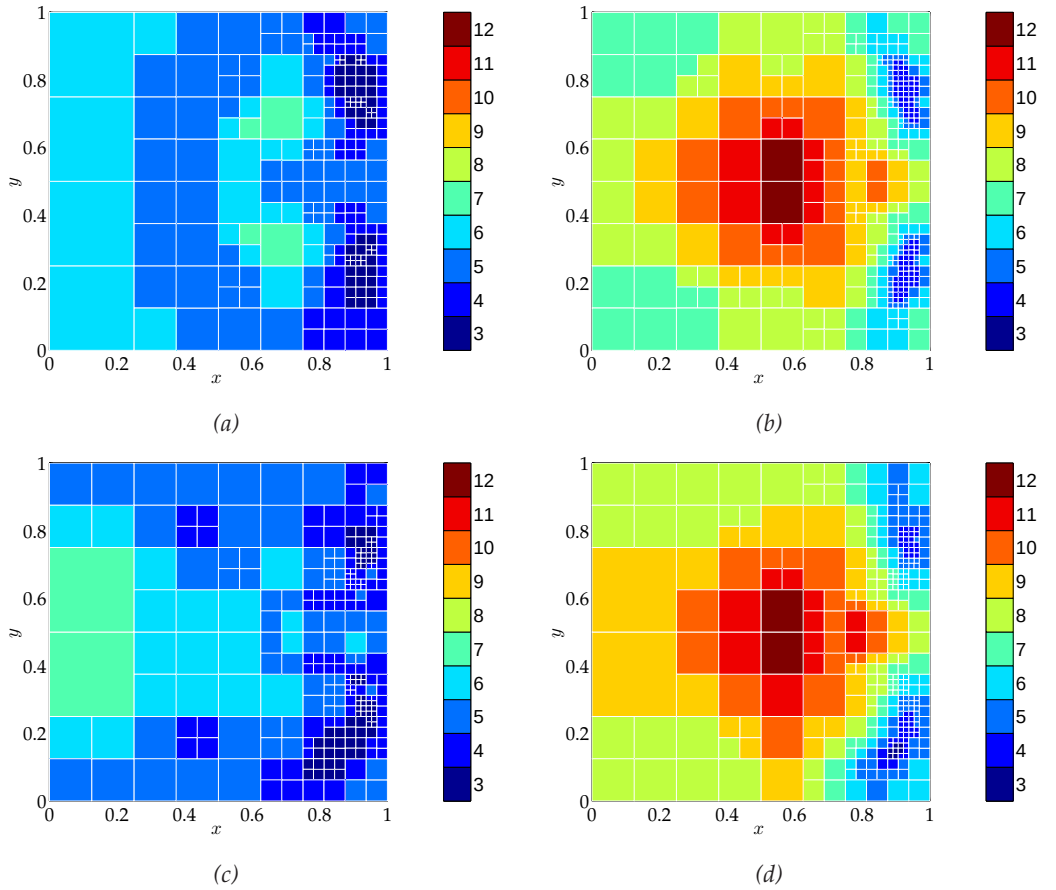

Figure 7.6: Example 1. Coarse and fine mesh after 13 *hp*-adaptive mesh refinements: (a) & (b) Coarse and fine mesh, respectively, for first two-grid method (Section 7.1); (c) & (d) Coarse and fine mesh, respectively, for second two-grid method (Section 7.2)

Example 2: Singular Solution

For this example we consider a nonlinear version of the singular solution from Verfürth [170, p. 113], see also Houston *et al.* [120], using the nonlinearity

$$\mu(|\underline{e}(\boldsymbol{u})|) = 1 + \mathrm{e}^{-|\underline{e}(\boldsymbol{u})|}.$$

We let Ω be the L-shaped domain $(-1,1)^2 \setminus [0,1) \times (-1,0]$ and select $\boldsymbol{f}$ so that the analytical solution to (7.1)–(7.3), where (r,φ) denotes the system of polar coordinates,

is given by

$$\boldsymbol{u}(r,\varphi) = r^{\lambda}\begin{pmatrix} (1+\lambda)\sin(\varphi)\Psi(\varphi) + \cos(\varphi)\Psi'(\varphi) \\ \sin(\varphi)\Psi'(\varphi) - (1+\lambda)\cos(\varphi)\Psi(\varphi) \end{pmatrix},$$
$$p(r,\varphi) = -r^{\lambda_s - 1}\frac{(1+\lambda_s)^2\Psi'(\varphi) + \Psi'''(\varphi)}{1-\lambda},$$

where

$$\Psi(\varphi) = \frac{\sin((1+\lambda)\varphi)\cos(\lambda\omega)}{1+\lambda} - \cos((1+\lambda)\varphi) \\ - \frac{\sin((1-\lambda)\varphi)\cos(\lambda\omega)}{1-\lambda} + \cos((1-\lambda)\varphi),$$

and $\omega = {}^{3\pi}/_{2}$. Here, the exponent λ is the smallest positive solution of

$$\sin(\lambda\omega) + \lambda\sin(\omega) = 0;$$

thereby, $\lambda \approx 0.54448373678246$. We note that $(\boldsymbol{u}, p)$ is analytic in $\bar{\Omega} \setminus \{\mathbf{0}\}$, but both $\nabla\boldsymbol{u}$ and p are singular at the origin; indeed, $\boldsymbol{u} \notin H^2(\Omega)^2$ and $p \notin H^1(\Omega)$.

We again compare in Figure 7.7(a) the true error, measured in the DGFEM norm, of the standard and two-grid DGFEMs with respect to the third root of the degrees of freedom (of the fine mesh) on a linear-log scale for both adaptive mesh algorithms. We notice that the error in the DG norm for the two-grid methods is roughly the same as the error in the DG norm for the standard DGFEM when employing the same number of degrees of freedom in the fine mesh as in the mesh for the standard DGFEM. Figure 7.7(b) compares the number of degrees of freedom in the two meshes for both two-grid methods. Both two-grid methods appear to have similar numbers of degrees of freedom in the coarse and fine meshes as each other. We also note that, although initially the number of degrees of freedom in the coarse meshes for h-refinement are considerably less than in the fine meshes, as refinement continues the number of degrees of freedom in the coarse and fine meshes converge. As before we are interested

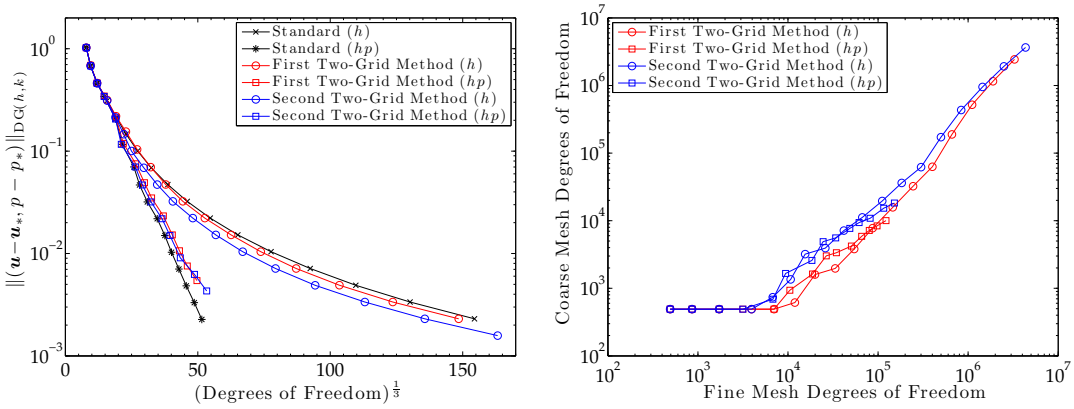

(a) *(b)*

Figure 7.7: Example 2. (a) Comparison of error in the DG norm, using the standard ($\boldsymbol{u}_* = \boldsymbol{u}_{h,k}$, $p_* = p_{h,k}$) and both two-grid methods ($\boldsymbol{u}_* = \boldsymbol{u}_{2G}$,$p_* = p_{2G}$), with respect to the number of degrees of freedom; (b) Comparison of number of degrees of freedom in coarse and fine mesh.

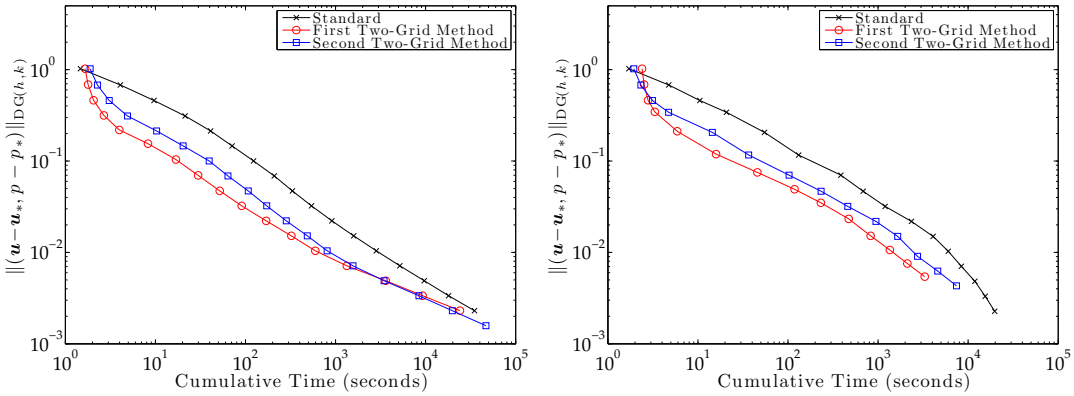

(a) h-refinement *(b)* hp-refinement

Figure 7.8: Example 2. Cumulative CPU timing of the standard ($\boldsymbol{u}_* = \boldsymbol{u}_{h,k}$,$p_* = p_{h,k}$) and both two-grid ($\boldsymbol{u}_* = \boldsymbol{u}_{2G}$,$p_* = p_{2G}$) solvers compared to the error in the DG norm.

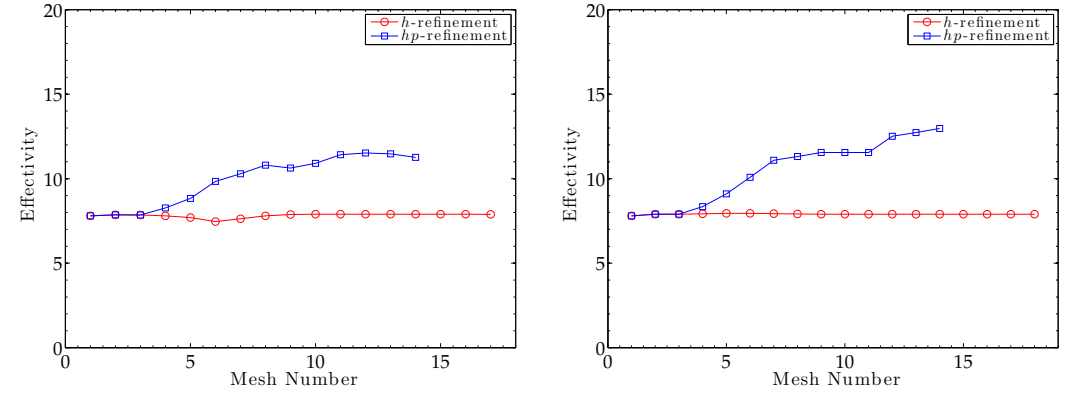

(a) First method (Section 7.1) *(b)* Second method (Section 7.2)

Figure 7.9: Example 2. Effectivity of the h- and hp-refinement using both two-grid methods.

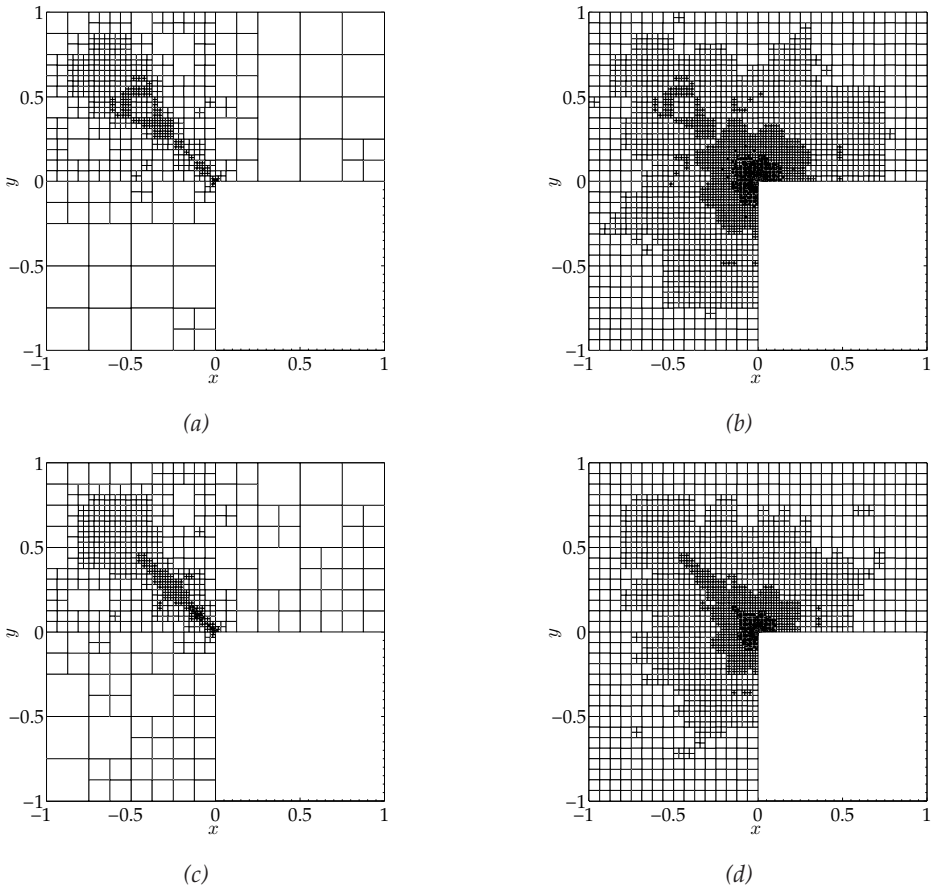

Figure 7.10: Example 2. Coarse and fine mesh after 11 h-adaptive mesh refinements: (a) & (b) Coarse and fine mesh, respectively, for first two-grid method (Section 7.1); (c) & (d) Coarse and fine mesh, respectively, for second two-grid method (Section 7.2)

in the performance improvement that is attained by undertaking the two-grid DGFEM as opposed to the standard DGFEM; therefore, in Figure 7.8 the true error, measured in the DGFEM norm, of the standard and two-grid DGFEMs is compared with the cumulative computation time, in seconds, on a log-log scale for both h- and hp-adaptive mesh algorithms. We note that a computational time improvement is seen for both the h- and hp-adaptive two-grid DGFEMs compared to the standard DGFEM. Unlike in the smooth problem the second two-grid method based on a single Newton iteration appears to perform slightly worse than the first two-grid method in terms of computation time reduction. Figure 7.9 illustrates that, for both the h- and hp-refinement strategy, that the effectivity constants are roughly constant indicating that the *a posteriori* error bound for both two-grid DGFEMs overestimate the true error by a roughly constant

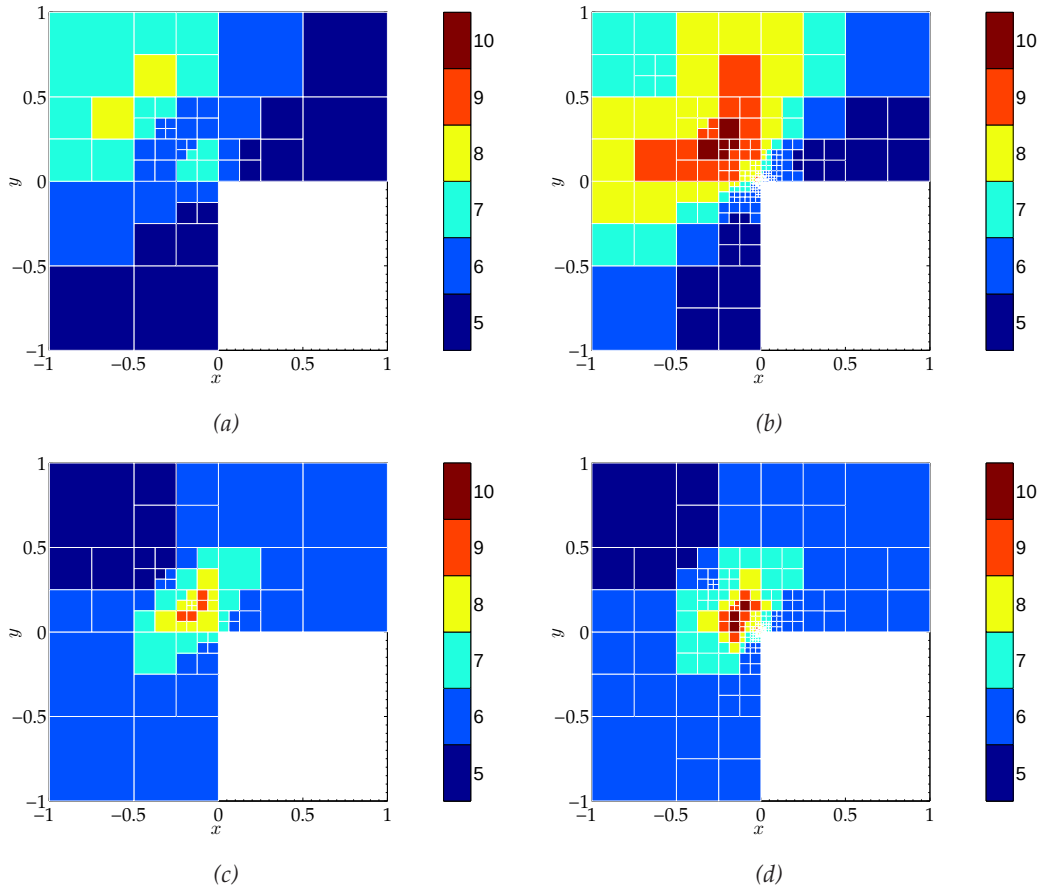

Figure 7.11: Example 2. Coarse and fine mesh after 11 hp-adaptive mesh refinements: (a) & (b) Coarse and fine mesh, respectively, for first two-grid method (Section 7.1); (c) & (d) Coarse and fine mesh, respectively, for second two-grid method (Section 7.2)

factor; indeed for the h-adaptive refinement it is almost exactly 8 for all meshes. For the hp-adaptive refinement the effectivity indices does rise initially before becoming constant at around 12 for the first two-grid method and rising slightly more in the second two-grid method based on a single Newton iteration.

We show the coarse and fine meshes for both two-grid DGFEMs after 11 h- and hp-adaptive mesh refinements in Figure 7.10 and Figure 7.11, respectively. In h-adaptive refinement we note that the focus of the refinement in the fine mesh appears to be around the singularity at the origin; however, in the coarse mesh the refinement appears to be centred around both the singularity and the line $y = -x$ coming from the singularity, where it appears that the coarse mesh needs to be almost as refined as the fine mesh. This behaviour is also demonstrated in the hp-adaptive mesh refinement,

although less noticeable, for the first two-grid method. The two methods have resulted in notably different hp-refinements with the second two-grid method doing very minimal refinement along the line $y = -x$.

7.4 Summary

In this chapter, we have extended the *a priori* and *a posteriori* analysis for the hp-interior penalty discontinuous Galerkin method developed for the quasi-Newtonian fluid flow problem considered in Chapter 6 to its so-called two-grid numerical approximation. We have studied both variants of the two-grid method previous studied for the quasilinear elliptic problem, cf. Chapter 3 and Chapter 5, and compared the results. We note that although the second method based on using a single Newton method results in better *a priori* error bounds, when conducting hp-adaptive mesh refinement based on the algorithms presented in Chapter 4 the two methods give similar results. We note that this is in keeping with the results for the quasilinear elliptic problem presented in Chapter 5. We also note that the computation time saving from utilising the two-grid methods for a quasi-Newtonian fluid flow are not as pronounced as for the quasilinear elliptic problem.

In this chapter and the previous chapters we have focused on *energy norm* based error estimation for strongly monotone elliptic PDEs. In the next chapter we study the use of dual weighted residual based error estimation for problems with more general nonlinearities for both quasilinear elliptic PDEs and non-Newtonian fluid flows.

CHAPTER 8

Dual Weighted Residual Error Estimation for Two-Grid hp-Version Discontinuous Galerkin Finite Element Methods

In the previous chapters we have studied the *a posteriori* error estimation with respect to the underlying energy norm. While this aims to minimise the error across the whole computational domain, it is not efficient for minimising the error with respect to a specific target functional. Therefore, in this chapter we study the use of *dual weighted residual* (DWR) *a posteriori* error estimation for estimating the error in a given target functional when exploiting a two-grid numerical method, cf. Becker & Rannacher [24], Bangerth & Rannacher [15], Harriman *et al.* [108] and Hartmann & Houston [110]. Here, we shall study both a scalar second-order quasilinear PDE and a non-Newtonian fluid flow problem.

8.1 Second-Order Quasilinear PDE

In this section, we start by analysing the hp-version of the two-grid IP DGFEM for the numerical solution of the following quasilinear elliptic boundary-value problem:

$$-\nabla \cdot (\mu(\boldsymbol{x}, u, \nabla u)\nabla u) = f(\boldsymbol{x}) \qquad \text{in } \Omega, \tag{8.1}$$

$$u = g_{\mathcal{D}} \qquad \text{on } \Gamma_{\mathcal{D}}, \tag{8.2}$$

$$(\mu(\boldsymbol{x}, u, \nabla u)\nabla u) \cdot \boldsymbol{n} = g_{\mathcal{N}} \qquad \text{on } \Gamma_{\mathcal{N}}, \tag{8.3}$$

where $\Omega \subset \mathbb{R}^d$, $d = 2, 3$, is a bounded polygonal Lipschitz domain with boundary $\Gamma = \Gamma_{\mathcal{D}} \cup \Gamma_{\mathcal{N}}$ and $f \in L^2(\Omega)$. Here, $\Gamma_{\mathcal{D}}$ and $\Gamma_{\mathcal{N}}$ denote the parts of the boundary $\partial\Omega$ with Dirichlet and Neumann boundary conditions, respectively. For ease of notation we shall suppress the dependence of μ on $\boldsymbol{x}$ and ∇u and write $\mu(u)$ instead of $\mu(\boldsymbol{x}, u, \nabla u)$.

Assumption F. We assume that the nonlinearity $\mu \in C^2(\bar{\Omega} \times (\infty, \infty) \times (\infty, \infty)^d)$.

Remark 8.1. We note that, unlike in the energy norm case, we do not impose the strongly monotone assumption on the nonlinearity μ, cf. Chapter 3 and Chapter 5.

As in Chapter 3 we use the notation from Section 2.1.2 to consider the fine $\mathcal{T}_h$ and coarse $\mathcal{T}_H$ partitions of the computational domain Ω, of granularity h and H, respectively. We again associate the corresponding polynomial degree distributions $\boldsymbol{k} = \{k_\kappa : \kappa \in \mathcal{T}_h\}$ and $\boldsymbol{K} = \{K_\kappa : \kappa \in \mathcal{T}_H\}$ and assume that Assumption B holds. Given $\mathcal{T}_h$, $\boldsymbol{k}$, $\mathcal{T}_H$, $\boldsymbol{K}$ we construct the fine and coarse hp-finite element spaces $V(\mathcal{T}_h, \boldsymbol{k})$ and $V(\mathcal{T}_H, \boldsymbol{K})$, respectively, which satisfy $V(\mathcal{T}_H, \boldsymbol{K}) \subseteq V(\mathcal{T}_h, \boldsymbol{k})$, cf. (3.7). We now state the two-grid IP DGFEM discretisation of (8.1)–(8.3) based on employing a single step of a Newton iteration:

1. Compute the coarse grid approximation $u_{H,K} \in V(\mathcal{T}_H, \boldsymbol{K})$ such that

$$A_{h,k}(u_{H,K}, v_{H,K}) = F_{H,K}(v_{H,K}) \tag{8.4}$$

   for all $v_{H,K} \in V(\mathcal{T}_H, \boldsymbol{K})$.

2. Determine the fine grid solution $u_{2G} \in V(\mathcal{T}_h, \boldsymbol{k})$ such that

$$A'_{h,k}[u_{H,K}](u_{2G}, v_{h,k}) = A'_{h,k}[u_{H,K}](u_{H,K}, v_{h,k}) - A_{h,k}(u_{H,K}, v_{h,k}) + F_{h,k}(v_{h,k}) \tag{8.5}$$

   for all $v_{h,k} \in V(\mathcal{T}_h, \boldsymbol{k})$.

Here,

$$\begin{aligned}
A_{h,k}(u,v) &= \sum_{\kappa\in\mathcal{T}_h}\int_\kappa \mu(u)\nabla u\cdot\nabla v\,\mathrm{d}\boldsymbol{x} - \sum_{F\in\mathcal{F}_h^{\mathcal{I}}\cup\mathcal{F}_h^{\mathcal{D}}}\int_F \{\!\{\mu(u)\nabla_h u\}\!\}\cdot[\![v]\!]\,\mathrm{d}s \\
&\quad + \theta\sum_{F\in\mathcal{F}_h^{\mathcal{I}}\cup\mathcal{F}_h^{\mathcal{D}}}\int_F \{\!\{\mu(u)\nabla_h v\}\!\}\cdot[\![u]\!]\,\mathrm{d}s + \sum_{F\in\mathcal{F}_h^{\mathcal{I}}\cup\mathcal{F}_h^{\mathcal{D}}}\int_F \sigma_{h,k}[\![u]\!]\cdot[\![v]\!]\,\mathrm{d}s, \\
F_{h,k}(v) &= \sum_{\kappa\in\mathcal{T}_h}\int_\kappa fv\,\mathrm{d}\boldsymbol{x} + \sum_{F\in\mathcal{F}_h^{\mathcal{D}}}\int_F \sigma_{h,k}g_{\mathcal{D}}v\,\mathrm{d}s + \sum_{F\in\mathcal{F}_h^{\mathcal{N}}}\int_F g_{\mathcal{N}}v\,\mathrm{d}s \\
&\quad + \theta\sum_{F\in\mathcal{F}_h^{\mathcal{D}}}\int_F \mu(g_{\mathcal{D}})g_{\mathcal{D}}\boldsymbol{n}\cdot\nabla_h v\,\mathrm{d}s,
\end{aligned}$$

and $A'_{h,k}[u](\cdot,v)$ denotes the Fréchet derivative of $u\to A_{h,k}(u,v)$, for fixed v, evaluated at u; thereby, given ϕ we have

$$A'_{h,k}[u](\phi,v) = \lim_{t\to 0}\frac{A_{h,k}(u+t\phi,v)-A_{h,k}(u,v)}{t}.$$

Here, $\mathcal{F}_h^{\mathcal{D}}$ and $\mathcal{F}_h^{\mathcal{N}}$ denote the sets of faces on the boundaries $\Gamma_{\mathcal{D}}$ and $\Gamma_{\mathcal{N}}$, respectively, ∇_h denotes the elementwise gradient operator, $\theta\in[-1,1]$ and the *interior penalty parameter* $\sigma_{h,k}$ is defined as

$$\sigma_{h,k} := \gamma k_F^2 h_F^{-1},$$

where $\gamma>0$ is a constant. We note that $[\![\cdot]\!]$, $\{\!\{\cdot\}\!\}$ and $\mathcal{F}_h^{\mathcal{I}}$ are defined as in Section 2.1. For brevity we employ only a two-grid method based on a single Newton iteration step.

8.1.1 *A Posteriori* Error Estimation

In order to state an *a posteriori* error estimate for a linear target functional $J(\cdot)$ we need to state the following dual problem for the two-grid method: find $z\in V$ such that

$$A'_{h,k}[u_{H,K}](v,z) = J(v) \tag{8.6}$$

for all $v\in V$, where V is some suitably chosen function space such that $V(\mathcal{T}_h,\boldsymbol{k})\subset V$. With this definition of the dual solution z we can state the following estimate.

Theorem 8.1. *Let $u \in H^1(\Omega)$ be the analytical solution of (8.1)–(8.3), $u_{H,K} \in V(\mathcal{T}_H, \boldsymbol{K})$ the numerical approximation obtained from (8.4) and $u_{2G} \in V(\mathcal{T}_h, \boldsymbol{k})$ the numerical approximation computed from (8.5); then, for a given linear functional $J(\cdot)$, we can estimate the error in the two-grid approximation by*

$$J(u) - J(u_{2G}) \approx F_{h,k}(z - z_{h,k}) - A_{h,k}(u_{H,K}, z - z_{h,k}) + A'_{h,k}[u_{H,K}](u_{H,K} - u_{2G}, z - z_{h,k}) - \mathcal{Q}(u_{H,K}, u_{2G}, z)$$

for all $v_{h,k} \in V(\mathcal{T}_h, \boldsymbol{k})$, where

$$\mathcal{Q}(v, w, z) = \int_0^1 (1-t) A''_{h,k}[v + t(w - v)](w - v, w - v, z)\,\mathrm{d}t.$$

Proof. From (8.6) and the linearity of $J(\cdot)$ we have that

$$\begin{aligned} J(u) - J(u_{2G}) = J(u - u_{2G}) &= A'_{h,k}[u_{H,K}](u - u_{2G}, z) \\ &= A'_{h,k}[u_{H,K}](u, z) - A'_{h,k}[u_{H,K}](u_{2G}, z). \end{aligned}$$

Given $z_{h,k} \in V(\mathcal{T}_h, \boldsymbol{k})$, from (8.5), we deduce that

$$\begin{aligned} J(u) - J(u_{2G}) = A'_{h,k}[u_{H,K}](u, z) - A'_{h,k}[u_{H,K}](u_{2G}, z) + A'_{h,k}[u_{H,K}](u_{2G}, z_{h,k}) \\ - A'_{h,k}[u_{H,K}](u_{H,K}, z_{h,k}) + A_{h,k}(u_{H,K}, z_{h,k}) - F_{h,k}(z_{h,k}). \end{aligned}$$

Letting $\xi(t) = u_{H,K} + t(u - u_{H,K})$ and $\eta(t) = A_{h,k}(\xi(t), z)$, we note the identity

$$\eta(1) = \eta(0) + \eta'(0) + \int_0^1 \eta''(t)(1-t)\,\mathrm{d}t;$$

thereby,

$$A_{h,k}(u, z) = A_{h,k}(u_{H,K}, z) + A'_{h,k}[u_{H,K}](u - u_{H,K}, z) + \mathcal{Q}(u_{H,K}, u, z).$$

Hence,

$$\begin{aligned} J(u) - J(u_{2G}) &= -A'_{h,k}[u_{H,K}](u_{2G}, z - z_{h,k}) - A'_{h,k}[u_{H,K}](u_{H,K}, z_{h,k}) \\ &\quad + A_{h,k}(u_{H,K}, z_{h,k}) - F_{h,k}(z_{h,k}) + A_{h,k}(u, z) - A_{h,k}(u_{H,K}, z) \\ &\quad + A'_{h,k}[u_{H,K}](u_{H,K}, z) - \mathcal{Q}(u_{H,K}, u, z), \\ &= F_{h,k}(z - z_{h,k}) - A_{h,k}(u_{H,K}, z - z_{h,k}) - A'_{h,k}[u_{H,K}](u_{2G}, z - z_{h,k}) \\ &\quad + A'_{h,k}[u_{H,K}](u_{H,K}, z - z_{h,k}) + A_{h,k}(u, z) - F_{h,k}(z) - \mathcal{Q}(u_{H,K}, u, z). \end{aligned}$$

By consistency $A_{h,k}(u, z) - F_{h,k}(z) = 0$ and, hence, approximating $\mathcal{Q}(u_{H,K}, u, z)$ with $\mathcal{Q}(u_{H,K}, u_{2G}, z)$ completes the proof. □

8.1.2 Two-Grid hp-Adaptive Mesh Refinement Algorithm

In order to perform two-grid mesh refinement we define

$$\eta_\kappa = F_{h,k}(z - z_{h,k})|_\kappa - A_{h,k}(u_{H,K}, z - z_{h,k})|_\kappa , \tag{8.7}$$

$$\xi_\kappa = A'_{h,k}[u_{H,K}](u_{H,K} - u_{2G}, z - z_{h,k})\big|_\kappa - \mathcal{Q}(u_{H,K}, u_{2G}, z)|_\kappa , \tag{8.8}$$

for all $\kappa \in \mathcal{T}_h$ and employ Algorithm 4.1; however, we need a new algorithm for selecting the elements for refinement/derefinement in the fine and coarse mesh in Step 2 of Algorithm 4.1. We note that unlike in the energy norm case η_κ and ξ_κ can be negative. In principle η_κ represents the coarse grid error and ξ_κ is the *two-grid correction*. With this in mind, we wish to design the coarse and fine meshes so that $\xi_\kappa \approx -\eta_\kappa$ as this minimises the error. As such we wish to develop an algorithm that refines the fine mesh when $|\eta_\kappa| > |\xi_\kappa|$ to perform more correction and the coarse mesh when $|\eta_\kappa| < |\xi_\kappa|$ to reduce the correction. We also note that if η_κ and ξ_κ are the same sign then the fine mesh is not correcting the error, so we refine the coarse mesh to reduce the total error. From this we generate the following algorithm.

Algorithm 8.1. *Elements in the coarse and fine meshes $\mathcal{T}_h$ and $\mathcal{T}_H$, respectively, are selected for refinement/derefinement based on employing the following algorithm.*

1. *Determine the sets* $\mathfrak{R}(\mathcal{T}_h) \subseteq \mathcal{T}_h$ *and* $\mathfrak{D}(\mathcal{T}_h) \subseteq \mathcal{T}_h$ *of fine elements to be (potentially) refined/derefined, respectively, based on the size of* $|\eta_\kappa + \xi_\kappa|$ *using a standard refinement algorithm, e.g., the fixed fraction refinement strategy.*

2. *For all elements selected for derefinement decide whether to perform derefinement of the fine or coarse mesh: for all* $\kappa \in \mathfrak{D}(\mathcal{T}_h)$

   - *if* $\xi_\kappa \eta_\kappa > 0$ *derefine the coarse element,*
   - *else*
     - *if* $\lambda_F |\xi_\kappa| \leq |\eta_\kappa|$ *derefine the fine element* κ*, and*
     - *if* $\lambda_C |\eta_\kappa| \leq |\xi_\kappa|$ *derefine the coarse element* $\kappa_H \in \mathcal{T}_H$*, where* $\kappa \subseteq \kappa_H$*.*

3. *For all elements selected for refinement decide whether to perform refinement of the fine or coarse mesh: for all* $\kappa \in \mathfrak{R}(\mathcal{T}_h)$

   - *if* $\xi_\kappa \eta_\kappa > 0$ *refine the coarse element,*
   - *else*
     - *if* $\lambda_F |\xi_\kappa| \leq |\eta_\kappa|$ *refine the fine element* κ*, and*
     - *if* $\lambda_C |\eta_\kappa| \leq |\xi_\kappa|$ *refine the coarse element* $\kappa_H \in \mathcal{T}_H$*, where* $\kappa \subseteq \kappa_H$*.*

Here, $\lambda_F, \lambda_C \in (0, \infty)$ *are steering parameters selected such that* $\lambda_F \lambda_C \leq 1$*.*

Remark 8.2. As for Algorithm 4.3 it is possible that a coarse element $\kappa_H \in \mathcal{T}_H$ may be marked for both refinement and derefinement. When this occurs the coarse element is refined, as refinement should take precedence over derefinement. We also note that for all elements $\kappa \in \mathfrak{R}(\mathcal{T}_h)$ either the fine element $\kappa \in \mathcal{T}_h$ or the coarse element $\kappa_H \in \mathcal{T}_H$, where $\kappa \subseteq \kappa_H$, will be marked for refinement as a corollary of Proposition 4.1 holds.

8.1.3 Numerical Experiments

In this section, we present a series of numerical experiments in two- and three-dimensions to demonstrate the performance of the *a posteriori* error estimate derived in Theorem 8.1 using Algorithm 8.1 for mesh refinement. We set the interior penalty

parameter constant γ to 10, $\lambda_C = 2/3$ and $\lambda_F = 1/2$. We also compute the numerical solutions with $\theta = 0$, i.e. we employ the IIP scheme. The nonlinear equations are solved by employing a damped Newton method [147, Section 14.4]. The solution of the resulting set of linear equations, emanating from either the fine mesh or at each step of the iterative nonlinear solver, was computed using either the direct Multifrontal Massively Parallel Solver (MUMPS) solver, see Amestoy *et al.* [2, 3, 4], for the two-dimensional problem or an ILU preconditioned GMRES algorithm, see Saad & Schultz [153], for the three-dimensional problem. We also calculate the error estimate stated in Theorem 8.1; here, the dual z is approximated by a DGFEM numerical solution of the dual problem on the fine mesh with augmented polynomial degree $\boldsymbol{k}^+ = \{k_\kappa^+ : \kappa \in \mathcal{T}_h\}$, where $k_\kappa^+ = k_\kappa + 1$ for all $\kappa \in \mathcal{T}_h$. We note that for the marking strategy required by the mesh refinement strategy we employ a fixed fraction strategy, where the refinement and derefinement fractions are set to 25% and 5%, respectively.

In the following problems we know the analytical solution so we can compute both the error estimate $\sum_{\kappa\in\mathcal{T}_h}(\eta_\kappa+\xi_\kappa)$ and the true error $J(u)-J(u_{2G})$. We can then calculate an effectivity index by dividing $\sum_{\kappa\in\mathcal{T}_h}(\eta_\kappa+\xi_\kappa)$ by the true error $J(u)-J(u_{2G})$. As the mesh is refined we expect the effectivity indices to tend to unity.

For comparison we also compute the numerical solution $u_{h,k}$ using a standard DGFEM formulation and compute the true error for the standard method. We are, therefore, able to compare the convergence of the standard and two-grid methods. As for the energy norm numerical experiments we calculate the computation time of both the standard and two-grid methods and compare them to assess the computational performance of the two-grid.

Example 1: 2D p-Laplacian

For the first example we consider the p-Laplacian problem from Ainsworth & Kay [1, Section 5.2] on the unit square $(0,1)^2 \subset \mathbb{R}^2$. To this end we define the nonlinearity μ to be

$$\mu(\nabla u) = |\nabla u|^{p-2}, \tag{8.9}$$

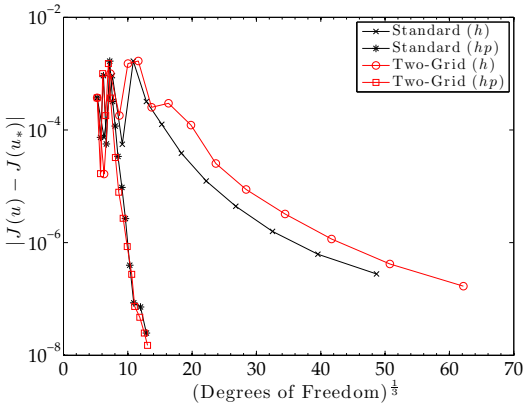

Figure 8.1: Example 1. Comparison of the error in the functional with respect to the number of degrees of freedom in the fine mesh for both the standard ($u_* = u_{h,k}$) and two-grid ($u_* = u_{2G}$) DGFEM.

where $p = 3$, set $\Gamma_{\mathcal{N}} = \emptyset$ and select f and $g_{\mathcal{D}}$ such that the analytical solution in polar coordinates (r, φ) is

$$u(r, \varphi) = r^{3/4}. \tag{8.10}$$

For simplicity we consider the point functional

$$J(u) = u(\widehat{\boldsymbol{x}}), \tag{8.11}$$

evaluated at the point $\widehat{\boldsymbol{x}} = (0.01, 0.01)$.

In Figure 8.1 we plot the absolute value of the error in the functional against the third root of the number of degrees of freedom for h- and hp-refinement for both the standard and two-grid DGFEM. We notice that after some initial oscillatory behaviour the hp-refinement converges exponentially with respect to the number of degrees of freedom, while the h-refinement converges much slower. As a result the hp-refinements use far less degrees of freedom for a lower error. Comparing the standard and two-grid methods we note that for hp-refinement, both methods follow a similar convergence rate; however, for h-refinement the two-grid method requires more fine grid degrees of freedom for the same error compared to the standard method.

Table 8.1 and Table 8.2 show the results of the h- and hp-refinements, respectively, for the two-grid method. These tables show the number of elements and degrees of

Fine Elems.	Fine DoFs	Coarse Elems.	Coarse DoFs	$J(u) - J(u_{2G})$	$\sum_{\kappa\in\mathcal{T}_h} \eta_\kappa$	$\sum_{\kappa\in\mathcal{T}_h} \xi_\kappa$	$\sum_{\kappa\in\mathcal{T}_h} (\eta_\kappa + \xi_\kappa)$	Eff.
16	144	16	144	3.7186×10^{-4}	2.3061×10^{-3}	3.3472×10^{-15}	2.3061×10^{-3}	6.20
28	252	16	144	1.6498×10^{-5}	2.6395×10^{-3}	-4.3715×10^{-4}	2.2023×10^{-3}	133.49
43	387	28	252	-1.0008×10^{-3}	1.3097×10^{-3}	-1.1955×10^{-3}	1.1428×10^{-4}	-0.11
73	657	40	360	-1.8013×10^{-4}	-1.2733×10^{-3}	5.2180×10^{-4}	-7.5146×10^{-4}	4.17
112	1008	67	603	1.5067×10^{-3}	-9.0499×10^{-5}	1.5273×10^{-3}	1.4368×10^{-3}	0.95
175	1575	118	1062	1.6764×10^{-3}	1.2992×10^{-3}	7.7588×10^{-6}	1.3069×10^{-3}	0.78
286	2574	172	1548	2.5243×10^{-4}	1.7173×10^{-3}	-1.5098×10^{-3}	2.0757×10^{-4}	0.82
484	4356	271	2439	2.9777×10^{-4}	2.8812×10^{-4}	-2.4254×10^{-5}	2.6387×10^{-4}	0.89
865	7785	421	3789	1.2210×10^{-4}	1.1779×10^{-4}	-3.9841×10^{-6}	1.1380×10^{-4}	0.93
1477	13293	748	6732	2.5403×10^{-5}	1.1915×10^{-4}	-9.5018×10^{-5}	2.4131×10^{-5}	0.95
2545	22905	1297	11673	8.7764×10^{-6}	3.8966×10^{-5}	-3.0588×10^{-5}	8.3784×10^{-6}	0.95
4543	40887	2275	20475	3.2287×10^{-6}	1.2569×10^{-5}	-9.4641×10^{-6}	3.1054×10^{-6}	0.96
8044	72396	4030	36270	1.1605×10^{-6}	4.0945×10^{-6}	-2.9734×10^{-6}	1.1210×10^{-6}	0.97
14518	130662	7198	64782	4.1766×10^{-7}	1.3864×10^{-6}	-9.8165×10^{-7}	4.0471×10^{-7}	0.97
26698	240282	13333	119997	1.6860×10^{-7}	4.9169×10^{-7}	-3.2739×10^{-7}	1.6430×10^{-7}	0.97

Table 8.1: Example 1. Error and effectivities for h-adaptive mesh refinement.

Fine Elems.	Fine DoFs	Coarse Elems.	Coarse DoFs	$J(u) - J(u_{2G})$	$\sum_{\kappa\in\mathcal{T}_h} \eta_\kappa$	$\sum_{\kappa\in\mathcal{T}_h} \xi_\kappa$	$\sum_{\kappa\in\mathcal{T}_h} (\eta_\kappa + \xi_\kappa)$	Eff.
16	144	16	144	3.7186×10^{-4}	2.3061×10^{-3}	3.3472×10^{-15}	2.3061×10^{-3}	6.20
19	192	16	144	1.6787×10^{-5}	2.6395×10^{-3}	-4.3695×10^{-4}	2.2026×10^{-3}	131.20
22	226	19	171	-1.0004×10^{-3}	1.3106×10^{-3}	-1.1959×10^{-3}	1.1465×10^{-4}	-0.11
25	283	22	198	-1.7969×10^{-4}	-1.2741×10^{-3}	5.2298×10^{-4}	-7.5110×10^{-4}	4.18
28	340	25	232	1.5077×10^{-3}	-9.4310×10^{-5}	1.5316×10^{-3}	1.4373×10^{-3}	0.95
28	391	28	280	3.6853×10^{-4}	1.5441×10^{-3}	-1.3170×10^{-3}	2.2709×10^{-4}	0.62
31	527	31	328	3.2411×10^{-5}	3.2923×10^{-4}	-3.1276×10^{-4}	1.6474×10^{-5}	0.51
34	635	34	403	7.8522×10^{-6}	1.1561×10^{-4}	-1.1263×10^{-4}	2.9791×10^{-6}	0.38
37	800	37	485	2.7016×10^{-6}	3.0341×10^{-5}	-2.9195×10^{-5}	1.1458×10^{-6}	0.42
40	974	40	597	8.5112×10^{-7}	8.3350×10^{-6}	-7.9797×10^{-6}	3.5530×10^{-7}	0.42
43	1193	43	706	2.7356×10^{-7}	1.4942×10^{-6}	-1.3832×10^{-6}	1.1096×10^{-7}	0.41
46	1356	46	867	7.3713×10^{-8}	2.1995×10^{-7}	-2.0740×10^{-7}	1.2551×10^{-8}	0.17
49	1669	49	1155	4.7330×10^{-8}	-1.2828×10^{-7}	1.5457×10^{-7}	2.6288×10^{-8}	0.56
52	1986	52	1313	2.4852×10^{-8}	-1.6751×10^{-7}	1.8248×10^{-7}	1.4973×10^{-8}	0.60
55	2236	55	1643	1.5017×10^{-8}	-1.0608×10^{-7}	1.0936×10^{-7}	3.2814×10^{-9}	0.22

Table 8.2: Example 1. Error and effectivities for hp-adaptive mesh refinement.

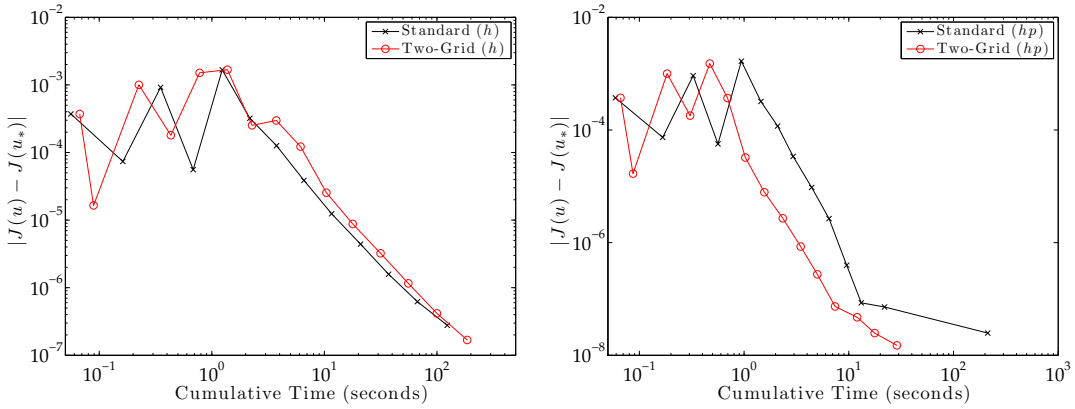

(a) h-Refinement *(b)* hp-Refinement

Figure 8.2: Example 1. Cumulative CPU timing of the standard ($u_* = u_{h,k}$) and two-grid ($u_* = u_{2G}$) solvers compared to the error in the functional: (a) h-refinement; (b) hp-refinement.

freedom (DoFs) in both meshes along with the true error, the error estimate, the sum of the individual parts η_κ and ξ_κ from (8.7) and (8.8), respectively, over the elements in the fine mesh, and the effectivity index. We notice that as the two-grid mesh refinement progresses η_κ and ξ_κ tend towards each other, which is as desired as we would like that $\eta_\kappa \approx -\xi_\kappa$. We notice also for the h-refinement case that the effectivity tends towards 1 as the refinement progresses. For hp-refinement we notice that the effecitivity indices are not converging towards 1; however, it should be noted that the standard method also has effectivities that do not tend towards 1 for hp-refinement.

Figure 8.2 compares the cumulative computation time for the standard and two-grid DGFEM against the absolute error in the functional. We notice that for h-refinement that the two-grid method does not save any time, and is in fact slightly more expensive; whereas, for the hp-refinement the two-grid is generally better.

We show in Figure 8.3 the coarse and fine meshes after 13 h- and hp-adaptive mesh refinements for the two-grid DGFEM. We notice that the h-refinement has focused its refinement around the corner containing the point $\widehat{\boldsymbol{x}}$ with the coarse mesh being slightly less refined than the fine mesh. For the hp-refinement case we notice that both meshes have performed identical h-refinement, which is minimal and focused around the point $\widehat{\boldsymbol{x}}$, and similar p-refinement, with bands of decreasing polynomial degrees as we move away from $\widehat{\boldsymbol{x}}$, where the fine mesh polynomial degrees are roughly two

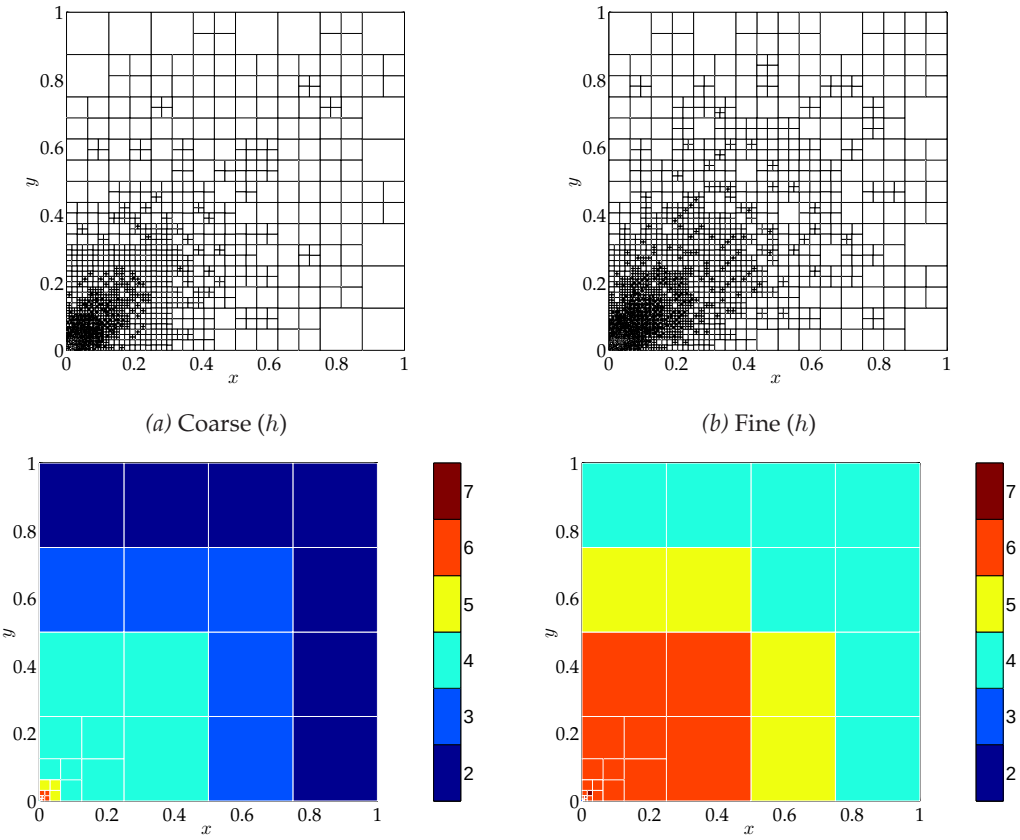

(a) Coarse (h) *(b)* Fine (h)

(c) Coarse (hp) *(d)* Fine (hp)

Figure 8.3: Example 1. Meshes after 13 h/hp-refinements.

degrees higher.

Example 2: 3D p-Laplacian

We now extend the p-Laplacian problem defined in the previous example to the Fichera corner $(-1,1)^3 \setminus [0,1)^3 \subset \mathbb{R}^3$. We set μ as in (8.9) with $p = 3$, $\Gamma_{\mathcal{N}} = \emptyset$ and select f and $g_{\mathcal{D}}$ such that the analytical solution in spherical coordinates (r, ϑ, φ) is given by (8.10). We again consider the point functional (8.11) evaluated at the point $\widehat{\boldsymbol{x}} = (-0.01, -0.01, -0.01)$.

In Figure 8.4 we plot the absolute value of the error in the functional against the fourth root of the number of degrees of freedom for h- and hp-refinement for both the standard and two-grid DGFEM. We notice that the hp-refinement converges exponentially with respect to the number of degrees of freedom while the h-refinements con-

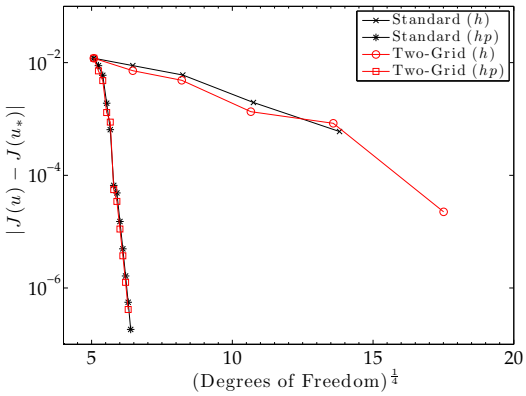

Figure 8.4: Example 2. Comparison of the error in the functional with respect to the number of degrees of freedom in the fine mesh for both the standard ($u_* = u_{h,k}$) and two-grid ($u_* = u_{2G}$) DGFEM.

verges much slower. We notice that both the standard and two-grid methods follow a similar convergence rate with roughly the same error for the same number of degrees of freedom in the fine mesh of the two-grid method as in the standard method.

In Table 8.3 and Table 8.4 we again show the results of the h- and hp-refinements, respectively, for the two-grid method. These tables show the number of elements and degrees of freedom (DoFs) in both meshes along with the true error, the error estimate, the sum of the individual parts η_κ and ξ_κ from (8.7) and (8.8), respectively, over the elements in the fine mesh, and the effectivity index. We again notice that η_κ and ξ_κ tend towards each other as the two-grid mesh refinement progresses. The h-refinement only performs a few steps before the number of degrees of freedom grows to a level that cannot be easily computed and, hence, not enough refinement has occurred for the effectivity indices to start to settle towards 1. By contrast, however, for hp-refinement the effectivities do start to tend towards 1 as refinement progresses.

Figure 8.5 compares the cumulative time for the computations to the absolute error in the functional employing h- and hp-adaptive refinement for both the standard and two-grid methods. Unlike in the previous example we notice that for both refinement strategies the two-grid method results in a lower computation time for the same error compared to the standard method, with hp-refinement giving the best improvement. We point that for a three-dimensional problem it is not unsurprising that the two-grid

Fine Elems.	Fine DoFs	Coarse Elems.	Coarse DoFs	$J(u) - J(u_{2G})$	$\sum_{\kappa \in \mathcal{T}_h} \eta_\kappa$	$\sum_{\kappa \in \mathcal{T}_h} \xi_\kappa$	$\sum_{\kappa \in \mathcal{T}_h} (\eta_\kappa + \xi_\kappa)$	Eff.
448	12096	448	12096	-1.1982×10^{-2}	-5.4828×10^{-3}	6.9599×10^{-17}	-5.4828×10^{-3}	0.46
1232	33264	448	12096	-7.1877×10^{-3}	-9.1976×10^{-3}	5.7897×10^{-3}	-3.4079×10^{-3}	0.47
3178	85806	1148	30996	-4.8588×10^{-3}	-8.4202×10^{-3}	4.6421×10^{-3}	-3.7782×10^{-3}	0.78
8715	235305	3241	87507	-1.3471×10^{-3}	-6.7584×10^{-3}	5.0013×10^{-3}	-1.7571×10^{-3}	1.30
23534	635418	9639	260253	8.3806×10^{-4}	-2.2058×10^{-3}	3.0762×10^{-3}	8.7039×10^{-4}	1.04
63420	1712340	26782	723114	2.2469×10^{-5}	6.0050×10^{-4}	-5.9928×10^{-4}	1.2271×10^{-6}	0.05

Table 8.3: Example 2. Error and effectivities for h-adaptive mesh refinement.

Fine Elems.	Fine DoFs	Coarse Elems.	Coarse DoFs	$J(u) - J(u_{2G})$	$\sum_{\kappa \in \mathcal{T}_h} \eta_\kappa$	$\sum_{\kappa \in \mathcal{T}_h} \xi_\kappa$	$\sum_{\kappa \in \mathcal{T}_h} (\eta_\kappa + \xi_\kappa)$	Eff.
448	12096	448	12096	-1.1982×10^{-2}	-5.4828×10^{-3}	6.9599×10^{-17}	-5.4828×10^{-3}	0.46
497	17452	448	12096	-7.1511×10^{-3}	-9.1974×10^{-3}	5.8222×10^{-3}	-3.3752×10^{-3}	0.47
546	24802	497	15121	-4.8047×10^{-3}	-8.4062×10^{-3}	4.6774×10^{-3}	-3.7288×10^{-3}	0.78
595	35333	546	20578	-1.2991×10^{-3}	-6.7202×10^{-3}	5.0071×10^{-3}	-1.7131×10^{-3}	1.32
644	48418	595	26419	8.7924×10^{-4}	-2.1830×10^{-3}	3.0930×10^{-3}	9.0998×10^{-4}	1.03
693	61773	644	32789	5.5718×10^{-5}	6.1881×10^{-4}	-5.8478×10^{-4}	3.4024×10^{-5}	0.61
742	79605	693	43071	3.4365×10^{-5}	5.6277×10^{-5}	-2.4795×10^{-5}	3.1482×10^{-5}	0.92
791	96791	742	52204	1.1108×10^{-5}	3.3350×10^{-5}	-2.3021×10^{-5}	1.0329×10^{-5}	0.93
840	115106	791	65597	3.7258×10^{-6}	8.8011×10^{-6}	-5.3089×10^{-6}	3.4921×10^{-6}	0.94
889	154172	840	92893	1.2589×10^{-6}	4.2534×10^{-6}	-3.0661×10^{-6}	1.1873×10^{-6}	0.94
938	191148	889	116829	4.1527×10^{-7}	1.6632×10^{-6}	-1.2724×10^{-6}	3.9075×10^{-7}	0.94

Table 8.4: Example 2. Error and effectivities for hp-adaptive mesh refinement.

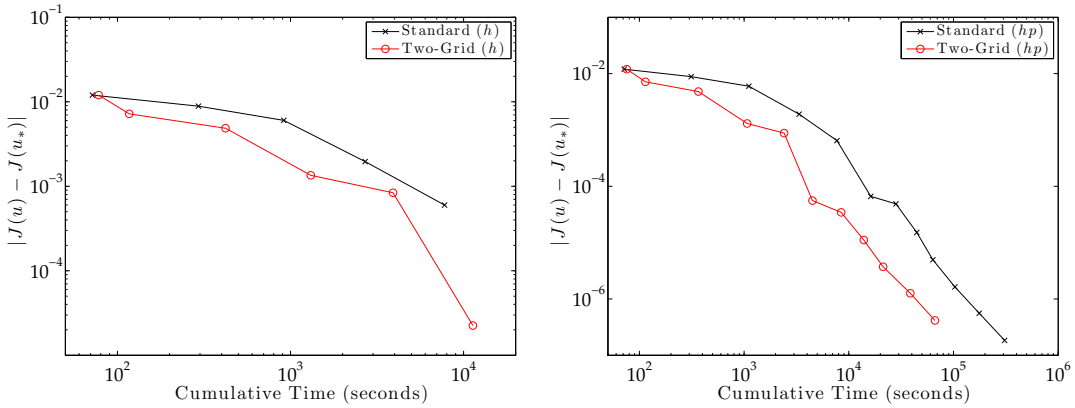

(a) h-Refinement *(b)* hp-Refinement

Figure 8.5: Example 2. Cumulative CPU timing of the standard ($u_* = u_{h,k}$) and two-grid ($u_* = u_{2G}$) solvers compared to the error in the functional: (a) h-refinement; (b) hp-refinement.

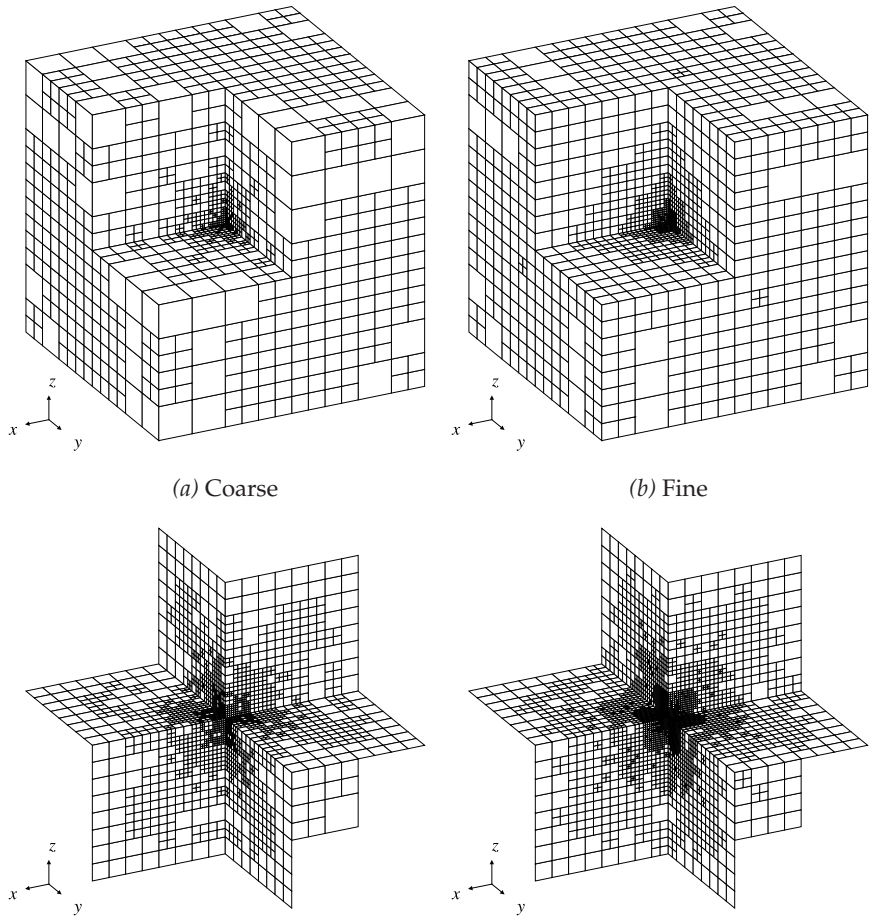

(a) Coarse *(b)* Fine

(c) Coarse 3-slice *(d)* Fine 3-slice

Figure 8.6: Example 2. Meshes after 5 h-refinements.

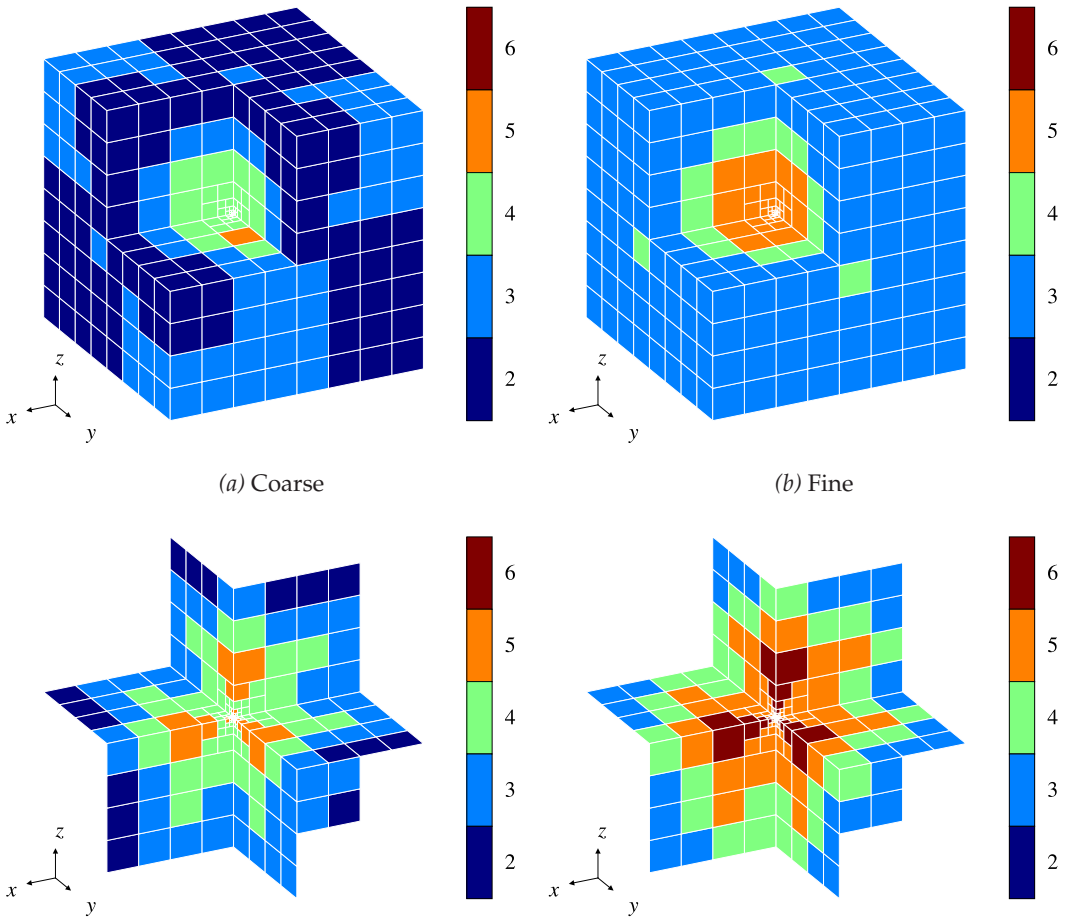

(a) Coarse *(b)* Fine

(c) Coarse 3-slice *(d)* Fine 3-slice

Figure 8.7: Example 2. Meshes after 8 hp-refinements.

method is faster as we use a GMRES iterative solver at each step of the Newton iteration; hence, solving only a coarse nonlinear problem greatly reduces the computation time.

Figure 8.6 shows the coarse and fine mesh after 5 h-adaptive mesh refinements. As can be seen both meshes refine around the point $\widehat{\boldsymbol{x}}$, with the h increasing as we move away from this point, and the coarse mesh is again less refined than the fine mesh. After 8 hp-adaptive mesh refinements, cf. Figure 8.7, the coarse and fine meshes contain the same amount of h-refinement focused around the point $\widehat{\boldsymbol{x}}$, with the element size increasing as we move away from this point. The p-refinement is similarly greatest around this point and reduces as we move away from the point in the fine mesh with

the coarse mesh having lower polynomial degree compared to the fine mesh.

8.2 Non-Newtonian Fluid Flow

We now study the use of dual weighted residual *a posteriori* error estimation for the hp-version of the two-grid IP DGFEM of the quasi-Newtonian fluid flow problem:

$$-\nabla \cdot (\mu\left(\boldsymbol{x}, \boldsymbol{u}, \underline{e}(\boldsymbol{u}), p\right) \underline{e}\left(\boldsymbol{u}\right)) + \nabla p = \boldsymbol{f}(\boldsymbol{x}) \qquad \text{in } \Omega, \tag{8.12}$$

$$\nabla \cdot \boldsymbol{u} = 0 \qquad \text{in } \Omega, \tag{8.13}$$

$$\boldsymbol{u} = \boldsymbol{g}_{\mathcal{D}} \qquad \text{on } \Gamma_{\mathcal{D}}. \tag{8.14}$$

$$\mu\left(\boldsymbol{x}, \boldsymbol{u}, \underline{e}(\boldsymbol{u}), p\right) \underline{e}\left(\boldsymbol{u}\right) \boldsymbol{n} - p\boldsymbol{n} = \boldsymbol{g}_{\mathcal{N}} \qquad \text{on } \Gamma_{\mathcal{N}}. \tag{8.15}$$

Here, $\Omega \subset \mathbb{R}^d$, $d = 2, 3$, is a bounded polygonal Lipschitz domain with boundary $\Gamma = \Gamma_{\mathcal{D}} \cup \Gamma_{\mathcal{N}}$, $\boldsymbol{f} \in \left[L^2(\Omega)\right]^d$ is a given source term, $\boldsymbol{u} = (u_1, \ldots, u_d)^\top$ is the velocity vector, p is the pressure and $\underline{e}(\boldsymbol{u})$ is the symmetric $d \times d$ strain tensor defined by

$$e_{ij}(\boldsymbol{u}) = \frac{1}{2}\left(\frac{\partial u_i}{\partial x_j} + \frac{\partial u_j}{\partial x_i}\right), \qquad i, j = 1 \ldots d.$$

Here, $\Gamma_{\mathcal{D}}$ and $\Gamma_{\mathcal{N}}$ denote the parts of the boundary $\partial\Omega$ with Dirichlet and Neumann boundary conditions, respectively.

Assumption G. We assume that $\mu \in C^2(\bar{\Omega} \times (\infty, \infty)^d \times (\infty, \infty)^{d \times d} \times (\infty, \infty))$.

Given $\mathcal{T}_h$, $\boldsymbol{k}$, $\mathcal{T}_H$, and $\boldsymbol{K}$ we construct the fine and coarse hp-finite element spaces $\boldsymbol{V}(\mathcal{T}_h, \boldsymbol{k}) \times Q(\mathcal{T}_h, \boldsymbol{k})$ and $\boldsymbol{V}(\mathcal{T}_H, \boldsymbol{K}) \times Q(\mathcal{T}_H, \boldsymbol{K})$, respectively, which satisfies $\boldsymbol{V}(\mathcal{T}_H, \boldsymbol{K}) \subseteq \boldsymbol{V}(\mathcal{T}_h, \boldsymbol{k})$ and $Q(\mathcal{T}_H, \boldsymbol{K}) \subseteq Q(\mathcal{T}_h, \boldsymbol{k})$; cf. (6.10)–(6.11).

Remark 8.3. We note that when $\Gamma_{\mathcal{N}} = \emptyset$ the function spaces $Q(\mathcal{T}_h, \boldsymbol{k})$ and $Q(\mathcal{T}_H, \boldsymbol{K})$ require that the integral of the pressure is zero over the domain to guarantee a unique solution; however, this requirement is not needed when $\Gamma_{\mathcal{N}} \neq \emptyset$.

We can now state the two-grid IP DGFEM discretisation of (8.12)–(8.15) based on employing a single Newton iteration:

1. Compute the coarse grid approximation $(\boldsymbol{u}_{H,K}, p_{H,K}) \in \boldsymbol{V}(\mathcal{T}_H, \boldsymbol{K}) \times Q(\mathcal{T}_H, \boldsymbol{K})$

such that

$$A_{H,K}((\boldsymbol{u}_{H,K}, p_{H,K}), \boldsymbol{v}_{H,K}) + B_{H,K}(\boldsymbol{v}_{H,K}, p_{H,K}) = F_{H,K}(\boldsymbol{v}_{H,K}), \tag{8.16}$$

$$-B_{H,K}(\boldsymbol{u}_{H,K}, q_{H,K}) = 0 \tag{8.17}$$

for all $(\boldsymbol{v}_{H,K}, q_{H,K}) \in \boldsymbol{V}(\mathcal{T}_H, \boldsymbol{K}) \times Q(\mathcal{T}_H, \boldsymbol{K})$.

2. Determine the fine grid solution $(\boldsymbol{u}_{2G}, p_{2G}) \in \boldsymbol{V}(\mathcal{T}_h, \boldsymbol{k}) \times Q(\mathcal{T}_h, \boldsymbol{k})$ such that

$$\begin{aligned} &A'_{h,k}[(\boldsymbol{u}_{H,K}, p_{H,K})]((\boldsymbol{u}_{2G}, p_{2G}), \boldsymbol{v}_{h,k}) + B_{h,k}(\boldsymbol{v}_{h,k}, p_{2G}) \\ &\qquad = A'_{h,k}[(\boldsymbol{u}_{H,K}, p_{H,K})]((\boldsymbol{u}_{H,K}, p_{H,K}), \boldsymbol{v}_{h,k}) \\ &\qquad\quad - A_{h,k}((\boldsymbol{u}_{H,K}, p_{H,K}), \boldsymbol{v}_{h,k}) + F_{h,k}(\boldsymbol{v}_{h,k}), \end{aligned} \tag{8.18}$$

$$-B_{h,k}(\boldsymbol{u}_{2G}, q_{h,k}) = 0 \tag{8.19}$$

for all $(\boldsymbol{v}_{h,k}, q_{h,k}) \in \boldsymbol{V}(\mathcal{T}_h, \boldsymbol{k}) \times Q(\mathcal{T}_h, \boldsymbol{k})$.

Here,

$$\begin{aligned} A_{h,k}((\boldsymbol{u}, p), \boldsymbol{v}) &= \int_\Omega \mu(\boldsymbol{u}, p)\underline{e}_h(\boldsymbol{u}) : \underline{e}_h(\boldsymbol{v})\,\mathrm{d}\boldsymbol{x} + \sum_{F \in \mathcal{F}_h^{\mathcal{I}} \cup \mathcal{F}_h^{\mathcal{D}}} \int_F \{\!\{\mu(\boldsymbol{u}, p)\underline{e}_h(\boldsymbol{u})\}\!\} : \underline{[\![\boldsymbol{v}]\!]}\,\mathrm{d}s \\ &\quad + \theta \sum_{F \in \mathcal{F}_h^{\mathcal{I}} \cup \mathcal{F}_h^{\mathcal{D}}} \int_F \{\!\{\mu(\boldsymbol{u}, p)\underline{e}_h(\boldsymbol{v})\}\!\} : \underline{[\![\boldsymbol{u}]\!]}\,\mathrm{d}s \\ &\quad - \theta \sum_{F \in \mathcal{F}_h^{\mathcal{D}}} \int_F (\mu(\boldsymbol{g}_{\mathcal{D}}, p)\boldsymbol{g}_{\mathcal{D}} \otimes \boldsymbol{n}) : \underline{e}_h(\boldsymbol{v})\,\mathrm{d}s + \sum_{F \in \mathcal{F}_h^{\mathcal{I}} \cup \mathcal{F}_h^{\mathcal{D}}} \int_F \sigma_{h,k} \underline{[\![\boldsymbol{u}]\!]} : \underline{[\![\boldsymbol{v}]\!]}\,\mathrm{d}s, \\ B_{h,k}(\boldsymbol{v}, q) &= \int_\Omega q \nabla_h \cdot \boldsymbol{v}\,\mathrm{d}s + \sum_{F \in \mathcal{F}_h^{\mathcal{I}} \cup \mathcal{F}_h^{\mathcal{D}}} \int_F \{\!\{q\}\!\}[\![\boldsymbol{v}]\!]\,\mathrm{d}s, \\ F_{h,k}(\boldsymbol{v}) &= \int_\Omega \boldsymbol{f} \cdot \boldsymbol{v}\,\mathrm{d}\boldsymbol{x} + \sum_{F \in \mathcal{F}_h^{\mathcal{D}}} \int_F \sigma_{h,k}\boldsymbol{g}_{\mathcal{D}} \cdot \boldsymbol{v}\,\mathrm{d}s + \sum_{F \in \mathcal{F}_h^{\mathcal{N}}} \int_F \boldsymbol{g}_{\mathcal{N}} \cdot \boldsymbol{v}\,\mathrm{d}s, \end{aligned}$$

and $A'_{h,k}[(\boldsymbol{u}, p)](\cdot, \boldsymbol{v})$ denotes the Fréchet derivative of $(\boldsymbol{u}, p) \to A_{h,k}((\boldsymbol{u}, p), \boldsymbol{v})$, for fixed $\boldsymbol{v}$, evaluated at $(\boldsymbol{u}, p)$; thereby, given $(\boldsymbol{\phi}, \psi)$ we have

$$A'_{h,k}[(\boldsymbol{u}, p)]((\boldsymbol{\phi}, \psi), \boldsymbol{v}) = \lim_{t \to 0} \frac{A_{h,k}((\boldsymbol{u} + t\boldsymbol{\phi}, p + t\psi), \boldsymbol{v}) - A_{h,k}((\boldsymbol{u}, p), \boldsymbol{v})}{t}.$$

Here, $\underline{e}_h(\cdot)$ and ∇_h denote the elementwise strain tensor and gradient operator, respectively, and $\theta \in [-1, 1]$. The *interior penalty parameter* $\sigma_{h,k}$ is defined as $\sigma_{h,k} := \gamma k_F^2 h_F^{-1}$, where $\gamma \geq 1$ is a constant.

8.2.1 *A Posteriori* Error Estimation

As before in order to state an *a posteriori* error estimate for a linear target functional $J(\cdot)$ we need the following dual problem for the two-grid method: find $(\boldsymbol{z}, s) \in \boldsymbol{V}$ such that

$$A'_{h,k}[(\boldsymbol{u}_{H,K}, p_{H,K})]((\boldsymbol{v}, q), \boldsymbol{z}) + B_{h,k}(\boldsymbol{z}, q) - B_{h,k}(\boldsymbol{v}, s) = J((\boldsymbol{v}, q))$$

for all $(\boldsymbol{v}, q) \in \boldsymbol{V}$, where $\boldsymbol{V}$ is some suitably chosen function space such that $\boldsymbol{V}(\mathcal{T}_h, \boldsymbol{k}) \times Q(\mathcal{T}_h, \boldsymbol{k}) \subset \boldsymbol{V}$. With this definition of the dual solution $(\boldsymbol{z}, s)$ we can state the following estimate.

Theorem 8.2. *Let $(\boldsymbol{u}, p) \in \left[H^1(\Omega)\right]^d \times L^2(\Omega)$ be the analytical solution of (8.12)–(8.15), $(\boldsymbol{u}_{H,K}, p_{H,K}) \in \boldsymbol{V}(\mathcal{T}_H, \boldsymbol{K}) \times Q(\mathcal{T}_H, \boldsymbol{K})$ the numerical approximation obtained from (8.16)–(8.17) and $(\boldsymbol{u}_{2G}, p_{2G}) \in \boldsymbol{V}(\mathcal{T}_h, \boldsymbol{k}) \times Q(\mathcal{T}_h, \boldsymbol{k})$ the numerical approximation computed from (8.18)–(8.19); then, for a given linear functional $J(\cdot)$, we can estimate the error in the two-grid approximation with:*

$$\begin{aligned} J((\boldsymbol{u}, p)) - J((\boldsymbol{u}_{2G}, p_{2G})) \approx\ & F_{h,k}(\boldsymbol{z} - \boldsymbol{z}_{h,k}) - A_{h,k}((\boldsymbol{u}_{H,K}, p_{H,K}), \boldsymbol{z} - \boldsymbol{z}_{h,k}) \\ & + A'_{h,k}[(\boldsymbol{u}_{H,K}, p_{H,K})]((\boldsymbol{u}_{H,K} - \boldsymbol{u}_{2G}, p_{H,K} - p_{2G}), \boldsymbol{z} - \boldsymbol{z}_{h,k}) \\ & - B_{h,k}(\boldsymbol{z} - \boldsymbol{z}_{h,k}, p_{2G}) + B_{h,k}(\boldsymbol{u}_{2G}, s - s_{h,k}) \\ & - \mathcal{Q}((\boldsymbol{u}_{H,K}, p_{H,K}), (\boldsymbol{u}_{2G}, p_{2G}), \boldsymbol{z}) \end{aligned}$$

for all $(\boldsymbol{z}_{h,k}, s_{h,k}) \in \boldsymbol{V}(\mathcal{T}_h, \boldsymbol{k}) \times Q(\mathcal{T}_h, \boldsymbol{k})$, where

$$\mathcal{Q}((\boldsymbol{v}, q), (\boldsymbol{w}, r), \boldsymbol{z}) = \int_0^1 (1 - t) A''_{h,k}[(\boldsymbol{\eta}_{\boldsymbol{u}}(t), \eta_p(t))]((\boldsymbol{w} - \boldsymbol{v}, r - q), (\boldsymbol{w} - \boldsymbol{v}, r - q), \boldsymbol{z})\, \mathrm{d}t,$$

with $\boldsymbol{\eta}_{\boldsymbol{u}}(t) = \boldsymbol{v} + t(\boldsymbol{w} - \boldsymbol{v})$ and $\eta_p(t) = q + t(r - q)$.

Proof. The proof of this theorem follows in an analogous manner to the proof of Theorem 8.1. □

8.2.2 Numerical Experiments

In this section, we present a series of numerical experiments in two-dimensions to demonstrate the performance of the *a posteriori* error estimate derived in Theorem 8.2 using Algorithm 8.1 for mesh refinement. We first define

$$\begin{aligned}
\eta_\kappa &= F_{h,k}(\boldsymbol{z}-\boldsymbol{z}_{h,k})|_\kappa - A_{h,k}((\boldsymbol{u}_{H,K},p_{H,K}),\boldsymbol{z}-\boldsymbol{z}_{h,k})|_\kappa \\
&\quad - B_{h,k}(\boldsymbol{z}-\boldsymbol{z}_{h,k},p_{2G})|_\kappa + B_{h,k}(\boldsymbol{u}_{2G},s-s_{h,k})|_\kappa\,, \\
\xi_\kappa &= A'_{h,k}[(\boldsymbol{u}_{H,K},p_{H,K})]((\boldsymbol{u}_{H,K}-\boldsymbol{u}_{2G},p_{H,K}-p_{2G}),\boldsymbol{z}-\boldsymbol{z}_{h,k})\big|_\kappa \\
&\quad - \mathcal{Q}((\boldsymbol{u}_{H,K},p_{H,K}),(\boldsymbol{u}_{2G},p_{2G}),\boldsymbol{z})|_\kappa\,,
\end{aligned}$$

for all $\kappa \in \mathcal{T}_h$, set the interior penalty parameter constant γ to 10, $\lambda_C = 1$ and $\lambda_F = 1$. We compute the numerical solutions with $\theta = 0$, i.e., we employ the IIP scheme, and calculate the error estimate stated in Theorem 8.2; here, the dual z is approximated by a DGFEM numerical solution of the dual problem on the fine mesh with augmented polynomial degree $\boldsymbol{k}^+ = \{k_\kappa^+ : \kappa \in \mathcal{T}_h\}$, where $k_\kappa^+ = k_\kappa + 1$ for all $\kappa \in \mathcal{T}_h$. We note that for the marking strategy required by the mesh refinement strategy we employ a fixed fraction strategy, where the refinement and derefinement fractions are set to 25% and 5%, respectively.

We consider the channel problem from Berrone & Süli [31, Section 6.2] using both a power law and a Carreau law nonlinearity, where we do not know the analytical solution. We define the domain Ω to be a channel of unit height and five units long with a two unit by two unit cavity in the lower wall; cf. Figure 8.8(a). We set the outflow boundary $\Gamma_{\mathcal{N}}$ to be the right-hand boundary of the channel at $x = 5$ and set $\boldsymbol{g}_{\mathcal{N}} = \boldsymbol{0}$ on this boundary. On the rest of the boundary $\Gamma_{\mathcal{D}}$ we prescribe Dirichlet boundary data as appropriate. We also set the forcing function $\boldsymbol{f} = \boldsymbol{0}$. For the target functional we use

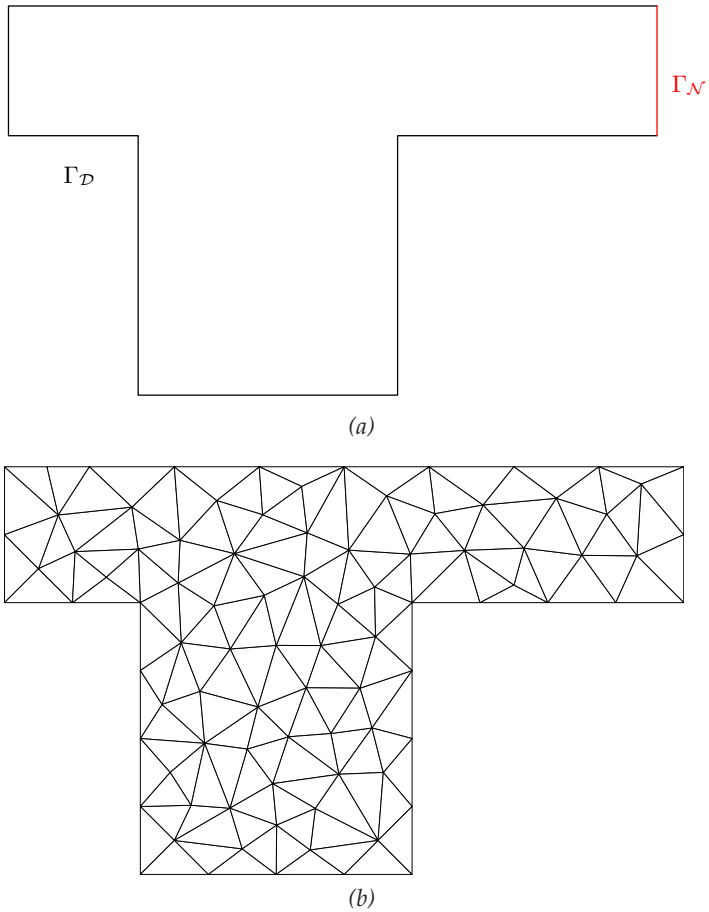

Figure 8.8: Example 4. (a) Geometry of the channel; (b) Initial mesh.

the weighted average of the vorticity

$$J((\boldsymbol{u},p)) = \int_{\Omega} \omega(\boldsymbol{u}) w(x,y)\,\mathrm{d}\boldsymbol{x},$$

where $\omega(\boldsymbol{u}) = \nabla \times \boldsymbol{u} = \partial u_y/\partial x - \partial u_x/\partial y$ is the vorticity of $\boldsymbol{u}$ and $w(x,y)$ is the two-dimensional Gaussian weight function

$$w(x,y) = \frac{10}{\pi} \exp\left(-10\left((x-x_v)^2 + (y-y_v)^2\right)\right)$$

centred at $(x_v, y_v) = (2, 0)$, which is the point at the top centre of the chamber in the south wall of the channel. For these numerics we use triangular elements with the initial mesh depicted in Figure 8.8(b).

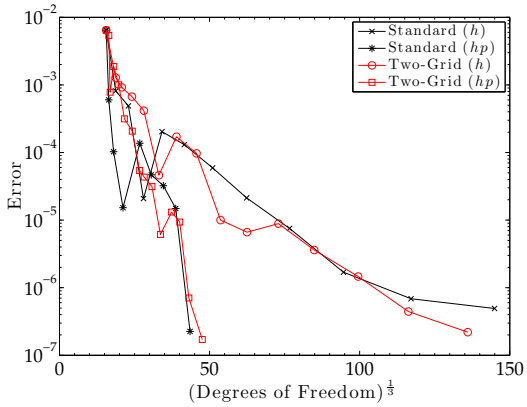

Figure 8.9: Example 3. Comparison of the estimate of the error in the functional with respect to the number of degrees of freedom in the fine mesh for both the standard and two-grid DGFEM.

Example 3: Power Law Nonlinearity

In this example we use the power law nonlinearity

$$\mu(|\underline{e}(\boldsymbol{u})|) = 2\nu|\underline{e}(\boldsymbol{u})|^{r-2},$$

with $r = 3.3$ and $\nu = 1.0 \times 10^{-2}$. We use the known inflow velocity profile for a power law flow in a simple channel at the left-hand inflow boundary $x = 0$ and no slip conditions on the rest of the Dirichlet boundary $\Gamma_{\mathcal{D}}$; i.e.

$$\boldsymbol{g}_{\mathcal{D}}(x,y) = \begin{cases} \left(1 - |1-2y|^{r/(r-1)}, 0\right)^{\top}, & \text{if } x = 0, \\ \boldsymbol{0}, & \text{otherwise.} \end{cases}$$

As we do not know the analytical solution for this problem, or the analytical value of the target function $J(\boldsymbol{u}, p)$, we plot in Figure 8.9 the absolute value of the error estimate from Theorem 8.2 against the third root of the number of degrees of freedom for both the standard and two-grid methods. The hp-adaptive mesh refinement results in the error estimate converging at a roughly exponential rate, which is clearly superior to the corresponding quantity computed with h-adaptive refinement. We also note that the two-grid and standard methods converge at a broadly similar rate, with the error in the two-grid method being lower in some regions but higher in other regions for the

Fine Elems.	Fine DoFs	Coarse Elems.	Coarse DoFs	$\sum_{\kappa\in\mathcal{T}_h}\eta_\kappa$	$\sum_{\kappa\in\mathcal{T}_h}\xi_\kappa$	$\sum_{\kappa\in\mathcal{T}_h}(\eta_\kappa+\xi_\kappa)$	$J((\boldsymbol{u}_{2G},p_{2G}))$
145	3770	145	3770	-6.4470×10^{-3}	1.4722×10^{-8}	-6.4470×10^{-3}	0.1821172316
253	6578	145	3770	-3.5298×10^{-3}	2.2494×10^{-3}	-1.2804×10^{-3}	0.1785641550
343	8918	226	5876	-3.6384×10^{-3}	2.7176×10^{-3}	-9.2087×10^{-4}	0.1784537135
541	14066	334	8684	-2.2379×10^{-3}	1.5678×10^{-3}	-6.7005×10^{-4}	0.1783608396
856	22256	520	13520	1.5397×10^{-5}	-4.3084×10^{-4}	-4.1544×10^{-4}	0.1785993839
1396	36296	829	21554	3.4003×10^{-5}	1.2141×10^{-5}	4.6144×10^{-5}	0.1784626565
2275	59150	1291	33566	1.3283×10^{-4}	3.8316×10^{-5}	1.7114×10^{-4}	0.1784458105
3661	95186	1972	51272	2.1459×10^{-4}	-1.1751×10^{-4}	9.7077×10^{-5}	0.1785123764
5941	154466	3100	80600	9.7702×10^{-5}	-8.7691×10^{-5}	1.0012×10^{-5}	0.1786039743
9379	243854	4975	129350	4.4378×10^{-5}	-3.7744×10^{-5}	6.6337×10^{-6}	0.1786137392
14914	387764	7939	206414	2.4290×10^{-5}	-1.5432×10^{-5}	8.8576×10^{-6}	0.1786137210
23494	610844	12679	329654	7.6685×10^{-6}	-4.0604×10^{-6}	3.6080×10^{-6}	0.1786202805
37885	985010	20125	523250	8.1668×10^{-6}	-6.7052×10^{-6}	1.4617×10^{-6}	0.1786243100
60409	1570634	32539	846014	2.4699×10^{-6}	-2.0261×10^{-6}	4.4377×10^{-7}	0.1786246907
96721	2514746	52108	1354808	2.2575×10^{-6}	-2.0378×10^{-6}	2.1975×10^{-7}	0.1786254421

Table 8.5: Example 3. Convergence of the error estimates for h-adaptive mesh refinement.

Fine Elems.	Fine DoFs	Coarse Elems.	Coarse DoFs	$\sum_{\kappa\in\mathcal{T}_h}\eta_\kappa$	$\sum_{\kappa\in\mathcal{T}_h}\xi_\kappa$	$\sum_{\kappa\in\mathcal{T}_h}(\eta_\kappa+\xi_\kappa)$	$J((\boldsymbol{u}_{2G},p_{2G}))$
145	3770	145	3770	-6.4470×10^{-3}	1.4722×10^{-8}	-6.4470×10^{-3}	0.1821172316
145	4442	145	3770	-3.2137×10^{-3}	8.6048×10^{-3}	5.3911×10^{-3}	0.1758367423
148	4800	148	4324	-1.2728×10^{-3}	4.9444×10^{-4}	-7.7841×10^{-4}	0.1792749963
154	5900	148	4437	-1.0380×10^{-3}	2.9087×10^{-3}	1.8706×10^{-3}	0.1775545261
178	7696	154	5351	-1.1303×10^{-4}	-8.9142×10^{-4}	-1.0045×10^{-3}	0.1788478223
214	10138	196	7996	2.1121×10^{-4}	1.0324×10^{-4}	3.1445×10^{-4}	0.1783283280
274	14281	220	9743	1.8143×10^{-4}	2.5276×10^{-5}	2.0671×10^{-4}	0.1784195258
343	19025	283	13499	1.4029×10^{-4}	-1.9446×10^{-4}	-5.4178×10^{-5}	0.1785574292
376	22462	319	16132	4.6363×10^{-5}	-3.0857×10^{-6}	4.3278×10^{-5}	0.1784782557
451	29276	361	19714	1.5146×10^{-4}	-1.2016×10^{-4}	3.1305×10^{-5}	0.1785338207
562	38037	442	25285	3.6522×10^{-5}	-3.0398×10^{-5}	6.1242×10^{-6}	0.1785927961
700	52075	517	31373	2.9282×10^{-5}	-1.6157×10^{-5}	1.3125×10^{-5}	0.1786085067
814	64377	583	37755	2.6430×10^{-5}	-1.7067×10^{-5}	9.3631×10^{-6}	0.1786180745
979	80128	706	48530	1.6706×10^{-5}	-1.6000×10^{-5}	7.0582×10^{-7}	0.1786232595
1252	107717	871	61812	5.7323×10^{-6}	-5.9037×10^{-6}	-1.7137×10^{-7}	0.1786242475

Table 8.6: Example 3. Convergence of the error estimates for hp-adaptive mesh refinement.

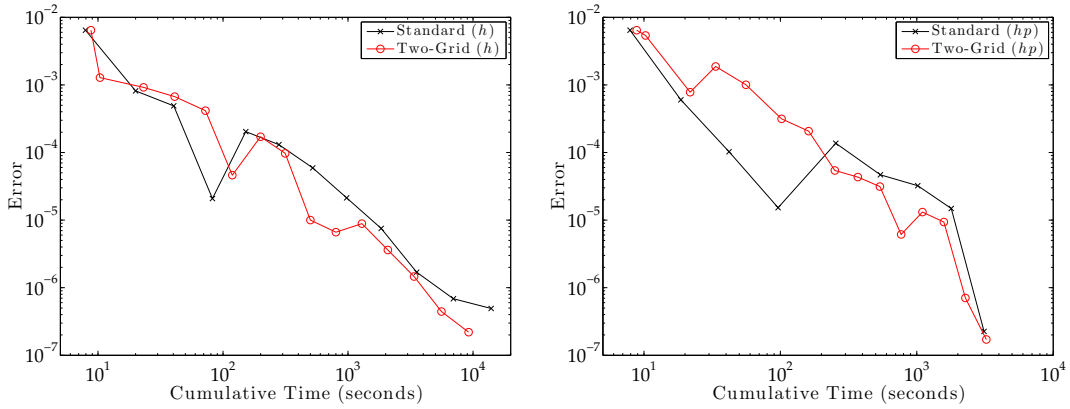

(a) h-Refinement *(b)* hp-Refinement

Figure 8.10: Example 3. Cumulative CPU timing of the standard and two-grid solvers compared to the estimate of the error in the functional: (a) h-refinement; (b) hp-refinement.

same number of degrees of freedom as the standard method.

We show the convergence of the h- and hp-adaptive mesh refinement of the two-grid method in Table 8.5 and Table 8.6, respectively. Here we show the number of coarse and fine elements and degrees of freedom (DoFs) along with the error estimate, the sum of the individual elements η_κ and ξ_κ, and the value of the error functional evaluated with the numerical solution $J((\boldsymbol{u}_{2G}, p_{2G}))$. We can see from these results that the error estimate converges towards zero as the refinement progresses and $J((\boldsymbol{u}_{2G}, p_{2G}))$ appears to converge towards a value (~ -0.17862).

In Figure 8.14(a) and Figure 8.10(b) we plot the absolute value of the error estimate from Theorem 8.2 against the cumulative computation time for both the h- and hp-refinement, respectively, for both the standard and two-grid methods. We note that initially for both h- and hp- refinement that the standard method appears to result in a lower error for the same computation time, more notably for hp-refinement, but as refinement progresses the two-grid method starts to show a marginal computational improvement.

We show in Figure 8.11 the coarse and fine meshes after 10 h-adaptive refinements. We note that the inflow velocity in the x-direction is a steep curve with a ridge along the $y = 0.5$ line, which propagates along the channel. As can be seen the h-refinement is focused along this line around the region of interest denoted by the Gaussian weight

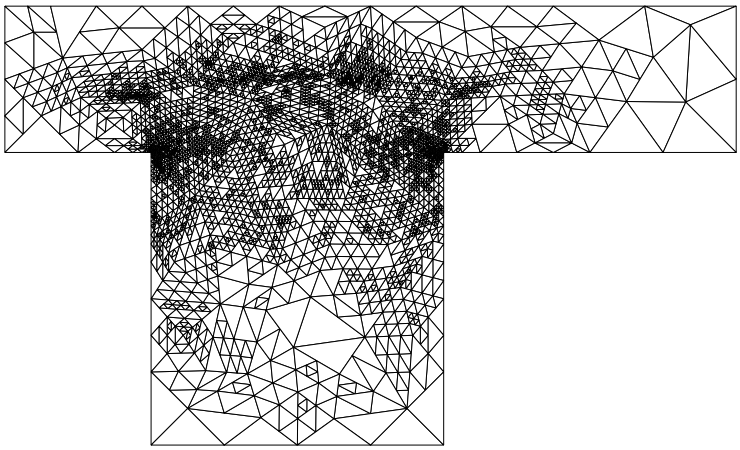

(a) Coarse

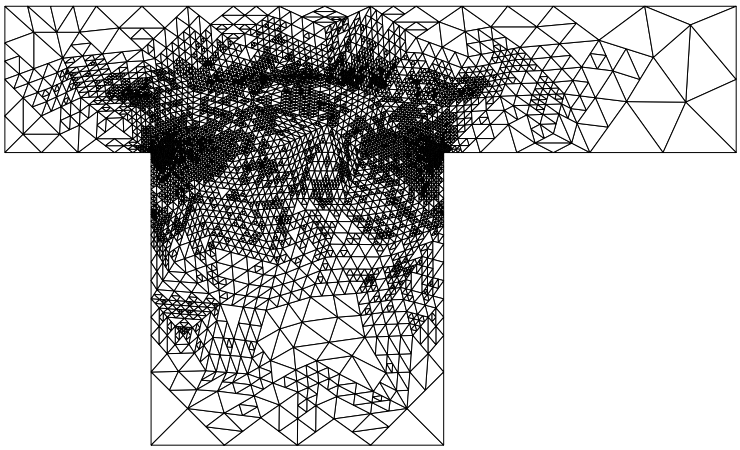

(b) Fine

Figure 8.11: Example 3. Meshes after 10 h-refinements.

function, as well as around the singularities caused by the reentrant corners. We note that the coarse mesh is slightly less refined than the fine mesh. We note that similar refinement occurs in the hp-refinement case, cf. Figure 8.12, with the refinement around the reentrant corners mostly h-refinement and the refinement along the ridge in the x-direction velocity flow is mostly p-refinement, with some h-refinement to assist in resolving the ridge.

Example 4: Carreau Law Nonlinearity

In this example we use the Carreau law nonlinearity

$$\mu(|\underline{e}(\boldsymbol{u})|) = k_\infty + (k_0 - k_\infty)(1 + \lambda|\underline{e}(\boldsymbol{u})|^2)^{(\vartheta-2)/2},$$

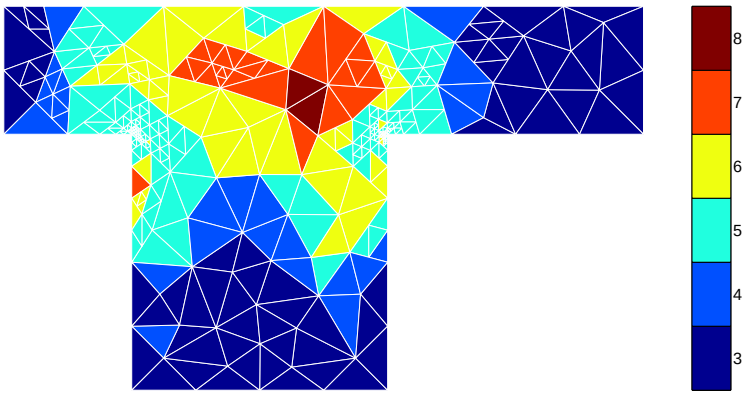

(a) Coarse

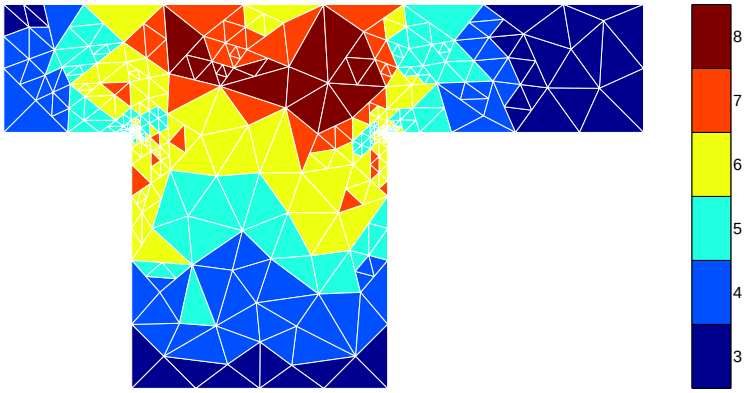

(b) Fine

Figure 8.12: Example 3. Meshes after 10 hp-refinements.

with $k_\infty = 1, k_0 = 2, \lambda = 1.0 \times 10^{-4}$ and $\vartheta = 1.5$. Unlike for the power law we do not know the velocity profile for a simple channel so we simply define a parabolic velocity profile in the x-direction at the left-hand inflow boundary $x = 0$ and no slip conditions on the rest of the Dirichlet boundary $\Gamma_{\mathcal{D}}$; i.e.

$$\boldsymbol{g}_{\mathcal{D}}(x,y) = \begin{cases} (4y(1-y),0)^\top, & \text{if } x = 0, \\ \mathbf{0}, & \text{otherwise.} \end{cases}$$

We again plot in Figure 8.13 the absolute value of the error estimate from Theorem 8.2 against the third root of the number of degrees of freedom for both the standard and two-grid methods, as we do not know the analytical value of the functional $J((\boldsymbol{u}, p))$. We can see that the hp-adaptive mesh refinement results in the error

Fine Elems.	Fine DoFs	Coarse Elems.	Coarse DoFs	$\sum_{\kappa\in\mathcal{T}_h}\eta_\kappa$	$\sum_{\kappa\in\mathcal{T}_h}\xi_\kappa$	$\sum_{\kappa\in\mathcal{T}_h}(\eta_\kappa+\xi_\kappa)$	$J((\boldsymbol{u}_{2G},p_{2G}))$
145	3770	145	3770	1.3607×10^{-3}	-3.4490×10^{-14}	1.3607×10^{-3}	-0.1524241467
253	6578	145	3770	2.8994×10^{-3}	-2.1880×10^{-3}	7.1139×10^{-4}	-0.1504401557
355	9230	220	5720	9.0186×10^{-4}	-1.0688×10^{-4}	7.9498×10^{-4}	-0.1505283786
592	15392	346	8996	9.9983×10^{-4}	-5.6445×10^{-4}	4.3538×10^{-4}	-0.1495991743
1000	26000	541	14066	5.8477×10^{-4}	-2.8699×10^{-4}	2.9778×10^{-4}	-0.1493290656
1723	44798	823	21398	5.9225×10^{-4}	-3.9225×10^{-4}	2.0000×10^{-4}	-0.1490637977
2869	74594	1228	31928	2.8739×10^{-4}	-1.8479×10^{-4}	1.0260×10^{-4}	-0.1488492816
4861	126386	2050	53300	2.1993×10^{-4}	-1.7960×10^{-4}	4.0332×10^{-5}	-0.1486952594
8122	211172	3379	87854	9.1008×10^{-5}	-7.0726×10^{-5}	2.0281×10^{-5}	-0.1486427843
13609	353834	5608	145808	4.7017×10^{-5}	-3.7882×10^{-5}	9.1347×10^{-6}	-0.1486131989
22603	587678	9394	244244	2.1428×10^{-5}	-1.5941×10^{-5}	5.4874×10^{-6}	-0.1486028487
37312	970112	15868	412568	1.2573×10^{-5}	-8.7711×10^{-6}	3.8016×10^{-6}	-0.1485974367

Table 8.7: Example 4. Convergence of the error estimates for h-adaptive mesh refinement.

Fine Elems.	Fine DoFs	Coarse Elems.	Coarse DoFs	$\sum_{\kappa\in\mathcal{T}_h}\eta_\kappa$	$\sum_{\kappa\in\mathcal{T}_h}\xi_\kappa$	$\sum_{\kappa\in\mathcal{T}_h}(\eta_\kappa+\xi_\kappa)$	$J((\boldsymbol{u}_{2G},p_{2G}))$
145	3770	145	3770	1.3607×10^{-3}	-3.4490×10^{-14}	1.3607×10^{-3}	-0.1524241467
223	5966	145	3770	2.8966×10^{-3}	-2.2006×10^{-3}	6.9595×10^{-4}	-0.1504239447
283	7829	202	5294	8.9869×10^{-4}	-8.8837×10^{-5}	8.0985×10^{-4}	-0.1505439839
391	11105	265	6946	1.0133×10^{-3}	-5.6733×10^{-4}	4.4596×10^{-4}	-0.1496120796
499	15461	349	9270	5.9626×10^{-4}	-3.2404×10^{-4}	2.7222×10^{-4}	-0.1492616128
634	20031	454	12098	5.3892×10^{-4}	-3.7332×10^{-4}	1.6560×10^{-4}	-0.1489934445
772	25332	556	15386	2.6511×10^{-4}	-1.7446×10^{-4}	9.0650×10^{-5}	-0.1488201885
949	32079	628	17673	2.1493×10^{-4}	-1.7803×10^{-4}	3.6902×10^{-5}	-0.1486841702
1120	40484	724	20629	1.2652×10^{-4}	-1.0805×10^{-4}	1.8475×10^{-5}	-0.1486372730
1318	48792	838	24996	6.3126×10^{-5}	-5.2350×10^{-5}	1.0776×10^{-5}	-0.1486148195
1570	60061	988	30638	3.3190×10^{-5}	-2.8270×10^{-5}	4.9203×10^{-6}	-0.1486000529

Table 8.8: Example 4. Convergence of the error estimates for hp-adaptive mesh refinement.

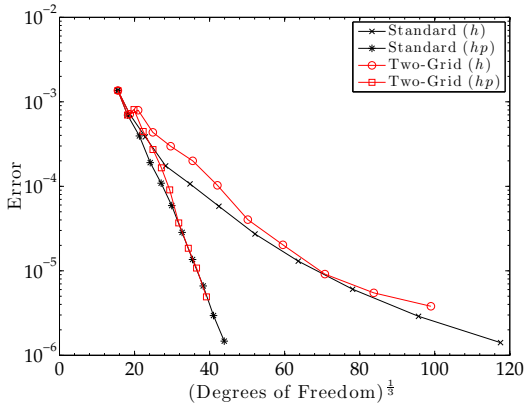

Figure 8.13: Example 4. Comparison of the estimate of the error in the functional with respect to the number of degrees of freedom in the fine mesh for both the standard and two-grid DGFEM.

estimate converging at an exponential rate, which is clearly superior to the corresponding quantity computed with h-adaptive refinement. We also note that the two-grid and standard methods converge at a broadly similar rate; although, the error in the two-grid method is slightly worse for the same number of degrees of freedom in the fine mesh compared to the corresponding quantity for the standard method.

In Table 8.7 and Table 8.8 we show the convergence of the the h- and hp-adaptive mesh refinement, respectively, of the two-grid method. These tables show the number of coarse and fine elements and degrees of freedom (DoFs) along with the error estimate, the sum of the individual elements η_κ and ξ_κ, and the value of the error functional evaluated with the numerical solution $J((\boldsymbol{u}_{2G}, p_{2G}))$. We can see from these results that the error estimate converges towards zero as the refinement progresses and $J((\boldsymbol{u}_{2G}, p_{2G}))$ appears to converge towards a value (~ -0.148597).

In Figure 8.14(a) and Figure 8.14(b) we plot the absolute value of the error estimate from Theorem 8.2 against cumulative computation time for both the h- and hp-refinement, respectively, for both the standard and two-grid methods. We note that for h-refinement there is no notable improvement from the two-grid method; whereas, for the hp-refinement the two-grid method does start to show a computational improvement as the adaptive algorithm progresses

We show in Figure 8.15 the coarse and fine meshes after 7 h-adaptive refinements.

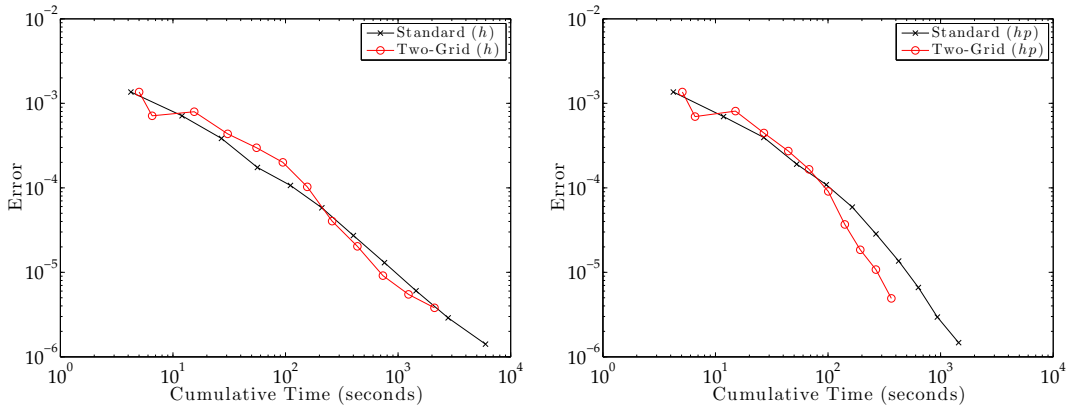

(a) h-Refinement *(b)* hp-Refinement

Figure 8.14: Example 4. Cumulative CPU timing of the standard and two-grid solvers compared to the estimate of the error in the functional: (a) h-refinement; (b) hp-refinement.

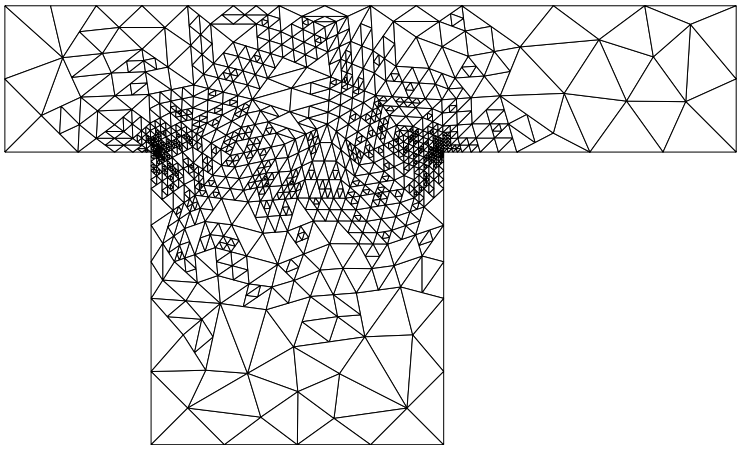

(a) Coarse

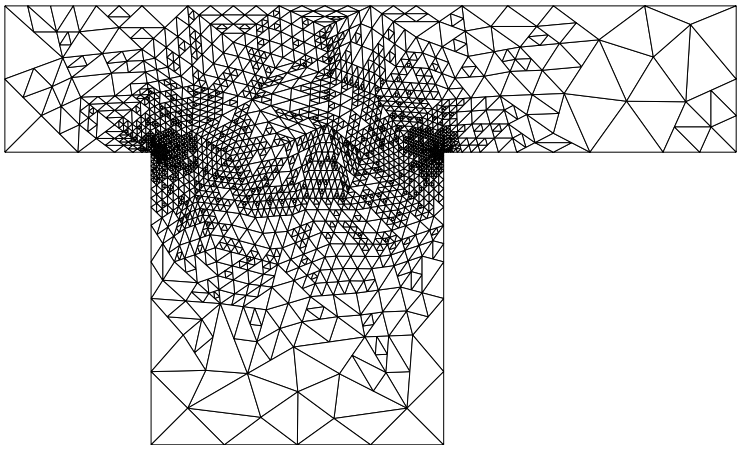

(b) Fine

Figure 8.15: Example 4. Meshes after 7 h-refinements.

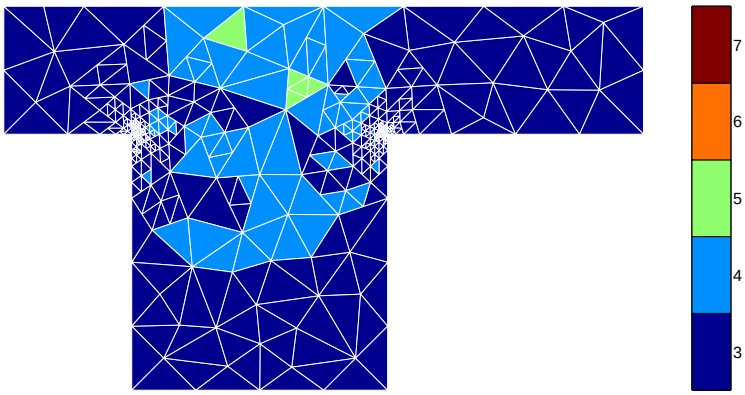

(a) Coarse

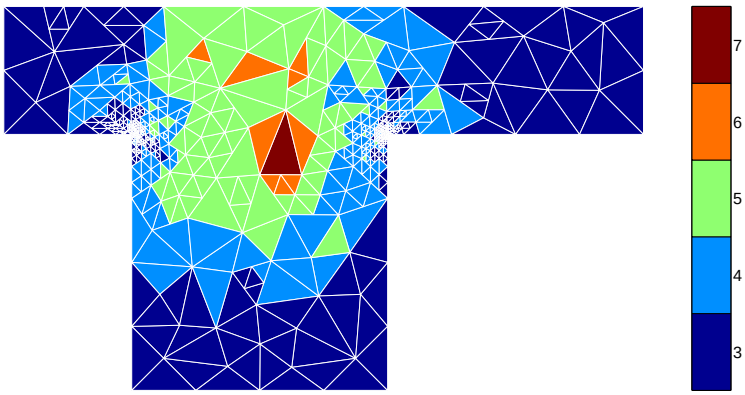

(b) Fine

Figure 8.16: Example 4. Meshes after 7 hp-refinements.

We note that the h-refinement has focused around the singularities in the vicinity of the reentrant corners initially and then generally around the centre of the Gaussian weight function (x_v, y_v) with the coarse mesh less refined than the fine mesh. We note that there is almost no mesh refinement around the corners at the outflow boundary as is seen in the energy norm based mesh refinement for the CGFEM, cf. Berrone & Süli [31]; this is because the target functional is not influenced by the error in that region. We note that similar refinement occurs in the hp-refinement case, cf. Figure 8.16, with the refinement around the reentrant corners mostly h-refinement and the refinement around the centre of the Gaussian weight function mostly p-refinement.

8.3 Summary

In this chapter, we have studied the *a posteriori* error analysis for the hp-interior penalty discontinuous Galerkin method for both a second-order quasilinear PDE and a quasi-Newtonian fluid flow problem based on the dual weighted residual framework and utilised this for goal-oriented mesh refinement. We have performed numerical experiments to validate the bound and the two-grid mesh refinement algorithm. For simple problems, we observe that the two-grid method does not yield a significant reduction in computation time, compared to the standard DGFEM, to achieve a specific error in a target functional. The improved efficiency of the two-grid method is clearly observed for three-dimensional problems when an iterative solver must be exploited to solve the linear matrix systems resulting from the nonlinear iterative solver.

CHAPTER 9

Conclusions and Further Work

9.1 Summary

In this thesis we have studied the *a priori* and *a posteriori* error analysis of the so-called two-grid variant of the discontinuous Galerkin finite element method for the numerical approximation of second-order quasilinear partial differential equations. We have studied both the energy norm and dual weighted residual based *a posteriori* error analysis, and developed automatic hp-adaptive mesh refinement strategies to utilise this analysis for the refinement of both the coarse and fine grid.

We started with analysing a simple second-order quasilinear elliptic partial differential equation in Chapter 3, where the nonlinearity was strongly monotone. For the two-grid method we solved the nonlinear problem on the coarse mesh and then passed this solution onto the fine mesh for the purposes of linearising the fine mesh problem. We deduced an *a priori* error bound that indicated that when refining the coarse mesh, for a fixed fine mesh and polynomial degree, the error between the standard DGFEM solution and the two-grid solution would converge to zero as $\mathcal{O}(H^K)$, and that an optimal converge rate for the full numerical error could be achieved when the fine mesh and coarse mesh are refined at the same rate ($h = \mathcal{O}(H)$), giving a convergence rate of $\mathcal{O}(h^k)$. We also developed an energy norm *a posteriori* error bound; this bound is similar to the corresponding estimate derived for the standard DGFEM, but contains an extra error term arising from the two-grid approximation.

In Chapter 4 we developed two different automatic hp-mesh refinement algorithms

for refining both the coarse and fine mesh of the two-grid method based on the elemental local error indicators of the *a posteriori* error bound. Numerical experiments in two- and three-dimensions were presented in order to demonstrate the practical performance of the two-grid mesh algorithms. Indeed, we noted that the two refinement strategies both produced fairly similar results for the problems considered. We also compared the computation time of the two-grid method with that of a standard DGFEM; in general the former approach leads to a lower computation time required to achieve a given accuracy.

In Chapter 5 we studied an alternative two-grid method based on employing a single Newton iteration step. More precisely, this scheme is constructed by first solving the nonlinear problem on the coarse grid as before, but on the fine grid we performed a single iteration of an *undamped* Newton solver for the underlying nonlinear problem based on using the coarse solution as the initial guess. We note for the *a priori* error bound that we got a higher order of convergence in the error between the standard and two-grid solutions, for a fixed fine mesh and polynomial degree, as we refined the coarse mesh of $\mathcal{O}(H^{2K})$; this results in allowing the coarse mesh to refine at a slower rate than the fine mesh, compared to the previous version of the two-grid method, to achieve the optimal $\mathcal{O}(h^k)$ convergence of the error in the numerical solution. However, when applying the two-grid mesh adaptation algorithm to the two-grid method based on a single Newton iteration the computational time required to attain the same level of accuracy as for the method proposed in Chapter 3 was very similar.

The next part of this thesis was devoted to the extension of these ideas to the discretisation of non-Newtonian fluid flows. To this end, in Chapter 6 we first considered the standard DGFEM for an incompressible quasi-Newtonian fluid flow problem, where the nonlinearity was strongly monotone. Here, we proved that the method was well-posed and derived both *a priori* and *a posteriori* error bounds and performed numerical experiments to validate these estimates. We then extended this analysis, in Chapter 7, to the two-grid variant of the DGFEM. Here, we studied both the original two-grid method based on using the coarse solution as the argument in the nonlinear

coefficient on the coarse mesh and the method based on using the coarse solution as the initial guess for a single iteration of an undamped Newton solver. We found that we get similar convergence rates for the two methods as for the second-order quasilinear elliptic problem, with the error between the standard and two-grid numerical solutions converging to zero as $\mathcal{O}(H^K)$ for the first method and $\mathcal{O}(H^{2K})$ for the method based on a single Newton iteration, for a fixed polynomial degree and fine mesh, as the coarse mesh is refined. For the first method, when the fine and coarse meshes were refined such that $h = \mathcal{O}(H)$ then an optimal convergence rate of $\mathcal{O}(h^k)$ for the error of the two-grid numerical solution was obtained; however, for the second method optimal convergence could be achieved when the coarse mesh is refined at a slower rate compared to the fine mesh. We derived similar *a posteriori* error bounds for both methods, with the method based on employing a single Newton iteration containing additional terms. We then performed numerical experiments using the second two-grid hp-mesh adaptation routine from Chapter 4 for both two-grid methods.

Finally, in Chapter 8 we studied the use of dual weighted residual *a posteriori* error estimation to control the error in a target functional for both the simple second-order quasilinear elliptic PDE and the quasi-Newtonian fluid flow problem. Here, more general nonlinearities were considered, which violates the strongly monotone condition previously required. We developed a modified two-grid mesh refinement algorithm, which allows for the fact that the error indicators in the dual weighted residual *a posteriori* error estimate can be negative, unlike in the energy norm case. We performed numerical experiments to validate the error estimates. For the simple problems that we considered we did not observe a significant saving in the computational time required to compute a target functional to a specific tolerance compared to the standard DGFEM. We do note, however, that in the three-dimensional problem studied a clear computational time improvement was observed; here, an iterative solver has to be employed to solve the resulting linear matrix systems and, hence, it appears that the two-grid method is more efficient when direct methods can not be employed.

We note that in this thesis we have focused mainly on the computational time sav-

ing from employing a two-grid method. There are potentially other benefits that can be made. Solving a nonlinear problem is not only computationally more expensive than a linear problem, it is more complex. Indeed, for more challenging problems than those considered in this thesis, it is not guaranteed that a nonlinear solver will find a solution as the complexity, i.e., the number of degrees of freedom, increases. Hence, solving the nonlinear problem only on a coarser mesh, where the solver can find a solution and then only solving a linear problem on the desired finer mesh could yield a more robust solver. The two-grid method also naturally has two meshes, which lends itself to the use of Schwarz domain decomposition preconditioners, cf. Antonietti & Ayuso [5], for solving the fine grid linear problem.

9.2 Further Work

Two-grid methods for discontinuous Galerkin methods are still early in development, especially the use of *a posteriori* error estimation for automatic mesh adaptation. As a result there is a large field of potential further work that could be performed, some of which we outline below.

9.2.1 Extension to Generic Nonlinearities

In this thesis we have mostly focused on strongly monotone nonlinearities, which are by definition usually a slightly weak nonlinearity. Exploiting ideas from Bi & Ginting [37], for example, the extension of the analysis presented in this thesis to nonmonotone quasilinear elliptic partial differential equations may be developed. The next natural step would be to then extend the analysis for the nonmonotone nonlinearity to the two-grid discretisation of the system of equations present in non-Newtonian fluid flows.

9.2.2 More Complex Problems and Time-Dependence

In this thesis we have only considered fairly simple partial differential equations. The two-grid method can be extended to more complex PDEs including systems of coupled equations and multiphase fluid flows. One obvious extension that we have not considered is the treatment of time-dependent equations; cf. Eriksson & John-

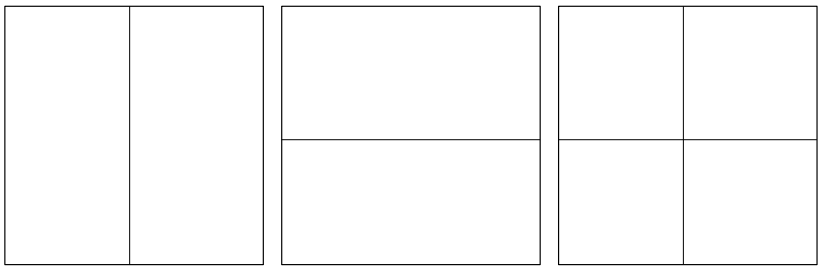

Figure 9.1: Rectangular element h-refinement: (a) Anisotropic x refinement; (b) Anisotropic y refinement; (c) Isotropic refinement.

son [76, 77, 78, 79, 80], Eriksson *et al.* [81], Georgoulis & Lakkis [89], Georgoulis *et al.* [95], Johnson [128], Lakkis & Makridakis [133], Makridakis & Nochetto [137], Schötzau [155], and the references cited therein.

9.2.3 Anisotropic Mesh Refinement

In this thesis we have focused on isotropic mesh refinement, where refining hypercube elements uniformly subdivides elements in every coordinate direction for h-refinement and increases the polynomial degree in each coordinate direction of tensor-product polynomials by one for p-refinement. It is also possible to anisotropically refine elements. For h-refinement this means subdividing the element in only one direction and for p-refinement only incrementing the polynomial degree of a tensor-product polynomial in one direction; cf. Figure 9.1. We refer to the articles by Georgoulis [87, 88], Georgoulis *et al.* [91, 92, 93], Giani & Houston [96], Giani *et al.* [97] and Hall [106], and the references cited therein, for recent work on developing anisotropic mesh refinement for discontinuous Galerkin finite element methods. A key factor in anisotropic mesh refinement is the decision on which coordinate direction to refine an element marked for refinement. Extension of this work to the two-grid DGFEMs presented in this thesis would be of interest.

9.2.4 General Elements

We have focused in this thesis on triangular, quadrilateral and hexahedral elements only. In three-dimensional space we have not considered prism, tetrahedral or pyra-

mid elements as the norm equivalence results, cf. Lemma 3.5, have only been proven in three-dimensions on hexahedral elements; cf. Zhu [181] and Zhu *et al.* [183]. Recently work has been performed on developing the DGFEM based on the use of general polygonal and polyhedral elements, cf. Antonietti *et al.* [6], Bassi *et al.* [19, 20] and Cangiani *et al.* [52]. Antonietti *et al.* [6] discusses the use of the composite discontinuous Galerkin finite element method, which is based on extending the ideas of the composite FEM method, cf. Frauböse & Sauter [86], Hackbusch & Sauter [103, 104, 105] and Sauter & Warnke [154], to the DG framework. Often the meshes used are referred to as agglomerated meshes, as each general polygonal/polyhedral element is an agglomeration of standard elements; in fact the composite finite element method works on large agglomerated elements using information about the small subelements. We note that for the two-grid DGFEM considered in this thesis we could consider an extension to a fine mesh of simple elements (triangles and tetrahedrons) and a coarse mesh based on an agglomeration of fine mesh elements. The construction of this coarse mesh could be generated automatically via the use of mesh partitioning techniques, cf. Karypis & Kumar [132] and the references cited therein. As a result the coarse mesh would consist of general polygonal/polyhedral elements and the fine mesh of standard elements.

Bibliography

[1] M. Ainsworth and D. Kay. The approximation theory for the p-version finite element method and application to non-linear elliptic PDEs. *Numer. Math.*, 82(3): 351–388, 1999.

[2] P. R. Amestoy, I. S. Duff, and J.-Y. L'Excellent. Multifrontal parallel distributed symmetric and unsymmetric solvers. *Comput. Methods Appl. Mech. Engrg.*, 184 (2–4):501–520, 2000.

[3] P. R. Amestoy, I. S. Duff, J. Koster, and J.-Y. L'Excellent. A fully asynchronous multifrontal solver using distributed dynamic scheduling. *SIAM J. Matrix Anal. Appl.*, 23(1):15–41, 2001.

[4] P. R. Amestoy, A. Guermouche, J.-Y. L'Excellent, and S. Pralet. Hybrid scheduling for the parallel solution of linear systems. *Parallel Comput.*, 32(2):136–156, 2006.

[5] P. F. Antonietti and B. Ayuso. Schwarz domain decomposition preconditioners for discontinuous Galerkin approximations of elliptic problems: non-overlapping case. *Math. Model. Numer. Anal.*, 41(1):21–54, 2007.

[6] P. F. Antonietti, S. Giani, and P. Houston. hp-version composite discontinuous Galerkin methods for elliptic problems on complicated domains. *SIAM J. Sci. Comput.*, 35(3):A1417–A1439, 2013.

[7] D. N. Arnold. An interior penalty finite element method with discontinuous elements. *SIAM J. Numer. Anal.*, 19(4):742–760, 1982.

[8] D. N. Arnold, F. Brezzi, B. Cockburn, and L. D. Marini. Discontinuous Galerkin methods for elliptic problems. In B. Cockburn, G. E. Karniadakis, and C.-W.

Shu, editors, *Discontinuous Galerkin Methods: Theory, Computation and Applications*, volume 11 of *Lecture Notes in Computational Science and Engineering*, pages 89–101. Springer, 2000.

[9] D. N. Arnold, F. Brezzi, B. Cockburn, and L. D. Marini. Unified analysis of discontinuous Galerkin methods for elliptic problems. *SIAM J. Numer. Anal.*, 39(5): 1749–1779, 2002.

[10] O. Axelsson and W. Layton. A two-level method for the discretization of nonlinear boundary value problems. *SIAM J. Numer. Anal.*, 33(6):2359–2374, 1996.

[11] I. Babuška and T. Strouboulis. *The Finite Element Method and its Reliablity*. Numerical Mathematics and Scientific Computation. Oxford University Press, Oxford, 2001.

[12] I. Babuška and M. Suri. The $h - p$ version of the finite element method with quasiuniform meshes. *RAIRO Modél. Math. Anal. Numér.*, 21(2):199–238, 1987.

[13] I. Babuška and M. Zlámal. Nonconforming elements in the finite element method with penalty. *SIAM J. Numer. Anal.*, 10(5):863–875, 1973.

[14] G. A. Baker. Finite element methods for elliptic equations using nonconforming elements. *Math. Comp.*, 31(137):45–59, 1977.

[15] W. Bangerth and R. Rannacher. *Adaptive Finite Element Methods for Differential Equations*. Lectures in Mathematics, ETH Zurich. Birkhäuser, 2003.

[16] J. W. Barrett and W. B. Liu. Quasi-norm error bounds for the finite element approximation of a non-Newtonian flow. *Numer. Math.*, 68(4):437–456, 1994.

[17] F. Bassi and S. Rebay. A high-order accurate discontinuous finite element method for the numerical solution of the compressible Navier-Stokes equations. *J. Comput. Phys.*, 131(2):267–279, 1997.

[18] F. Bassi, S. Rebay, G. Mariotta, S. Pedinotti, and M. Savini. A high order discontinuous finite element method for invisid and viscous turbomachinery flows. In R. Decuypere and G. Dibelius, editors, *Proceedings of the 2nd European Conference on Turbomachinery, Fluid Dynamics and Thermodynamics*, pages 99–108, Technologisch Instituut, Antwerpen, Belgium, 1997.

[19] F. Bassi, L. Botti, A. Colombo, D. A. D. Pietro, and P. Tesini. On the flexibility of agglomeration based physical space discontinuous Galerkin discretizations. *J. Comput. Phys.*, 231(1):45–65, 2012.

[20] F. Bassi, L. Botti, A. Colombo, and S. Rebay. Agglomeration based discontinuous Galerkin discretization of the Euler and Navier–Stokes equations. *Comput. & Fluids*, 61:77–85, 2012.

[21] G. K. Batchelor. *An Introduction to Fluid Dynamics*. Cambridge University Press, Cambridge, 1967.

[22] C. E. Baumann and J. T. Oden. A discontinuous *hp* finite element method for convection–diffusion problems. *Comput. Methods Appl. Mech. Engrg.*, 175(3–4): 311–341, 1999.

[23] R. Becker and R. Rannacher. A feed-back approach to error control in finite element methods: Basic analysis and examples. *East–West J. Numer. Math.*, 4:237–264, 1996.

[24] R. Becker and R. Rannacher. Weighted a posteriori error control in FE methods. Technical Report Preprint 1, Universität Heidelburg, Interdisziplinäres Zentrum für Wissenschaftliches Rechnen, 1996.

[25] R. Becker and R. Rannacher. An optimal control approach to a posteriori error estimation in finite element methods. *Acta Numerica*, 10:1–102, 2001.

[26] R. Becker, P. Hansbo, and M. G. Larson. Energy norm a posteriori error estima-

tion for discontinuous Galerkin methods. *Comput. Methods Appl. Mech. Engrg.*, 192(5–6):723–733, 2003.

[27] L. Beilina, S. Korotov, and M. Křížek. Nonobtuse tetrahedral partitions that refine locally towards Fichera-like corners. *App. Math.*, 50(6):569–581, 2005.

[28] L. Belenki and L. Diening. Optimality of an adaptive finite element method for the p-Laplacian equation. *IMA J. Numer. Anal.*, 32(2):484–510, 2012.

[29] C. Bernardi and Y. Maday. Spectral methods. In P. Ciarlet and J. Lions, editors, *Techniques of Scientific Computing (Part 2)*, volume 5 of *Handbook of Numerical Analysis*, pages 209–485. Elsevier, 1997.

[30] C. Bernardi, N. Fiétier, and R. G. Owens. An error indicator for mortar element solutions to the Stokes problem. *IMA J. Numer. Anal.*, 21(4):857–886, 2001.

[31] S. Berrone and E. Süli. Two-sided a posteriori error bounds for incompressible quasi-Newtonian flows. *IMA J. Numer. Anal.*, 28(2):382–421, 2008.

[32] K. S. Bey and J. T. Oden. hp-version discontinuous Galerkin methods for hyperbolic conservation laws. *Comput. Methods Appl. Mech. Engrg.*, 133(3–4):259–286, 1996.

[33] K. S. Bey, A. Patra, and J. T. Oden. hp-version discontinuous Galerkin methods for hyperbolic conservation laws: A parallel strategy. *Internat. J. Numer. Methods Engrg.*, 38(22):3889–3908, 1995.

[34] K. S. Bey, J. T. Oden, and A. Patra. A parallel hp-adaptive discontinuous Galerkin method for hyperbolic conservation laws. *Appl. Numer. Math.*, 20(4):321–336, 1996.

[35] C. Bi and V. Ginting. Two-grid finite volume element method for linear and nonlinear elliptic problems. *Numer. Math.*, 108(2):177–198, 2007.

[36] C. Bi and V. Ginting. Two-grid discontinuous Galerkin method for quasi-linear elliptic problems. *J. Sci. Comput.*, 49(3):311–331, 2011.

[37] C. Bi and V. Ginting. A posteriori error estimates of discontinuous Galerkin method for nonmonotone quasi-linear elliptic problems. *J. Sci. Comput.*, 55(3): 659–687, 2013.

[38] P. Binev, W. Dahmen, and R. DeVore. Adaptive finite element methods with convergence rates. *Numer. Math.*, 97(2):219–268, 2004.

[39] E. C. Bingham. An investigation of the laws of plastic flow. *Bull. Nat. Bur. Stand.*, 13:309–353, 1916.

[40] H. Blatter. Velocity and stress fields in grounded glaciers:a simple algorithm for including deviatoric stress gradients. *J. Glaciol.*, 41(138):333–344, 1995.

[41] K. Böhmer. *Numerical methods for nonlinear elliptic differential equations*. Numerical Mathematics and Scientific Computation. Oxford University Press, Oxford, 2010.

[42] D. Braess. *Finite elements. Theory, fast solvers, and applications in solid mechanics*. Cambridge University Press, Cambridge, second edition, 2001.

[43] S. C. Brenner. Poincaré-Friedrichs inequality for piecewise H^1 functions. *SIAM J. Numer. Anal.*, 41(1):306–324, 2003.

[44] S. C. Brenner. Korn's inequalities for piecewise H^1 vector fields. *Math. Comp.*, 73 (73):1067–1087, 2004.

[45] S. C. Brenner and L. R. Scott. *The Mathematical Theory of Finite Element Methods*. Texts in Applied Mathematics. Springer-Verlag, New York, third edition, 2008.

[46] F. Brezzi and M. Fortin. *Mixed and Hybrid Finite Element Methods*. Springer Series in Computational Mathematics. Springer-Verlag, New York, 1991.

[47] F. Brezzi, G. Manzini, D. Marini, P. Pietra, and A. Russo. Discontinuous finite elements for diffusion problems. In *Francesco Brioschi (1824-1897) Convegno di Studi*

Matematici, Istituto Lombardo, Accademia di Scienze e Lettere, Milan, Italy, pages 197–217, 1997.

[48] F. Brezzi, G. Manzini, D. Marini, P. Pietra, and A. Russo. Discontinuous Galerkin approximations for elliptic problems. *Numer. Methods Part. Diff. Eqs.*, 16(4):365–378, 2000.

[49] A. N. Brooks and T. J. R. Hughes. Streamline upwind/Petrov-Galerkin formulations for convection dominated flows with particular emphasis on the incompressible Navier-Stokes equations. *Comput. Methods Appl. Mech. Engrg.*, 32(1–3): 199–259, 1982.

[50] R. Bustinza and G. N. Gatica. A local discontinuous Galerkin method for nonlinear diffusion problems with mixed boundary conditions. *SIAM J. Sci. Comput.*, 26(1):152–177, 2004.

[51] R. Bustinza and G. N. Gatica. A mixed local discontinuous Galerkin method for a class of nonlinear problems in fluid mechanics. *J. Comput. Phys.*, 207(2):427–456, 2005.

[52] A. Cangiani, E. H. Georgoulis, and P. Houston. *hp*-version discontinuous Galerkin methods on polygonal and polyhedral meshes. Submitted for publication.

[53] A. Cangiani, E. H. Georgoulis, and M. Jensen. Continuous and discontinuous finite element methods for convection-diffusion problems: a comparison. In G. Lube and G. Rapin, editors, *Proceedings of the International Conference on Boundary and Interior Layers (BAIL) — Computational and Asymptotic methods*, 2006.

[54] P. Castillo. An optimal error estimate for the local discontinuous Galerkin method. In B. Cockburn, G. E. Karniadakis, and C.-W. Shu, editors, *Discontinuous Galerkin Methods: Theory, Computation and Applications*, volume 11 of *Lecture Notes in Computational Science and Engineering*, pages 285–290. Springer, 2000.

[55] P. Castillo, B. Cockburn, D. Schötzau, and C. Schwab. Optimal a priori error estimates for the *hp*-version of the Local Discontinuous Galerkin method for convection-diffusion problems. *Math. Comp.*, 71(238):455–478, 2002.

[56] O. Cazacu and N. Cristescu. Constitutive model and analysis of creep flow of natural slopes. *Ital. Geotech. J.*, 34:44–54, 2000.

[57] L. Chen and Y. Chen. Two-grid method for nonlinear reaction-diffusion equations by mixed finite element methods. *J. Sci. Comput.*, 49(3):381–401, 2011.

[58] R. W. Clough and E. L. Wilson. Early finite element research at Berkeley. In *Fifth U.S. National Conference on Computational Mathematics*, Boulder, CO, 1999.

[59] B. Cockburn and C.-W. Shu. The local discontinuous Galerkin method for time-dependent convection-diffusion systems. *SIAM J. Numer. Anal.*, 35(6):2440–2463, 1998.

[60] B. Cockburn, G. E. Karniadakis, and C.-W. Shu. The development of discontinuous Galerkin methods. In B. Cockburn, G. E. Karniadakis, and C.-W. Shu, editors, *Discontinuous Galerkin Methods: Theory, Computation and Applications*, volume 11 of *Lecture Notes in Computational Science and Engineering*, chapter 1, pages 3–50. Springer, 2000.

[61] B. Cockburn, G. Kanschat, I. Perugia, and D. Schötzau. Superconvergence of the local discontinuous Galerkin method for elliptic problems on Cartesian grids. *SIAM J. Numer. Anal.*, 39(1):264–285, 2002.

[62] J. Colinge and J. Rappaz. A strongly nonlinear problem arising in glaciology. *Math. Model. Numer. Anal.*, 33(2):395–406, 1999.

[63] S. Congreve and P. Houston. Two-grid *hp*-DGFEM for second order quasilinear elliptic PDEs based on a single Newton iteration. In J. Li and H. Yang, editors, *Proceedings of the 8th International Conference on Scientific Computing and Applica-*

tions, Contemporary Mathematics, pages 135–142, University of Nevada, Las Vegas, 2012. AMS.

[64] S. Congreve, P. Houston, and T. P. Wihler. Two-grid hp-version DGFEMs for strongly monotone second-order quasilinear elliptic PDEs. *Proc. Appl. Math. Mech.*, 11:3–6, 2011.

[65] S. Congreve, P. Houston, E. Süli, and T. P. Wihler. Discontinuous Galerkin finite element approximation of quasilinear elliptic boundary value problems II: Strongly monotone quasi-Newtonian flows. *IMA J. Numer. Anal.*, 33(4):1386–1415, 2013.

[66] S. Congreve, P. Houston, and T. P. Wihler. Two-grid hp-version discontinuous Galerkin finite element methods for second-order quasilinear elliptic PDEs. *J. Sci. Comput.*, 55(2):471–497, 2013.

[67] N. Cristescu. Plastic flow through conical converging dies, using a viscoplastic constitutive equation. *Int. J. Mech. Sci.*, 17(6):425–433, 1975.

[68] N. Cristescu. On the optimum die angle in fast wire drawing. *J. Mech. Work. Technol.*, 3(3–4):275–287, 1980.

[69] C. N. Dawson, M. F. Wheeler, and C. S. Woodward. A two-grid finite difference scheme for nonlinear parabolic equations. *SIAM J. Numer. Anal.*, 35(2):435–452, 1998.

[70] C. N. Dawson, S. Sun, and M. F. Wheeler. Compatible algorithms for coupled flow and transport. *Comput. Methods Appl. Mech. Engrg.*, 193(23–26):2565–2580, 2004.

[71] B. A. de Dios, F. Brezzi, O. Havle, and L. D. Marini. L^2-estimates for the DG IIPG-0 scheme. *Numer. Methods Part. Diff. Eqs.*, 28(5):1440–1465, 2012.

[72] A. Demlow and R. Stevenson. Convergence and quasi-optimality of an adaptive

finite element method for controlling L_2 errors. *Numer. Math.*, 117(2):185–218, 2011.

[73] V. Dolejší and O. Havle. The L^2-optimality of the IIPG method for odd degrees of polynomial approximation in 1D. *J. Sci. Comput.*, 42(1):122–143, 2010.

[74] W. Dörfler. A convergent adaptive algorithm for Poisson's equation. *SIAM J. Numer. Anal.*, 33(1996):1106–1123, 1996.

[75] J. Douglas and T. Dupont. Interior penalty procedures for elliptic and parabolic Galerkin methods. In R. Glowinski and J. Lions, editors, *Computing Methods in Applied Sciences*, volume 58 of *Lecture Notes in Physics*, pages 207–216. Springer, Berlin, 1976.

[76] K. Eriksson and C. Johnson. Error estimates and automatic time step control for nonlinear parabolic problems, I. *SIAM J. Numer. Anal.*, 24(1):12–23, 1987.

[77] K. Eriksson and C. Johnson. Adaptive finite element methods for parabolic problems I: A linear model problem. *SIAM J. Numer. Anal.*, 28(1):43–77, 1991.

[78] K. Eriksson and C. Johnson. Adaptive finite element methods for parabolic problems II: Optimal error estimates in $L_\infty L_2$ and $L_\infty L_\infty$. *SIAM J. Numer. Anal.*, 32 (3):706–740, 1995.

[79] K. Eriksson and C. Johnson. Adaptive finite element methods for parabolic problems IV: Nonlinear problems. *SIAM J. Numer. Anal.*, 32(6):1729–1749, 1995.

[80] K. Eriksson and C. Johnson. Adaptive finite element methods for parabolic problems V: Long-time integration. *SIAM J. Numer. Anal.*, 32(6):1750–1763, 1995.

[81] K. Eriksson, C. Johnson, and V. Thomée. Time discretization of parabolic problems by the discontinuous Galerkin method. *RAIRO Anal. Numér.*, 19(4):611–643, 1985.

[82] K. Eriksson, D. J. Estep, P. Hansbo, and C. Johnson. Introduction to adaptive methods for differential equations. *Acta Numerica*, 4:105–158, 1995.

[83] T. Fankhauser, T. P. Wihler, and M. Wirz. *hp*-adaptive FEM based on continuous Sobolev embeddings: Isotropic refinements. *Comput. Math. Appl.*, 2013. doi: 10.1016/j.camwa.2013.05.024.

[84] B. Fischer, A. Ramage, D. J. Silvester, and A. J. Wathen. On parameter choice and iterative convergence for stabilised discretisations of advection-diffusion problems. *Comput. Methods Appl. Mech. Engrg.*, 179(1–2):179–195, 1999.

[85] L. P. Franca, S. L. Frey, and T. J. Hughes. Stabilized finite element methods: I. application to the advective-diffusive model. *Comput. Methods Appl. Mech. Engrg.*, 95(2):253–276, 1992.

[86] N. Frauböse and S. A. Sauter. Composite finite elements and multigrid. Part I: Convergence theory in 1-d. In *17th GAMM-Seminar Liepzig on Construction of Grid Generation Algorithms*, MPI Leipzig, 2001.

[87] E. H. Georgoulis. *Discontinuous Galerkin methods on shape-regular and anisotropic meshes.* D. Phil. thesis, Oxford University, 2003.

[88] E. H. Georgoulis. *hp*-version interior penalty discontinuous Galerkin finite element methods on anisotropic meshes. *Int. J. Numer. Anal. Model.*, 3(1):52–79, 2006.

[89] E. H. Georgoulis and O. Lakkis. A posteriori error bounds for discontinuous Galerkin methods for quasilinear parabolic problems. In G. Kreiss, P. Lötstedt, A. Målqvist, and M. Neytcheva, editors, *Numerical Mathematics and Advanced Applications. Proceedings of ENUMATH 2009, the 8th European Conference on Numerical Mathematics and Advanced Applications*, Uppsala University, Uppsala, Sweden, 2010. Springer.

[90] E. H. Georgoulis and E. Süli. *hp*-DGFEM on shape-irregular meshes: reaction-diffusion problems. Technical Report NA 01-09, Oxford University, Computing Laboratory, 2001.

[91] E. H. Georgoulis, E. Hall, and P. Houston. Discontinuous Galerkin methods for advection-diffusion-reaction problems on anisotropically refined meshes. *SIAM J. Sci. Comput.*, 30(1):246–271, 2007.

[92] E. H. Georgoulis, E. Hall, and P. Houston. Discontinuous Galerkin methods on *hp*-anisotropic meshes I: A priori error analysis. *Int. J. Comput. Sci. Math.*, 1(2–3): 221–244, 2007.

[93] E. H. Georgoulis, E. Hall, and P. Houston. Discontinuous Galerkin methods on *hp*-anisotropic meshes I: A posteriori error analysis and adaptivity. *Appl. Numer. Math.*, 59(9):2179–2194, 2009.

[94] E. H. Georgoulis, E. Hall, and J. Melenk. On the suboptimality of the *p*-version interior penalty discontinuous Galerkin method. *J. Sci. Comput.*, 42(1):54–67, 2010.

[95] E. H. Georgoulis, O. Lakkis, and J. M. Virtanen. A posteriori error control for discontinuous Galerkin methods for parabolic problems. *SIAM J. Numer. Anal.*, 49(2):427–458, 2011.

[96] S. Giani and P. Houston. Anisotropic *hp*-adaptive discontinuous Galerkin finite element methods for compressible fluid flows. *Int. J. Numer. Anal. Model.*, 9(4): 928–949, 2012.

[97] S. Giani, D. Schötzau, and L. Zhu. An a-posteriori error estimate for *hp*-adaptive DG methods for convection-diffusion problems on anisotropically refined meshes. *Comput. Math. Appl.*, 10.1016/j.camwa.2012.10.015, 2012.

[98] V. Girault and J.-L. Lions. Two-grid finite-element schemes for the transient Navier-Stokes problem. *Math. Model. Numer. Anal.*, 35(5):945–980, 2001.

[99] R. Glowinski and J. Rappaz. Approximation of a nonlinear elliptic problem arising in a non-Newtonian fluid flow model in glaciology. *Math. Model. Numer. Anal.*, 37(1):175–186, 2003.

[100] T. Gudi and A. K. Pani. Discontinuous Galerkin methods for quasi-linear elliptic problems of nonmonotone type. *SIAM J. Numer. Anal.*, 45(1):163–192, 2007.

[101] T. Gudi, N. Nataraj, and A. K. Pani. *hp*-discontinuous Galerkin methods for strongly nonlinear elliptic boundary value problems. *Numer. Math.*, 109(2):233–268, 2008.

[102] T. Gudi, N. Nataraj, and A. K. Pani. An *hp*-local discontinuous Galerkin method for some quasilinear elliptic boundary value problems of nonmonotone type. *Math. Comp.*, 77(262):731–756, 2008.

[103] W. Hackbusch and S. A. Sauter. Composite finite elements for problems containing small geometric details. Part II: Implementation and numerical results. *Comput. Vis. Sci.*, 1(1):15–25, 1997.

[104] W. Hackbusch and S. A. Sauter. Composite finite elements for the approximation of PDEs on domains with complicated micro-structures. *Numer. Math.*, 75(4): 447–472, 1997.

[105] W. Hackbusch and S. A. Sauter. A new finite element approach for problems containing small geometric details. *Arch. Math. (Brno)*, 34(1):105–117, 1998.

[106] E. Hall. *Anisotropic adaptive refinement for discontinuous Galerkin methods*. PhD thesis, University of Leicester, 2007.

[107] P. Hansbo and M. G. Larson. Discontinuous Galerkin methods for incompressible and nearly incompressible elasticity by Nitsche's method. *Comput. Methods Appl. Mech. Engrg.*, 191(17–18):1895–1908, 2002.

[108] K. Harriman, P. Houston, B. Senior, and E. Süli. *hp*-version discontinuous Galerkin methods with interior penalty for partial differential equations with

nonnegative characteristic form. In C.-W. Shu, T. Tang, and S.-Y. Cheng, editors, *Recent Advances in Scientific Computing and Partial Differential Equations*, volume 330 of *Contemporary Mathematics*, pages 89–119. AMS, 2003.

[109] K. Harriman, D. G. Davaghan, and E. Süli. The importance of adjoint consistency in the approximation of linear functionals using the discontinuous Galerkin finite element method. Technical Report NA 04-18, Oxford University, Computing Laboratory, 2004.

[110] R. Hartmann and P. Houston. Symmetric interior penalty DG methods for the compressible Navier-Stokes equations II: Goal-oriented a posteriori error estimation. *Int. J. Numer. Anal. Model.*, 3(2):141–162, 2006.

[111] R. Hartmann and P. Houston. An optimal order interior penalty discontinuous Galerkin discretization of the compressible Navier-Stokes equations. *J. Comput. Phys.*, 227(22):9670–9685, 2008.

[112] R. Hartmann and P. Houston. Error estimation and adaptive mesh refinement for aerodynamic flows. In H. Deconinck, editor, *VKI LS 2010-01: 36th CFD/ADIGMA course on hp-adaptive and hp-multigrid methods, Oct. 26–30, 2009*. Von Karman Institute for Fluid Dynamics, Rhode Saint Genése, Belgium, 2009.

[113] P. Hild, I. R. Ionescu, T. Lachand-Robert, and I. Roşca. The blocking of inhomogeneous Bingham fluid: an application to landslides. *Math. Model. Numer. Anal.*, 36(6):1013–1026, 2002.

[114] C. O. Horgan. Korn's inequalities and their applications in continuum mechanics. *SIAM Review*, 37(4):491–511, 1995.

[115] P. Houston and E. Süli. Stabilised *hp*-finite element approximation of partial differential equations with nonnegative characteristic form. *Computing*, 66(2):99–119, 2001.

[116] P. Houston and E. Süli. A note on the design of *hp*-adaptive finite element methods for elliptic partial differential equations. *Comput. Methods Appl. Mech. Engrg.*, 194(2–5):229–243, 2005.

[117] P. Houston, R. Rannacher, and E. Süli. A posteriori error analysis for stabilised finite element approximations of transport problems. *Comput. Methods Appl. Mech. Engrg.*, 190(11–12):1483–1508, 2000.

[118] P. Houston, C. Schwab, and E. Süli. Stabilized *hp*-finite element methods for first-order hyperbolic problems. *SIAM J. Numer. Anal.*, 37(5):1618–1643, 2000.

[119] P. Houston, C. Schwab, and E. Süli. Discontinuous *hp*-finite element methods for advection-diffusion-reaction problems. *SIAM J. Numer. Anal.*, 39(6):2133–2163, 2002.

[120] P. Houston, D. Schötzau, and T. P. Wihler. *hp*-adaptive discontinuous Galerkin finite element methods for the Stokes problem. In P. Neittaanmäki, T. Rossi, S. Korotov, J. Périaux, and D. Knörzer, editors, *Proc. of the European Congress on Computational Methods in Applied Sciences and Engineering*, volume II, 2004.

[121] P. Houston, D. Schötzau, and T. P. Wihler. Mixed *hp*-discontinuous Galerkin finite element methods for the Stokes problem in polygons. Technical Report 2004/02, University of Leicester, School of Mathematics & Computer Science, 2004.

[122] P. Houston, J. Robson, and E. Süli. Discontinuous Galerkin finite element approximation of quasilinear elliptic boundary value problems I: the scalar case. *IMA J. Numer. Anal.*, 25(4):726–749, 2005.

[123] P. Houston, D. Schötzau, and T. P. Wihler. Energy norm a posteriori error estimation for mixed discontinuous Galerkin approximations of the Stokes problem. *J. Sci. Comput.*, 22(1):347–370, 2005.

[124] P. Houston, D. Schötzau, and T. P. Wihler. Energy norm a posteriori error estima-

tion of *hp*-adaptive discontinuous Galerkin methods for elliptic problems. *Math. Models Methods Appl. Sci.*, 17(1):33–62, 2007.

[125] P. Houston, E. Süli, and T. P. Wihler. A posteriori error analysis of *hp*-version discontinuous Galerkin finite-element methods for second-order quasi-linear PDEs. *IMA J. Numer. Anal.*, 28(2):245–273, 2008.

[126] T. J. Hughes, L. P. Franca, and G. M. Hulbert. A new finite element formulation for computational fluid dynamics: VIII. the galerkin/least-squares method for advective-diffusive equations. *Comput. Methods Appl. Mech. Engrg.*, 73(2):173–189, 1989.

[127] I. R. Ionescu and B. Vernescu. A numerical method for a viscoplastic problem. an application to wire drawing. *Int. J. Eng. Sci.*, 26(6):627 – 633, 1988.

[128] C. Johnson. Error estimates and adaptive time-step control for a class of one-step methods for stiff ordinary differential equations. *SIAM J. Numer. Anal.*, 25(4): 908–926, 1988.

[129] C. Johnson and U. Nävert. An analysis of some finite element methods for advection-diffusion problems. In O. Axelsson, L. Frank, and A. V. D. Sluis, editors, *Analytical and Numerical Approaches to Asymptotic Problems in Analysis*, volume 47 of *North-Holland Mathematics Studies*, pages 99–116. North-Holland, 1981.

[130] C. Johnson and J. Pitkäranta. An analysis of the discontinuous Galerkin method for a scalar hyperbolic equation. *Math. Comp.*, 46(173):1–26, 1986.

[131] O. A. Karakashian and F. Pascal. A posteriori error estimates for a discontinuous Galerkin approximation of second-order elliptic problems. *SIAM J. Numer. Anal.*, 41(6):2374–2399, 2003.

[132] G. Karypis and V. Kumar. A fast and high quality multilevel scheme for partitioning irregular graphs. *J. Sci. Comput.*, 20(1):359–392, 1998.

[133] O. Lakkis and C. Makridakis. Elliptic reconstruction and a posteriori error estimates for fully discrete linear parabolic problems. *Math. Comp.*, 75(256):1627–1658, 2006.

[134] P. LeSaint and P. A. Raviart. On a finite element method for solving the neutron transport equation. In C. de Boor, editor, *Mathematical aspects of finite element in partial differential equations*, volume 33 of *Publication of the Mathematics Research Center, University of Wisconsin*, pages 89–145. Academic Press, 1974.

[135] Q. Lin. Full convergence for hyperbolic finite elements. In B. Cockburn, G. E. Karniadakis, and C.-W. Shu, editors, *Discontinuous Galerkin Methods: Theory, Computation and Applications*, volume 11 of *Lecture Notes in Computational Science and Engineering*, pages 167–177. Springer, 2000.

[136] W. B. Liu and J. W. Barrett. Quasi-norm error bounds for the finite element approximation of some degenerate quasilinear elliptic equations and variational inequalities. *RAIRO Modél. Math. Anal. Numér.*, 28(6):725–744, 1994.

[137] C. Makridakis and R. Nochetto. Elliptic reconstruction and a posteriori error estimates for parabolic problems. *SIAM J. Numer. Anal.*, 41(4):1585–1594, 2003.

[138] M. Marion and J. Xu. Error estimates on a new nonlinear Galerkin method based on two-grid finite elements. *SIAM J. Numer. Anal.*, 32(4):1170–1184, 1995.

[139] C. Mavriplis. Adaptive mesh strategies for the spectral element method. *Comput. Methods Appl. Mech. Engrg.*, 116(1–4):77–86, 1994.

[140] J. M. Melenk and B. I. Wohlmuth. On residual-based a posteriori error estimation in *hp*-FEM. *Adv. Comp. Math.*, 15(1–4):311–331, 2001.

[141] M. Metcalf, J. Reid, and M. Cohen. *Fortran 95/2003 explained*. Numerical Mathematics and Scientific Computation. Oxford University Press, Oxford, 2004.

[142] W. F. Mitchell and M. A. McClain. A comparison of *hp*-adaptive strategies for elliptic partial differential equations. 2011. (Submitted for publication).

[143] W. F. Mitchell and M. A. McClain. A comparison of *hp*-adaptive strategies for elliptic partial differential equations. Technical Report NISTIR 7824, National Institute of Standards and Technology, 2011.

[144] P. Morin, R. H. Nochetto, and K. G. Seibert. Convergence of adaptive finite element methods. *SIAM Review*, 44(4):631–658, 2002.

[145] J. T. Oden, I. Babuška, and C. E. Baumann. A discontinuous *hp* finite element method for diffusion problems. *J. Comput. Phys.*, 146(2):491–519, 1998.

[146] J. G. Oldroyd. A rational formulation of the equations of plastic flow for a Bingham solid. *Math. Proc. Cambridge Philos. Soc.*, 43(1):100–105, 1947.

[147] J. M. Ortega and W. C. Rheinboldt. *Iterative Solution of Nonlinear Equations in Several Variables*. Computer Science and Applied Mathematics. Academic Press, New York, 1970.

[148] C. Ortner and E. Süli. Discontinuous Galerkin finite element approximation of nonlinear second-order elliptic and hyperbolic systems. *SIAM J. Numer. Anal.*, 45 (4):1370–1397, 2007.

[149] T. E. Peterson. A note on the convergence of the discontinuous Galerkin method for a scalar hyperbolic equation. *SIAM J. Numer. Anal.*, 28(1):133–140, 1991.

[150] W. H. Reed and T. R. Hill. Triangular mesh methods for the neutron transport equation. Technical Report LA-UR-73-479, University of California, Los Alamos Scientific Laboratory, 1973.

[151] G. R. Richter. An optimal-order error estimate for the discontinuous Galerkin method. *Math. Comp.*, 50(181):75–88, 1988.

[152] B. Rivière, M. Wheeler, and V. Girault. Improved energy estimates for interior penalty, constrained and discontinuous Galerkin methods for elliptic problems. Part I. *Comput. Geosci.*, 3(3–4):337–360, 1999.

[153] Y. Saad and M. H. Schultz. GMRES: A generalized minimal residual algorithm for solving nonsymmetric linear systems. *SIAM J. Sci. Stat. Comput.*, 7(3):856–869, 1986.

[154] S. A. Sauter and R. Warnke. Composite finite elements for elliptic boundary value problems with discontinuous coefficients. *Computing*, 77(1):29–55, 2006.

[155] D. Schötzau. *hp-DGFEM for parabolic evolution problems*. PhD thesis, ETH Zürich, 1999.

[156] D. Schötzau and T. P. Wihler. Exponential convergence of mixed *hp*-DGFEM for Stokes flow in polygons. *Numer. Math.*, 96(2):339–361, 2003.

[157] D. Schötzau, C. Schwab, and A. Toselli. Mixed *hp*-DGFEM for incompressible flows. *SIAM J. Numer. Anal.*, 40(6):2171–2194, 2002.

[158] C. Schwab. *p- and hp-FEM — Theory and Applications in Solid and Fluid Mechanics*. Numerical Mathematics and Scientific Computation. Oxford University Press, Oxford, 1998.

[159] K. G. Siebert. A convergence proof for adaptive finite elements without lower bound. *IMA J. Numer. Anal.*, 31(3):947–970, 2011.

[160] P. Šolín, K. Segeth, and I. Doležel. *Higher-order Finite Element Methods*. Studies in advanced mathematics. Chapman & Hall/CRC, Boca Raton, FL, 2004.

[161] B. Stamm and T. P. Wihler. *hp*-optimal discontinuous Galerkin methods for linear elliptic problems. *Math. Comp.*, 79(272):2117–2133, 2010.

[162] R. Stevenson. An optimal adaptive finite element method. *SIAM J. Numer. Anal.*, 42(5):2188–2217, 2005.

[163] E. Süli, C. Schwab, and P. Houston. *hp*-DGFEM for partial differential equations with non-negative characteristic form. In B. Cockburn, G. E. Karniadakis, and C.-W. Shu, editors, *Discontinuous Galerkin Methods: Theory, Computation and*

Applications, volume 11 of *Lecture Notes in Computational Science and Engineering*, pages 221–230. Springer, 2000.

[164] S. Sun. *Discontinuous Galerkin methods for reactive transport in porous media*. PhD thesis, University of Texas at Austin, 2003.

[165] S. Sun and M. F. Wheeler. Symmetric and nonsymmetric discontinuous Galerkin methods for reactive transport in porous media. *SIAM J. Numer. Anal.*, 43(1): 195–219, 2005.

[166] A. Toselli. *hp* discontinuous Galerkin approximations for the Stokes problem. *Math. Models Methods Appl. Sci.*, 12(11):1565–1597, 2002.

[167] C. Tropea, A. Yarin, and J. F. Foss, editors. *Springer handbook of experimental fluid mechanics*, volume 1, chapter 9, pages 619–744. Springer, 2007.

[168] T. Utnes. Two-grid finite element formulations of the incompressible Navier-Stokes equations. *Comm. Numer. Methods Engrg.*, 13(8):675–684, 1997.

[169] A. Veeser. Convergent adaptive finite elements for the nonlinear Laplacian. *Numer. Math.*, 92(4):743–770, 2002.

[170] R. Verfürth. *A Review of a Posteriori Error Estimation and Adaptive Mesh-Refinement Techniques*. Teubner, 1996.

[171] M. F. Wheeler. An elliptic collocation-finite element method with interior penalties. *SIAM J. Numer. Anal.*, 15(1):152–161, 1978.

[172] T. P. Wihler. An *hp*-adaptive strategy based on continuous Sobolev embeddings. *J. Comput. Appl. Math.*, 235(8):2731–2739, 2011.

[173] T. P. Wihler. An *hp*-adaptive FEM procedure based on continuous sobolev embeddings. *Proc. Appl. Math. Mech.*, 11:11–14, 2011.

[174] T. P. Wihler and M. Wirz. Mixed *hp*-discontinuous Galerkin FEM for linear elasticity and Stokes flow in three dimensions. *Math. Models Methods Appl. Sci.*, 22(8), 2012.

[175] T. P. Wihler, P. Frauenfelder, and C. Schwab. Exponential convergence of the *hp*-DGFEM for diffusion problems. *Comput. Math. Appl.*, 46(1):183–205, 2003.

[176] L. Wu and M. B. Allen. A two-grid method for mixed finite-element solution of reaction-diffusion equations. *Numer. Methods Part. Diff. Eqs.*, 15(3):317–332, 1999.

[177] J. Xu. A new class of iterative methods for nonselfadjoint or indefinite problems. *SIAM J. Numer. Anal.*, 29(2):303–319, 1992.

[178] J. Xu. A novel two-grid method for semilinear elliptic equations. *SIAM J. Sci. Comput.*, 15(1):231–237, 1994.

[179] J. Xu. Some two-grid finite element methods. In A. Quarteroni, J. Periaux, Y. A. Kuznetsov, and O. B. Widlund, editors, *Domain decomposition methods in science and engineering: the sixth international conference on domain decomposition*, volume 157 of *Contemporary Mathematics*, pages 79–87. AMS, 1994.

[180] J. Xu. Two-grid discretization techniques for linear and nonlinear PDEs. *SIAM J. Numer. Anal.*, 33(5):1759–1777, 1996.

[181] L. Zhu. *Robust a-posteriori error estimation for discontinuous Galerkin methods for convection-diffusion equations*. PhD thesis, University of British Columbia, 2010.

[182] L. Zhu and D. Schötzau. A robust a posteriori error estimate for *hp*-adaptive DG methods for convection-diffusion equations. *IMA J. Numer. Anal.*, 31(3):971–1005, 2010.

[183] L. Zhu, S. Giani, P. Houston, and D. Schötzau. Energy norm a posteriori error estimation for *hp*-adaptive discontinuous Galerkin methods for elliptic problems in three dimensions. *Math. Models Methods Appl. Sci.*, 21(2):267–306, 2011.